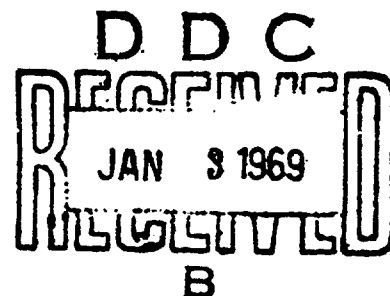


AD 679911



RDTR No. 131  
1 October 1968

PROCEEDINGS OF FIRST  
PYROTECHNIC SEMINAR



U. S. NAVAL AMMUNITION DEPOT  
CRANE, INDIANA



Reproduced by the  
CLEARINGHOUSE  
for Federal Scientific & Technical  
Information Springfield Va. 22151

This document has been approved  
for public release and sale; its  
distribution is unlimited

440

U. S. NAVAL AMMUNITION DEPOT  
Crane, Indiana 47522

RDTR No. 131  
1 October 1968

PROCEEDINGS OF FIRST  
PYROTECHNIC SEMINAR

R. M. Blunt  
General Chairman  
Denver Research Institute,

This report was reviewed for adequacy and technical accuracy  
by B. E. Douda.

RELEASED

*BH Calkins*  
B. H. CALKINS, Manager  
Concept Development Division  
Research and Development Department

PAGES \_\_\_\_\_  
ARE  
MISSING  
IN  
ORIGINAL  
DOCUMENT

## INTRODUCTION

These Proceedings contain the majority of the papers presented at the First Military Pyrotechnics Seminar.

The purpose of the seminar was primarily that of encouraging a free and lively exchange of information and viewpoints by the participants and the promotion of a more scientific approach to the solution of pyrotechnic problems. The solicitation of the opinions of interested and qualified persons regarding professional courses in ordnance engineering were also objectives.

During the week of August 12th, 1968, approximately sixty-five representatives of commercial, government and private organizations interested in military pyrotechnics attended the seminar at Estes Park, Colorado. The seminar was sponsored by the Mechanics Division, Denver Research Institute, University of Denver, Denver, Colorado 80210, and enthusiastically supported and aided by the Concepts Development Division, Research and Development Department, U. S. Naval Ammunition Depot, Crane, Indiana 47522.

The success of the seminar was due in large measure to those who presented the papers that are contained in these Proceedings. It is hoped that an even larger number of papers of equal quality will become available for the next seminar. Those who wish to participate are urged to communicate the title and a brief abstract of proposed papers to Mr. R. M. Blunt, Denver Research Institute.

It is a pleasure to acknowledge the invaluable assistance of Mr. Ralph Williams of D. R. I. during the seminar. Mr. B. E. Douda of the U. S. Naval Ammunition Depot and Mr. William S. Cronk, Ft. Walton Beach, Florida were instrumental in the promotion of the seminar during many hours of discussion in 1966-67. Sincere thanks are also due the chairmen of the several sessions who so ably directed the discussion periods.

The report of the 11th International Pyrotechnics Conference includes:

# TABLE OF CONTENTS

	Page
PYRO RESEARCH AREAS FOR FURTHER EXPLORATORY DEVELOPMENT - J. T. Hamrick . . . . .	1
→ COLORED SMOKE SIGNALS, CASTABLE COMPOSITIONS; - George A. Lane and Erwin M. Jankowiak. . . . .	25
→ IGNITION AND OUTPUT CHARACTERISTICS OF PYROTECHNICS FOR ELECTRO-EXPLOSIVE DEVICE APPLICATIONS; - James L. Austing and James E. Kennedy . . . . .	39
→ AN INTRODUCTION TO ADVANCED DELAY CORDS; - D.C. Orlander. . . . .	99
→ SPECTRAL OBSERVATIONS IN ILLUMINATING FLARES; - B. E. Douda . . . . .	113
THE SORCERY AND SCIENCE OF AEROSPACE EXPLOSIVE ORDNANCE - S. A. Moses . . . . .	129
DESIGN FOR EDUCATION OF PYROTECHNICISTS - R. M. Blunt. . . . .	149
→ COMPUTER SOLUTION OF PYROTECHNIC THERMOCHEMISTRY PROBLEMS; - Edward J. Davis . . . . .	157
→ MATHEMATICAL SIMULATION MODELS; - Jerry L. Kemp. . . . .	167
→ MEASUREMENT OF ILLUMINATION-SOURCE-RELATED CHARACTERISTICS OF THE CYANOGEN-OXYGEN-BORON TRICHLORIDE FLAME SYSTEM; - Robert L. Tischer and Karl Scheller . . . . .	175
→ ULTRASONIC ENHANCEMENT OF PYROTECHNIC PROCESSING, PRESSING, EXTRUSION, CASTING; - Richard Pheasant and C. Dana McKinney. . . . .	207
→ CHARACTERIZATION AND CHEMICAL REACTIVITY; - William Ripley. . . . .	225
→ NOVEL PYROTECHNIC COMPOSITIONS FOR SCREENING SMOKE; - George A. Lane, W. Arthur Smith and Erwin M. Jankowiak. . . . .	263
→ HEATS OF REACTION PLOTS AS DESIGN CRITERIA FOR PYROTECHNIC REACTIONS; - J. H. McLain. . . . .	293
SLURRIES ARE SAFER - R.D. Sheeline and J.J. Vrolyk . . . . .	305
→ ULTRASONIC WELD ENCAPSULATION -- HEATLESS, HERMETIC SEALING; - Charles Zglenicki . . . . .	349

Table of Contents Cont.

	Page
→ PRINCIPLES AND APPLICATIONS OF EXPLOSIVE BONDING, W. W. Cavell J. F. Kowalick, and H. J. Addison Jr. . . . .	363
→ EARLY EXPLOSION PHENOMENA, John Wisotski and Ralph E. Williams.	383
→ THE EXPLOSIVE FORMING OF METALS, Arthur A. Ezra . . . . .	393
→ COLORIMETRY AND RADIOMETRY, - James A. Swinson. . . . .	419

PYRO RESEARCH  
AREAS FOR FURTHER EXPLORATORY DEVELOPMENT

J. T. Hamrick

Aerospace Research Corporation

Roanoke, Virginia

The information presented herein is based on work performed by a team composed of personnel from Ordinance Research Inc.; The University of Minnesota; Thokol Chemical Corporation; Hollins College; John D. Stanitz, consultant; and headed by Aerospace Research Corporation under U.S. Air Force Contract F08635-67-C-0161. The work was administered under the Illumination Branch, Targets and Missiles Division, Air Force Armaments Laboratory, Eglin Air Force Base, Florida. Mr. Larry W. Moran is Project Engineer for the Armaments Laboratory.

## INTRODUCTION

There are several areas which, after study of the exploratory development work by members of the Aerospace Research Corporation team and others during the past year, submit to further analysis and evaluation. It is most apparent from this study that the interdependence of parameters is such that isolation of the variables is a very difficult task and is possibly the most severe of the problems encountered. It is likely as a result of this work and the work of others that most, if not all, of the relevant variables have been determined. It is shown by the results that although the assumption of a given set of equilibrium conditions in the flare plume allows fruitful treatment of many of the parameters, a state of overall equilibrium does not exist and a group of superimposed submechanisms probably are responsible for a significant amount, if not most, of the light production.

It is the objective in the following pages to discuss the nature of the light producing mechanisms in view of the work done in this program and that referenced. These are, in order, temperature measurements and correlation with luminous intensity, analysis of particle behavior in the plume, effects of magnesium particle size, effect of velocities of particles in the plume, effect of the surrounding gaseous medium, effect of flare diameter variation, binder formulations, and case effects. It must be emphasized that the conclusions reached in these analyses are tentative. In many of the analyses the data are inadequate either to prove or disprove the conclusions reached, but an attempt has been made to provide a sound base for planning of further experimentation and study.

Temperature Measurements and Correlation with Luminous Intensity - For most of

the plumes shown in figure 1 the point of maximum luminous intensity is approximately 3 inches from the burning face of the flare along the flare centerline. The temperature as measured by thermocouple for all flares at this three inch point varied from approximately 2200 to 2700°F. Only for AeKeCo 868 flares was this the point of maximum temperature. That the maximum luminous intensity point does not necessarily occur at the point of maximum average temperature may possibly be explained by the results obtained at the University of Minnesota for which maximum temperatures of 2700 to 2900°K (4400 to 4760°F) at wavelengths of 5800 to 6000 Å were detected by spectrometer. The existence of these temperatures within the plume which are so high above the computed equilibrium temperature indicates continued sporadic combustion of magnesium throughout the plume. Inasmuch as the thermocouple temperature measurements were made within a chamber in which there was only nitrogen or argon, whereas the isolation from air was not so complete with the Ordnance Research and University of Minnesota experiments, comparisons of luminous intensity with temperature away from the maximum luminous intensity point are less meaningful than near it. The fact that at Ordnance Research the flares were burned in a downward facing position whereas the thermocouple measurements were made with flares burning in an upward facing position probably makes little difference near the maximum luminous intensity point in view of the apparent constancy of that position with varying flare compositions.

If for the upward facing flares, particles of magnesium were ejected as they were with the downward facing flares as observed at the University of Minnesota a substantial amount of sodium nitrate must have also been ejected, at least for flares containing 60 and 68 percent magnesium. This statement is based on the fact that the maximum temperatures as measured by thermocouple

Figure 1 - Lower Half

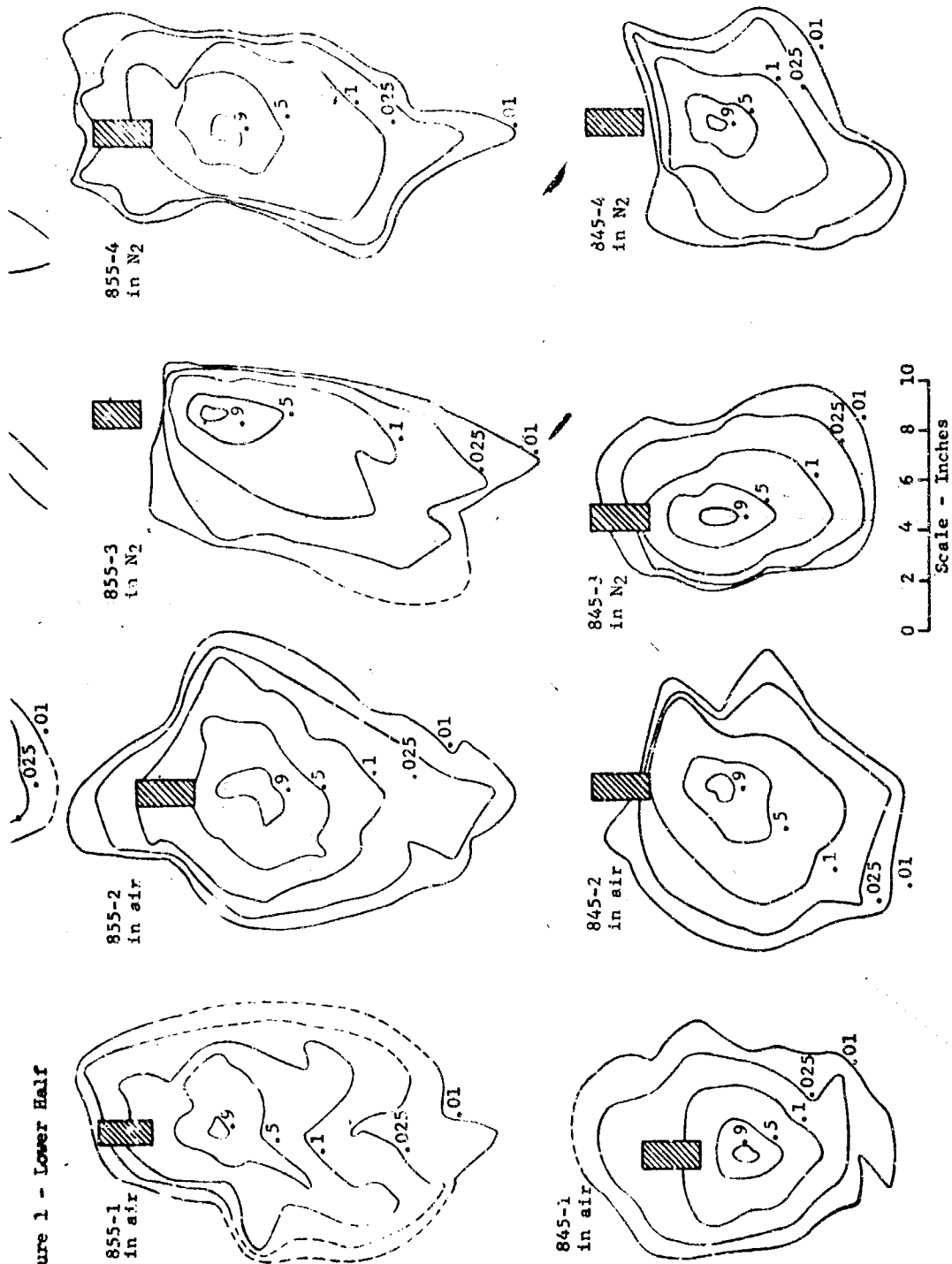


Figure 1 - Relative luminous intensity of AzReCo 800 type flares burning in air and nitrogen. Last two digits indicate percent magnesium. Nitrogen velocity was approximately 6 feet per second upward.

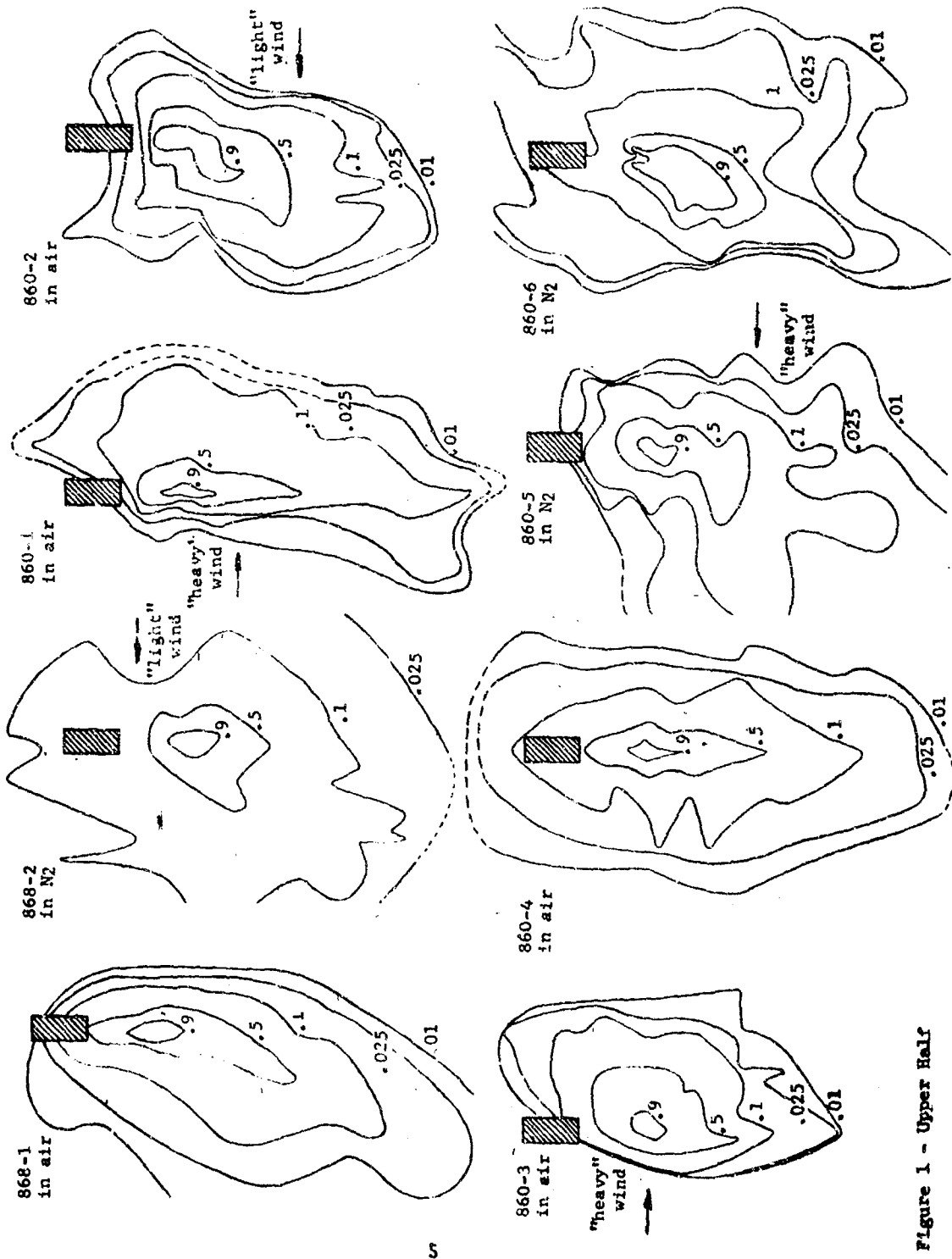


Figure 1 - Upper Half

were in such close agreement with the computed equilibrium temperature.

The sodium nitrate, with its low decomposition temperature (716°F) would rapidly decompose in the plume and immediately react with the surrounding magnesium vapor which is greatly in excess. This could account for the high temperatures observed by spectrometer and may also explain the higher illumination intensity with the large magnesium excess. Further discussion of this effect is provided in the next subsection on analysis of particle behavior.

Analysis of Particle Behavior in the Plume - As conjectured in the previous section, the ejection of particles of magnesium into the plume may be accompanied by substantial amounts of sodium nitrate. It can be logically supposed that the magnesium particle leaves the flare surface coated with molten sodium nitrate which upon evaporating and decomposing cools the magnesium particle and reacts more readily with the surrounding magnesium vapor than with the solid particle. The foregoing analysis is based upon the assumption that adequate melting of the sodium nitrate (melting point 584°F) and binder at the flare surface occurs to allow the particles of solid magnesium (melting point 1204°F) to float in the liquid sodium nitrate in the case of upward burning flares. In the case of downward burning flares, magnesium probably would tend to fall but may be held to some extent by surface tension. Thus, the size and quantity of the magnesium particles as well as the orientation of the flares would have a significant effect upon flare performance. It is highly probable that some of the larger magnesium particles are forcefully unseated by the melting and decomposition of confined sodium nitrate and binder in which the particles are embedded.

If the foregoing analysis is correct the probability of the computed equilibrium temperature equalling that measured by thermocouple in the plume of a downward burning flare is lower than for an upward burning flare. This is an

area which requires further investigation as it may hold the key to particle size selection as well as a clear understanding of the combustion mechanisms.

Effects of Magnesium Particle Size - In view of the foregoing analysis there

is good indication that the burning mechanisms are such that not only the average size but the combinations of magnesium particle sizes may be very important. Currently, production flares utilize granulations specified by MIL P-14067 and primarily Type I magnesium, 30/50 nominal mesh size. The particle size is nominally  $350 \pm 50$  microns. If the light producing mechanism is enhanced by particles of magnesium being dispersed through the plume then the magnesium particles serve at least three functions: (1) initial combustion with oxidizer to form the basic plume, (2) formation of magnesium vapor which reacts with the oxidizer as it is dispersed throughout the plume, and (3) as carriers of the molten sodium nitrate during ejection through the plume. These three separate functions might be carried out most efficiently by providing three (or more) particle sizes, one which would control burning rate, another formation of magnesium vapor, and another particle dispersal. Thus, the 30/50 magnesium which contains a maximum of 5 percent of particles of a size less than 149 microns may be inefficient for some functions which it performs. For example, if large particles are required for provision of highest illumination efficiency as indicated by Picatinny results and small particles are required for highest burn rate, then a mix of 350 micron and 22 micron particles might provide the desired burn rate and a higher luminous efficiency. Indeed, a larger average particle size than 350 microns in combination with the 22 micron particles could prove even more effective. If the oxidizer melts on the burning surface of the flare, it can be assumed that oxidizer particle size would not significantly affect flare performance. This assumption is given some support by the results of tests reported by Ordnance Research Inc. on cast flares.

Their results show that increasing sodium perchlorate particle size from 100/200 mesh to 325 mesh did not change flare burn rate or performance. The results are not conclusive, however, because of the partial solubility of the sodium perchlorate in the binder. The degree of obscuration of oxidizer particle size was not reported.

A second factor to consider with regard to the results reported by Ordnance Research Inc. is that best luminous efficiencies were obtained with a one to one ratio of magnesium and oxidizer. This may have resulted from the magnesium particle size chosen which was limited to a maximum of 200 microns. In the (1) Picatinny results pressed flare particle size did not appear to be a factor between performances of .62 and 1.35 inch diameter flares for particle sizes at or below 200 microns. Further, it was shown by Ordnance Research Inc. that with a 350 micron average particle size the maximum luminous efficiency was 57,400 candle-seconds per gram for a one inch pressed flare with 68 percent magnesium. This luminous efficiency was determined with the same EG&G 580 radiometer system that was used to measure the luminous efficiencies of the (3) 3.2 and 4.0 inch diameter cast flares made by Ordnance Research Inc. and mentioned previously and for which the maximum luminous efficiencies were 51000 candleseconds per gram. On the basis of a 68 percent magnesium pressed flare and comparisons of thermochemical computations at 4000°F the maximum luminous efficiency for the cast flare could occur with a 48 percent magnesium, 37 percent oxidizer, and 15 percent binder ratio if MIL P-14067, 30/50 magnesium particle size were used. This, of course, is based on the assumption that the particle ejection mechanism theory is correct. It should be noted that the burn rates of the cast flares are in the 4 to 5 inch per minute range which is approximately the same as for the 68 percent magnesium 30/50 particle size flares. The amount of magnesium gas in the plume is only slightly less for the cast flare than for the pressed flare,

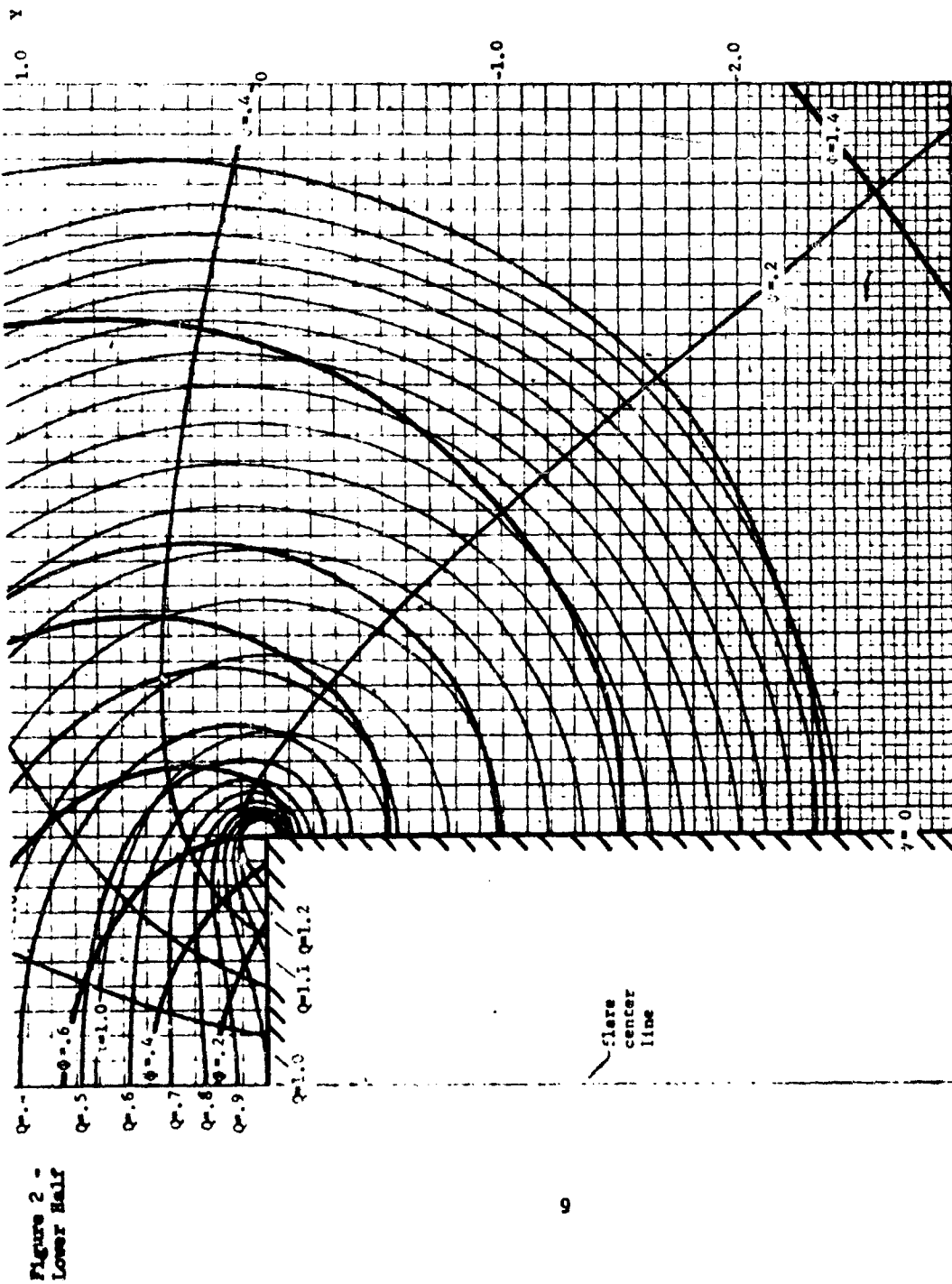


Figure 2 - Streamlines ( $\psi = \text{constant}$ ) and velocity potential lines ( $\phi = \text{constant}$ ) in X-Y plane for two dimensional flare with dimensionless drop rate given by  $K = 0$ . Also shown are lines of constant gas velocity  $Q$  (local velocity divided by constant velocity  $v_B$  normal to burning flare surface) and line of constant time ratio,  $\tau$ .

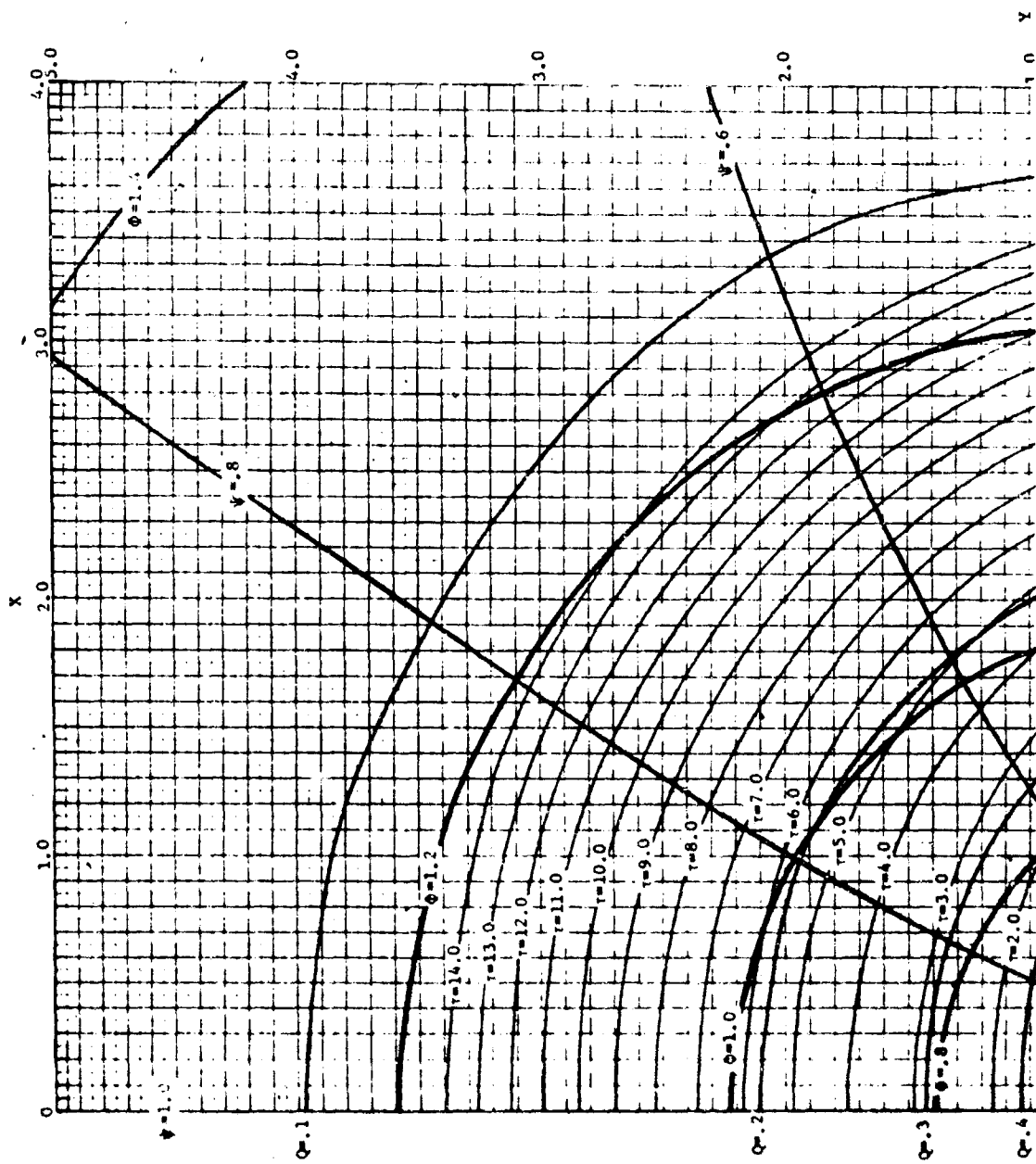


Figure 2 -  
Upper Half

Figure 3 -  
Lower Half

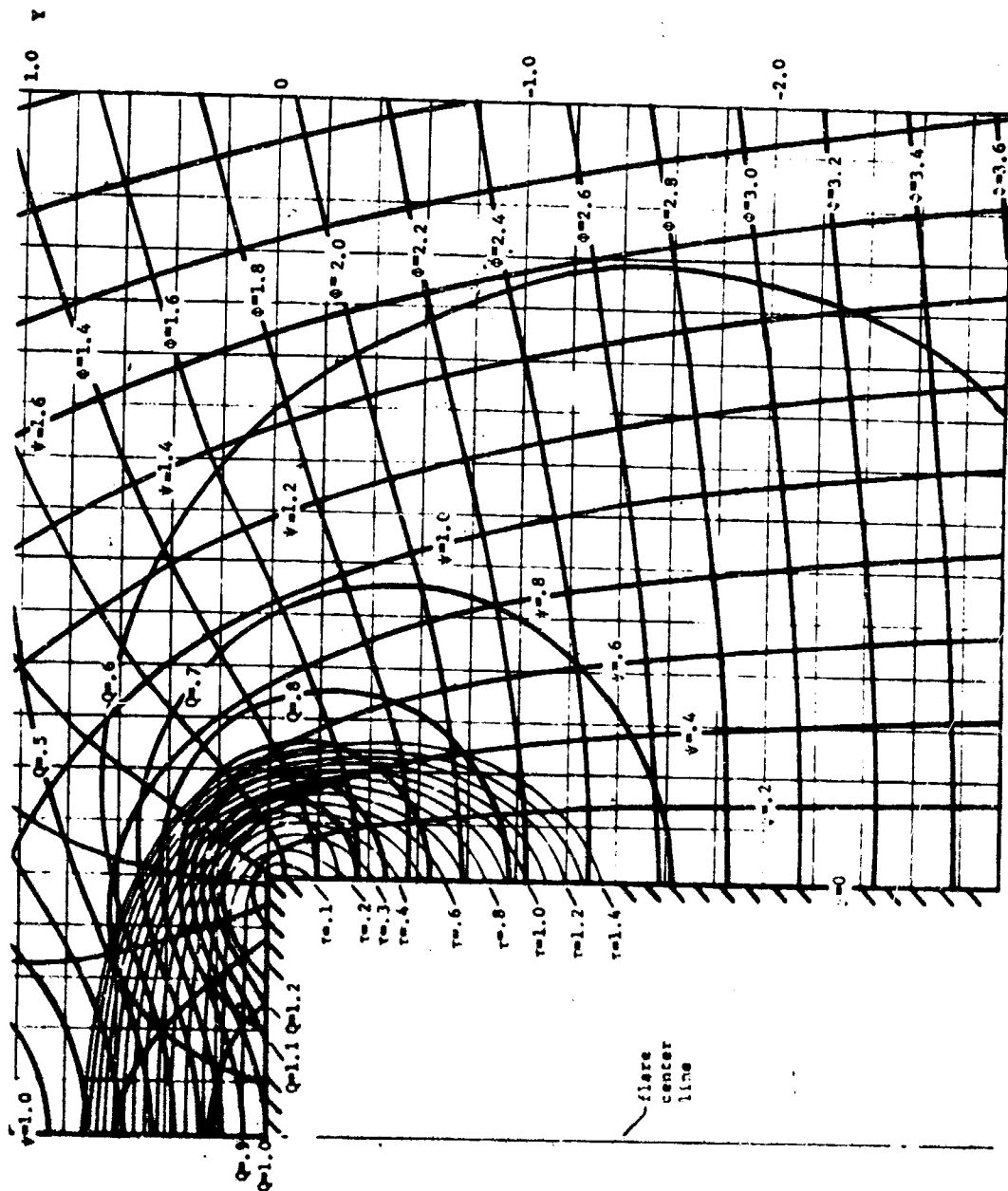


Figure 3 - Streamlines ( $\psi = \text{constant}$ ) and velocity potential lines ( $\phi = \text{constant}$ ) in  $x$ - $y$  plane for two dimensional flame with dimensionless drop rate given by  $K = 0.5$ . Also shown are lines of constant gas velocity  $Q$  (local velocity divided by constant velocity  $V_g$  normal to burning flame surface) and lines of constant time ratio,  $r$ .

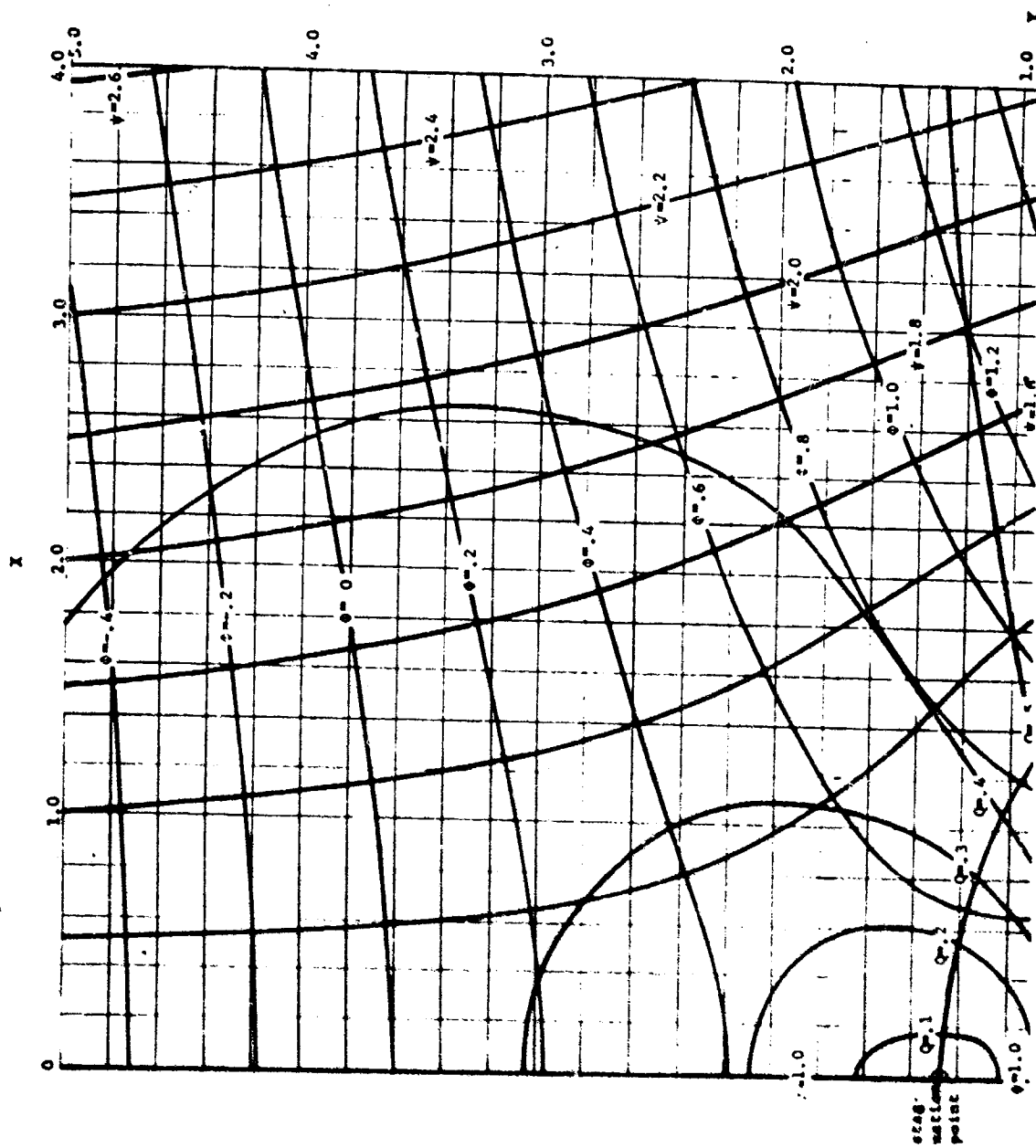


Figure 3 -  
Upper Half

but it has not been determined if the velocities in the two plumes were similar.

Perhaps clues to the effects of particle sizes can be obtained by considering the velocities of particles within the plume.

Effect of Velocities of Particles Within the Plume - It is indicated by the results of computations using the mathematical model, figures 2 and 3, that the residence time (which is a measure of velocity) of a particle at least within a radius of one half of the flare diameter in the plume is not greatly affected by fall rate. Experimentally this appears to be true not only with differing counter flows but also for flares with the same magnesium particle size and varying percents of magnesium, an observation which is based on the constancy of the maximum luminous intensity position evident in figure 1. There is some indication that longer residence time, which is assumed to be in some degree synonymous with low burn rate, provides higher luminous efficiency. This is generally supported by the Picatinny results, but is not supported by the <sup>(1)</sup> Ordnance Research results in which the burn rate decreases with decreasing magnesium content below 60 percent along with a decrease in luminous efficiency. There is indication in the Picatinny results that higher velocities generated by thick walled casings may have contributed to conditions in .62 inch casing diameters which resulted in the same low luminous efficiency with 30/50 magnesium as was obtained with 50/100 magnesium. As the casing diameter was increased to 1.33 inches, the 30/50 system was superior to the 50/100 system. It is assumed that the slower burn through of the thicker casing resulted in a rim which caused a jet effect in the .62 inch casing and thus higher velocities occurred in the plume. The jet effect is not the only factor involved as will be discussed in a subsequent section but it is clear that particle size effects and study of these effects will require carefully controlled conditions including type and thickness of inhibitor as well as exact sizing of particles. Factors

related to the problems that may be encountered in simulated fall rates as well as the surrounding medium are discussed in the following section.

Effect of Surrounding Gaseous Medium - It has been indicated that the edge effect on the burning plume surface should be subjected to further theoretical study. This should be extended to include evaluation of a rim simulating the casing which produces the jet. It has been indicated by Blackshear that producing the jet effect enhances plume mixing with air, causing lower flare efficiency.

If this thesis is correct then the lower luminous intensities obtained with nitrogen as reported by Ordnance Research are readily explained. The flares burned in air experienced no counter velocities (other than those due to convection) as the air was not being ejected upward as was the nitrogen. One consequence of increased mixing of the plume with surrounding air is provided by comparing the first four AeReCo 860 flares in figure 1. Three of the flares 860-1, 860-2, and 860-3 were subjected to cross winds and the resulting plumes were smaller than the plume for the flare 860-4 for which there was no cross wind. For the 868 and 860 flares burned in nitrogen it appears that mixing of air with the nitrogen in the edge of the plume resulted in scattered burning of magnesium (and perhaps sodium) in the lower velocity oxygen-lean mixture, with consequent broader plumes than those for still air. The plumes for the AeReCo 855 and 845 flares were smaller and apparently adequately enveloped by the nitrogen to prevent this broadening. Tests of flares in a still nitrogen atmosphere as well as in counterflow air and nitrogen atmospheres will have to be performed to check the validity of the foregoing tentative explanation. In the future the upward flowing columns of air and nitrogen should be large enough to preclude effects on the plume due to mixing or slowing down of gases in the column due to the surrounding air. The results of such tests are a

necessary input for optimizing flare fall rate. For example, the average luminous efficiency for all flares subjected to upward flowing nitrogen was 95 percent of those in still air. If a similar reduction should be experienced with upward flowing air, a close examination of fall rates is in order. Such an examination should include the effect of varying the flare diameter. A discussion of diameter effects is included in the following section.

Effects of Flare Diameter Variation - It has been pointed out by Stanitz that for a given value of time ratio at a given point in the flow field (see figure 2 and 3), the larger the flare radius and the lower the burning rate the longer the time that the fluid particle has existed in the plume. He concluded that if a longer time in the plume results in lower particle temperature, it can be concluded that the luminosity per unit area of burning surface is higher for smaller diameter flares. Blackshear has shown that radiation properties of a 30 percent MgO, 10 percent sodium mixture are such that the efficacy of the mixture drops rapidly as the body of gas thickens. He has also shown that the cooling rate of the mixture is more than 10 times as great at 3500°K (5840°F) as it is at 2000°K (3140°F.) Both of these factors support the thesis that a longer particle residence time in the plume reduces its luminous output, for although the plume constituents may block luminous radiation they do not necessarily block infrared radiation which plays a large part in particle cooling. Thus, by the time a particle has moved through the optically thick portion of the plume it may have cooled to a temperature at which it is a much less effective illuminant than it would have been in an optically thin plume. This analysis is based on the assumption that the hot particle is generated near the flare surface, and that the smallest diameter flare would provide the highest luminous efficiency. It has been demonstrated that this is not the case, which gives further support to the assumption that oxidizer

is ejected into the plume where it burns with magnesium vapor. It should be emphasized that this in no way impairs the usefulness of the conclusions regarding particle residence time or the results obtained by Blackshear. However, it does suggest that arrival at the optimum flare diameter will require inclusion of the path length of the ejected particles as a contributing function and that the originating point of the hot particle must be clearly defined.

Some information relevant to this problem may be drawn from the results obtained by Picatinny. For thin cased flares using 22 micron magnesium, the 1.33 inch diameter flares were slightly less efficient than the 0.62 inch diameter flares. The same is true for the flares in which 200 micron magnesium was used. However, for the flares using 350 micron magnesium there was a thirty percent increase in luminous efficiency in going to the larger diameter. The size of this change is such as to preclude the jet effect and mixing as the dominant factors and to suggest that an additional light-producing mechanism was introduced with the increased diameter. A plausible explanation is that the ejected particles of oxidizer left the plume of the 0.62 inch diameter flare before decomposing sufficiently to burn completely with the magnesium vapor whereas in the 1.33 inch diameter flare there was adequate time to complete the process. Further tests to determine the flare and plume diameter at which the maximum rate of drop in luminous efficiency occurs might supply some clue as to the nature of the change in mechanisms. Luminous efficiencies for varying diameters and magnesium percentages have been obtained at Crane NAD, Ordnance Research, and Picatinny. An attempt was made to integrate all of their results in order to provide greater comprehensiveness, but this was not possible due to differences in formulations, processing methods, particle sizes, inhibitors, and light measuring techniques. This is emphasized by results in which the luminous efficiency equal to 57,400 candle-seconds per gram for the 68 percent magnesium

flare burned in air at Ordnance Research exceeds the maximum of 46,000 candle-seconds per gram for a 4.25 inch diameter flare tested at NAD Crane. As the formulations and magnesium particle sizes are identical the major difference appears to be in the luminosity measuring system. This does not impair the usefulness of the data derived from a given system but emphasizes the precariousness of comparing data obtained in different experiments of this kind. (4)

With this in view an analysis of the results using a single system from NAD Crane by Douda et al was attempted. Douda shows that the efficiency of 30/50 magnesium, sodium nitrate, Laminac flares increases with diameter up to approximately 4.25 inches. Above this diameter the luminous efficiency drops off rapidly. For cast flare compositions he shows that the efficiency continues dropping to between 5000 and 10,000 candle-seconds per gram depending upon the binder system and remains constant for diameters above approximately 15 inches. It is indicated by these results that the mechanism involving particle ejection is more effective with increase in flare diameter to approximately four inches for the 30/50 magnesium, sodium nitrate, Laminac system. In plumes of flares of the same composition above that diameter the increasing optical thickness of the plume with diameter causes an observed fall off in luminous efficiency, until finally most of the illumination is provided by gray body radiation from the luminous cloud of magnesium oxide particles. It is estimated by Blackshear that extinction lengths in MgO clouds are approximately  $10^{-6}$  cm at the D-lines and 60 cm away from the D-lines. With flares from which a great deal of illumination is derived from D-line radiation, this would require that oxidation of the magnesium vapor and heating of the sodium vapor take place on the fringes of the plume. It is indicated from Picatinny data that the optimum path length of the sodium nitrate particles probably far exceeds two inches for the flares tested there. The sizes of the plumes were not given for those tests, but

based on the results of figure 1, a four-inch diameter pressed flare would exhibit a plume on the order of 40 inches in diameter, and 60 inches high, which places the optimum path length of the oxidizer particles at approximately twenty inches, a distance which would require approximately one second to traverse. Without experimental evidence to the contrary it is assumed at this point that unused sodium nitrate escaped from the plume for flare diameters below 4.25 inches and that the optical thickness of the plume caused blockage of a great deal of the radiation for the 7.35 inch diameter flares. For cast flares exceeding 15 inches in diameter the projected plume size would be on the order of 100 inches in diameter by 175 inches high based on the plume sizes obtained at Ordnance Research Inc. The plume radius of 50 inches exceeds the 20 inch optimum by approximately 30 inches (76 cm.) This exceeds by 16 cm the optical path length of 60 cm as computed by Blackshear. If the foregoing analysis is correct, it explains why the luminous efficiency levels out above 15 inches for cast flares. It also demonstrates that plume size rather than flare diameter determines the luminous efficiency. Therefore, the optimum flare diameter will vary with flare composition and processing methods. If the ejection theory is correct, a study of the rate of rise and decline in luminous efficiency with varying diameter for various magnesium ratios and for different particle size combinations may provide the basis for a more complete understanding of the light producing mechanisms. As ejection of particles can be greatly affected by the type and percentage of binder, the merits of different binder systems might also be more easily evaluated by such a study. Both the binder and the inhibitor (or casing) present problems that have been evaluated to some extent in the past. The problems involved are discussed briefly in the next two sections.

Binder Formulations - With pressed flares the percent of binder required is approximately one fourth of that required for casting because consolidation of ingredients depends upon both binder and pressure. However, production problems anticipated with large flares using available presses has led to experimentation with casting of flares. The binders used in both pressed and cast flares are usually relatively low viscosity liquids which polymerize upon addition of chemicals that cross link the binder molecules. Binders which contain fluorocarbons may be better because they are oxidizers. However, it is not known how they will behave with regard to ejection into the plume or as illuminants. Both magnesium and sodium fluorides are stable at high temperatures and their behavior as illuminants is not well known. Binders that are oxygenated and also dissolve the oxidizers have been investigated at Ordnance Research Inc., but primary emphasis was placed upon physical integrity rather than upon the effect on burning mechanisms. The results obtained at Ordnance Research Inc. show rapidly decreasing luminous efficiency with increase in binder content. The amount of decrease appears to be much in excess of what would be expected from the decrease in fuel and oxidizer due to displacement by the binder. This could be due to effects on the ejection mechanism. It has already been stated under the discussion of particle size that the luminous efficiency might be increased by introducing a larger average magnesium particle size. Just how the increased binder content might affect ejection and other mechanisms is not known. The effects of such factors as melting point of the binder versus that of the oxidizer, heat transfer coefficient of the binder, and oxidizer dilution may be significant and should be evaluated.

Casing Effects - The rim effect and experimental results obtained with changing inhibitor thickness have already been mentioned. However, there are a few additional remarks regarding effects of the casing upon performance. If the

formation of a rim is beneficial, for example, in inverted burning, then the inhibitor material should be so designed as to form the optimum rim height. It is conceivable, however, that if the rim were burned off so as to present a rounded edge, the ejection of particles with a large radial component outward could occur which could be highly beneficial. There are methods of designing such inhibitors such as by the use of metals, binders partially loaded with oxidizer, or combinations of the two. As previously indicated a theoretical evaluation of the flow around the rim should be incorporated into the study of the edge effect.

## SUMMARY

In the programs pursued in the past year by the Aerospace Research Corporation team and others most, if not all, of the relevant variables have been identified. To provide more definitive information about these variables, the following recommendations are made:

1. The mathematical model should be modified to include more detailed information about the flow pattern at the edge or corner of the burning flare surface including the rim which is left by the flare casing or inhibitor.
2. The computations for the mathematical model should be expanded to include density variations, heat exchange in turbulent mixing of the plume gases with air cooling of the flare plume due to heat radiation, and enthalpy distribution.
3. Temperature measurements with thermocouples should be made in magnesium-sodium nitrate flares up to at least four inches in diameter. These flares should incorporate a range of magnesium particle sizes.
4. A study of particle history should be made from the time the particle begins to heat up on the flare surface until it leaves the plume. This would include movies of action on the flare surface, movies of the plume, and spectroscopic measurements for flares having both small particles alone and a mixture of small and large magnesium particle sizes. The spectroscopic measurements in this case should be primarily concerned with absorption broadening and techniques of derivation of temperature from sodium doublet broadening.
5. Luminosity distribution in plumes of one inch diameter flares in still air and nitrogen as well as in counter flow air and nitrogen should be obtained for flares containing both small and a mixture of small and large magnesium particle sizes. Luminous distribution should also be

obtained in plumes of flares up to at least four inches in diameter in still air.

6. Spectral distribution in the plume should be determined by means of a scanning spectrometer. This would provide identification of the chemical species and possibly their temperature in direct association with their luminous intensity.

#### LIST OF REFERENCES

1. The Effects of Processing on Pyrotechnic Compositions Part III: Dimensional Effects of Paper Cases on Illuminance and Burning Rate of Flare Compositions, by D. E. Middlebrooks, S. M. Kaye, and G. Weingarten, T. R. 3275, Jan 1966, Picatinny Arsenal, Dover, New Jersey.
2. Study of Visual Cast Flare Binder Material, RDTR No. 113, January 1968, Hal R. Waite, Yoshiyuki Arikawa, Ordnance Research Incorporated.
3. Binder Study - Visual Cast Flares, RDTR 92, AD655821, March 1967, by H. R. Waite and Y. Arikawa, Ordnance Research Incorporated, Fort Walton Beach, Florida.
4. 25 Million Candle Cast Flare, Diameter and Binder Study, RDTR No. 105, January 1968, Volumes I and II, by Bernard E. Douda, U.S. Naval Ammunition Depot, Crane, Indiana.



COLORED SMOKE SIGNALS:  
CASTABLE COMPOSITIONS

George A. Lane  
Erwin M. Jankowiak

The Dow Chemical Company  
Midland, Michigan

## COLORED SMOKE SIGNALS: CASTABLE COMPOSITIONS

George A. Lane and Erwin M. Jankowiak

The Dow Chemical Company  
Midland, Michigan\*

### ABSTRACT

A promising castable, polymer-fueled red smoke composition has been developed. This mix is a suitable replacement for the pressed composition used in munitions such as the M-18 grenade, or the XM-168 smoke signal.

The program involved developing and optimizing pyrotechnic formulations based on epoxy and polysulfide resins. It was shown that a significant improvement can be achieved by using a large particle size red dye.

These formulations exhibit high burning rates and are not suitable for the internal-burning M-18 grenade. They were tested in an end-burning configuration, however, and appeared promising. It was also shown that the burning rate of these formulations can be adjusted over a wide range by using different particle sizes of oxidizer.

Application of the improved castable red smoke formulations to the small XM-168 munition was studied with favorable results. A 3-4 fold variation in burning rate was produced by changes in composition of the binder and mix.

Physical properties of the polymer-based items are superior to those of the pressed items. Likewise, safety tests on the polymer-fueled formulations indicated a marked improvement in impact sensitivity, and a very high safety level for the uncured mix.

### I. INTRODUCTION

This paper presents the results of a program to develop castable or extrudable pyrotechnic formulations for the thermal dissemination of colored smoke. The advantages of these formulations over the conventional pressed grains are increased safety, ease of processing, improved economics, and wider applicability.

\*This work was supported by U. S. Army Munitions Command, Dover, N. J.

In order to be useful, the formulations developed should have the properties of curing at room or slightly elevated temperature to a tough, strong grain which will maintain its shape and performance under surveillance at 70°C. The goal also has been to produce an easily ignited, reproducible, smooth burning formulation, which will yield a colored smoke of a quality comparable to that of current pressed-grain standard formulations.

## II. FEASIBILITY STUDIES

A screening program showed epoxy resins to be most versatile and promising as fuel binders. Dow CX-2679, an aromatic, sulfide-containing epoxy, proved a highly desirable binder when copolymerized with the polysulfide resin LP-3 (Thiokol Chemical Co.). Glycerine diglycidyl ether (GDGE) also showed utility as a copolymer. Butyl glycidyl ether (BGE), added as a reactive diluent, increased the castability, but interfered with curing if present above a certain quantity. The tertiary amine catalyst, benzyldimethylamine (BDMA), was selected for this system.

Several promising formulations based on MAAQ-D (dextrinized methylaminoanthraquinone red dye), KClO<sub>3</sub>, CX-2679, LP-3, GDGE, BGE, and BDMA were subjected to more intensive study, and evaluation in full-scale M-18 munitions. Results were encouraging for Formulation #285, shown in Table I.

Table I

### Composition and Properties of Formulation No. 285

<u>Parameter</u>	<u>Formulation No. 285</u>
<u>Composition, wt. %</u>	
MAAQ <sup>a</sup>	40.0
KClO <sub>3</sub>	30.0
CX-2679.1	12.9
LP-3	3.5
GDGE	3.5
BDMA	10.1
Castability, cps.	1.2 x 10 <sup>6</sup>
<u>Process Life, cps.</u> (90 min. R.T.)	4.5 x 10 <sup>6</sup>
<u>Combustion Rate,</u> in./sec.	0.0145
<u>Efficiency, %</u>	75-80
<u>Yield, %</u>	25-27

<sup>a</sup>85% Methylaminoanthraquinone,  
15% dextrin.

This formulation is non-flaming and efficient, producing a burning time and quality of smoke equivalent to that of the standard M-18. Its shortcomings are limited processing life, and high initial viscosity. Because the primary limitations of No. 285 center about processability, formulation development efforts were directed toward lowering viscosity and extending pot life.

### III. FORMULATION DEVELOPMENT AND PROCESS STUDIES

#### A. GRANULAR MAAQ

Substitution of a large particle size MAAQ for the fine particle size dextrinized MAAQ markedly improves castability and processability. The effectiveness of the reduced surface area of granular MAAQ is illustrated in Table II.

Table II

#### Effects of MAAQ Particle Size on Processability and Combustion

<u>Effect</u> <u>Visc., cps.</u>	<u>Formulation No. 285</u>		<u>Formulation No. 023</u>	
	<u>Fine</u>	<u>Coarse</u>	<u>Fine</u>	<u>Coarse</u>
Initial	$1.2 \times 10^8$	23,800	V. High	10 - 20,000
15 min.		52,000	Rapid	
30 min.		73,250	exo-	
45 min.		93,750	therm	
60 min.		243,550	and	
75 min.		486,750	curing	
90 min.	$3.2 \times 10^8$	$>1 \times 10^8$		$>1 \times 10^8$
<u>Combustion</u>				
ln./sec.	0.0145	0.016	0.036	0.080
Flaming	No	No	Yes	No
Effic., %	75-80	80.	>80.	>80.
Yield, %	25-27	30-32	30	38.

The dependence of initial viscosity on minimal solids surface area is apparent. There is also a gain in processing life, probably due to the lower initial viscosity and perhaps improved heat transfer in the resin. An additional desirable effect is that of increased yields, resulting from the use of pure MAAQ.

Substitution of granular MAAQ for powdered dextrinized MAAQ results in combustion rate acceleration. However, because of the processing advantages gained by the use of large particle size granular MAAQ, it has been employed in all subsequent formulation studies.

#### B. BINDER STUDIES

Because critical formulation properties, such as viscosity, processing life, rate and extent of curing, physical properties, surveillance behavior, and combustion properties, are a function of binder composition, a study was undertaken to investigate and optimize the effects of each binder component in Formulation No. 285.

The results are portrayed in Figures 1 through 3. Figure 1 shows that improvements in initial mix viscosity can be obtained by minimizing CX-2679.1 and increasing GDGE content. Pot life was also found to be improved by lowering the CX-2679.1 content of the binder. In Figure 1, a viscosity of over 1,000,000 cps. was obtained for the composition represented by point A after 90 minutes of mixing. This viscosity level was reached after 45 minutes for composition B and 75 minutes for C. On the other hand, composition D reached only 17,000 cps. in 90 minutes.

The combustion rate and dye yield are shown in Figures 2 and 3. An increase in burning rate accompanies the reduction in CX-2679.1 content. A rate of 0.089 in./sec. is reached with elimination of CX-2679.1. Standard M-18 combustion rates range from 0.012 to 0.018 in./sec. Dye yield, the weight of dye disseminated per 100 g. of formulation, remains relatively unaffected by the binder variations experienced in these studies. Because of the adverse effect of CX-2679.1 on pot life and mix viscosity, this material was eliminated as a binder component.

Continuing studies of the binder system, using neat binders, revealed the data represented in Figure 4, which shows the viscosity after 40 minutes at 25°C. At high BDMA levels, the excess curing agent tends to separate, resulting in a heterogeneous mix. Rapid gelation occurs at high LP-3 levels. Only the area of high GDGE content proved worthy of further investigation. Extended exposures were conducted at 70°C. of the compositions represented by points A, B, and C in Figure 4. For composition A, viscosity increase failed to materialize, indicating insufficient catalyst. At points B and C useful processing possibilities were exhibited. After 6 hours at 25°C., viscosity increased only slightly to 20,000 cps.; however, an additional 1-2 hours at 70°C. resulted in a firm gel.

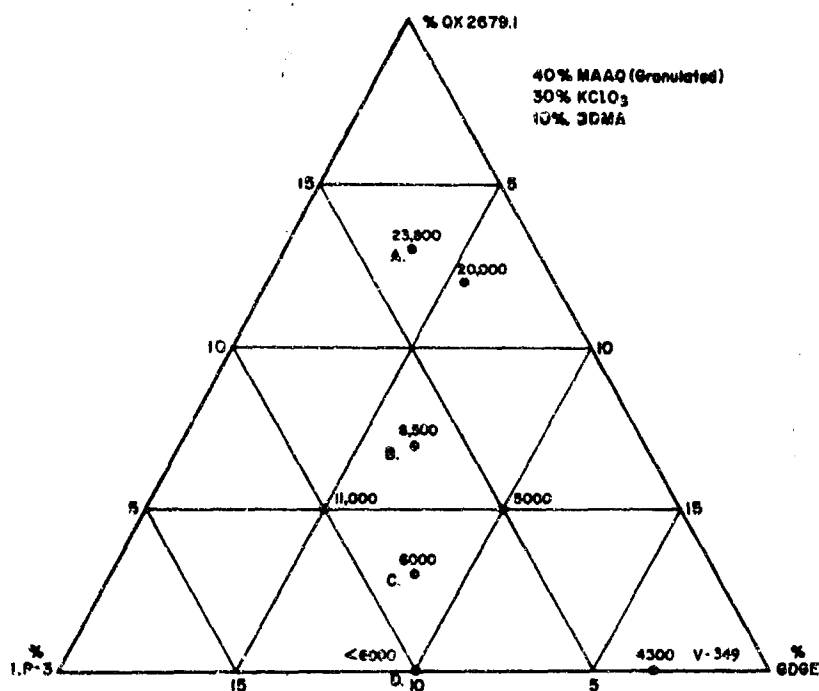


Fig. 1 - Castability vs. Binder Composition,  
Initial Mix Viscosity (cps.)

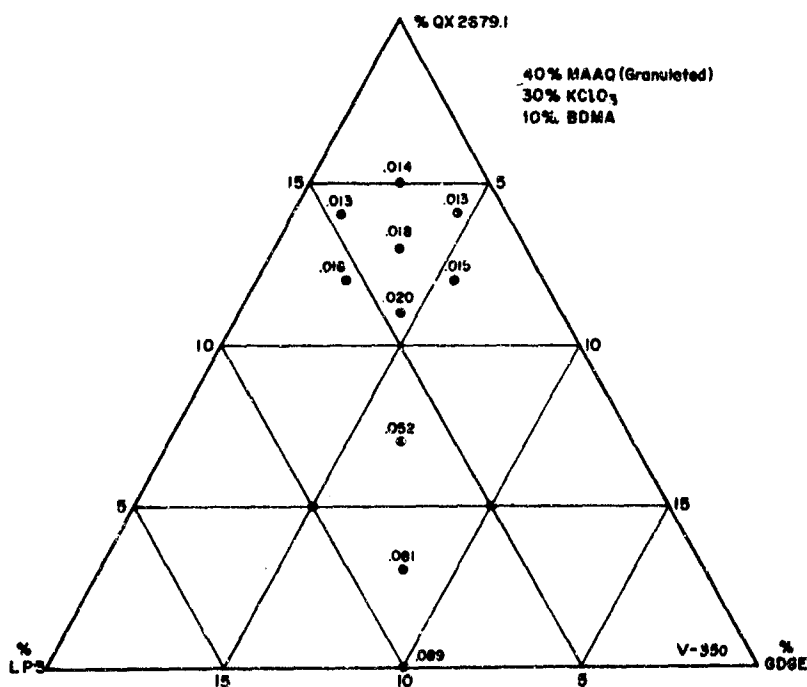


Fig. 2 - Rate of Combustion (in./sec.)  
as a Function of Binder Composition



A formulation designated No. 157, shown in Table III, was chosen, based upon binder ratios suggested by this study. This composition displayed desirable castability, adequate processing life, and a rapid cure at elevated temperature.

Table III

Composition and Properties of Formulation No. 157

<u>Parameters</u>	<u>Formulation No. 157</u>
<u>Composition, wt. %</u>	
MAAQ (Granulated)	45.5
KClO <sub>3</sub>	27.3
GDGE	15.1
LP-3	3.0
BDMA	9.1
<u>Viscosity (init.), cps.</u>	47,000
<u>Processing Life</u>	>2 hr. @ R.T.
<u>Curability</u>	<6 hr. @ 70°C.
<u>Combustion,</u>	
Time, sec./25 gm.	34
Rate, in./sec.	0.024

Since adequate processability is available from the GDGE/LP-3/BDMA binder, particularly if controlled low temperature mixing is used, most of the remaining effort was directed toward combustion control.

C. OPTIMIZATION STUDIES

To increase the versatility of the system, efforts were initiated to tailor the combustion rate of formulations based on the LP-3/GDGE/BDMA binder-fuel system, while maintaining processability. This involved optimizing complete formulations, with the primary variables being MAAQ, KClO<sub>3</sub>, and binder content.

The composition area for combustion rates equivalent to the standard internal burning M-18 grenades, 0.014 in./sec. proved quite limited, as shown in Figure 5. At high dye and low binder concentrations it is not possible to maintain processability. Low oxidizer content is conducive to low pressure, inefficient combustion. As a result of these investigations, it appears that, using the 1:1:1 LP-3/GDGE/BDMA

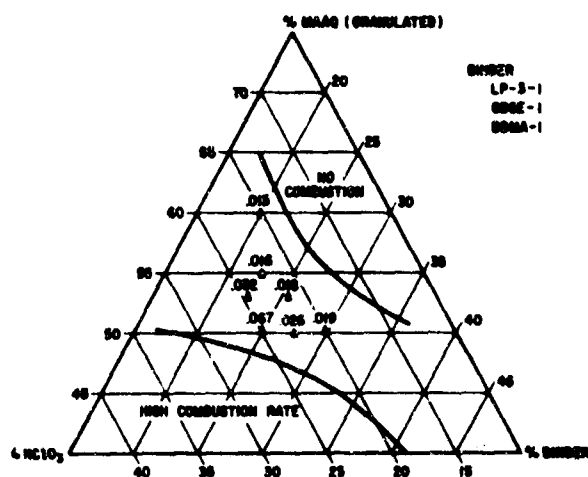


Fig. 5 - Combustion Rate (in./sec.)  
as a Function of Formulation Composition

binder system, it is not possible to attain simultaneously processability, efficiency, and a combustion rate suitable for the internal burning M-18 grenade.

### 1. End-Burning M-18 Configuration

An end-burning configuration would be advantageous for the M-18 grenade. With this in mind, formulations were selected on the basis of combustion rates, and end-burning M-18 munitions were prepared. Flaming was prevented by substituting four 1/4" exhaust smoke openings for the single 1/2" hole of the standard M-18. "Filtering," or production of pale smoke in latter phases of the combustion, was no worse than for the standard M-18 munition.

Two formulations representing different burning rates are shown in Table IV. Duplicate items were fired and compared directly with standard M-18 munitions. At this time the end-burning grain configuration for M-18 application appears promising. Additional features, such as loading and curing without a mandrel, and greater loading per unit volume, contribute to its desirability.

Table IV

#### Composition and Properties of End-Burning Items

<u>Parameter</u>	<u>Formulation</u>	
	<u>No. 023</u>	<u>No. 055</u>
<u>Composition, Wt. %</u>		
MAAQ (granulated)	45	50
KClO <sub>3</sub>	25	25
LP-3	10	6.65
GDGE	10	10
BDMA	10	8.35
<u>Viscosity, cps.</u>		
Initial	13,500	17,000
90 minutes	<500,000	<750,000
<u>Processing Life</u>	<6 hr. @ 70°C.	<6 hr. @ 70°C.
<u>Combustion, 25 g. grain</u>		
Time, sec.	10-12	17-20
Rate, in./sec.	0.073	0.045
<u>Efficiency, %</u>	80	86
<u>Yield, %</u>	>32	>40
<u>Combustion, M-18 size</u>		
Time, sec.	49	78
Rate, in./sec.	0.076	0.048
<u>Flaming</u>	No	No

## 2. XM-168 Configuration

Efforts were directed at investigating the applicability of castable, curable pyrotechnic systems to the small XM-168 red ground smoke signal. Because this is an end-burning munition that burns in an overall time of approximately 20-30 seconds, the castable formulations appear well suited for this application.

Three different values of burning time were set as goals for the XM-168 application: 11 seconds, 23 seconds, and 34 seconds.

The approach taken was to meet these rate requirements in two different ways; first, by manipulation of the composition of the formulations; and, second, by varying  $KClO_3$  particle size. The formulations, shown in Table V, were selected to meet the required combustion rates, and a series of tests was conducted on units containing the selected formulations.

Table V  
Formulations Selected for XM-168

<u>Parameter</u>	<u>Formulation</u>		
	<u>023</u>	<u>055</u>	<u>157</u>
<u>Composition, Wt. %</u>			
MAAQ (Granulated)	45	50	45.47
$KClO_3$	25	25	27.27
LP-3	10	6.65	3.04
GDGE	10	10	15.12
BDMA	10	8.35	9.10
<u>Combustion Time, sec.</u>	11.0	23.0	34.0

### a. Flaming Tendencies

Initial firings of several formulations, using XM-168 hardware, revealed a distinct tendency toward flaming. This was completely overcome by reducing the diameter of the exhaust opening from  $3/8$ " diameter to  $1/4$ " diameter.

### b. Reproducibility of Functioning

Multiple firings of Formulation Nos. 023, 055, and 157 showed reproducible color quality, and an average deviation of about 10% in burning time.

#### c. Effect of Cure Time on Functioning

The relationship of curing time to munition functioning behavior was studied. The data indicate that optimum cure can be achieved in two hours or less at 70°C., and that effects of further curing on combustion behavior are minor.

#### d. High and Low Temperature Firings

To test the effect of temperature on functioning behavior, munitions were tested at -40°C. and +50°C. The items were stored at the desired temperature long enough to insure a uniform temperature, removed from the oven or cold box, and fired immediately. The tests at +50°C. showed no appreciable difference from ambient. The tests at -40°C. showed a marked rate reduction for Nos. 023 and 055. A standard XM-168 functioned equally at ambient outdoor, +50°C., and -40°C. temperatures.

#### e. KClO<sub>3</sub> Particle Size Effects

The effect of KClO<sub>3</sub> particle size on combustion was investigated, as shown in Figure 6. Oxidizers of varied average particle size were obtained by blending a coarse screened fraction (100-150  $\mu$ ) with Mil-P-150B, Grade B, Class 7 (72.5% through 325 mesh). It can be seen that a wide range of burning rates can be obtained for a single pyrotechnic composition by selection of the oxidizer particle size.

#### f. Flame Arresting Screens

The use of copper screen for flame arresting was investigated, and proved successful. In these experiments, the exhaust port was covered with a grid of copper screen. Mesh sizes 20, 40, 50, and 80 were tested, with good results.

#### g. Caseless Munitions

A "caseless" munition configuration was produced by forming a small hole in the center of a cured pellet. The case was formed by dipping and painting the entire pellet with a flame inhibiting polymeric coating. After the coating was dry, ignitacord was fitted into the center opening. First-fire was not used. A 24-g. pellet and a 130-g. pellet were prepared and studied. Upon functioning, the smaller munition showed flaming for a fraction of a second, then functioned smoothly for 7.5-8.5 sec. Clouds were a dense, highly colored red smoke. The 130-g. unit displayed no flaming, and burned for 66 sec., yielding a dense, high quality smoke.

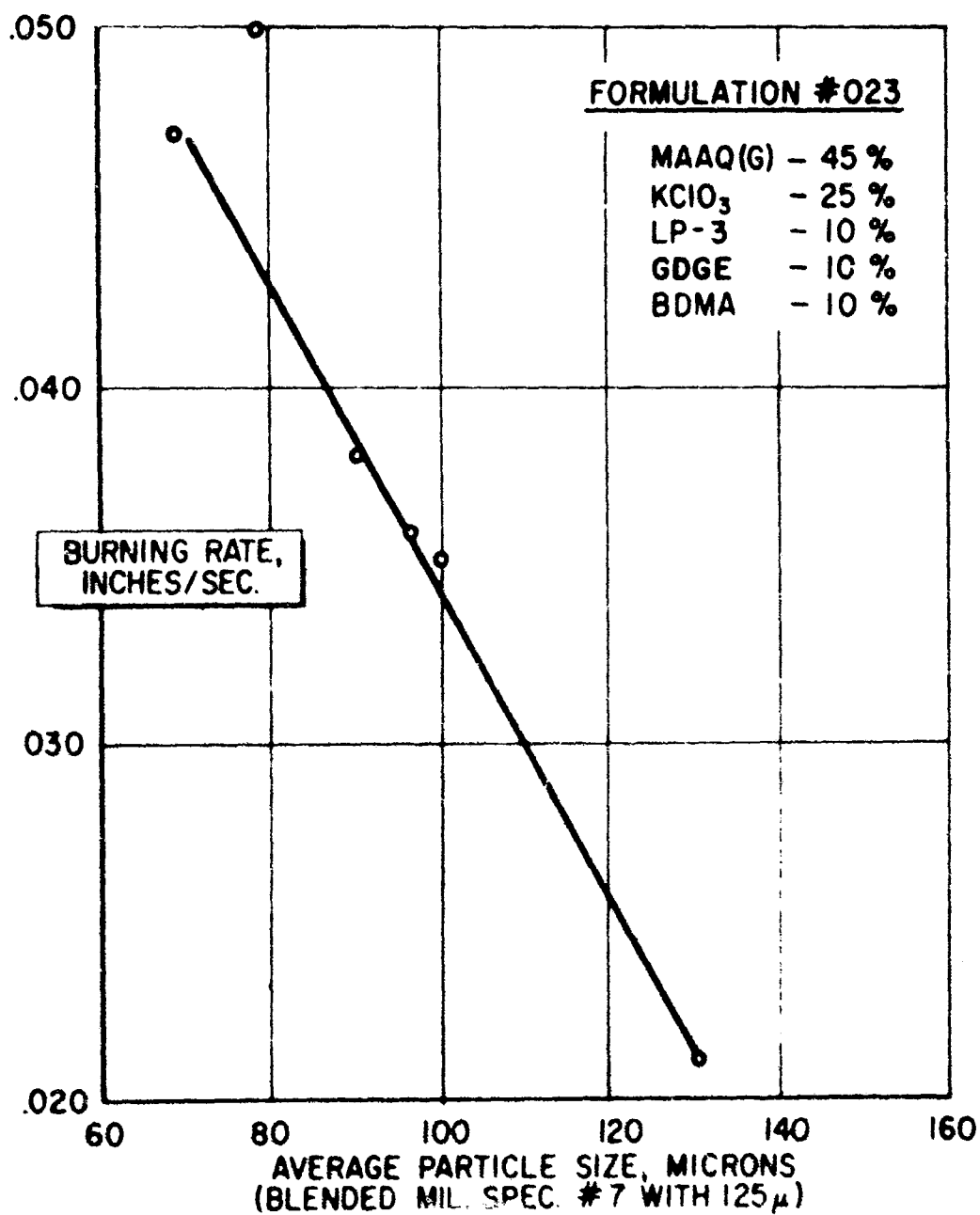


Fig. 6 - Effect of KClO<sub>3</sub> Particle Size on Combustion Rate

## D. PHYSICAL PROPERTIES, SAFETY, AND SURVEILLANCE

### 1. Physical Properties

Preliminary examination of the physical properties of the cured compositions was conducted. Grain hardness was determined by the Shore Durometer test at 25 and 80°C. Type A Shore Durometer values of 83-93 were obtained. There is every indication that the physical properties of these formulations are fully adequate, both at ambient and elevated storage temperatures.

### 2. Safety

Sensitivity tests were conducted on cured grains of Formulations 023, 055, and 157, as well as the M-18 standard pressed mix. Using the Olin Drop Weight Tester, cured specimens of grains representing Formulations 023, 055, and 157 were tested and none exploded at the maximum test level of 300 kg. cm.

All these castable systems are less sensitive than the Standard M-18 mix, which yields an E<sub>50</sub> to low level explosion of 220 kg. cm. Experience has shown that the uncured polymer-based pyrotechnic mix will be less sensitive than the cured formulations.

### 3. Surveillance

Sufficient 25-g. munitions were prepared and cured 6 hours at 74°C. for triplicate stability and surveillance studies of Formulations Nos. 023, 055, and 157. These were to be run under the following conditions: 2 days and 6 months at 20°C.; and 2, 3, and 6 months at 74°C.

After seven weeks exposure of the samples at 74°C., a malfunctioning oven temperature control caused ignition and combustion of five of the munitions, seriously affecting the triplicate check program. The maximum temperature reached in the oven is not known, but undoubtedly it was greatly in excess of 74°C. The surveillance program is currently being repeated.

IGNITION AND OUTPUT CHARACTERISTICS  
OF PYROTECHNICS FOR ELECTROEXPLOSIVE DEVICE APPLICATIONS

James L. Austing  
James E. Kennedy  
IIT Research Institute  
Chicago, Illinois 60616

IGNITION AND OUTPUT CHARACTERISTICS  
OF PYROTECHNICS FOR ELECTROEXPLOSIVE DEVICE APPLICATIONS\*

James L. Austing  
James E. Kennedy\*\*  
IIT Research Institute  
Chicago Illinois 60616

John P. Weber  
Sandia Corporation  
Albuquerque, New Mexico 87115

ABSTRACT

Experimental studies on the ignition and output of metal-metal oxidant pyrotechnic mixtures in contact with electrically pulsed bridgewires for electroexplosive device applications have been performed. The systems that were studied extensively included aluminum-tungstic oxide, aluminum-cupric oxide, aluminum-potassium perchlorate, and aluminum-ammonium perchlorate. Representative data show that electric initiators incorporating the proper metal-metal oxidant system (1) are capable of withstanding static electric discharge pulses in excess of those generated by the human body, and (2) can be designed to provide a 5-amp, 5-watt no-fire capability.

Constant current ignition tests were conducted over a range of 5 to 50 amperes, using a low-inductance firing circuit that had a rise time of 10  $\mu$ sec. The metal-metal oxidant power was pressed into initiators containing headers bridged with wire or ribbon. At a given current, the data showed a general increase in ignition time as metal-metal oxidant loading density and aluminum content of the mixture were increased. Excellent correlation of burning rate with density was obtained for the aluminum-tungstic oxide system.

The output characteristics of gas-producing pyrotechnic mixtures were studied with the goal of designing a charge that propelled a 5-gram piston according to the same distance-time profile generated by a 250-mg lead styphnate charge. The distance-time data were recorded photographically. It was found that a 280-mg aluminum-potassium perchlorate charge met the above goal in the first 1/8 in. of piston travel, which was the displacement of most interest. A graphical double differentiation of the piston distance-time profiles presented a picture of the burning characteristics of the various systems and permitted experimental verification of the force constants from a van der Waals equation of state.

---

\* Work supported by the U.S. Atomic Energy Commission.

\*\* Present Address: Sandia Corporation, Albuquerque, New Mexico, 87115.

## INTRODUCTION

Electroexplosive devices (EED's), or electric initiators as they are frequently called, are used in ordnance and aerospace systems to convert an electrical pulse into a chemical burning or detonation reaction for reliably initiating a subsequent propellant or explosive charge, or for performing useful work. The typical design of the electroexplosive device consists of a suitable electrical bridge element which is in physical contact with an explosive or pyrotechnic flash charge; the electrical pulse heats or explodes the bridge, and this in turn initiates the flash charge. Research and development activities in the area of electroexplosive devices over the last several years have been directed towards improving the safety of these devices, while maintaining their inherent high reliability. Specifications and standards have been drawn up which require that EED's dissipate without functioning input no-fire currents and powers of 1-amp and 1-watt for 5 minutes or 5-amp and 5-watts for 15 minutes. Furthermore, EED's must not be sensitive to electrostatic discharges such as those produced by the human body. By designing EED's to meet these standards, the probability of accidental initiation is significantly reduced. The work described in this paper was part of several programs to develop EED's of improved safety.

The metal-metal oxidant pyrotechnic is a mixture of a metal powder and a metal oxidant powder that upon ignition will react generally in an oxidation-reduction type reaction, with liberation

of a large amount of heat, such that the products may be in the liquid or the vapor state, depending on the system of interest. This paper discusses the experimental efforts related to the development of an electrostatic-insensitive 5-amp, 5-watt no-fire initiator and a 1-amp, 1-watt no-fire actuator each of which contain pressed metal-metal oxidants; this includes all-fire constant current ignition studies of metal-metal oxidants pressed against wire and ribbon bridges. The gas producing pyrotechnic mixtures aluminum-potassium perchlorate and aluminum-ammonium perchlorate were used as propellants to redesign a valve actuator that previously contained a 250-mg lead styphnate charge.

Metal-metal oxide mixtures, such as aluminum-tungstic oxide, have an enhanced thermal stability. These mixtures have been used to initiate detonation in insensitive explosives. This work, which was concerned with transition from burning to detonation, is described in Reference 1.

#### PHYSICAL PROPERTIES OF PYROTECHNIC MIXTURES

##### Particle Size Distribution of Aluminum and Metal Oxidant Powders

The particle size distribution of the spherical aluminum powders and of the metal oxidant powders that were studied is summarized in Table 1. The data for the finer powders were obtained on the IITRI centrifugal disc photosedimentometer (ref. 2) while that for the coarser powders with particles greater than 10 microns were obtained from a gravity sedimentation analysis.

Table 1  
PARTICLE SIZE DISTRIBUTION OF ALUMINUM AND METAL OXIDANT POWDERS

Powder	Product Identification	for 95% oversize	Particle Diameter, microns for 70% oversize	for 50% oversize	for 30% oversize	for 10% oversize
Aluminum <sup>1</sup>	H-3	0.3	1.0	1.4	2.1	3.2
	H-5	1.0	2.1	2.9	4.1	5.9
Tungstic Oxide <sup>2</sup>	TO-2	0.3	1.4	2.1	2.7	3.8
Cupric Oxide <sup>3</sup>	--	0.3	0.8	1.1	1.5	1.9
Potassium Perchlorate <sup>4</sup>	Batch 1	0.4	1.3	2.8	6.1	25.4
	Batch 2	5.8	11.1	13.0	16.3	21.8
Ammonium Perchlorate <sup>5</sup>	Fine	0.7	1.9	7.1	12.2	--

<sup>1</sup>Valley Metallurgical Company, Essex, Connecticut

<sup>2</sup>Sylvania Electric Products Corporation, Towanda, Pennsylvania

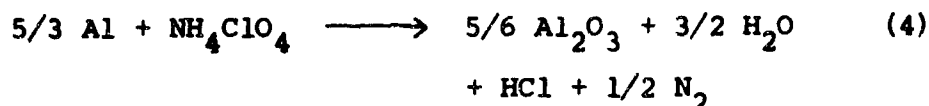
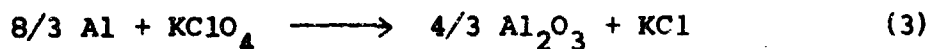
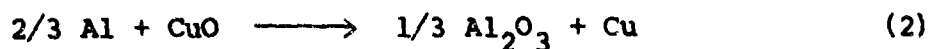
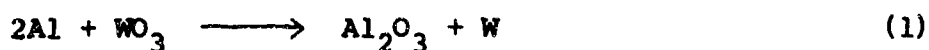
<sup>3</sup>The Glidden Company, Hammond, Indiana

<sup>4</sup>Hummel Chemical Company, Newark, New Jersey

<sup>5</sup>Thiokol Chemical Corporation

### Formulation of Pyrotechnic Mixtures

The pyrotechnic mixtures were formulated in quantities of approximately 20 g according to the stoichiometric mole ratios indicated in the following equations:



However, mixtures both deficient in aluminum and rich in aluminum were also formulated for subsequent evaluation; specifically, the former contained 2/3 of the stoichiometric quantity of aluminum, while the latter contained 30 to 33.33% excess aluminum.

No problems were encountered in formulating the mixtures, except that the perchlorate powders tended to agglomerate somewhat, so it was necessary to force the required quantity through a fine sieve; a No. 100 sieve appeared to be a convenient size to use. The aluminum and metal oxidant powders were then put in a closed jar and rotated for approximately 10 minutes on a bench-top roller mill. This rotation resulted in a mixture that visually appeared to be uniform.

### Loading of Powders

The following procedure was used in loading the initiators and actuators for the ignition and output studies to be described later. A weighed quantity of metal-metal oxidant, 250 to 500 mg,

was pressed into the cup of each initiator at a specific, pre-determined loading pressure that ranged from 2500 to 20,000 psi. The ram used in the pressings was a drill blank of such a diameter as to have a slip fit inside the initiator. The height of the column of pressed powder was calculated by subtracting the depth of the initiator after loading from the depth prior to loading, both measurements having been made with a depth micrometer.

The density variation at each loading pressure follows a normal probability distribution. This is illustrated in Figure 1, in which the individual densities for 2/3 stoichiometric H-3 aluminum + TO-2 tungstic oxide at 4800 psi are plotted versus probability coordinates. Similar results were obtained at other loading pressures and for other systems in which a sufficient number of points permitted calculation of standard deviation. The data are summarized in Table 2. There appears to be a general decrease in standard deviation as the loading pressure increases.

#### INITIATORS AND ACTUATORS

Two types of EED's were evaluated extensively -- initiators having 5-amp, 5-watt no-fire capability and actuators possessing a 1-amp, 1-watt no-fire capability.

The initiator is depicted in Figure 2. It consisted of a steel sleeve case assembled to a Kovar-glass header in such a manner as to form a cup approximately 0.540 in. deep. The components were held together by epoxy resin. The Kovar-glass

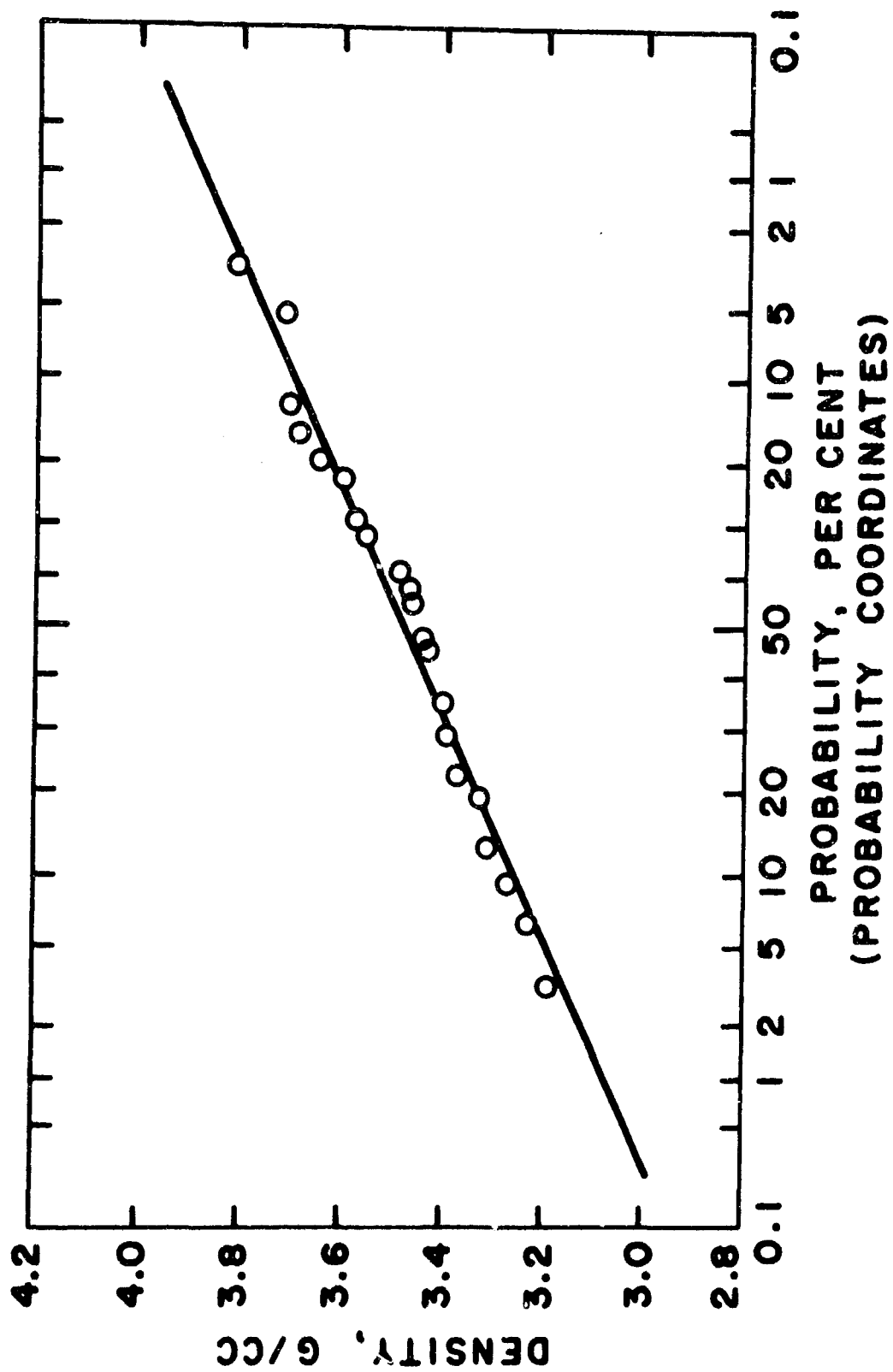


Figure 1

DENSITY DISTRIBUTION FOR H-3 Al + TO-2 WO<sub>3</sub>,  
2/3 STOICHIOMETRIC, AT 4800 PSI.

Table 2  
DENSITY VARIATION OF PRESSED METAL-METAL OXIDANT POWDERS

System	Amount of Al	Loading Pressure, psi	Density, g/cc	
			Average	Standard Deviation
H-3 Al + TO-2 WO <sub>3</sub>	2/3 stoich.	4,800	3.42	0.19
H-3 Al + TO-2 WO <sub>3</sub>	2/3 stoich.	20,000	3.81	0.04
H-5 Al + TO-2 WO <sub>3</sub>	2/3 stoich.	4,800	3.59	0.08
H-3 Al + Glidden CuO	2/3 stoich.	4,800	3.16	0.20
H-3 Al + Glidden CuO	2/3 stoich.	20,000	3.14	0.06
H-5 Al + Glidden CuO	2/3 stoich.	4,800	2.98	0.07
H-3 Al + NH <sub>4</sub> ClO <sub>4</sub>	33.33% excess	4,840	1.78	0.03
H-3 Al + KClO <sub>4</sub> (Batch 1)	2/3 stoich.	3,100	2.00	0.07
H-3 Al + KClO <sub>4</sub> (Batch 2)	2/3 stoich.	10,000	2.12	0.02

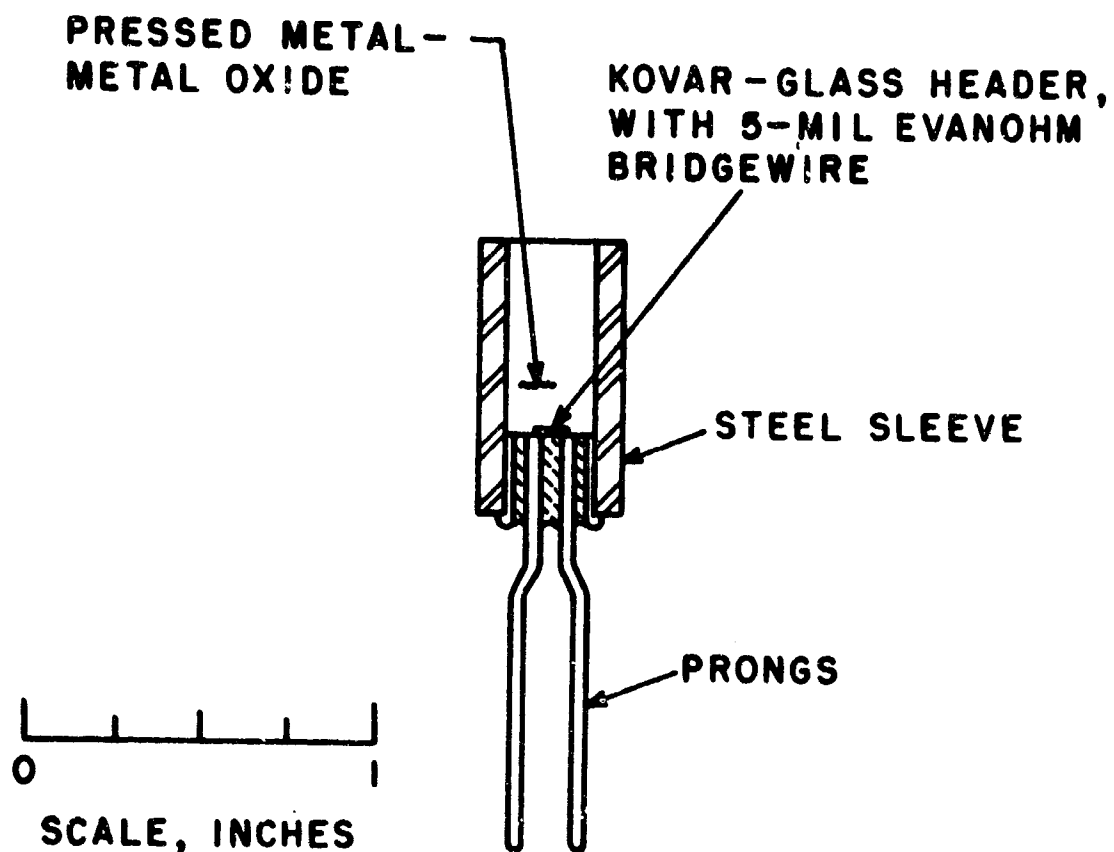


Figure 2

**METAL-METAL OXIDE INITIATOR**  
(Nominal bridge resistance = 0.20 ohm.  
Initiator has 5-amp, 5-watt no-fire capability.)

header was bridged with a 5-mil-diameter Evanohm\* wire each end of which was welded to the pins (prongs). The nominal resistance of this initiator was 0.20 ohm.

The actuator that was used most extensively is shown in Figure 3. Basically, it was an electric initiator consisting of an Inconel-glass-stainless steel header to the prongs of which the bridge was welded. Two types of bridge elements were evaluated, namely a 2-mil-diameter Tophet-C\* wire bridge and a 0.13-mil-thick by 25-mil-wide Resistvar II\*\* ribbon bridge. In line with the 1-amp, 1-watt no-fire requirements, the nominal resistance of these bridges was 1 ohm. The ribbon bridges were included in the investigation because they dissipate heat into the surroundings faster than wire bridges of the same material and resistance, and hence the actuator would more easily meet the no-fire requirements.

The stainless steel charge holder was designed to have an internal volume of 0.133 cc. Hence, at a pressure of 10,000 psi it was possible to load 280 mg of  $\text{Al-KClO}_4$  or 250 mg of  $\text{Al-NH}_4\text{ClO}_4$ , and the top of the pressing was flush with the top of the actuator. The pressed density of  $\text{Al-KClO}_4$  at these conditions was 2.10 g/cc, while that of  $\text{Al-NH}_4\text{ClO}_4$  was 1.88 g/cc. To load quantities greater than the above amounts, it was necessary to omit the charge holder from the actuator assembly. This procedure increased the available volume to 0.254 cc.

---

\* Wilber B. Driver Company, Newark, New Jersey

\*\* Hamilton Watch Company, Lancaster, Pennsylvania

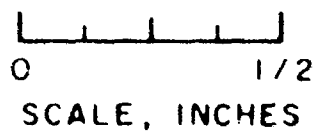
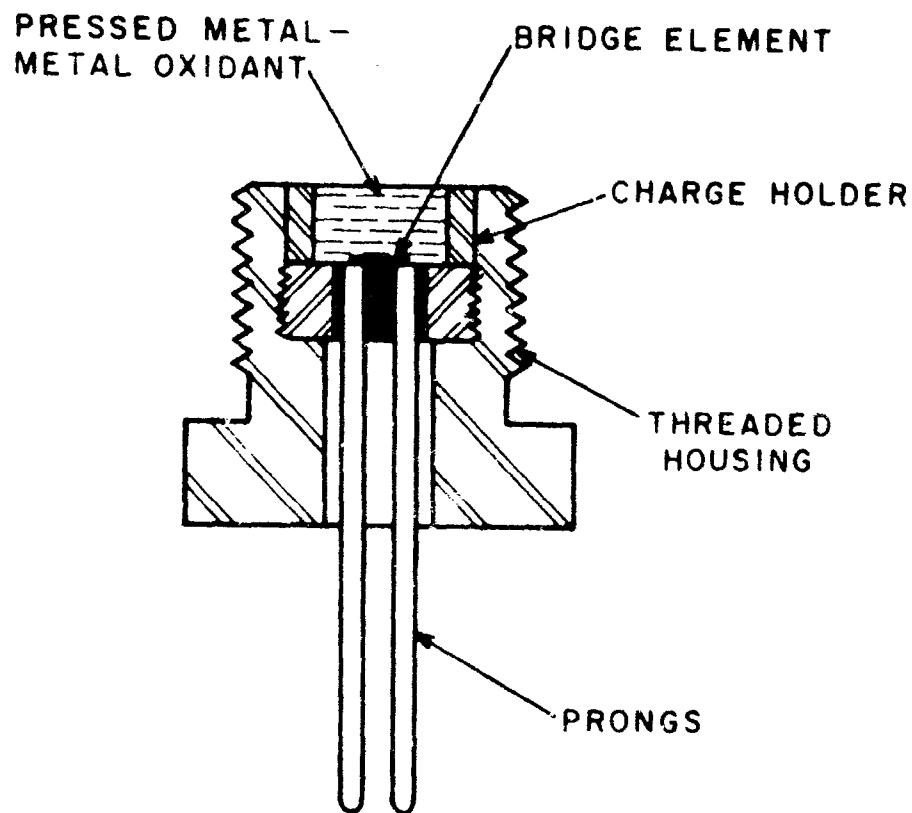


Figure 3

#### ACTUATOR

(Bridge element was either a 2-mil diameter wire or a 0.13-mil thick ribbon, each of nominal 1-ohm resistance. Actuator has 1-amp, 1-watt no-fire capability. Charge holder was fabricated from stainless steel.)

## ENVIRONMENTAL EVALUATIONS

### Thermal Stability of Metal-Metal Oxidants

One method for evaluating the thermal stability of a system is differential thermal analysis (DTA). The sample under study is heated continuously at a controlled rate side by side with a thermally inert reference material. A thermocouple embedded in the sample and in the reference material permits continuous monitoring of the temperature difference between the two as a function of temperature magnitude. As long as no change takes place in the sample, the temperature difference ideally is zero. If the sample changes phase or reacts endothermally, a thermal arrest occurs. If the sample reacts exothermally, the temperature difference becomes positive, and may be so large that the slope of the curve becomes vertical.

The DTA instrument used was the Fisher model 260 Differential Thermalizer, which consists of three separate units, a furnace, a solid-state programmer, and a sample holder. A Microcord 44 recorder (Photovolt Corporation) completes the instrumentation system.

Thermograms for three metal-metal oxidant systems are shown in Figure 4. The peaks that can be readily identified are the rhombic to cubic transition in  $\text{KClO}_4$  at  $300^\circ\text{C}$ , the decomposition of  $\text{KClO}_4$  at  $500^\circ\text{C}$ , the fusion of product  $\text{KCl}$  at  $770^\circ\text{C}$ , and the fusion of aluminum at  $660^\circ\text{C}$ . The curve for  $\text{Al-NH}_4\text{ClO}_4$  is not shown, but is similar with the transition occurring at  $240^\circ\text{C}$  and the decomposition occurring at  $370^\circ\text{C}$ .

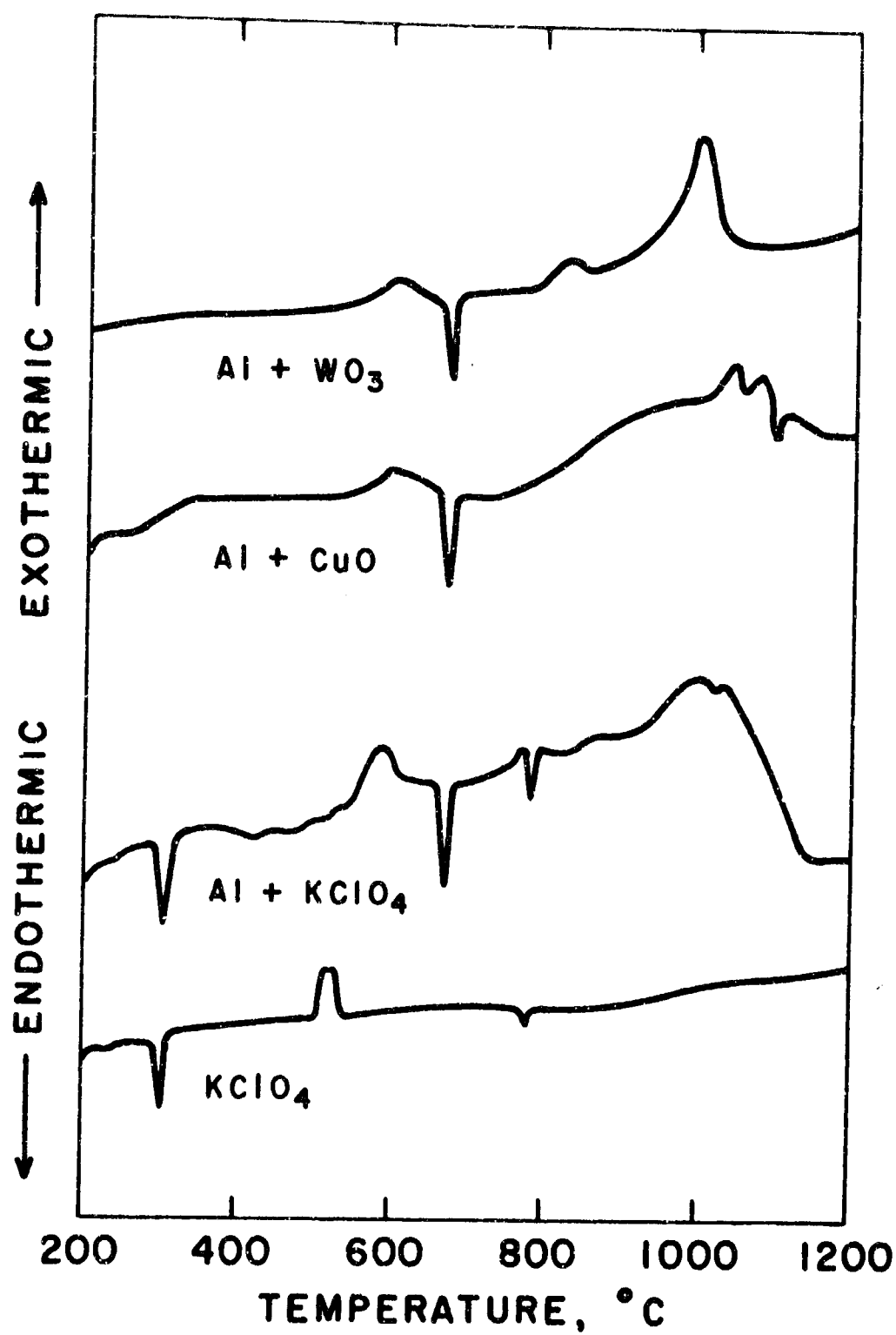


Figure 4  
DTA THERMOGRAMS  
(Heating Rate = 10°C/min)

For the metal-metal oxide traces, the absence of appreciable exothermic peaks up to temperatures as high as 800°C suggests that these systems have an enhanced thermal stability. The large exotherm in the Al-WO<sub>3</sub> trace beginning at approximately 825°C is believed to be associated with autoignition of the mixture. Accordingly, we have assumed that 825°C is the autoignition temperature, and have used this value in the development of the ignitability criterion for the Al-WO<sub>3</sub> system (ref. 3). The fact that propagating reaction was initiated at marginal currents where the calculated bridge temperature was not much in excess of 825°C suggests that this temperature is a good estimate of the auto-ignition temperature.

#### Sensitivity to Electrostatic Discharge Pulses

The ability of an electric initiator to withstand electrostatic discharges such as those produced by the human body is an important safety consideration. A number of tests were conducted on initiators loaded with pressed Al-CuO and Al-KClO<sub>4</sub> mixtures. The tests were conducted by discharging a 600-pf condenser at a maximum of 25 kv through the metal-metal oxidant mixture, that is, from pin to case. No 500-ohm series resistor was used,\* so that effectively the electrostatic discharge was in excess of what can be generated by the human body.

Under the above conditions, it was found that mixtures of H-3 spherical grade aluminum and cupric oxide were not initiated at 25 kv. In fact, a given pressing could dissipate repeated

---

\*The function of the series resistor, when used, is to simulate the resistance of the human body, which under discharge conditions is approximately 500 ohms.

discharges at this voltage without being initiated. Identical results were obtained from mixtures of flaked aluminum and potassium perchlorate. It is conceivable that many other metal-metal oxidant systems such as Al-WO<sub>3</sub> subjected to this environment would behave the same way, although these other systems were not tested.

On the basis of these results, a family of electrostatic-insensitive initiators with a 5-amp, 5-watt no-fire capability has been developed for aerospace applications. The basic charge in these initiators is a mixture of flaked aluminum and potassium perchlorate (ref. 4).

#### CONSTANT CURRENT IGNITION STUDIES

The constant current ignition studies of the pyrotechnic mixtures have been described in detail in Reference 5. Hence, only a brief summary of the method will be given here.

##### Firing Circuit

The firing circuit used was the IITRI low inductance, short rise-time constant current circuit, a schematic drawing of which is shown in Figure 5. The basic power supply consisted of lead storage batteries connected in series. The operation of the circuit is as follows. The resistance,  $R_1$ , is set equal to the resistance of the initiator under test. The current,  $I_1$ , through  $R_1$  is adjusted to the desired value by moving the rheostat. Then the calibrating circuit switch is opened, and the circuit to the initiator is completed by closing the mercury switch. The initial current through the initiator is equal to preselected

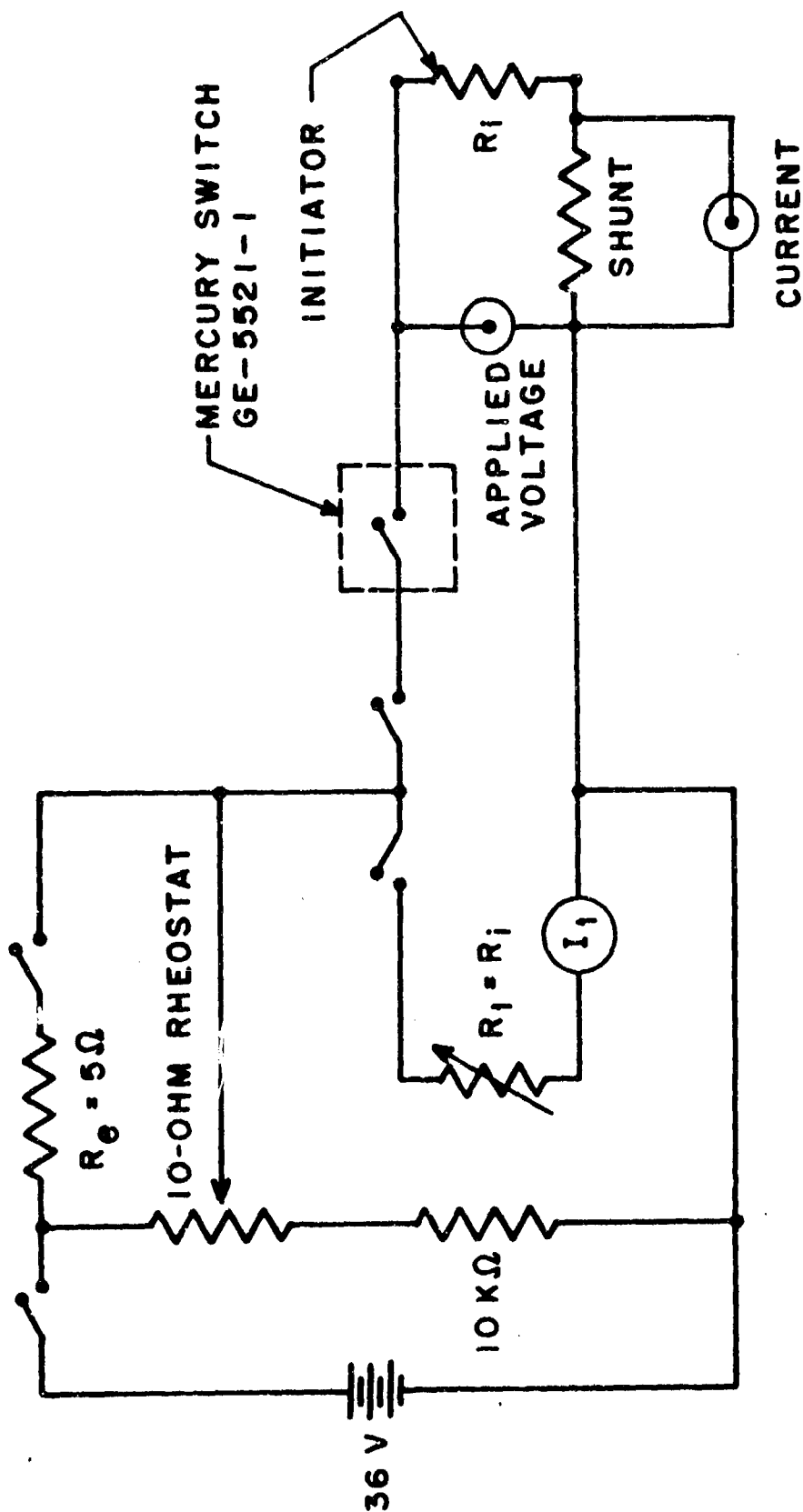


Figure 5

SCHEMATIC DIAGRAM OF CONSTANT CURRENT FIRING CIRCUIT  
(Resistance of shunt was in range 0.02 to 0.10 ohm.)

value of  $I_1$ . The switching of resistance,  $R_e$ , into the circuit permits higher currents at a given rheostat setting. The current,  $I_1$ , was read with Singer-Metrics Sensitive Research ammeters that were accurate to the nearest 0.04 amp or 0.25 amp.

The short rise time, which is in the range 4 to 10  $\mu$ sec, was achieved by using cables of low inductance. The cables, from the batteries to the initiator, consisted of two flat copper conductors separated by a Teflon tape dielectric, as indicated schematically in Figure 6. These three components were held together by a tight wrapping of Scotch No. 33 electrical tape. Cables to switches and resistors were constructed in the same manner to minimize inductive loops.

#### Instrumentation

The instrumentation included continuous monitoring of resistance of the EED during firing, and measurement of overall function time.

The performance of the EED's during firing was monitored by a Tektronix type 555 dual-beam oscilloscope equipped with a Polaroid camera. The upper beam was chopped into two channels by means of a type CA dual-trace plug-in unit. Channel A recorded the voltage drop across the shunt resistor in Figure 5. Since the shunt resistor was made from a heavy piece of resistance wire, its resistance changed very little during the few milliseconds required for EED functioning. Hence, this voltage drop is proportional to the current. Channel B recorded the applied voltage drop across both the EED (initiator) and shunt resistor. In

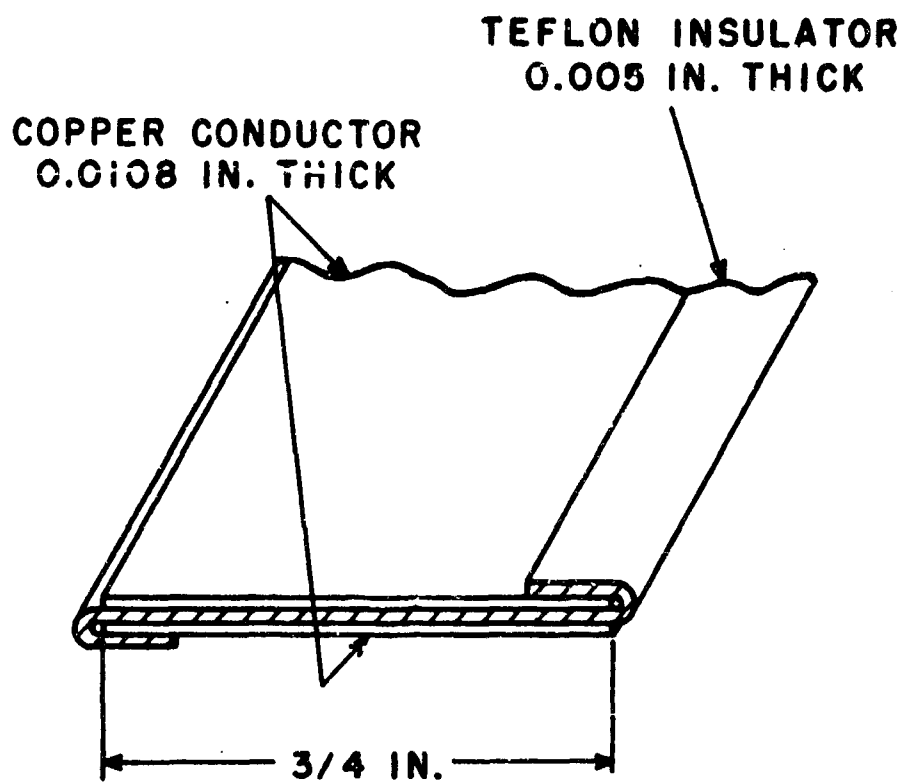


Figure 6

SCHEMATIC DRAWING OF FLAT CABLE USED  
IN CONSTANT CURRENT FIRING CIRCUIT  
OF FIGURE 5

this way, the simultaneous recording of current through and voltage drop across the EED provided a continuous picture of EED resistance during firing.

The lower beam of the oscilloscope was used in conjunction with a condenser discharge type ion probe system to measure overall function time, defined as the time from first application of firing pulse to emergence of the reaction wave from the end of the pyrotechnic column. The ion probe, which consisted of a two-prong Kovar-glass header, was positioned at the top of the pressed pyrotechnic charge. Further details about the ion probe system, including a circuit diagram, may be found in Reference 5.

#### Ignition at 15 amp

The constant-current ignitability studies on various combinations of aluminum and metal oxide are summarized in Tables 3 through 6, and a typical record from which the data were obtained is shown in Figure 7. The data in each table are arranged in the order of decreasing current. Initial currents were varied within a range of 49.6 amp to 7.1 amp, with the majority of the tests being conducted at or near 15 amp, which is the design all-fire current for the 5-amp, 5-watt no-fire initiator previously shown in Figure 2. The record in Figure 7 shows that the voltage trace decreases slightly from its initial value. This pattern indicates that the resistance of the initiator decreases during firing. At 37 msec the voltage trace becomes rather erratic, which as explained in Reference 5 was caused by the ignition of the metal-metal oxide bed; this phenomenon permitted measurement of ignition time of the pyrotechnic. The overall function time of the initiator was 66 msec.

Table 3

IGNITION OF H-3 ALUMINUM + TO-2 TUNGSTIC OXIDE  
(Initiator is shown in Figure 2.)

Amount of Al	Shot No.	Density g/cc	Resistance, ohms after Loading	at Ignition	Initial Current, amp	Ignition Time, msec	Column Height, in.	Unit Burning Time, msec/in.
2/3 stoich.	220	3.65	0.228	0.158	37.0	2.5	0.221	183
	362	3.83	.199	.180	36.2	1	.201	169
	219	3.58	.222	.164	25.7	5	.215	181
	361	3.84	.232	.195	21.0	6	.200	170
	47	3.52	.243	.173	15.7	14	.219	178
	166	3.60	.268	.170	15.7	14	.214	178
	150	4.07	.228	.143	15.7	34	.150	187
	146	4.13	.191	.139	15.7	42	.148	189
	153	4.05	.205	.140	15.5	37	.151	192
	167	3.44	.229	.164	15.2	14	.224	165
	46	3.83	.215	.160	15.2	18	.201	194
	149	3.93	.217	.158	15.2	26	.196	199
	145	3.81	.235	.158	14.8	26	.202	183
	357	3.84	.213	.196	14.8	14	.200	200
	152	3.87	.216	.158	14.8	30	.199	196
	48	3.71	.194	.153	14.8	20	.208	188
	49	3.77	.222	.158	14.8	22	.204	196
	50	3.87	.231	.149	14.8	27	.199	186
	51	3.99	.219	.151	14.8	29	.193	192
	52	3.89	.219	--	14.8	24	.198	197
	168	3.60	.192	.158	14.2	23	.214	173
	169	3.56	.221	.169	13.0	29	.217	170
	358	3.86	.200	.181	12.7	23	.199	196
	170	3.56	.229	.161	12.2	34	.217	175
	172	3.72	.203	--	11.3	>180	.207	--
	173	3.71	.183	No go	10.4 <sup>a</sup>	No go	.208	--

Table 3 (cont.)

Amount of Al	Shot No.	Density g/cc	Resistance after Loading	Resistance, ohms at Ignition	Initial Current, amp	Ignition Time, msec	Column Height, in.	Unit Burning Time, msec/in.
Stoich.	313	3.56	.204	.171	23.0	4	.217	111
	41	3.33	.204	.155	15.7	16	.232	99
	45	3.57	.227	.145	15.2	30	.216	111
	42	3.59	.205	.118	15.2	52	.215	107
	44	3.81	.229	No go	15.2a	No go	.202	--
	355	3.58	.211	.156	15.1	24	.215	98
	43	3.40	.264	.161	14.8	20	.227	106
	286	3.14	.211	.205	14.5	12	.246	77
	287	3.31	.201	.180	13.2	23	.233	90
	356	3.49	.222	No go	12.9a	No go	.221	--
	268	3.25	.194	No go	11.1a	No go	.237	--
30% excess	40	3.45	.235	No go	16.1a	No go	.224	--
	39	3.09	.223	.169	15.7	18	.251	72
	52	3.25	.262	.141	14.8	30	.238	88
	54	3.29	.211	.135	14.8	29	.235	85
50% excess	55	3.11	.236	.134	15.2	34	.249	88
	56	3.17	0.225	No go	14.8a	No go	0.254	--

a One-minute pulse.

Table 4  
IGNITION OF H-5 ALUMINUM + TO-2 TUNGSTIC OXIDE  
(Initiator is shown in Figure 2.)

Amount of Al.	Shot No.	Densit', g/cc	Resistance, ohms after loading	at initiation	Initial Current, amp	Ignition Time, msec	Column Height, in.	Unit Burning Time msec/in.
2/3 stoich.	228	3.57	0.204	0.154	44.4	2	0.216	199
	323	3.85	.211	.190	35.0	2	.200	210
	226	3.58	.202	.158	32.6	3	.215	216
	225	3.50	.237	.157	26.3	5	.220	186
	322	3.79	.208	.187	24.4	4	.203	212
	34	4.01	.207	.154	17.4	19	.192	234
	31	3.69	.217	.150	17.0	13.5	.209	213
	33	3.79	.223	.158	17.0	16	.203	227
	32	3.72	.215	.142	16.3	15	.207	227
	224	3.55	.210	.160	16.1	16	.217	193
	30	3.71	.222	.157	15.2	19	.208	226
	142	4.05	.222	.160	15.2	29	.151	219
	141	4.01	.214	.161	15.0	33	.192	219
	337	3.85	.208	.181	14.5	15	.200	220
	104	3.57	.238	.167	12.9	20	.216	208
	333	3.79	.209	.169	12.7	36	.203	226
	105	3.54	.218	.168	11.8	25	.218	206
	106	3.47	.220	.168	11.3	23	.222	198
	339	3.88	.215	.164	11.1	75	.198	227
	108	3.49	.253	.173	10.1	41	.221	195
	109	3.46	.220	.172	9.4	48	.223	197
	340	3.81	.223	No go	9.0a	No go	.202	-
	110	3.50	.248	No go	6.3a	No go	.220	-

<sup>a</sup>One-minute pulse

Table 5

IGNITION OF H-3 ALUMINUM + GLIDDEN CUPRIC OXIDE  
(Initiator is shown in Figure 2.)

Amount of Al	Shot No.	Density, g/cc	Resistance, ohms after Loading	at Ignition	Initial Current, amp	Ignition Time, msec	Column Height, in.	Unit Burning Time, msec/in.
2/3 stoich.	241	2.89	0.202	0.157	33.5	2	0.267	101
	321	3.07	.219	.196	28.8	3	.252	143
	320	3.19	.219	.180	21.5	5	.242	153
	127	3.21	.270	.169	20.3	9	.241	179
	240	2.94	.225	.163	18.3	11	.263	114
	138	3.29	.197	.161	16.5	20	.187	182
	137	3.08	.190	.160	16.3	16	.251	156
	129	3.11	.244	.166	16.3	16	.198	167
	135	3.21	.198	.165	16.1	18	.241	170
	121	3.07	.224	.162	15.7	20	.252	163
	120	3.10	.200	.165	15.6	21	.250	156
	86	3.08	.221	.162	15.4	22	.251	191
	128	3.19	.201	.169	15.4	24	.242	149
	87	3.04	.200	.163	15.2	19	.255	173
	89	3.23	.230	.163	15.2	25	.239	213
	88	3.29	.232	.164	15.2	26	.235	208
	239	2.82	.201	.162	15.0	14	.274	58
	119	3.12	.232	.171	14.6	22	.248	169
	332	3.18	.217	.185	14.5	16	.243	161
	333	3.17	.210	.182	13.0	26	.244	148
	334	3.17	.210	.180	11.0	108	.244	156
	283	2.91	.210	.202	10.6	40	.266	60
	335	3.10	.211	.180	9.0	220	.249	-
	336	3.10	.211	No go	7.1a	No go	.249	-
Stoich.	85	3.25	.212	.162	15.2	50	.238	80
	83	2.96	.192	.153	15.0	30	.262	99
	84	3.20	.225	.162	15.0	48	.242	87
	82	2.87	0.271	0.167	14.5	20	0.270	126

Table 3 (cont.)

Amount of Al	Shot No.	Density, g/cc	Resistance, ohms after Loading	Ign. Time, sec	Initial Current, amp	Ignition Time, msec	Column Height, in.	Unit Burning Time, msec/in.
30% excess	79	3.16	0.250	0.156	16.1	38	0.245	82
	77	3.06	.241	.151	15.7	36	.253	83
	78	3.06	.245	.154	15.7	51	.253	91
	80	3.02	.249	.159	15.2	30	.256	94
	75	2.86	.192	.143	14.9	26	.271	96
	76	2.75	.210	.164	14.8	51	.282	114
	74	2.80	.238	.168	14.8	24	.267	101
	81	3.01	0.241	-	14.4	6 sec	0.257	-

<sup>a</sup>One-minute pulse.

Table 6

IGNITION OF H-5 ALUMINUM + GLIDDEN CUPRIC OXIDE  
(Initiator is shown in Figure 2.)

Amount of Al	Shot No.	Density, g/cc	Resistance, ohms after Loading	at Ignition	Initial Current, amp	Ignition Time, msec	Column Height, in.	Unit Burning Time, msec/in.
2/3 Stoich.	236	2.94	0.207	0	157	1	0.263	141
	326	3.15	.213	.180	35.5	2	.245	175
	235	2.96	.210	.166	35.2	2	.261	103
	234	2.88	.229	.165	25.2	5	.268	127
	324	3.15	.203	.173	24.0	4	.245	175
	174	3.04	.236	.164	15.7	15	.254	150
	103	3.32	.236	.162	15.5	27	.233	210
	101	2.93	.216	.167	15.0	21	.264	136
	328	3.25	.193	.176	15.0	21	.238	198
	102	3.19	.200	.162	14.2	33	.242	190
	175	2.95	.190	.161	14.1	30	.262	134
	176	2.97	.232	.160	13.5	28	.260	127
	329	3.15	.213	.176	12.5	35	.245	167
	177	3.04	.226	.171	12.2	50	.254	138
	330	3.13	.212	.184	10.8	60	.247	162
	178	3.07	.233	-	10.4	20 sec	.252	-
	331	3.20	.201	-	9.0	3 sec	.241	-
Stoich.	96	2.97	.199	.155	15.5	30	.261	106
	98	3.11	.253	.160	15.1	44	.249	96
	97	3.08	.235	.159	15.0	47	.251	106
	99	3.10	.222	.170	15.0	31	.250	116
30% excess	100	2.98	.232	.154	14.6	29	.260	127
	92	2.96	.229	.155	15.4	49	.262	69
	91	3.08	.248	.166	15.2	22	.251	88
	94	2.92	.253	.156	14.8	35	.265	72
	93	3.06	0.197	No go	14.8 <sup>a</sup>	No go	0.253	..

<sup>a</sup>One-minute pulse.

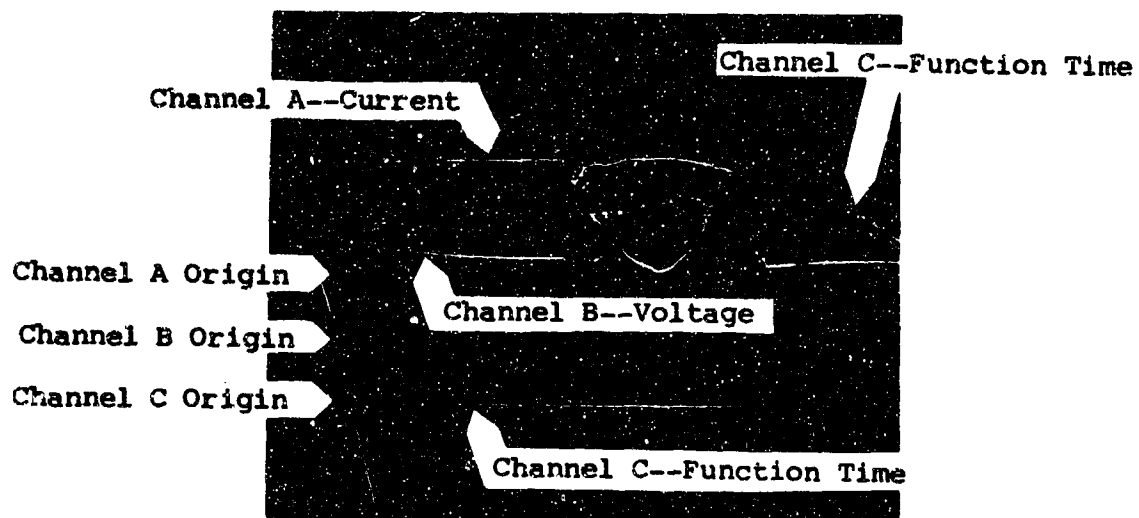


Figure 7

OSCILLOSCOPE RECORD FROM FIRING  
OF METAL-METAL OXIDE INITIATOR  
(Shot No. 153, H-3 Al + TO-2 WO<sub>3</sub>.  
Vertical Sensitivities: A, 0.2 volt/cm;  
B, 2 volt/cm; C, 10 volt/cm.  
Sweep Rate on all channels = 10 msec/cm.)

The unit burning time in Tables 3 through 6 was calculated by subtracting the ignition time from the overall function time and then dividing this difference by the column height. Overall function time was not reported in the tables in order to conserve space but can be calculated from the following:

$$\begin{aligned} \text{Function time} &= \text{ignition time} + & (5) \\ &(\text{column height}) \times (\text{unit burning time}) \end{aligned}$$

The unit burning time data for two metal-metal oxide systems are plotted in Figures 8 and 9. Unit burning time is the reciprocal of burning rate. Note how well the burning rate correlated with density, particularly in the aluminum-tungstic oxide systems. The scatter in the points for these systems is within the experimental error of the measurements, that is  $\pm 2$  msec in burning time and  $\pm 0.002$  in. in column height. The correlation for the aluminum-cupric oxide systems was not as good, possibly because the pressed columns were inadvertently allowed to exceed one diameter (0.222 in.) in length. This occurrence may have caused excessive density gradients in the column.

Increasing the amount of aluminum caused the mixture to burn more rapidly in all systems. Increasing the density slowed the burning except for H-3 aluminum-Glidden cupric oxide system. As shown in Figure 9, mixtures that contained a stoichiometric quantity of aluminum or 30% excess aluminum exhibited more rapid burning as the density was increased.

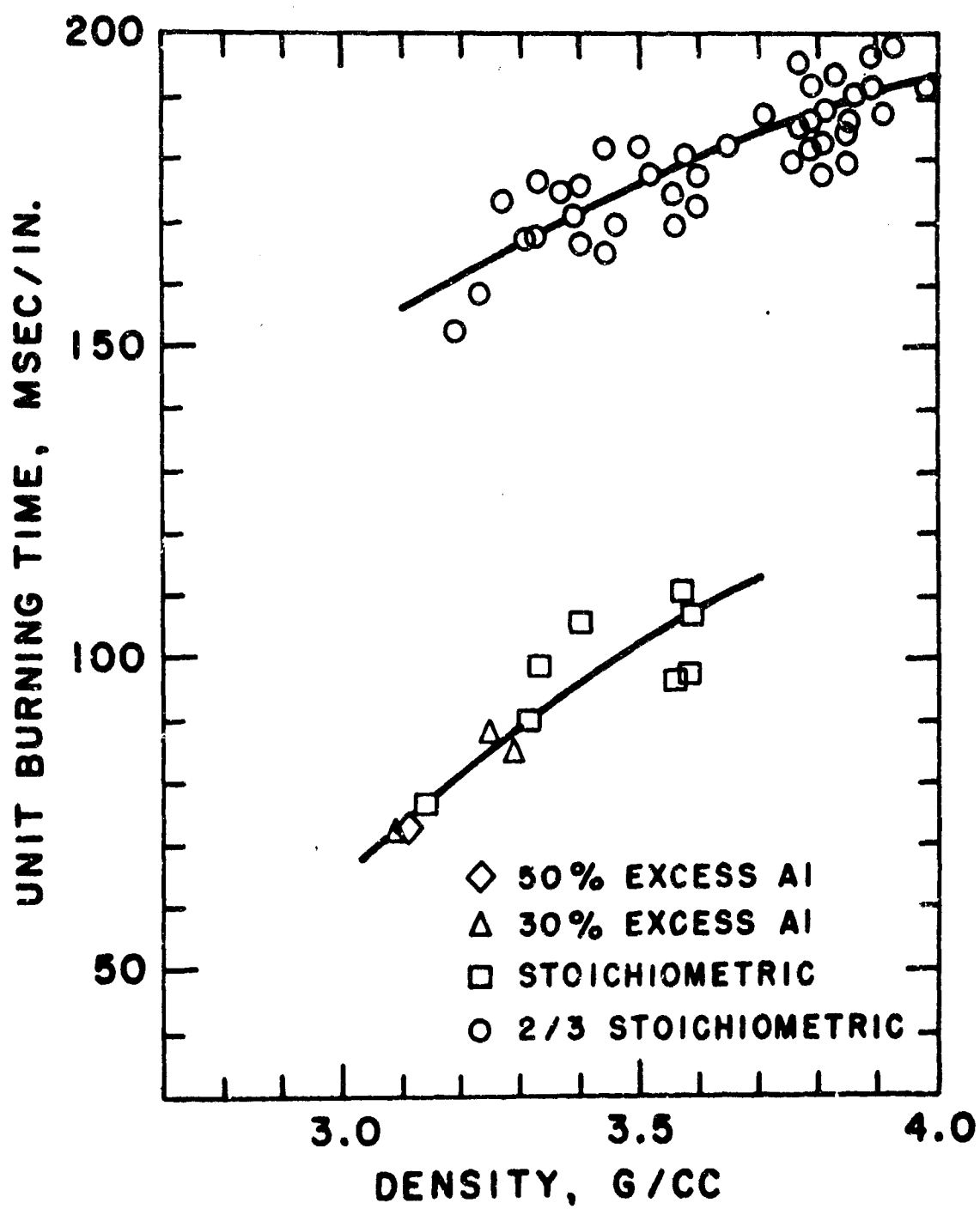


Figure 8

UNIT BURNING TIME OF H-3 Al + TO-2 WO<sub>3</sub>

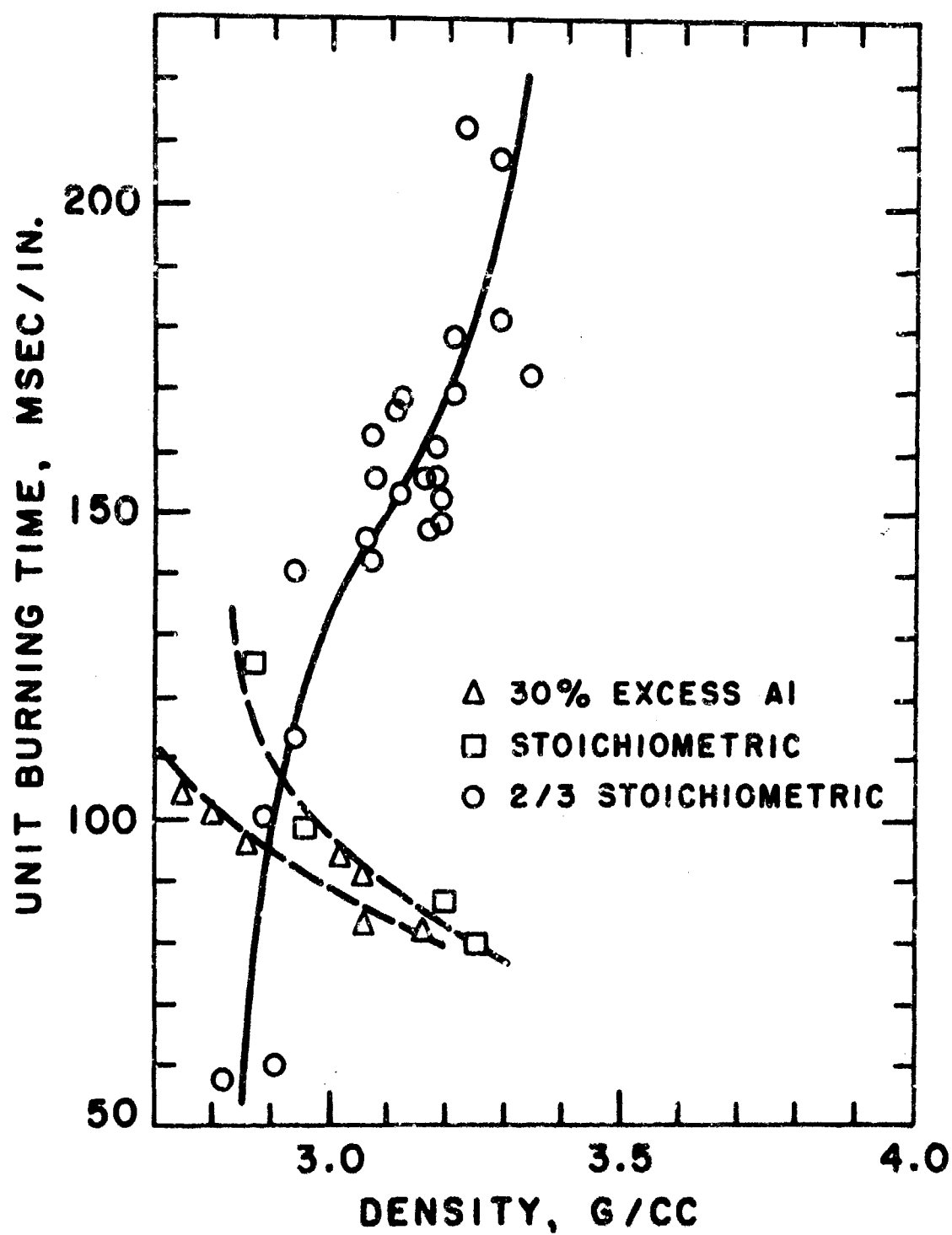


Figure 9  
UNIT BURNING TIME OF H-3 Al + GLIDDEN CuO

The data in Tables 3 through 6 show that loading density had a observable effect on ignition time. Generally speaking, at a given current an increase in density caused an increase in ignition time. The implication, of course, is that accurate control of overall function time of the initiator requires control of metal-metal oxide loading density, particularly for a system such as Al-CuO where not only ignition time but also burning rate varies significantly with density.

#### Ignition at 5 amp

The 5-amp ignition tests on the Al-KClO<sub>4</sub> and Al-NH<sub>4</sub>ClO<sub>4</sub> systems are summarized in Tables 7 through 9. The principle variant in these studies was the loading density, which was controlled by varying loading pressure. The actuators shown in Figure 3 were used for these ignition studies. These actuators have a 1-amp, 1-watt no-fire capability.

The majority of the studies were conducted using mixtures formulated from H-3 spherical grade aluminum powders. In the initial tests, however, two flaked aluminum grades were evaluated -- 28-XD and 40-XD, manufactured by the Reynolds Metals Company, Louisville, Kentucky. Previous studies showed certain pyrotechnic mixtures such as Al-KClO<sub>4</sub> offer much improved resistance to electrostatic discharges if the mixture were formulated from flaked aluminum, as compared with spherical aluminum (ref. 4); however, in the current work severe tendency for the flaked aluminum mixtures to fail to compact under pressure was encountered, to the extent that misfires occurred. For this reason

Table 7

IGNITION OF H-3 ALUMINUM + HUMMEL  $KClO_4$  (BATCH 1) AT 5 AMP\*

Amount of Aluminum	Shot No.	Density, g/cc	Type of Bridge	Resistance, ohms		Ignition Time, msec
				after Loading	at Ignition	
33.33% excess	115	1.98	Wire	0.835		2.3
	112	2.01	Wire	.81	0.78	6.4
	116	2.01	Wire	.82		6.2
	114	2.08	Wire	.825		Delay
	119	2.10	Wire	.825	.70	12.2
	113	2.12	Wire	.95		8.4
	117	2.14	Wire	.865		6.2
	111	2.16	Wire	.86	.75	9.1
	118	2.16	Wire	.815		2 sec
2/3 stoich.	107	1.95	Wire	.94	1.06	1.3
	104	1.97	Wire	.83	.90	1.6
	105	1.99	Wire	.82		2.7
	103	2.08	Wire	.86	.99	1.6
	106	2.12	Wire	.82		2.7
	108	2.12	Wire	.83	.86	3.4
	110	2.20	Wire	.83	.86	3.4

Table 8

IGNITION OF H-3 ALUMINUM + HUMMEL  $KClO_4$  (BATCH 2) AT 5 AMP\*

Amount of Aluminum	Shot No.	Density, g/cc	Type of Bridge	Resistance, ohms		Ignition Time, msec
				after Loading	at Ignition	
2/3 stoich.	191	2.10	Wire	0.788	0.86	1.3
	192	2.10	Wire	1.244	.96	1.2
	193	2.10	Wire	.892	.94	1.4
	194	2.10	Wire	.940		2.6
	195	2.10	Wire	.987	.94	1.1
	196	2.10	Wire	1.056	.90	2.7
	208	2.11	Wire	.936		1.5
	197	2.13	Wire	0.939	0.96	2.7

\* Actuator is shown in Figure 3.

Table 9

IGNITION OF H-3 ALUMINUM + THIOKOL  $\text{NH}_4\text{ClO}_4$  AT 5 AMP\*

Amount of Aluminum	Shot No.	Density, g/cc	Type of Bridge	Resistance, ohms		Ignition Time, msec
				after Loading	at Ignition	
33.33% excess	82	1.56	Ribbon	0.625		11
	86	1.59	Ribbon	.680		10
	85	1.66	Ribbon	.707		10
	78	1.74	Ribbon	.672		14
	79	1.74	Ribbon	.622		14
	92	1.75	Ribbon	.69	0.78	11
	29	1.76	Ribbon	.678	.76	14
	30	1.73	Ribbon	.687	.71	16
	80	1.78	Ribbon	.622		12
	83	1.84	Ribbon	.650		12
	84	1.87	Ribbon	.664		12
2/3 stoich.	39	1.74	Ribbon	.637		8.6
33.33% excess	94	1.75	Wire	.87	.88	2.3
	19	1.78	Wire	.832	.84	3.3
	18	1.83	Wire	.843		3.3
	17	1.84	Wire	.850		3.1
2/3 stoich.	59	1.54	Wire	.812		2.0
	70	1.54	Wire	.787		2.3
	47	1.60	Wire	.803		2.3
	49	1.63	Wire	.841		2.2
2/3 stoich.	73	1.70	Wire	.795		2.3
	74	1.71	Wire	.795		2.0
	11	1.80	Wire	.817	.84	2.4
	14	1.81	Wire	.831	0.93	2.4
	13	1.87	Wire	.802		No go
	12	2.04	Wire	0.792		No go

\* Actuator is shown in Figure 3.

further work with flaked aluminum mixtures was suspended and the majority of the effort was diverted to evaluating spherical aluminum mixtures.

The resistance of the 2-mil Tophet-C wire bridge during firing at first increased and then decreased. The resistance at ignition has been calculated for some of the shots in Tables 7 through 9 to show this behavior. The Resistvar-II ribbon bridge, on the other hand, exhibited only a tendency to increase in resistance.

No unit burning times have been reported in Tables 7 through 9. This omission is explained by the very high burning rate of the  $\text{Al-KClO}_4$  and  $\text{Al-NH}_4\text{ClO}_4$  systems. Pitts in Reference 6 obtained values of 0.05 in/ $\mu\text{sec}$  for  $\text{Al-KClO}_4$ , which would indicate that the burning time of our pressing would be only 3  $\mu\text{sec}$ . Such a short time is not resolvable on an oscilloscope which is being swept in the milliseconds-per-centimeter range. In the tables, therefore, only the ignition time has been reported, and the overall function time is understood to be only microseconds greater.

The performance of the  $\text{Al-KClO}_4$  mixtures with excess aluminum at 5-amp was erratic, judging from the wide variation in ignition time as reported in Table 7. Noticeable delays were observed in some of the shots. The aluminum-deficient (2/3 stoichiometric) mixtures performed much more reproducibly, however. For  $\text{Al-NH}_4\text{ClO}_4$  mixtures in Table 9, it can be observed that ignition times were longer for the ribbon bridges than for the wire bridges. This was expected, since the greater surface

area of the flat ribbon in contact with the surroundings causes its heating rate at a given current to be lower. All  $\text{Al-NH}_4\text{ClO}_4$  systems performed reproducibly, however, with the exception that the last two entries showed that too high a density caused misfires.

#### 5-Watt No-Fire Experiments

The ability of metal-metal oxide initiators bridged with a 5-mil wire to dissipate a constant 5-amp. 5-watt pulse without functioning or seriously degrading the performance is shown in Table 10. Ten initiators illustrated in Figure 2 were loaded with 2/3 stoichiometric mixtures of either  $\text{Al-WO}_3$  or  $\text{Al-CuO}$ , in the same manner as for the constant current ignition studies. A current of 5 amp was then delivered to the initiator for a period of 15 minutes. The input power at this current was somewhat greater than 5-watts, except for the test where the initiator resistance was less than 0.200 ohm. The initiators became very hot; however none fired under these conditions.

After each initiator cooled to ambient temperature, an attempt was made to fire it at the design all-fire current of 15 amp. The performance at 15 amp is summarized in columns 5 through 8 of Table 10. The ignition times are essentially the same as for initiators which have been tested only at 15 amp, as previously reported in Tables 3 and 5. However, the unit burning times (i.e., burning rate) of the metal-metal oxide was affected somewhat by the 5-amp exposure. The  $\text{Al-WO}_3$  system burned more slowly than that studied in Table 3, while the

Table 10  
SUMMARY OF 5-AMP, 5-WATT NO-FIRE EXPERIMENTS \*

System	Density, g/cc	Resistance after Loading, ohms	5-amp 15-min Test	Ignition Current, amp.	Ignition Time, msec.	After Cooling Column Height, in.	Unit Burning Time, msec/in.
H-3 Al + TO-2 WO <sub>3</sub> , 2/3 Stoich.	3.65	0.221	No go	15.5	15	0.426	317
	3.72	.221	No go	15.0	16	.419	320
	3.77	.202	No go	14.0	23	.412	286
	3.60	.203	No go	15.0	15	.433	305
	3.61	0.210	No go	15.0	17	0.431	308
H-3 Al + Glidden CuO, 2/3 Stoich.	3.27	0.207	No go	15.0	15	0.381	165
	3.22	.207	No go	15.0	16	.396	161
	3.29	.207	No go	15.0	16	.378	175
	3.13	.193	No go	15.0	16	.398	83
	3.11	0.210	No go	15.0	15	0.400	137

\* Initiator is shown in Figure 2.

Al-CuO burned more rapidly than that in Table 5. However, the burning rates under both sets of conditions are of the same order of magnitude, so that the observed differences are of no major concern.

#### One-Watt No-Fire Experiments

The ability of pyrotechnic-loaded actuators bridged with either a 2-mil wire or a 0.13-mil thick ribbon to dissipate a constant 1-amp, 1-watt pulse was determined in the experiments that are summarized in Tables 12 through 14. The actuators were lined with the stainless steel charge holders. Each actuator (Figure 3) was loaded with the appropriate pyrotechnic in the same manner as for the 5-amp ignition studies. A current of appropriate value for dissipation of 1 watt was then delivered to the actuator for a period of 5 minutes; the actual value for each test is indicated in column 5 of the Tables. Column 6 shows that none of the actuators fired under these conditions.

After each actuator cooled to ambient temperature, an attempt was made to fire it at the all-fire current of 5-amp. The performance of the actuators under these conditions is shown in columns 7 through 10 of the Tables. The interesting results are those for the  $\text{Al-NH}_4\text{ClO}_4$  system with excess aluminum in Table 11. The advantages of the ribbon bridge versus the wire bridge are demonstrated. All of the ribbon-bridged actuators that had been exposed to the 1-watt pulse fired at 5-amp; furthermore, the ignition times agreed very well with those for actuators that were tested only at 5-amp, as previously reported in Table 9.

Table 11

ONE-WATT NO-FIRE EXPERIMENTS FOR H-3 ALUMINUM + THIOKOL  $\text{NH}_4\text{ClO}_4$  \*

Amount of Aluminum	Density, g/cc	Type of Bridge	Resistance after Loading, ohms	5-minute Test:		Ignition Current, amp	Ignition Time, msec
				Current, amp	Results		
33.33% excess	1.71	Ribbon	0.684	1.21	No go	5.0	13
	1.71	Ribbon	.66	1.23	No go	5.0	13
	1.73	Ribbon	.738	1.16	No go	5.0	12
	1.73	Ribbon	.67	1.22	No go	5.0	12
	1.73	Ribbon	.68	1.21	No go	5.0	11
	1.80	Ribbon	.651	1.24	No go	5.0	17
	1.80	Ribbon	.652	1.00	No go	5.0	15
33.33% excess	1.72	Wire	.795	1.00	No go	5.1	No go
	1.73	Wire	.791	1.13	No go	5.0	No go
	1.77	Wire	.797	1.00	No go	5.0	3.6
	1.81	Wire	.781	1.00	No go	5.0	Delay
2/3 stoich.	1.69	Ribbon	.672	1.22	No go	5.0	6.5
	1.76	Ribbon	0.670	1.22	No go	5.0	No go

\* Actuator is shown in Figure 3.

Table 12  
ONE-WATT NO-FIRE EXPERIMENTS FOR H-3 ALUMINUM + KClO<sub>4</sub> (BATCH 1)\*

Amount Of Aluminum	Density, g/cc	Type of Bridge	Resistance after Loading, ohms	5-minute Test:		After Cooling	
				Current, amp	Results	Ignition Current, amp	Time, msec
33.33% excess	1.97	Wire	0.805	1.12	No go	5.0	8.2
	2.01	Wire	.81	1.11	No go	5.0	4.9
	2.05	Wire	.76	1.15	No go	5.0	2.0
	2.06	Wire	.82	1.10	No go	5.0	3.2
	2.09	Wire	.83	1.00	No go	5.0	2.6
2/3 stoich.	1.87	Wire	.79	1.13	No go	5.0	2.4
	2.02	Wire	.785	1.13	No go	5.0	2.8
	2.05	Wire	.81	1.11	No go	5.0	2.2
	2.06	Wire	.81	1.11	No go	5.0	1.9

\* Actuator is shown in Figure 3.

Table 13  
ONE-WATT NO-FIRE EXPERIMENTS FOR H-3 ALUMINUM + KClO<sub>4</sub> (BATCH 2) \*

Amount of Aluminum	Density, g/cc	Type of Bridge	Resistance after Loading, ohms	5-minute Test:		After Cooling	
				Current, amp	Results	Ignition Current, amp	Ignition Time, msec
2/3 stoich.	2.10	Wire	1.142	0.94	No go	5.0	2.8
	2.10	Wire	1.038	0.98	No go	5.0	1.5
	2.14	Wire	0.967	1.02	No go	5.0	1.5
	2.16	Wire	0.887	1.06	No go	5.0	1.5
	2.17	Wire	0.911	1.05	No go	5.0	2.9

\* Actuator is shown in Figure 3.

On the other hand, the wire-bridged actuators at 5-amp behaved very erratically, and Table 11 shows that some misfires were encountered. A logical explanation of the above behavior is that the greater surface area of the ribbon bridge in contact with the surroundings permits it to dissipate its heat more effectively than would the wire bridge. Hence the ribbon-bridge, as well as the pyrotechnic adjacent to the bridge, stays cooler during the 1-watt exposure. There is less chance for the pyrotechnic to be heated to temperatures at which phase changes would alter its ignition characteristics or at which thermal expansion would alter the physical contact between the bridge and charge.

Tables 12 and 13 show that both aluminum-rich and aluminum-deficient  $\text{Al-KClO}_4$  mixtures could be ignited at 5-amp after the 1-watt test. The interesting aspect was that these results were achieved with the wire bridges; hence the performance with ribbon bridges was not evaluated. The greater thermal stability of  $\text{KClO}_4$  as compared to that of  $\text{NH}_4\text{ClO}_4$  probably explains why wire bridges were more effective for  $\text{Al-KClO}_4$  pressings than for  $\text{Al-NH}_4\text{ClO}_4$  pressings.

#### OUTPUT OF GAS-PRODUCING PYROTECHNICS

The output characteristics of gas-producing pyrotechnic mixtures such as aluminum-potassium perchlorate and aluminum-ammonium perchlorate were studied with the goal of redesigning a valve actuator that is electrically fired and actuated by a

250-mg lead styphnate charge. The main objective of the output studies was to design a pyrotechnic charge that would propel a 5.00-gram piston over a distance of approximately 1/8 in. according to the same displacement-time profile as provided by the lead styphnate charge. The principle variants in these studies were the charge weight and the aluminum/oxidant ratio in the pyrotechnic mixtures.

#### Theoretical Force Constant

A prime consideration in the selection of candidate compositions was the value of the force constant of the candidate as compared with that for lead styphnate. The force constant calculations are summarized in Table 14. In the calculations, it was assumed that only the most stable products are formed. That is, first, all the aluminum, when used, is permitted to react with oxygen to form aluminum oxide ( $\text{Al}_2\text{O}_3$ ). Then, hydrogen combines with oxygen to form water. Finally, any oxygen left over is permitted to react with the carbon, when present, to form carbon monoxide. Typical reactions under these assumptions are as follows:

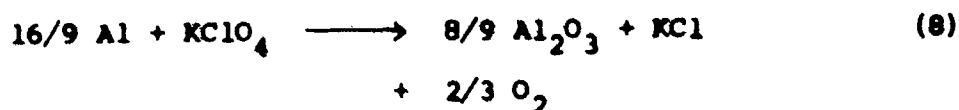
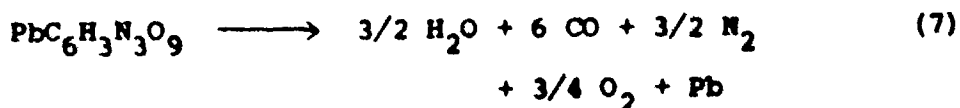
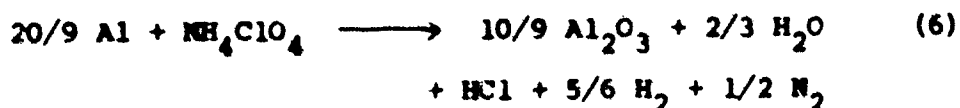


Table 14  
CALCULATED THEORETICAL FORCE CONSTANTS FOR CANDIDATE COMPOSITIONS

System	Amount of Al	Molecular Weight	Reaction Temp., °K	Amount of Gas, mole/g of reactant	Force Constant, ft-lb <sub>f</sub> /g
5/3 Al + NH <sub>4</sub> ClO <sub>4</sub>	Stoich.	163	3770	0.0244	565
20/9 Al + NH <sub>4</sub> ClO <sub>4</sub>	33.33% excess	178	3770	.0243	563
Nitroguanidine	--	104	2370	.0385	559
Lead styphnate	--	468	2880	.0230	406
16/9 Al + KClO <sub>4</sub>	2/3 stoich.	187	3770	.0143	332
8/3 Al + KClO <sub>4</sub>	Stoich.	211	3770	.0143	331
32/9 Al + KClO <sub>4</sub>	33.33% excess	235	3770	0.0141	327

The reaction temperature was calculated from an enthalpy balance in which the heat released 298°K was permitted to heat the products to the final temperature. Heats of formation and heat capacities were obtained from Glassner (ref. 7) and Perry (ref. 8). In the case of the aluminum-perchlorate systems, a significant portion of the product,  $\text{Al}_2\text{O}_3$ , decomposes at 3770°K according to the reaction (ref. 9):



The force constant is then calculated from the relationship:

$$F = \frac{n}{M} RT \quad (10)$$

where

- n = moles of gas produced
- M = molecular weight of reactants
- R = gas constant
- T = reaction temperature.

These calculations confirmed most of the systems under consideration showed potential promise as candidates to replace lead styphnate in the actuator. The explosive nitroguanidine was included to provide an alternative system in the event that reaction kinetics precluded the pyrotechnics from exhibiting a performance equivalent to that of lead styphnate; in retrospect, however, little or no experimental work was done with the explosive system, because the performance of the pyrotechnics in all respects was satisfactory.

### Experimental Method

A photographic method based on the use of a Fastax smear camera was employed to obtain piston displacement-time data. The experimental arrangement and typical records are shown in Figure 10. The charges were pressed into actuators previously described and depicted in Figure 3. The 5.00-gram piston was positioned initially in a breechblock into which the loaded actuator was screwed. When the charge was fired, the emerging piston passed in front of an accurately machined slit through which an intense light shined. The movement of the piston past the slit blocked out a steadily increasing portion of the light, which was then prevented from reaching the camera focused on the slit. As can be seen from Figure 10, the method produced a clear, very sharp trace of the displacement of the piston. Distance reference on the records was obtained from the width of the trace, which corresponded to a slit length of 0.500 in. Time reference was obtained from the timing marks which occurred at 1-msec intervals. The brilliant flash visible on the record for Shot No. 186 ( $\text{Al-KClO}_4$ ) was observed with all pyrotechnic charges, and was believed to be caused by the shifting  $\text{Al}_2\text{O}_3$  equilibrium as described by Equation 9.

The piston was machined from 0.39060-in. diameter drill rod to a length of 0.557 in. The weight was controlled to the nearest 0.05 g. The clearance between the piston and the hole from which it was propelled was approximately 0.001 in.

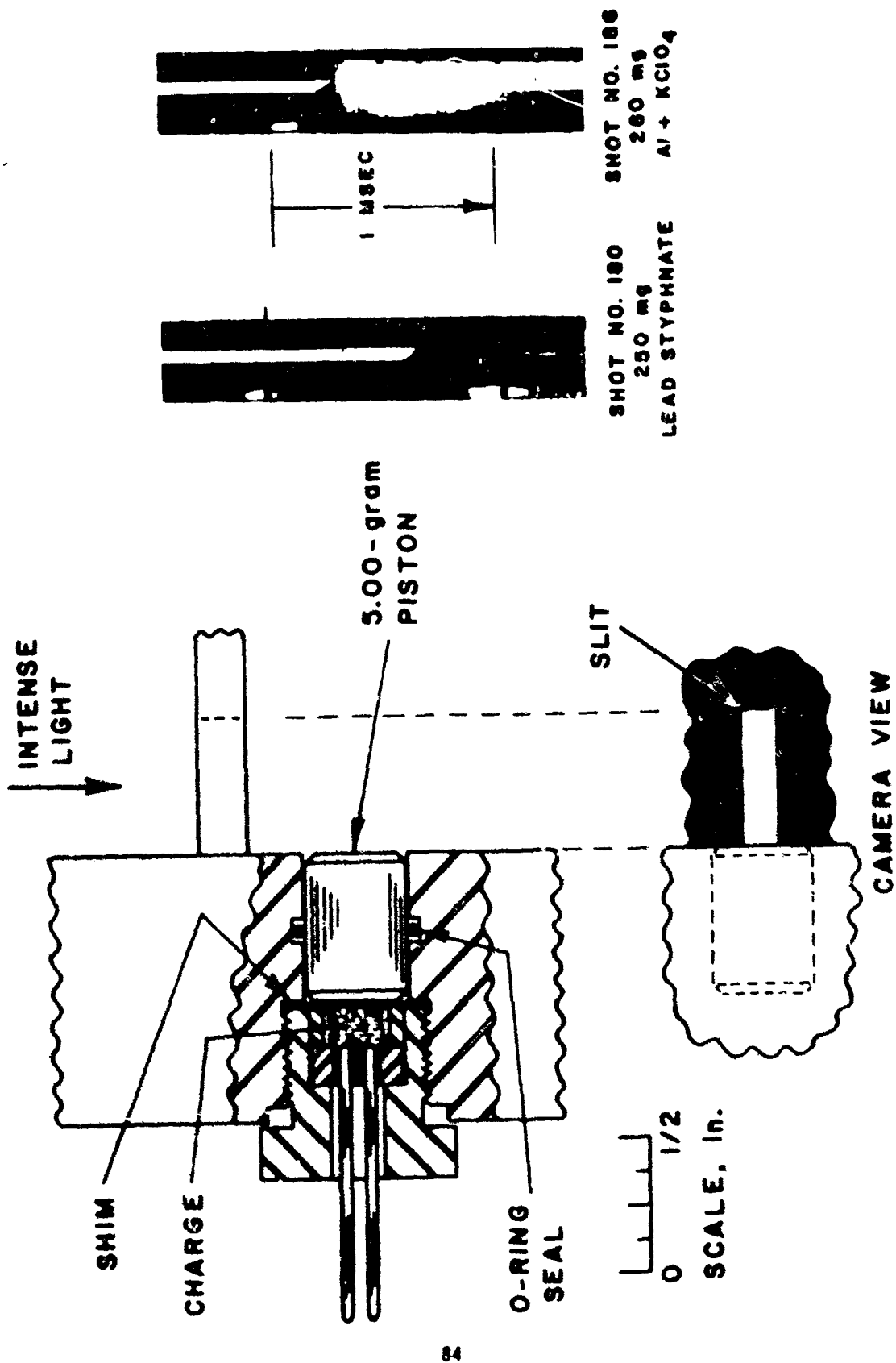


Figure 10 EXPERIMENTAL ARRANGEMENT FOR OBSERVATION OF PISTON MOTION

Figure 10 shows the presence of a shim which was held securely between the charge and piston by the actuator and breechblock hardware. The purpose of the shim, which was used on all pyrotechnic firings, was to provide a shot-start effect by delaying the motion of the piston until the charge had reacted more completely than would have been possible without a shim.

A brass shim was not used for the lead styphnate charges, because these were supplied as loaded actuators. The tops of the charge was sealed with a thin metal disc which provided the required shot-start effect.

#### Summary of Pertinent Output Data

The output characteristics of lead styphnate and selected pyrotechnic charges as measured by the piston displacement-time data are summarized in Table 15.\* The data show that the 280-mg  $16/9 \text{ Al} + \text{KClO}_4$  system, which contains  $2/3$  of the stoichiometric amount of aluminum, comes very close to duplicating the piston motion produced by lead styphnate in the first 0.15 in. of travel. This displacement is the region of most interest in valve actuator design. The volumes occupied by the 280-mg  $\text{Al-KClO}_4$  and 250-mg lead styphnate charges were identical.

Systems containing a stoichiometric or excess amount of aluminum, such as  $8/3 \text{ Al} + \text{KClO}_4$  or  $32/9 \text{ Al} + \text{KClO}_4$ , respectively, did not duplicate the piston motion produced by styphnate nearly

---

\* The lead styphnate charges were fired at a current of approximately 0.67 amp d.c.; the pyrotechnic charges were fired at 7 amp d.c.

Table 15

PISTON DISPLACEMENT-TIME DATA FOR SELECTED SYSTEMS<sup>a</sup>

System	Shot No.	Charge Weight, mg	Time, $\mu$ sec									
			at 0 in.	at 0.05 in.	at 0.1 in.	at 0.15 in.	at 0.2 in.	at 0.3 in.	at 0.4 in.	at 0.5 in.	at 0.6 in.	at 0.7 in.
Lead styphnate	190	250	0	17	27	35	42	54	65	75		
	190	250	0	17	29	38	44	57	68	79		
	209	250	0	15	25	33	40	54	66	76		
16/9 Al + KClO <sub>4</sub> (Batch 1)	149	260	0	17	31	42	52	69	84	97		
	150	280	0	15	29	40	50	67	82	94		
	186	280	0	17	30	41	51	67	81	94		
	181	280	0	19	32	43	51	67	81	91		
16/9 Al + KClO <sub>4</sub> (Batch 2)	210	280	0	17	32	45	57	80	96	113		
	211	280	0	15	29	41	51	71	89	103		
8/3 Al + KClO <sub>4</sub> (Batch 1)	182	280	0	21	35	47	58	75	90			
	187	280	0	19	35	47	57	77	94	108		
32/9 Al + KClO <sub>4</sub> (Batch 1)	147	275	0	27	48	64	77	99	117	133		
	148	290 <sup>b</sup>	0	21	35	48	59	80				
	152	500 <sup>b</sup>	0	14	27	38	48					
5/3 Al + NH <sub>4</sub> ClO <sub>4</sub>	183	250	0	19	31	41	49	65	74			
	193	250	0	16	31	43	52	69	85	96		
20/9 Al + NH <sub>4</sub> ClO <sub>4</sub>	145	230	0	30	47	57	66	80	90			
	146	250	0	21	36	48	59	73	86	97		
	189	250	0	19	32	42	51	66	78	88		
	184	250	0	22	35	48	58	74	89	102		
	27	450 <sup>b</sup>	0	10	18							
Nitroguanidine (+ Ignition charge)	151	160	0	22	39	52	63	85	103	114		
		(50)										

<sup>a</sup>For all systems except Lead Styphnate, a 0.002-in. thick brass shim was used as shot-start device (see Figure 10).<sup>b</sup>No charge holder.

as well, unless the charge holder in the actuator housing was removed to allow more charge to be loaded. Likewise, the 20/9 Al + NH<sub>4</sub>ClO<sub>4</sub> system did not perform as well, in spite of its very high calculated force constant in Table 14.

The last entry in Table 15 shows the results of the very little work which was done using explosives. The principle drawback with the explosives was that they were not ignitable with a hot bridge. Hence, a pyrotechnic ignition charge in contact with the bridge was required; for Shot No. 151 this charge was 50 mg of Al-NH<sub>4</sub>ClO<sub>4</sub>. The remaining volume in the actuator was loaded with 160 mg of nitroguanidine in two equal increments at a pressure of 10,000 psi; the pressed density of the nitroguanidine was 1.46 g/cc. Several other shots of a similar nature were also attempted, but in these the nitroguanidine wafers were found lying on the table after the shots were fired. Because of these problems and because the excellent performance of the pyrotechnics had already been demonstrated, further work with explosives was halted.

Experimental Determination of Force Constant from  
van der Waals Type Equation of State

The van der Waals equation of state for real gases is

$$\left[ P + \frac{a}{(V/n)^2} \right] \left( \frac{V}{n} - \beta \right) = RT \quad (11)$$

where

$a$  = a proportionality constant

$\beta$  = the covolume term

$n$  = the number of moles of gas

The term  $a/(V/n)^2$  is a measure of the attractive force between the molecules, and the covolume term is related to the volume occupied by the molecules of the gas. The number of moles of gas is proportional to the weight of propellant,  $m$ , hence

$$n = k m$$

Substitution of this expression into Equation 11 for  $n$  results in

$$\left[ P + \frac{a}{(V/m)^2} \right] \left( \frac{V}{m} - b \right) = \frac{n}{m} RT \quad (12)$$

where  $a = k^2 \alpha$  and  $b = k\beta$ . If it is assumed that equation 12 applies at the time the propellant has completely burned and that the burning proceeds adiabatically,  $T$  is the adiabatic reaction temperature and the right side of equation 12 is the force constant. Hence equation 12 reduces to

$$\left[ P + \frac{a}{(V/m)^2} \right] \left( \frac{V}{m} - b \right) = F \quad (13)$$

Equation 13 provides a means of measuring the force constant, as well as the van der Waals constants, from the piston displacement-time data. For each propellant system, three shots were selected and values of maximum pressure and total volume,  $V$ , at maximum pressure were substituted into Equation 13. The resulting three equations were then solved simultaneously to yield values of  $F$ ,  $a$ , and  $b$ .

The maximum pressure was calculated by graphically differentiating the displacement-time data twice to obtain the acceleration imparted to the piston, and then by applying Newton's Second Law:

$$P = \frac{f}{A} = \frac{m_p}{A} \left( \frac{d^2 s}{dt^2} \right) \quad (14)$$

where

$f$  = the force on the piston

$A$  = The piston across-sectional area,  
0.120 in<sup>2</sup> or 0.773 cm<sup>2</sup>

$m_p$  = the mass of the piston, 5.00 g

$\frac{d^2 s}{dt^2}$  = the acceleration

$s$  = the displacement of the piston

The volume at maximum pressure was calculated from the relationship

$$V = V_0 + A s_{mp} \quad (15)$$

where

$V_0$  = the internal volume occupied by the charge  
in the actuator

$s_{mp}$  = the piston displacement at maximum pressure

Typical graphical differentiations are shown for lead styphnate and Al-KClO<sub>4</sub> firings in Figures 11 and 12, respectively. These shots are the same two for which the original records were shown in Figure 10. In all cases, the displacement-time data were plotted in straight line increments, and the average slope (the velocity) of each increment was calculated. These velocities in turn were plotted and likewise connected in straight line increments, and now the acceleration of each increment was obtained.

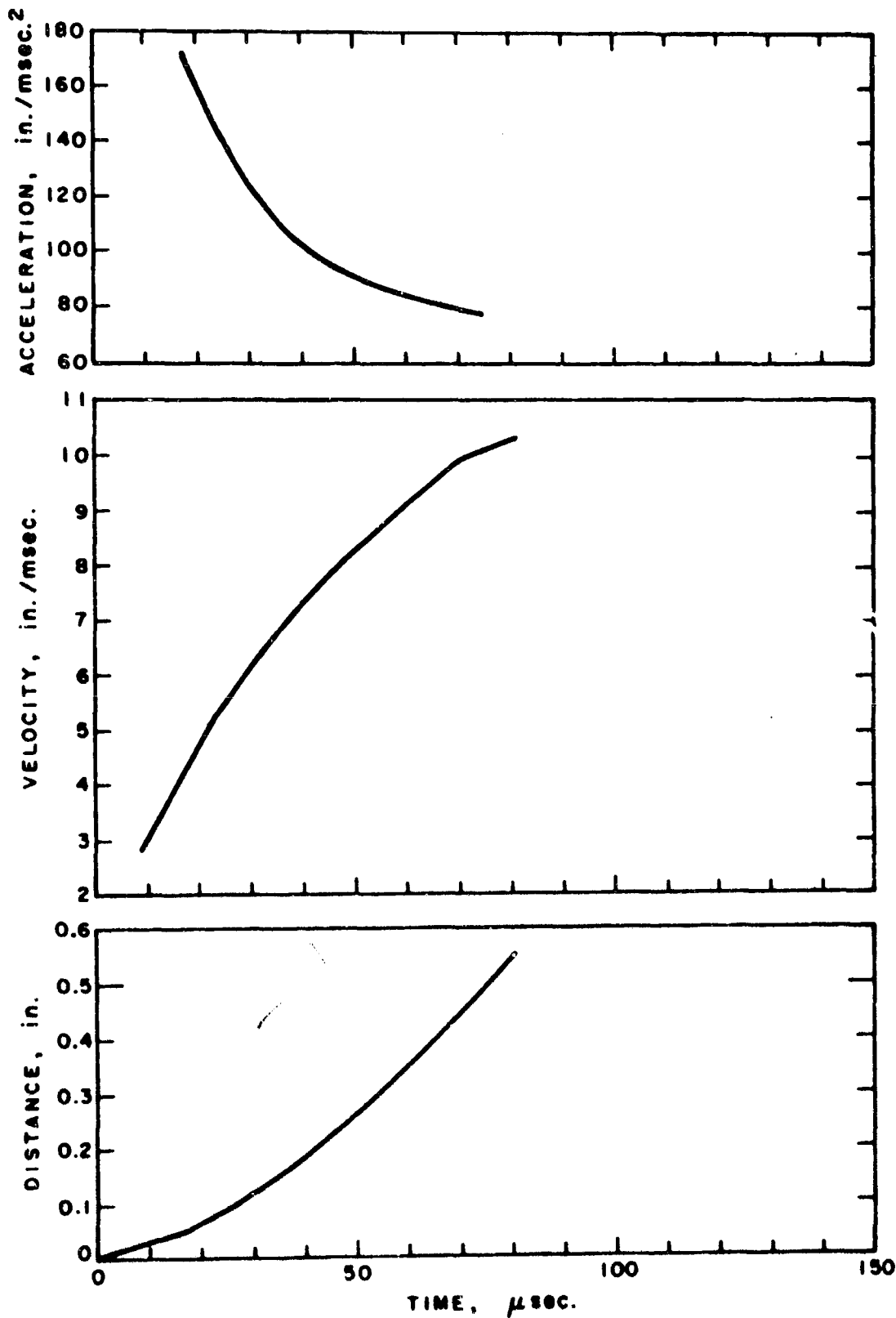


Figure 11

OUTPUT PERFORMANCE OF 250-mg LEAD STYPHNATE CHARGE  
(Data reduced from Shot No. 180)

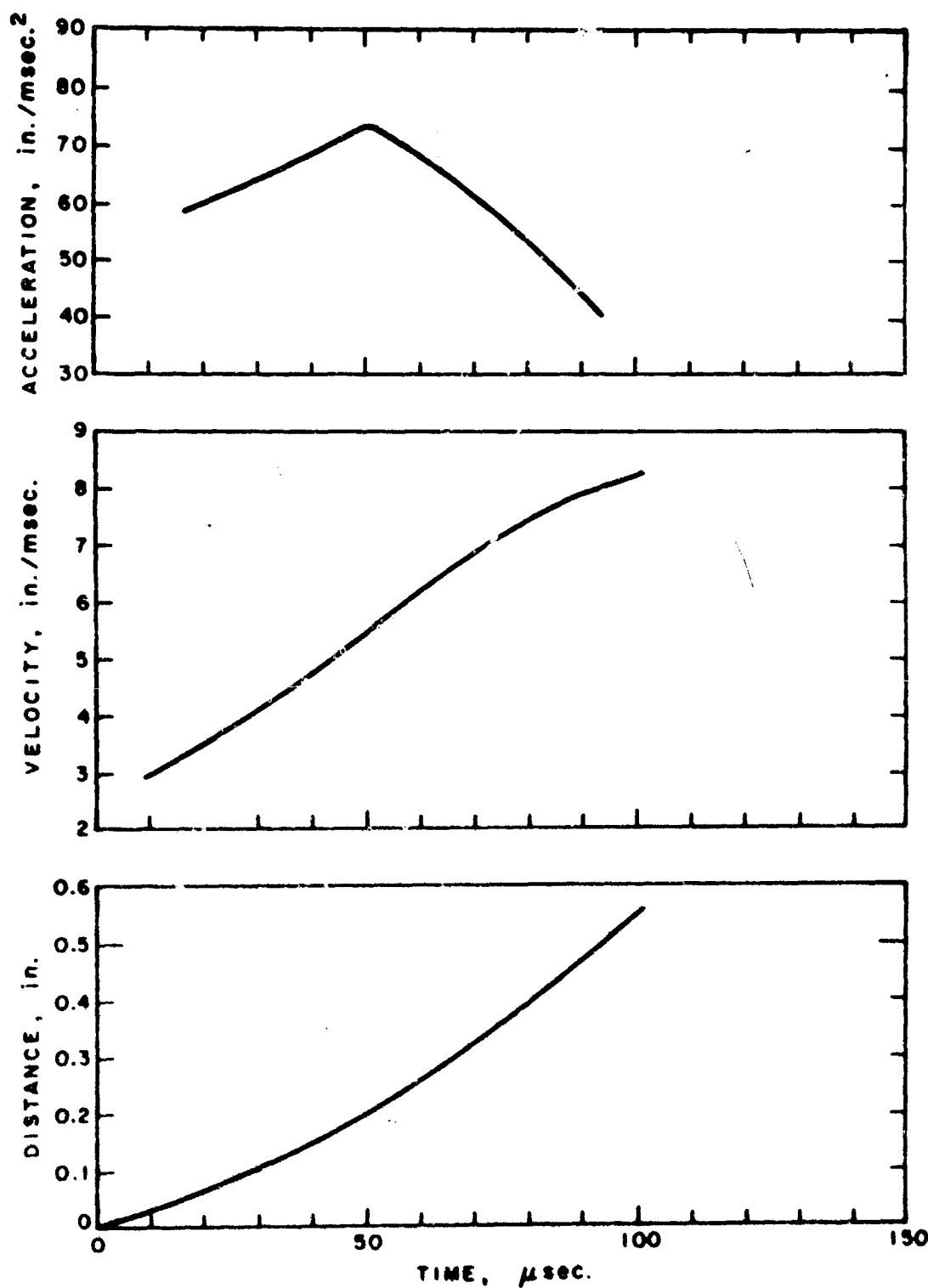


Figure 12  
OUTPUT PERFORMANCE OF 280-mg  $\text{Al-KClO}_4$  CHARGE  
(Data reduced from Shot No. 186.  
Mixture is 2/3 stoichiometric.)

The accelerations were plotted versus time, and the maximum acceleration and the displacement at this point permitted calculation of pressure and volume from Equations 14 and 15.

Table 16 shows the input data to the van der Waals equation for determination of force constant for each propellant system. The various quantities were calculated as outlined above, and charge weights were obtained from Table 15. From these data, the simultaneous solution of the three equations for each system gives the results which are summarized in Table 17. The experimental force constant so obtained is compared with the theoretical value which was calculated in Table 14 for an assumed equilibrium reacting at adiabatic conditions. For lead styphnate and  $16/9 \text{ Al} + \text{KClO}_4$  (2/3 stoichiometric), the agreement is very good. This indicates, for example, that the equilibrium for the pyrotechnic reaction as suggested in Equation 8 actually occurs experimentally. For lead styphnate, the dissociation of some of the gaseous species as indicated in Equation 7 to produce more moles of gas probably explains why the experimental force constant is slightly higher than the theoretical one.

The agreement for the two aluminum-rich systems,  $32/9 \text{ Al} + \text{KClO}_4$  and  $20/9 \text{ Al} + \text{NH}_4\text{ClO}_4$ , is not as good. The possible explanation here is that all of the aluminum does not react as predicted. This would lower the reaction temperature, which in turn would decrease the amount of gas produced by the reaction. Both effects would result in a smaller force constant value.

Table 16  
INPUT DATA FOR CALCULATION OF FORCE CONSTANT

System	Shot No.	Maximum Acceleration, in/msec <sup>2</sup>	Maximum Pressure, bars	Volume, V, at Maximum Pressure, cc	Charge Weight, m, mg	V/m, cc/g
Lead styphnate	180	172	2820	0.231	250	0.924
	190	162	2660	.330	250	1.320
	209	184	3020	.133	250	0.532
16/9 Al + HClO <sub>4</sub>	149	75.0	1230	.330	260	1.270
	150	73.1	1200	.330	280	1.179
	186	72.4	1187	.546	280	1.951
32/9 Al + HClO <sub>4</sub>	147	57.7	946	.428	275	1.557
	148	64.2	1053	.231	290	0.797
	152	58.9	966	.451	500	0.903
20/9 Al + NH <sub>4</sub> ClO <sub>4</sub>	145	115	1890	.428	230	1.841
	146	121	1980	.428	250	1.712
	184	125	1730	0.526	250	2.104

Table 17

## RESULTS OF FORCE CONSTANT DETERMINATION AND COMPARISON WITH THEORETICAL VALUE

System	van der Waals Constants		Force Constant, ft-lb/g	
	a, psi-cc <sup>2</sup> /g <sup>2</sup>	b, cc/g	Experimental	Theoretical (Table 14)
Lead Styphnate	87,900	0.265	482	407
16/9 Al + KClO <sub>4</sub>	70,300	0.321	294	332
32/9 Al + KClO <sub>4</sub>	34,800	0.350	164	327
20/9 Al + NH <sub>4</sub> ClO <sub>4</sub>	66,900	0.329	362	563

The validity of the van der Waals analysis rests on the assumption that adiabatic conditions prevail. In every case complete burning as measured by the time to maximum pressure occurred in 50  $\mu$ sec or less. This length of time was short enough to permit such an assumption.

#### Qualitative Observation of Burning Characteristics

The one observation which became very apparent in the van der Waals analysis was that the pyrotechnic mixtures consistently took longer to burn than the lead styphnate charges. This can be readily seen by glancing at Figures 11 and 12. Here, the burning time of the Al-KClO<sub>4</sub> as measured by the time to peak acceleration was about 50  $\mu$ sec, whereas that for the lead styphnate was about 17  $\mu$ sec. Variations in burning characteristics are believed partly responsible for the difference in times at various displacements in Table 15.

One factor which influences burning characteristics is the particle size distribution of the powders. It is recalled that two lots of  $\text{KClO}_4$  were evaluated, and that Batch 2 was a much coarser powder. Figure 13 shows a comparison of the performance of two  $\text{Al-KClO}_4$  mixtures at identical charge weights and using identical shot-start shims, but formulated from different lots. The burning characteristics of the two mixtures are appreciably different. The upper curves show that the coarser Batch-2 mixture (Shot No. 210) took almost twice as long to burn completely. The explanation is that the larger  $\text{KClO}_4$  particles require a longer time to react completely than do the smaller ones.

#### Conclusions from Output Studies

The overall conclusion based on the output studies is that the  $2/3$  stoichiometric mixture  $16/9 \text{ Al} + \text{KClO}_4$  offers a satisfactory solution to the problem of redesigning the actuator. This mixture in the first  $1/8$  in. duplicates the piston motion produced by the lead styphnate charge presently used in the actuator. This distance represents the displacement of most interest in actuator operation. Although the graphical double differentiation required for evaluation of the data has definite shortcomings, it did provide estimates of the pressure-time histories of the various propellants. These histories made it possible to infer something about the burning characteristics of the propellants under various experimental conditions, and to determine the force constant experimentally from a van der Waals

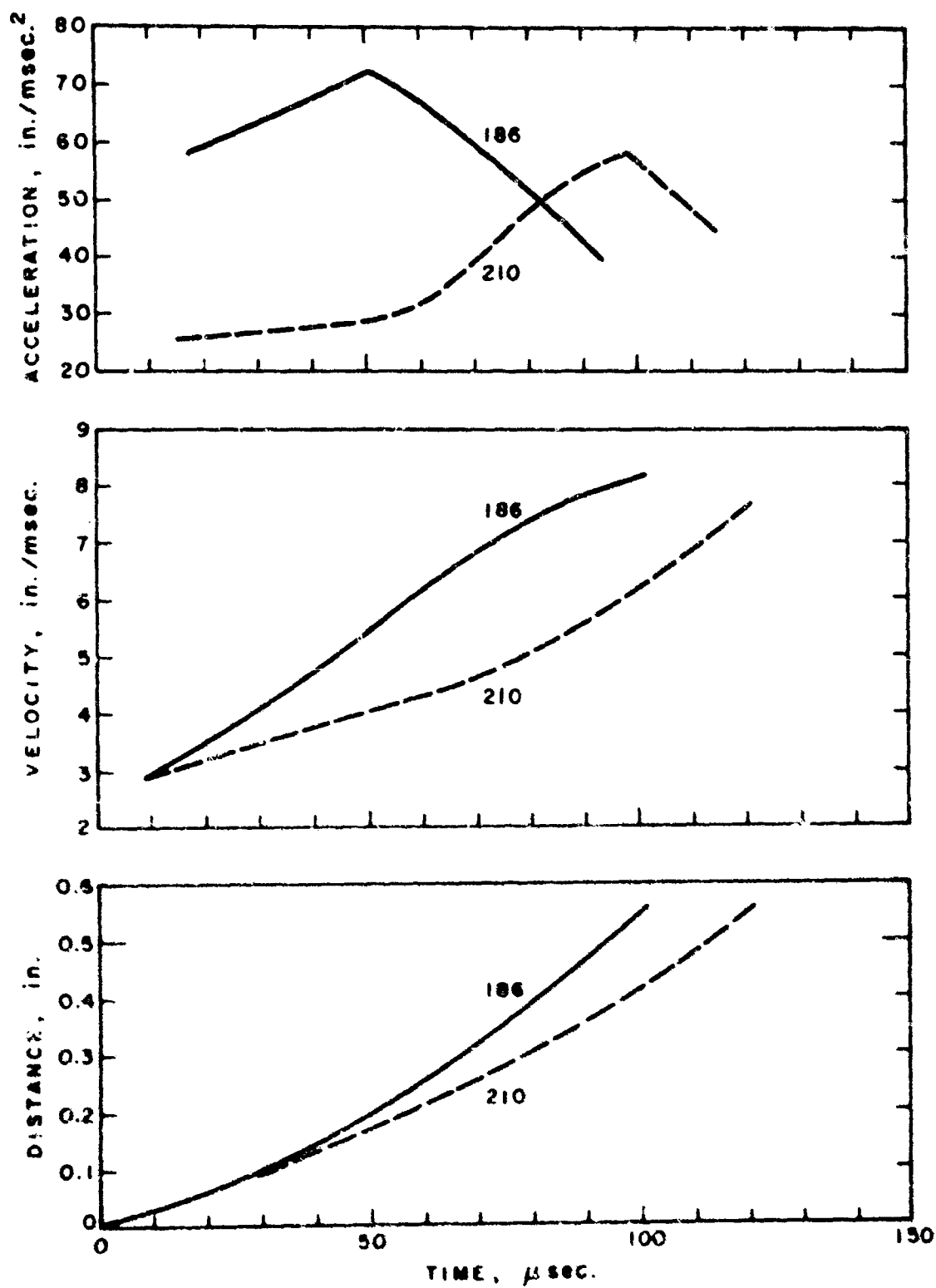


Figure 13

COMPARISON OF PERFORMANCE OF Al-KClO<sub>4</sub> MIXTURES

(Shot No. 186, Batch 1 KClO<sub>4</sub>;

Shot No. 210, Batch 2 KClO<sub>4</sub>)

equation of state. In future work, pressure-time will be measured directly using a high response pressure transducer. This would mean that a double integration would replace the double differentiation with a corresponding increase in accuracy. The effects of experimental variants such as particle size of the powders on the performance of the propellant could in this way be measured directly.

#### ACKNOWLEDGEMENTS

The authors are indebted to all personnel of IIT Research Institute and Sandia Corporation who assisted in the investigations discussed in this paper. IITRI personnel who contributed to the work included: Dr. Brian H. Kaye and Mr. Reg Davies, who performed the particle size studies; Mr. James A. Erickson, who performed the differential thermal analysis studies; Messrs. Douglas E. Baker, Kenneth W. Jones, Dennis W. Stombaugh, and Arthur L. Usher, who assisted in the constant current ignition studies; and Mr. James E. Daley, who assisted in the output studies. Sandia Corporation personnel who contributed to the work included: Messrs. Paul J. Langdon and William Thompson, who directed the electrostatic sensitivity studies and the development of the 5-amp, 5-watt no-fire initiators; Messrs. James Craig, Rex Steele, and Louis N. Tallerico, who formulated the requirements for the output studies and served as consultants to the work.

#### REFERENCES

1. Austing, James L., "The Initiation of Insensitive Explosives with Metal-Metal Oxides", Manuscript to be published
2. Kaye, B. H., Paint and Varnish Production 55, No. 9, p. 87, September 1965.
3. Austing, J. L., Kennedy, J. E., Chamberlain, D. H., and Stresau, R. H., "A Heat Transfer Study of Hot Wire Ignition of a Metal-Metal Oxide Mixture", Paper No. 3-8P, Proceedings Fifth Symposium on Electroexplosive Devices, The Franklin Institute, Philadelphia, June 1967.
4. Langdon, Paul J., "High Energy Initiators", AIAA Sounding Rocket Vehicle Technology Conference, February 1967.
5. Austing, James L. and Weber, John P., "Constant Current Ignition of Metal-Metal Oxide Mixtures", Paper No. 3-3, Proceedings Fifth Symposium on Electroexplosive Devices, The Franklin Institute, Philadelphia, June 1967.
6. Pitts, Locha D., "Electrical Probe Technique for Measurement of Detonation and Deflagration Velocities", Proceedings Fourth Symposium (International) on Detonation, ONR Report No. ACR-126, October 1965.
7. Glassner, A., "The Thermochemical Properties of the Oxides, Fluorides, and Chlorides to 2500°K", Report No. ANL-5750, U.S. Government Printing Office, 1957.
8. Perry, J. H., Ed., CHEMICAL ENGINEERS' HANDBOOK, Third Ed., McGraw-Hill Book Company, Inc. New York, 1950.
9. Brewer, L. and Searcy, A. W., J.A.C.S., 73, 5308, 1951.

1003(01)SR

Special Report

AN INTRODUCTION TO ADVANCED DELAY CORDS

Presented to

University of Denver  
Pyrotechnics Seminar  
13 August 1968

by

D. E. Olander

Explosive Technology  
Systems Division  
Fairfield, California

## An Introduction to Advanced Delay Cord

(Abstract)

D. E. Glander

Explosive Technology has developed a series of standard gasless delay cords with burning times ranging from 0.1 to 35 seconds per inch. Both aluminum and lead sheaths are available. Typically, a coefficient of variation of less than 3 percent for a 1-inch length of cord has been maintained.

Principal advantages of this new type of product are:

- (1) Elimination of density discontinuities and the resultant interface ignition problems.
- (2) Availability of delays for use by ordnance-item manufacturers who do not have delay capability.
- (3) Capability of envelope shapes other than the conventional small-diameter, long-length envelope.
- (4) Increased precision achieved through the statistical improvement experienced by long delay columns. The precision of a delay column improves at least in accordance with the square root of increase of column length.
- (5) Decreased gaseousness achieved through the use of smaller column diameters used for the faster delay cords.

Seven standard cord configurations are now available, and custom configurations are available upon special request.

## AN INTRODUCTION TO ADVANCED DELAY CORDS

D. E. Olander

Explosive Technology, Inc.

Historically, mankind develops, improves, and redevelops processes, theories, and items in interwoven spirals of sophistication. A potential answer to a problem or a step toward a new goal is discovered, and development is carried out to the satisfaction of the interested parties in relation to their time, place, and goal. Then at some later date, the concept is rediscovered and redeveloped at a more sophisticated level and perhaps in relation to a new, or at least more complex, goal. My organization's recent announcement of the availability of pyrotechnic cords embodying precise time delays is an excellent example of this historical spiral trend. The delay cords I refer to meet today's need for precise timing normally found in pyrotechnic columnar increments, while re-imparting the longitudinal flexibility offered by the now-unsophisticated fabric fuzes.

The first pyrotechnic time delay to be formally developed and manufactured was undoubtedly the black-powder fuze. This early fuze was merely a piece of string impregnated with black powder. Later development - a part of a new spiral - brought about fabric-sheathed black-powder fuzes. Their limitations, however, were great - so great that an incremental fuze was developed, consisting of a column of black powder pressed into a sleeve. The design controls and the widespread applications offered by the delay-cartridge concept allowed - actually led to - a new realm of development. Research and development brought about a whole new family of gas-less pyrotechnic delay compositions pressed into cartridges of various designs.

The past 20 years have seen the development of a large number of different compositions in the gasless pyrotechnic realm. During the Korean war, this type was produced in various compositions and columns with remarkably high precision in large quantities, i.e., 2 to 3 million units of any given design. Since that time, however, production of delays in significantly larger

quantities has been relegated to a few isolated cases. In greater demand today are pyrotechnic time delays produced in small quantities, perhaps no more than a few hundred, for highly specialized applications. These delays are more reliable under environmental extremes, including much higher temperatures, and assure longer storage life than those previously manufactured.

Many of today's applications, however, do not lend themselves to the conventional pressed column delay configuration. Often the spaces available are short with allowance for a large diameter rather than for the long-length, small-unit diameter that was so prevalent during the Korean war. To meet this new demand, certain limited-edition delay cords have been made in the industry. Such tentative approaches have invariably used lead sheathing because that is the principal material used for explosive cords. Always, the pyrotechnics manufacturer has assembled these cords into units and, for their applications, performance has been satisfactory. But the nature of the compositions used has required a great deal of knowledge of the exact performance phenomena and design parameters inherent to the cord being used. As a consequence, these were not products that could be disseminated to other manufacturers for incorporation into independent units. We, therefore, decided to attempt development of a series of delay cords that could be supplied as components to organizations wishing to incorporate them into larger units of advanced design.

To be successful in this endeavor, we saw that we would have to develop materials that were gasless, were not detonable, and that could be handled under normal atmospheric conditions. In addition, the sheath material would have to be one that would provide geometrical stability and be easy to machine. It was also obvious that the precision of such delay cords would have to be competitive with that of well-controlled pressed delay production line products. We established quantitative design goals

of 4 milliliter per gram at standard temperature and pressure as an upper limit of gaseousness that would be permitted in a delay composition, and 3 percent coefficient of variation for burning rate through a 1-inch length of delay cord.

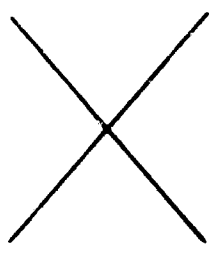
This 1-inch length is very important to predictable reliability and for specification of precision because of the increased accuracy that is obtained in longer lengths. Statistically, the standard deviation of a timed event will increase in proportion to the square root of the number of events that are put in sequence. Therefore, if the number of events are represented by "n" and the variation from the mean is the square root of "n", precision is enhanced by the square root of "n". From that, one can ideologically anticipate that the increase of precision of a delay can be no worse than the square root of the increase in the column length itself. Of course, ignition and end effects influence the burning time of a delay column, but these occur only once each time. The longer the delay column, therefore, the greater the potential accuracy.

Gas evolutions are determined in our laboratory by a simple method. We burn a composition sample in a small bomb, which after burning is placed in a bath at 145°C, to assure complete vaporization of the water generated during burning. The pressure is read and, using ideal gas laws, the gas evolution is ascertained at standard temperature and pressure.

We have produced a variety of delay cords of dependable burning times ranging from 0.1 second per inch to 35 seconds per inch.

Typical gas evolution, coefficient of variation, and burning times at various temperatures of these cords are shown in Table 1. The data in Table 1 indicates that our basic design objectives have, in the main,

Table 1. Cord Functioning Parameters.

Sheath Material	0.2 Second/Inch	3 Seconds/Inch	15 Seconds/Inch	35 Seconds/Inch
Aluminum	Temp $\bar{X}$ (ms) C.V.% 75 215.3 2.86 165 214.4 3.2 -65 219.7 4.4 Gas Evolution = 1.4 ml/gm	Temp $\bar{X}$ (sec) C.V.% 75 3.07 1.2 Gas Evolution = 4.5 ml/gm	Temp $\bar{X}$ (sec) C.V.% 75 13.99 3.0 165 11.63 1.8 -65 14.48 2.6 Gas Evolution = 3.8 ml/gm	Temp $\bar{X}$ (sec) C.V.% 75 33.95 2.6 -100 38.88 1.6 Gas Evolution = 3.8 ml/gm
Lead (Pb)	Temp $\bar{X}$ (ms) C.V.% 165 213.8 1.4 -65 213.9 3.0 Gas Evolution = 1.4 ml/gm		Temp $\bar{X}$ (sec) C.V.% 75 13.72 2.8 165 12.47 3.6 -65 15.11 2.4 Gas Evolution = 0.3 ml/gm	Temp $\bar{X}$ (sec) C.V.% 75 31.81 2.3 165 34.99 2.5 -65 29.47 0.66 Gas Evolution = 4.0 ml/gm

been achieved. The only coefficient of variation listed greater than 3 percent is at 165°F with the 0.2000 second/inch cord. In this burning rate realm, maintaining a 3 percent coefficient of variation, in using pressed delays at high temperature, is difficult.

All time ranges are at least as precise as normally expected, using high-quality production techniques. The gas evolution for the 3-second cord, however, is greater than the goal of 4 milliliters/gram. The gas evolution for this range could be held at our goal if we used a cord containing either a tungsten or a molybdenum composition. In fact, we could make satisfactory lead-sheathed cords in such a range, using such compositions. The superior temperature coefficient of delay materials containing chromium, however, is so great that we have selected them instead of the tungsten or molybdenum compositions. The temperature coefficient of most delays is approximately .08 percent per degree Fahrenheit, but the typical chromium delay exhibits only about .04 percent per degree Fahrenheit. The use of such gaseous material would seem questionable were it not for the small diameter of the delay column. Although it may be possible to press columns of very small diameter and of significant length, it has not been the usual practice, and would appear to be quite difficult to achieve. As a result, the typical pressed delay column would have about eight times as much material per unit length (in comparison with cord delays). Therefore, on a unit/length basis, we have more than achieved the equivalent of our design goal of 4 milliliters/gram.

The coiling and bending of such cords have not significantly affected their precision. Therefore, the small size allows the fuse designer to build better precision into his unit by using, for example, a coiled piece of 3-second cord instead of a pressed column that is only 1 inch long.

Table 2 compares various delay time elements. Typical values for burning time and gas evolution are listed. A standard deviation consisting of

Table 2. Comparison of Cord\* vs Column\*\* Delays.

\* 3 second/inch delay cord.

\*\* Standard pressed-column delays.

Delay	$\sigma$ of a 3-second/inch Cord	$\sigma$ of a 1-inch (long) Column	$\pm 3 \sigma$ -65°F to +160°F		Ratio of Cord $\sigma$ to Column $\sigma$
			Cord	Column	
3 Second	3.0 %	3.0 %	18.2 %	18.2 %	1:1
10 Seconds	1.73 %	3.0 %	14.4 %	27.4 %	1:1.9
20 Seconds	1.15 %	3.0 %	12.7 %	27.4 %	1:2.2
30 Seconds	0.95 %	3.0 %	12.0 %	27.4 %	1:2.28
40 Seconds	0.82 %	3.0 %	11.7 %	27.4 %	1:2.34

3-percent (for a 1-inch length), along with perfect ignition and actuation are assumed. In addition, the effects at extremes in temperature are shown because of the smaller change of burning time with changes of temperature of this delay material compared to slower burning delay materials.

The ratios shown in Table 2 clearly indicate that a design using a coiled cord has the capability of reducing the overall ranges of delays in this realm by half. Of course, each range and each design must be evaluated separately, but the trends in Table 2 should be generally valid.

Let us compare the vent space requirements using the smaller cord sizes with those required for conventionally pressed delays that feature the common 0.203-inch column diameter, using 750 psia, and 4.0 milliliters/gram as the conventional column design parameters. The details of the calculations are summarized in Table 3. Column 2 lists the typical specific gas evolutions of the material used; Column 3 presents the weights of material per inch in cord, and those of the conventional (pressed) column. The gas evolutions of cord and of columns per inch of length are shown in the fourth column. For these calculations, an average temperature of 546 degrees Kelvin is assumed. Column 5 lists the first-fire gas that must be added; Column 6 lists the recommended vent space for cord and columns, and Column 7 gives the ratio of vent space of cord to vent space of columns. The advantage of cord in this connection is obvious. Of course, in the design of complete units, vent space must be allocated for the gaseous products of the ignition source.

It can be seen that basic objectives have been achieved - that is to manufacture delay cords that compare in performance with pressed delays. Seven standard cords are now in stock. These cord configurations are shown in Table 4. The physical dimensions of the cords dictate the types of delay

Table 3. Comparative Gas Evolutions.

1 Delay Time (Second)	2 Specific Gas Evolution (In milli- liters per gram)	3 Height of De- lay per Inch (grams)		4 Gas Evolution per Inch (milliliters)		5 Gas From First-fire (milliliters)		6 Minimum Vent Space (cubic inch)		7 vent-space Ratio (Cord to Pressed Column)
		Cord	Pressed	Cord	Pressed	Cord	Pressed	Cord	Pressed	
0.200	2	0.231	3.81	0.462	7.61	0	0	.0055	.0091	1 : 16.5
3	5	0.352	3.02	1.76	5.1	0.21	1.8	.0047	.090	1 : 5.5

Table 4. Standard Delay Cords.

Burning Time in Seconds per inch	Outside Diameter (Nominal)	Inside Diameter (Nominal)	Sheath Material	Minimum 180-degree Bend Diameter
0.200	0.100 in.	0.050 in.	Aluminum	0.064 inch
0.200	0.100 in.	0.050 in.	Lead	0.032 inch
3.000	0.150 in.	0.071 in.	Aluminum	0.050 inch
15	0.500 in.	0.264 in.	Aluminum	—
15	0.500 in.	0.264 in.	Lead	—
35	0.500 in.	0.256 in.	Aluminum	—
35	0.500 in.	0.256 in.	Aluminum	—

elements that can be designed. The 0.10-inch and the 0.15-inch-diameter cords can be bent very sharply as indicated. Specifically, the figures given represent the limit of capability of the respective cords to sustain a 180-degree bend around a mandrel.

In designing units, it is recommended that somewhat less sharp radii be selected, especially in helical designs. The larger cords appear to be impractical to bend, although they are easily machined -- especially those with aluminum sheathing. They can be faced off and counterbored on a production basis and given whatever external configurations the designer requires. Naturally, cutting oil cannot be used and care should be taken to prevent excessive quantities of pyrotechnic waste. It is recommended that the machined pieces be transferred to desiccated storage as soon as practical.

The chromium and tungsten delay cords require a first-fire. This first-fire can be added to the cords by any of several means: For instance an increment of first-fire cord can be pressed against the surface of the pyrotechnic core exposed at the end of the delay cord.

The Explosive Technology first-fire is a proprietary product for which a patent is pending. It has approximately 50 percent greater output than the well-known AlA mixture and is much safer to handle. Surprisingly, the autoignition temperature, determined by means of differential thermal analysis, is 732°C. Its static sensitivity is slightly less than one joule, and it is insensitive to standard impact and friction tests.

#### Advantages of Delay Cords

A principal advantage is that no density discontinuity occurs in contradistinction to pressed columns. One would therefore expect a greater reliability than that experienced with pressed columns because of freedom from interface ignition problems as well

as the lack of relatively unconsolidated and therefore weaker center sections of pressed increment.

In the realm of advanced design, standard delay cords afford several advantages. The most important is the availability of shelf-stock delays for application in small or large production quantities, and also for the use by ordnance designers whose organizations do not make their own delay formulations and components. Of special advantage to aerospace and defense rocketry are the bends that can be applied in fast-burning delay cords, thus permitting the optimum use of space available. In many applications the cost of a unit that has been designed with delay cord in mind can be considerably less than that using a conventional multi-increment, pressed delay column. The longer the delay column used in the comparable pressed unit, the more the economic advantage of delay cord is realized. Of course, the basic, accurate delay, using cord, is obtained at lower cost because it is inherently less costly to make a long cord using our manufacturing techniques than it is to press multiple pyrotechnic increments.

#### Delay Cord Limitations

As is so often found in our discipline, no single development offers a panacea. We do not feel that delay cords in lengths the order of 1/4 inch are practical. One or two increments of delay material is usually more economical to press and might prove slightly more accurate.

Although lot-to-lot variation of the mean burning time is not greater than 10 percent, good design practice should allow for lot-to-lot variations.

While we have made pressed delays that burn as fast as 60 milliseconds per inch, we have been unsuccessful in our attempts to produce delay cord that burns accurately if it is significantly faster than 100 milliseconds per inch.

### Delay Cord Application Design

Delay cord affords additional flexibility for fuze train designers; yet standard, good pyrotechnic design practices must prevail as always. First, a proper vent space must be maintained in an internally vented item. Normally, it is poor practice to pressurize this vent space to over 750 psi.

As noted earlier, with all but the very fast delay cords, a first-fire properly interfaced with the delay material, is still required.

The slower and large-diameter delay cords require provision for ash retention, although fortunately this is not required in the smaller diameter, fast delays. Without a proper ash retainer, variability can be expected. Generally, fast-burning pyrotechnic delays require some sort of mechanical retention at each end of the column. The fact that in delay cord it is not required is surprising, at first, but when one considers the small cross-sectional area of the core of fast-burning delay cord, the lack of a need for additional retention for significantly long cord lengths can be at least intuitively understood.

If sensitive materials such as lead azide and lead styphnate are placed on the output side of a delay cord, and a high-pressure internal vent is being maintained, a gas stop is necessary to prevent complete gas passage from the vent through the unburned column, which will initiate the sensitive material. This is no different, of course, from any standard pressed delay, but it has, in the past, been a problem in some designs.

In summary, we in the pyrotechnics field now have an additional time delay fuze family available for a variety of applications. This new family, in the form of linear, metal-sheathed deflagrating compositions, is expected to find extensive application by the technological community. It answers a broad spectrum of problems related to today's design requirements.

SPECTRAL OBSERVATIONS IN ILLUMINATING FLARES

Bernard E. Douda  
U. S. Naval Ammunition Depot  
Crane, Indiana

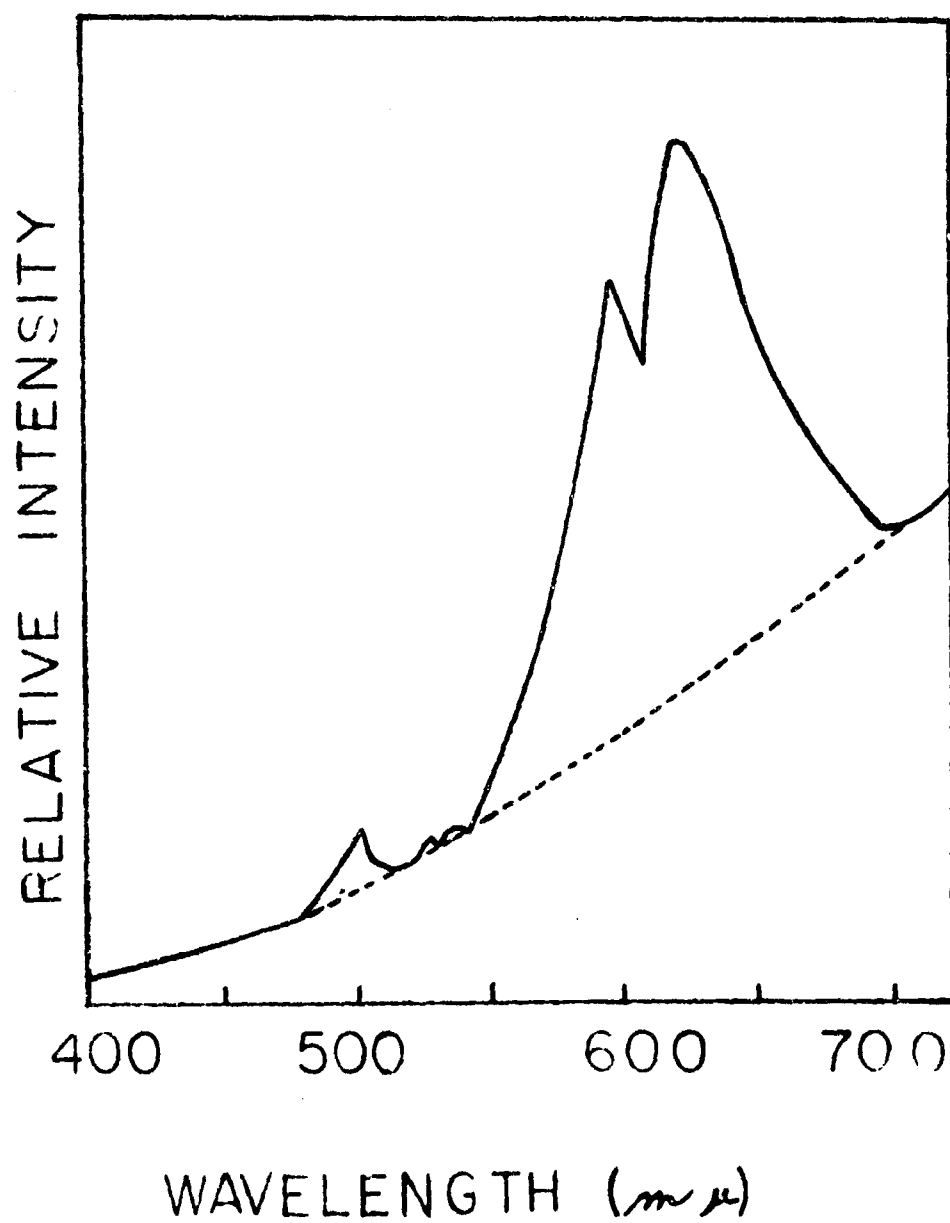
## SPECTRAL OBSERVATIONS IN ILLUMINATING FLAMES\*

Bernard E. Douda  
U.S. Naval Ammunition Depot  
Crane, Indiana

The purpose of this presentation is to describe some of the progress being made toward the interpretation of the spectral features of an illuminating flame utilizing theories developed to explain the shape and shift of spectral lines. The illuminating flame being studied is that which is produced from combustion of magnesium, sodium nitrate and some binder. Such a flame produces an enormous amount of luminous energy. To study the distribution of that energy, we took spectra both with a scanning spectrometer and a grating spectrograph.

The spectrum on the next page was taken with a Perkin-Elmer Model 108 Scanning Spectrometer operating at 30 scans per second.<sup>(1)</sup> As you can see, the spectrum of the flame shows a strong broad continuum distributed about the sodium resonance line. This continuum is superimposed on a weaker background continuum which extends throughout the visible region. The sodium related continuum, which may in fact be the broadened sodium D lines, extends from about 5500 angstroms to 7000 angstroms.

\*Presented at Pyrotechnics Seminar 12-16 August 1968, Estes Park Colorado sponsored by the Denver Research Institute, Mechanics Division, University of Denver, Denver, Colorado, 80210, Mr. R.M. Blunt, General Chairman.



Some absolute energy measurements have been made on this flame. Of the total energy produced by the combustion reaction, we find 11 percent in the visible region. Also, there is 17 percent of the total radiated energy in the visible. The effective emitting temperature of the flame is in the neighborhood of 2900°Kelvin. If we separate the background region from the region about the sodium D lines, we find that about 45 percent of the energy in the visible is around the resonance lines, whereas the background is composed of about 55 percent of the total energy in the visible. It might therefore be said that sodium alone accounts for 45 percent of the energy in the visible. If we correct this information for the eye response, the sodium feature becomes even more important.

Next I will show you a different form of the same spectrum which was taken with a 1.5 meter grating spectrograph which has a dispersion of 15 angstroms per millimeter. The slit opening is about 10 microns. All of these spectra may be found in Blunt's report as Plates 2, 4, 6, 8 and 9 of reference 2. One important feature to notice is the drastic reduction in the background continuum region as one goes from pressures of 630 torr down to 20 torr. At the same

time, a narrowing or lessening of the continuum region around the sodium resonance lines is also observed. Furthermore at about 150 torr, one clearly sees the band head which is formed near 5500 angstroms.

The band head at 5500 is as yet unexplained, a shift of the sodium D line towards the red region is predicted but as yet has not been observed experimentally in these flames. The reduction in the background intensity and the narrowing of the continuum above the sodium resonance lines is attributed to two conditions. First, at atmospheric pressures, the flame is not optically thick or thin. It can be described as being somewhere inbetween. As the pressure is reduced, the flame changes from a tendency to be optically thick toward an optically thin condition. This change, in theory, should cause a lessening of the sodium line broadening. In addition, one can speculate that a flame temperature reduction accompanies the change from an optically thick toward an optically thin system. In accordance with Planck's function a reduction in temperature will cause a reduction in the background continuum.

This concludes the description of the flame spectrum itself. Next, I will review the theories of spectral line

formation which may help to explain why the sodium D line region assumes the form that it does.

One of the objectives of this work is to determine the nature of the interaction which causes the continuum about the sodium resonance lines to be so strong and broad. Thus, let us examine the processes which contribute to the formation of a spectral line of a gas.

- (1) Natural line broadening is due to the finite lifetime of the excited state.
- (2) Doppler broadening is due to the motions of the atoms.
- (3) Lorentz broadening is due to collisions with foreign gases.
- (4) Holtsmark broadening is due to collisions with other atoms of the same kind.
- (5) Stark broadening is due to collisions with electrons and ions.
- (6) Instrumentation broadening is that due to the apparatus utilized in the experiment and measurement of the spectral line.

Because of the low temperature involved and information provided by Gaydon,<sup>(3)</sup> the Stark effect will be neglected because of its small contribution. Because the Lorentz and Holtsmark broadening theories both deal with collision, no further distinction will be made in the remainder of this paper and both will be included under the term Lorentz broadening.

If for the moment we neglect the problem of instrumentation broadening, we can, at this point, say that our line is composed of natural, Lorentz and Doppler components. These individual profiles can be folded together through a convolution integral to give the Voigt profile. I have listed the analytical representations of each of these profiles in the appendix. For further information one should consult Mitchell and Zemansky<sup>(4)</sup> and Breene.<sup>(5)</sup>

The important thing to know about these distributions is that natural line broadening is a function only of the lifetime of the atom in its excited state. The Doppler profile is a Gaussian distribution which is a function of only the temperature and molecular weight of the atoms. It is not a function of the concentration of the atoms in the gas. The general analytical form of the Lorentz distribution is the same as that for the natural broadening coefficient. However, the Lorentz broadening profile is a function of temperature, particle molecular weight, and concentrations of the colliding particles. These variables are utilized to compute a Maxwellian distribution of velocities along the lines of classical kinetic theory. The Lorentz line width is derived from this distribution and the effective velocity cross section. All these parameters are needed to evaluate the Voigt profile.

If we review the literature concerning natural line, Doppler, and Lorentz broadening, we find that at reasonably low pressures and low concentrations, these effects often total to less than one angstrom of line broadening. Furthermore, because each of these distributions is symmetrical, they can not account for line shift or asymmetry.

Let us for the moment neglect the possibility of line shift or line asymmetry and consider only how we might explain a 1000 angstrom broadened sodium doublet whereas the theory we just reviewed might at best account for a few angstroms broadening. The reason for this, is that all of the theories are developed for systems which approach the optically thin condition. In contrast to this, we know that the flame from an illuminating flare is neither optically thin nor optically thick and that there is a gross temperature gradient over the cross section of this flame. This means that the theory developed for optically thin systems is not valid and also that since thermodynamic equilibrium does not exist as evidenced by the non-Planckian spectral distribution, we also cannot apply the radiation theory suitable for optically thick equilibrium systems. Clearly then, there is a need for a new function. Such a function must play the same role in our non-equilibrium radiation transfer problem as does the Planck function to equilibrium situations.

Let us call this new function a source function and define it as the ratio of emissivity to opacity. In this fashion, we include the notion of thinness to thickness ratio. The source function therefore is the primary quantity in non-equilibrium theory. It is a function of position, the radiation field and the atomic level population

Before we go further, let us consider what essential physical mechanisms we must include in our model. First, photons are fed into the line by collisional excitation to the upper level and leave the line ultimately either by escaping from the atmosphere or by being reconverted into kinetic energy through collisional de-excitation of the upper level. Secondly, photons experience slight changes in frequency in non-coherent scattering, so that photons created near the line center can diffuse into the line wings where the opacity is less and the mean free path is greater. Therefore, this so called non-coherent scattering is important since it sets the scale of variations in the radiation field by controlling the distribution of mean free paths. A number of mechanisms cause non-coherence. The most important for our flames are associated with Doppler and collision broadening.

The next step is to express the source function in terms of the radiation field such that in the limit of optical

thickness, the source function becomes the Planck function. Included in this function is a term which defines the probability per scattering that a photon is lost from the line, its energy going back into kinetic energy. In general, this probability term will depend on depth in the flame and represent the influence of the rest of the flame on the line in question.

Finally, we need to express the source function in terms of the rate that the intensity in the radiation field is varying with the thickness of the flame. Once again the intensity here is a function of frequency and the direction of propagation of the photons. After it has been mathematically manipulated into convenient form, it is this transfer equation that we hope to use to interpret the broadening observed around the sodium resonance line. I hasten to add that although the solution of this problem is not simple, it is not hopeless. Hummer<sup>(6)</sup> has already successfully used this radiative transfer theory to solve problems in stellar atmospheres. The notions associated with the radiative transfer problem and the mathematical algorithm which I presented follow closely the approach taken by Hummer.

The graphs on the next page are included to illustrate how the radiation transfer theory coupled with broadening theory

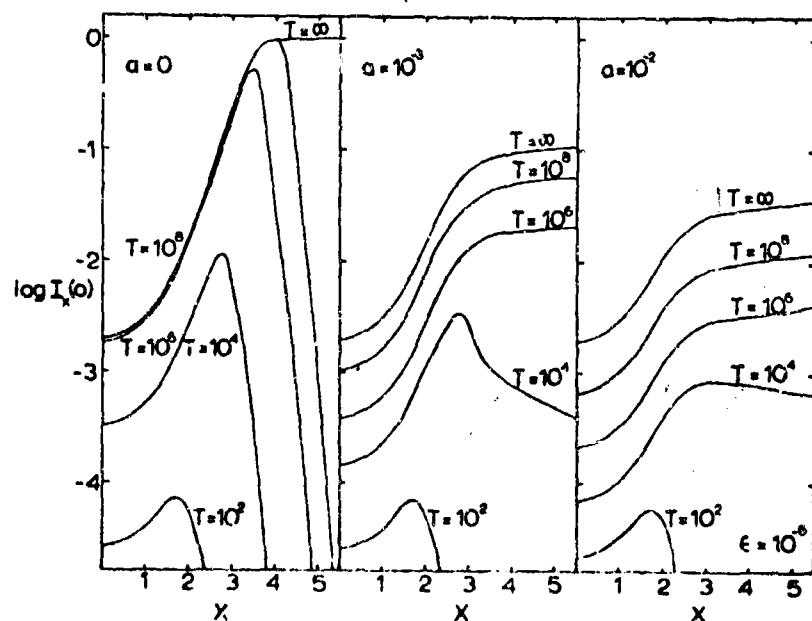


FIG. 5. Normally emergent intensities for atmospheres with  $B = 1$ ,  $\epsilon = 10^{-6}$ , and various values of  $T$ , with  $\alpha = 0, 0.001$  and  $0.01$ .

From: J. Quant. Spectrosc. Radiative Transfer, Vol 8,  
193-217, (1968)

might be used to describe the spectral features in the flame.

The plots are line intensity,  $I$ , against frequency,  $\chi$ .

$T$  is a measure of optical thickness and " $a$ " is the ratio of collision to Doppler broadening. All panels are plotted for  $\epsilon = 10^{-6}$  where  $\epsilon$  is the probability per scattering that a photon is lost from the line.

The left panel shows the line in the Doppler broadened form only. Note the self-reversed emission form at the line center and the line broadening as a function of optical thickness. As the ratio of collision to Doppler broadening increases, we see in the second and third panels that the lines become extremely broad, with a characteristic kink at the frequency where the transition from Doppler to collision broadening occurs. Some of these shapes are remarkably similar to the line shape recorded in our flame.

In conclusion, it is important to understand that this is not the end of a study but is only a meager beginning. The approach is not one which involves the derivation of an entirely new theory. Rather, for the first time, we are attempting to adapt radiative transfer and line broadening theory to explain the behavior of the broadened region around the sodium D lines. The theory has potential for describing line changes due to Doppler and Lorentz broadening as well

as those due to the non-equilibrium nature of the flame. Thus it appears quite probable that this approach will not only allow us to describe the flame features more completely but also will allow us to learn more about the flame in terms of its optical properties, temperature and spectral distribution with position in the flame, particle concentration and other parameters.

#### REFERENCES

1. George Laramore and Duane M. Johnson, "A Method for Determining the Effective Emitting Temperature of a Radiating Body", RDTR No. 44, USNAD Crane, Indiana, August 1964.
2. R. M. Blunt, "Evaluation of Processes Occurring in Pyrotechnic Flames", RDTR No. 91, USNAD Crane, Indiana, March 1967.
3. Gaydon, A.G. and Wolfhard, H.G., "Flames; Their Structure, Radiation, and Temperature," Chapman and Hall, London, 1960, p. 304.
4. Mitchell, A.C.G. and Zemansky, M.W., "Resonance Radiation and Excited Atoms", Cambridge University Press, London, 1961.
5. Breene, R.G., Jr., "The Shift and Shape of Spectral Lines," Pergamon Press, New York, 1961.
6. Hummer, D.G., "Summary-Introduction to Radiative Transfer Problems in Stellar Atmospheres", J. Quant. Spectrosc. Radiat. Transfer, 8, 193-217 (1968).

## APPENDIX

### 1. NATURAL LINE PROFILE

$$k_{\nu_N} = \frac{1}{1 + \left[ \frac{2(\nu - \nu_0)}{\Delta \nu_N} \right]^2}, \quad \Delta \nu_N = \frac{1}{2\pi\tau}$$

### 2. DOPPLER PROFILE

$$k_{\nu_D} = k_0 e^{-\left[ \frac{2(\nu - \nu_0)}{\Delta \nu_D} \sqrt{\ln 2} \right]^2}, \quad \Delta \nu_D = \frac{2\sqrt{2R\ln 2}}{c} \nu_0 \sqrt{\frac{T}{M}}$$

### 3. LORENTZ PROFILE

$$k_{\nu_L} = \frac{\text{const.}}{1 + \left[ \frac{2(\nu - \nu_0)}{\Delta \nu_L} \right]^2}, \quad \Delta \nu_L = \frac{Z_L}{\pi}$$

$$Z(T, \sigma^2) = 2Nn\sigma^2 \sqrt{2\pi RT \left( \frac{1}{M_1} + \frac{1}{M_2} \right)}$$

### 4. VOIGT PROFILE

$$k_{\nu_V} = \frac{2k_0}{\pi(\nu_0 + \Delta \nu_L)} \int_{-\infty}^{\infty} \frac{\exp - \left[ \frac{2\delta}{\Delta \nu_D} \sqrt{\ln 2} \right]^2}{1 + \left[ \frac{2}{(\Delta \nu_N + \Delta \nu_L)(\nu - \nu_0 - \delta)} \right]^2} d\delta$$

$$y = \frac{2(\nu - \nu_0)}{\Delta \nu_D} \sqrt{\ln 2}, \quad y = \frac{2\delta}{\Delta \nu_D} \sqrt{\ln 2}, \quad \sigma' = \frac{\Delta \nu_N + \Delta \nu_L}{\nu_0} \sqrt{\ln 2}$$

$$k_{\nu} = k_0 \frac{\sigma'}{\pi} \int_{-\infty}^{\infty} \frac{e^{-y^2} dy}{\sigma'^2 + (\omega - y)^2}$$

From: A.C.G. Mitchell and M.W. Zemansky, "Resonance Radiation and Excited Atoms", Cambridge University Press, London, 1961.



THE SORCERY AND SCIENCE  
OF AEROSPACE EXPLOSIVE ORDNANCE

by S. A. Moses

Douglas Missile & Space Systems Division  
McDonnell Douglas Corporation

THE SORCERY AND SCIENCE  
OF AEROSPACE EXPLOSIVE ORDNANCE

by S. A. Moses

Douglas Missile & Space Systems Division  
McDonnell Douglas Corporation

"We don't need ordnance engineers; we need sorcerers!" This was my greeting as I entered the office of the manager of a high-priority aerospace program to discuss a recent problem. "Why can't explosive devices be engineered the way we engineer other mechanical devices?"

As an engineer, I was baffled by the manager's assertion that aerospace ordnance devices couldn't be "engineered" the same as other mechanical devices. Was this because the manager wasn't aware of the engineering that goes into some of these devices? Or could it be because he and I had different definitions for engineering? To this manager, "engineering" is the ability to put formulas into a computer and produce a series of pat answers for any specific problem. This idea is intriguing and is worth examining. Can greater use be made of the computer for the development of aerospace ordnance devices?

While I lack the ability to develop the necessary computer formulas, it is possible to take a good hard look at aerospace explosive ordnance to indicate areas in which scientific principles might be applied and those that are still wrapped in a cloak of mystery.

Before proceeding further, perhaps the term "aerospace explosive ordnance" should be defined and placed in its proper perspective with other explosive applications. The military defines explosive ordnance as: "a term used to denote military material which normally contains or consists of explosives as, for example, bombs, missiles, projectiles, and the like." In the aerospace industry, it is common practice to

divide explosive ordnance into several categories such as armament or weapons, propulsion, escape systems, destruct and/or separation systems, pyrotechnics and explosively operated devices - although there is no hard and fast rule concerning this.

For the purpose of this discussion, aerospace explosive ordnance will be defined as: "Devices on aircraft, missiles or space vehicles, excluding armament and propulsive units, which contain deflagrating or detonating explosives."

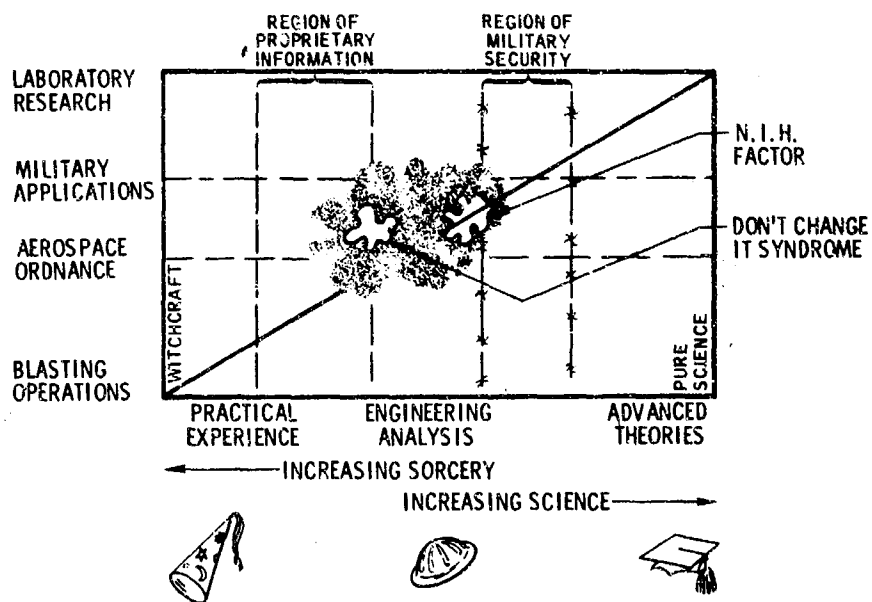
I have prepared a graph indicating the entire field of explosives and the probable position of aerospace ordnance in this field. Along the abscissa, I have plotted increasing degrees of knowledge. Along the ordinate, I have plotted various explosive applications with the diagonal line tying these applications to knowledge.

The first application, blasting, leans heavily upon field experience. Although there is a moderate background of theoretical work concerning blasting, this has not yet progressed to the point where the arrangement, size, and firing sequence of the explosive charges are determined by a computer program. Rather, these are determined by a field supervisor with years of practical experience but little knowledge of rock mechanics or shock kinetics.

At the top of the list of applications I have placed laboratory research which leads to a better understanding of explosive phenomena. In between these two limits lie the areas of military applications and aerospace ordnance.

Omitting military applications for the time being, the shaded area encompassing aerospace ordnance encroaches on both practical experience and advanced theories. It intrudes on and is limited by the region of proprietary information in one direction and on the region of military security in the other. Whether these are actually two separate regions

## GRAPH OF THE SORCERY AND SCIENCE OF EXPLOSIVES



or whether this is one region, inhabited jointly by both private corporations and government bureaucups is open to question.

The shaded area is still further limited by the two amoeba-shaped parasites, the N.I.H. (Not Invented Here) Factor and the Don't Change It Syndrome. The former has the ability to move anywhere along the diagonal. It has the interesting property that the higher up the diagonal it moves, the larger it becomes. Remarkably, as it moves down into the region of proprietary information, it occupies negative area. In this region, it is typical to practice a reverse N.I.H. technique, more commonly called piracy. Surprisingly, it grows out of all proportions when it reaches the rarefied atmosphere found in the advanced theoretical regions, as anyone can testify who has heard two scientists arguing over minuscule details of their own particular theories.

The Don't Change It Syndrome is a malignant growth which characterizes those programs that are in a rundown condition due to lack of green stuff. The more rundown the program, the more pronounced this malignancy becomes until, with some programs, it completely dominates the entire field of aerospace ordnance. Interestingly, the best cure for this condition is a malfunction resulting in a critical injury or fatality. Although this may seem like bitter medicine, the results are almost miraculous. Green stuff is immediately pumped into the program and the necessary surgery to remove the parasite can then be performed.

This then is the (black) magical kingdom in which aerospace ordnance must operate. With the help of my scoffing manager I will attempt to survey a few of the mazy byways of this land, suggesting possible improvements which might lead to a computerized Utopia. Although this Utopia may be many years in the future, it is hoped that some of the paths suggested may be at least pointed in the right direction.

### Those Bewitching Names

"Why," asked the program manager, "do you have such cabalistic names for explosives? You come in here one day chanting about TNT or PETN which I understand are acronyms of chemical compounds, and the next time I hear some incantation about cyclotol or Composition A which are neither acronyms nor chemical names. Why can't explosives be neatly categorized in some simple system like the AISI numerical code for metals?"

I must admit that my first reaction was to tell him all the things that I thought wrong with the AISI code. Then I remembered that this coding system did have merit. Furthermore, the present system of naming explosives certainly contributes to their being identified as ingredients from the witches' cauldron.

Among the common high explosives, for example, there are several different methods for naming new compounds and mixtures.

As indicated previously, there is one group identified by acronyms of chemical compounds. TNT (trinitrotoluene), DDNP (diazodinitrophenol), and PETN (pentaerythrite tetranitrate) are good examples.

A smaller group is known by chemical names without the use of acronyms. These include lead azide, lead styphnate, and mercury fulminate, to list some common ones.

A group of castable explosives, the "tol" group, consists of mixtures of TNT and other materials in various percentages. Examples include amatol, baratol, cyclotol, and tetrytol.

Then there are the compositions which are mixtures of cyclonite (RDX) and other chemicals. I rather suspect that we inherited these from the British who coined the acronym, RDX, from "Research Department Explosive." These compositions appear to have an ordered grouping

with all the "A" compositions being suitable for press loading, the "B" compositions suitable for casting, and the "C" compositions being hand moldable.

There are other explosives named for individuals (Haleite named for Dr. Hale of Picatinny Arsenal is an example) or for a particular use such as the Depth Bomb Explosive, DBX. Although several other categories could be mentioned, I think these few examples will indicate that there is no standard method for naming high explosives.

In the field of propellants where there is a wide variety of proprietary materials, the names are even more confusing. The Army gave the "gun" propellants "M" number as they were standardized. As a result, we have M1, M3, M4, etc., which are single base powders and M2, M5, M8, etc., which are double base powders. Those propellants which did not reach the standardization stage were given consecutive "T" numbers (for "Technical," which was the original name of the Ordnance Corps, Research and Development Division). In addition, the Army also uses a number of commercial pistol powders which are known by their trade names.

In the case of proprietary propellants, the situation is even more confusing. Each manufacturer of propellants has its own system of nomenclature but there is certainly no standardization between these companies. Thus, the Solid Propellant Manual lists propellants such as: ANP-2569ED and ANP-2608AF, made by Aerojet-General; AFU and CYH, manufactured by Allegany Ballistics Laboratory; Arcite 251 and 362, which are compositions of Atlantic Research; and JPL-131 and 601, manufactured by Jet Propulsion Laboratory to name only a few.

Is it really too much to expect that, in this day of instant information retrieval, a codified nomenclature system could be achieved and put into use? In the far distant future it might even be possible to pick up a telephone, dial a central information center

and a code number and immediately receive a print-out containing everything known about any given explosive.

#### Incantations, Spells, and Explosive Testing

"I am sure," said the program manager, "that the rifle bullet test for explosives has some meaning for the Army, but it reeks of witchcraft to me. I'm used to dealing with engineering units. Except for propellant burn rate, impulse values, and explosive temperature, most explosive tests don't help me in selecting the right explosive for a given application. Can't explosive tests be designed to produce real numbers that can be used for design rather than meaningless comparisons to TNT?"

Let's examine a few of the test methods used for both high explosives and propellants to determine which have any real meaning for solving design problems.

Many of these are rather ingenious tests which were developed long before modern electronic test equipment was available. Speaking quite broadly, these tests can be divided into those concerning the sensitivity, power, and stability of the material along with measurements of the detonation or burn rate.

The Picatinny Arsenal and Bureau of Mines drop weight testers give only quantitative data on the sensitivity of explosives. These data would be much more meaningful if the drop height was defined statistically rather than the present system of indicating the height that will produce one explosion in ten trials. It is possible that this statistical information converted into terms of kinetic energy might be useful in designing initiating systems.

The recent work by the Naval Ordnance Laboratory goes a long way toward placing sensitivity tests on a scientific basis. In their

extensive experiments with gap tests, the sensitivity of a number of explosives has been determined as a function of the shock strength required for initiation. Sufficient data have been collected to establish both "no fire" and "all fire" criteria on a statistical basis.

For those not familiar with the small scale gap test, a standardized donor explosive is separated from the test explosive (the acceptor) by a plastic spacer or attenuator. Both donor and acceptor explosives are pressed into brass sleeves. When the donor is detonated, a shock is transmitted through the plastic into the acceptor. High order or low order detonation of this acceptor is indicated by the depth of dent formed in a steel block. A low order is indicated by a dent which is less than half the depth of one formed by high order detonation. A determination is made of the thickness of spacer through which initiation is achieved in 50% of the tests. The thicker the spacer, the more sensitive the explosive. A relationship has been established between the shock pressure and the required gap such that:

$$\text{Log pressure (kilobars)} = 4.72 - 1.40 \log \text{ gap (mils)}.$$

Tests which measure the power of various explosives are just as mystical as most of the sensitivity tests described previously. There are tests which measure the number of grams of sand crushed by detonation of a given explosive, the volume of a cavity formed in a lead block, or the number and size of slivers into which an artillery shell is fragmented. Unfortunately, with the exception of the sand test, the results are usually given as a comparison with TNT. Perhaps this has some meaning to the military in the testing of new explosives but has little use for the aerospace engineer. However, with some modification, the dent test does provide extremely useful information. As previously mentioned, the NOL small scale gap test identifies between stable and non-stable detonations by the differences in dents formed in thick steel blocks. The tests would be even more useful if

the depth of dent could be calibrated in terms of the energy output of the explosive and I predict that this will be done some day.

Tests of the stability of explosive materials are of extreme interest to manufacturers and users of aerospace ordnance. Devices are frequently required to be stored for long periods of time, or to be exposed to high temperatures, and then function satisfactorily. There are a number of different types of stability tests for explosives. Each of these gives some indication of the decomposition characteristics at a given temperature when stored for a given time, but no single test or combination of tests gives any real indication of the storage life of an explosive device.

Without going into details - these older high explosive and propellant tests include the following hodgepodge:

1. 75°C, 48 hour test
2. 100°C, 48 and 96 hour tests
3. Vacuum stability tests at 100°C, 120°C, and 150°C (40 hours)
4. 65.5°C surveillance test (up to 20 days and longer)
5. 120°C and 134.5°C heat tests (up to 5 hours)
6. Taliani test (110°C test for 100 minutes)

Of more recent origin are differential thermal analysis (DTA) and thermal gravimetric analysis (TGA). The DTA test provides information on the occurrence of exothermic and endothermic reactions as the sample material is heated at a given rate. With TGA, the percentage of weight lost at any temperature may be determined.

There appear to be two major drawbacks to using any of the above tests to estimate the storage life of an explosive device.

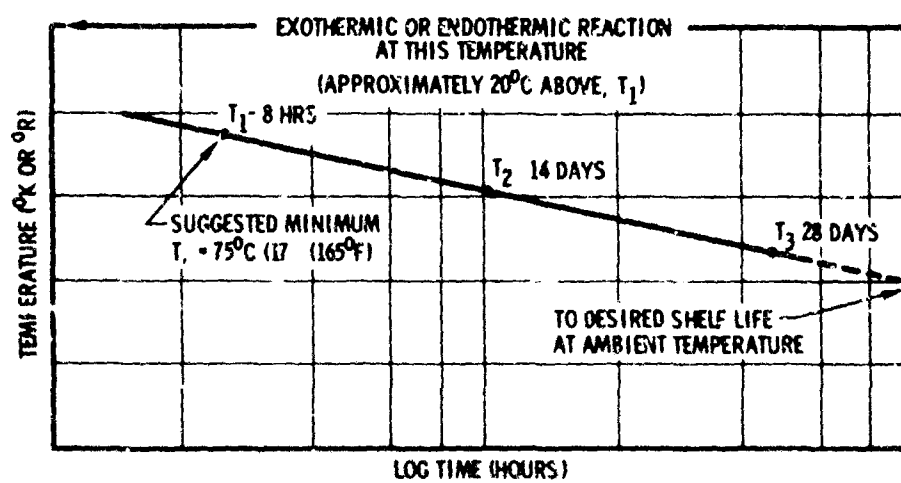
1. The device usually contains not one but a combination of materials which may be reactive or catalytic. This indicates that the whole device, rather than individual materials, should be subjected to the heat.
2. None of the above tests provide an indication of the performance degradation of the material. This indicates that the device should be given a performance test following the heating cycle.

Although there is no standard test for estimating the shelf life of an ordnance device, with reasonable assumptions an accelerated shelf life test appears entirely feasible and no more difficult or time consuming than the well-known temperature-humidity tests.

As a suggestion, this test may include the following:

1. DTA tests of the reaction components. These should provide information on the maximum temperature to which the device may be exposed without causing exothermic or endothermic reactions. The highest temperature in the following tests should be less than this maximum temperature.
2. Subjecting sample devices to three different storage conditions at elevated temperatures. When plotted on a semi-log time-temperature graph, these three conditions should lie on a straight line with the projected storage life at ambient temperature.
3. Following the storage tests, sample devices should be examined for possible degradation and other samples should be put through performance tests.

## SUGGESTED ACCELERATED STORAGE TEST



This type of testing is certainly not the ultimate but is a step above the present crystal ball system of estimating storage life.

#### Formulas for Magic and Mathematics

"Are military applications utilizing explosives conjured up by trial and error like most aerospace ordnance devices?" asked the program manager. "Can't some of the same math models be used for both military and aerospace applications?"

Without crossing the barbed wire boundary into the region of military security, I will attempt to examine the explosive applications for which there is a large background of theoretical and practical information susceptible to computerized analysis. In the broad categories outlined, it will be pointed out that for military applications, computer analysis is available, whereas this is rarely the case with similar aerospace explosive applications. The first of these categories has to do with interior ballistics.

An artillery shell or rifle bullet is normally designed to have a given muzzle velocity. This must be accomplished while maintaining the pressure in the gun tube below a certain critical level. The gas laws for solving this problem are well-known and it is safe to say that both arsenals and gun manufacturers have the ability to computerize this problem, thereby selecting the correct weight and type of propellant required for optimum performance.

In the field of aerospace ordnance, interior ballistic formulas are used for the development of drogue guns and items which fall under the broad category of propellant actuated devices (PAD). Whether these are designed by computer analysis or the sorcerer's slip stick will depend largely on the quantities desired. If the manufacturing potential is sufficiently large to interest one of the giants of the explosives industry, computer analysis will be called into play to

solve the associated interior ballistics problems. If, on the other hand, only a limited number of devices are required, the contract will usually go to one of the smaller explosive ordnance companies and be solved by an engineer working without the aid of a computer. Because the engineer may be familiar with the burn characteristics of only a few propellants and as he cannot rely on the huge memory bank of a computer, the final design may not be "optimum" but, through trial and error, can be made both workable and reliable.

The second explosive category I would like to discuss has to do with the development of solid propellant rockets. Here it goes without saying that the design of the propellant grain for all military rockets and aerospace vehicles is subjected to computer analysis.

As I have eliminated propulsive units from my definition of aerospace ordnance, this leaves only such items as spin rockets, retrorockets, and, by stretching a point, gas generators to consider. Assuming that the designs of all rocket motor grains, whether large or small, are subjected to computer analysis, I will turn my attention to the design of gas generator grains. These have a wide range of applications in aerospace. To name a few: gas generators are often used to pressurize hydraulic systems, to supply hot gas for control systems, to inflate floatation devices, and for many other purposes.

Designing the propellant grain for a gas generator is in some cases much simpler and in others more complex than designing a rocket propellant grain. In the simplest case, a gas generator may be desired in which an equal volume of gas per unit time is to be delivered for a required period. For this, it is relatively easy to design a cigarette burning grain with its necessary controlling orifice.

Greater difficulty is experienced when the heat-sinking characteristics of the system must be taken into account. The size, shape, and material

of the propellant grain will depend, to a large extent, on the waste heat lost to the system. Unfortunately, some of the companies manufacturing gas generators do not have math models for complicated heat loss equations and although good approximations can be made, final shaping of the gas generator grain is usually made on a trial and error basis. This process will be largely eliminated in the future as more and more small explosive companies make use of computer programming service organizations.

Another application of explosives has to do with the formation and acceleration of metal fragments. A grenade, warhead, or other fragmentation munition is normally designed to be effective against certain classes of targets. For optimum performance, the designer should know the characteristics of the target as well as the mass, velocity, and distribution of the fragments from the munition. These can then be related back into the munition design to determine such factors as the size and shape of the munition, the type of explosive, and the fuzing characteristics.

Utilizing such aids as the Gurney or Stern formulas for determining fragment velocities, the Shapiro formula for fragment direction and DeMaro's empirical equation for target penetration, the design engineer can make any number of computer runs simulating different munition and target characteristics to obtain information on the expected effectiveness prior to committing expensive hardware for test purposes.

Unfortunately, this well-established technique finds little application for aerospace devices because of the limited need for high velocity fragments. With the exception of some destruct systems, almost the only requirement involving high velocity fragments comes when it is necessary to initiate detonating fuse end fittings separated by an air gap. When the gap is small, the donor fitting initiates the acceptor by a combination of shock and fragment impact.

As the gap is increased, the shock impacting on the acceptor is less and may not result in reliable initiation. At this distance and beyond, initiation of the acceptor may be achieved by fragment impact.

This appears to be a situation that is amenable to computer analysis, yet as far as is known, this has not been done. When this analysis is accomplished, undoubtedly the aerospace industry will be benefited by the development of more effective and fitting designs.

Again, in the area of shaped charge development, there is good evidence that military munitions are designed utilizing well-established formulas relating the pressure in the detonation front, the formation of the jet, and the penetration of the target by this jet. In the field of aerospace ordnance, linear shaped charges (LSC) are generally used for skin cutting applications, while conical shaped charges are used in some destruct systems.

As most companies manufacturing linear shaped charges supply information regarding the thickness of various materials which can be cut by their charges, the application of LSC is relatively straightforward. However, when it comes to the use of conical shaped charges for the destruction of solid rocket motors, this is indeed a "black art." As far as can be ascertained, no work has been published on the penetration of the jet into propellants or the mechanism whereby solid propellants may be initiated (destructively) by a shaped charge jet. As a result, destruct charges of this nature are normally oversized. The typical attitude is that if a quarter pound charge will suffice, a pound charge will do it better. This is usually satisfactory to range safety personnel because this results in a big "bang" when the destruct button is pushed. However, the attitude is rather frustrating for an engineer attempting to establish design criteria.

Although only a few applications have been cited here, the picture is rather clear. Knowledge exists of many of the basic fundamentals which allow computer analysis for the development of aerospace devices. In fact, many computer programs may now exist, hidden in the regions of proprietary information or military security.

Whether the programs exist or not, the desire for this type of analysis must be generated and funded by the using organization. This is, of course, far different from the typical request in which the manufacturer is asked for a small number of already qualified "off the shelf" items for immediate delivery.

Even should time and funds be made available for computer analysis, the requirement for this type of work must be clearly transmitted to the manufacturer. I remember one development program for which a proposal was sent to a number of manufacturers of ordnance devices. The proposal work statement indicated that "in the selection of materials, mathematical analysis was desired but not mandatory."

Of the nine proposals received, not one offered an analysis for the selection of the explosive materials, although one manufacturer did perform an analysis to determine the strength of the screw threads.

As this paper has touched on magic and sorcery, I'd like to end it by recalling a scene from that classic motion picture, "The Wizard of Oz."

In that scene, the Great Oz grants some longed-for wishes in an interesting fashion.

The Scarecrow, who wanted a brain, receives a diploma, Magna Cum Laude. Who would question his having a brain if he had such an imposing diploma?



The Tin Woodman, who wanted a heart, received a testimonial praising his benevolence for who can show benevolence without a heart?

The Cowardly Lion was satisfied with his medal for bravery. With this on his chest, who would dare call him a coward?

I only wish that I could play the Great Oz and conjure up computerized solutions for aerospace ordnance. Only then would the program manager be convinced that explosive devices could be engineered.



DESIGN FOR EDUCATION OF PYROTECHNICISTS

R. M. BLUNT

DENVER RESEARCH INSTITUTE

## DESIGN FOR EDUCATION OF PYROTECHNICISTS

R. M. BLUNT

DENVER RESEARCH INSTITUTE

Some background information is necessary to an understanding of the reasons for this discussion. On 29-30 November, 1967, the Military Pyrotechnics Section of the Artillery Division of the American Ordnance Association met at Fort Bragg, North Carolina. I had been honored by a Request to speak at that meeting and discussed "Education for Ordnance Scientists & Engineers". That discussion was based upon a meeting that had been held on August 17-18, 1967 at Hall Lodge, Grand Lake, to consider the areas and depth of treatment that would be appropriate in a series of formal courses aimed at the research people working in Ordnance. This latter meeting was attended by Mr. William Cronk, of the Illumination Branch, Targets and Missiles Division, Air Force Armament Laboratory, Eglin Air Force Base, Florida; Mr. B. E. Douda, Research Branch, Concept Development Division, Research & Development Department, U. S. Naval Ammunition Depot, Crane, Indiana; Messrs. R. Fay, R. E. Williams, J. Kottenstette, R. Blunt, Denver Research Institute, University of Denver. Invitations also were extended to personnel of Picatinny Arsenal and Frankford Arsenal, but they were unable to attend. This Grand Lake meeting in turn stemmed from one held on March 22, 1967 at which Dr. R. Griskey of the Department of Chemical Engineering, Dr. A. Ezra, Dr. R. Evans and Mr. R. Blunt of DRI, Mechanics Division and Mr. C. Lundin of DRI, Metallurgy Division, discussed the concepts of an ordnance engineering option and a summer course in ordnance engineering. It was agreed that these ideas should be developed, beginning with the summer course. This present seminar is not a formal course, but it does represent the first step in the direction of a summer course and, hopefully, the creation of a series of related courses that might be termed an ordnance option in, say, mechanical engineering. In view of the current strong feelings of some of the members of the University community in the United States, it may be necessary to de-emphasize the association with military terms such as ordnance. Several possible titles for an option have been suggested, but no choice is really needed just yet.

I hope that this bit of history will give you who are attending this seminar a better perspective on it. Brigadier General Hiester, Colonel Hinricks of the Army Office of Personnel Operations, Dr. Simecha of Eglin Air Force Base, Dr. J. T. Thomas of the Army Materiel Command, Brigadier General Erwin Graham, Aberdeen Proving Ground, Mr. Burton Calkins, U. S. Naval Ammunition Depot, Crane, and many others have been kind enough to write and encourage us to develop this idea. I hope that all of you will express your opinions of this seminar, of what formal courses in ordnance research should encompass and of the duration and content of a summer course. Express your opinions in a letter, if you will, and be completely frank.

At present there is no formal course in Ordnance Engineering or Science available at any of the public or private U. S. universities so far as is known. Those of us who are now working in ordnance problems

have received our formal education in diverse fields encompassing most of those considered a part of the usual engineering or science curriculum. This background has obviously been of value when one views the accomplishments of ordnance research over the years. There is, however, an induction or learning period involved when someone first enters this field. To a lesser extent, this is also true when a shift in work requires a person to move from, say, smokes to flares. Consequently, a longer period is required for the ordnance scientist to progress on his own than is needed in other fields. In addition, there is often an element of hazard associated with this area of research that is absent or at a much lower level in the work done in other fields. This hazard element further slows the progress of the new worker for he must acquire reliable data on it before he can proceed with his main task of research. The quality of the work that is done may also suffer because of excessive caution on the part of the inexperienced, or conversely because of its absence when experience would dictate prudence.

With that bit of background as a basis, I would like to offer some suggestions as to the material that would be useful to someone working in the specific ordnance area of pyrotechnics. These suggestions are drawn from personal experience and from discussions with a number of people. It is my hope that by presenting them before this group, further helpful comments and opinions will be expressed. Perhaps next summer it will be possible to offer a useful course, in which the substance of these suggestions or requests can be incorporated.

As a starting point from which a design may be constructed for the education of pyrotechnicists, I believe the basic areas of study should be defined. To me, these would be General Chemistry, Physical Chemistry, General Analytical Chemistry and Chemical Instrumentation from the general field of chemistry. Optics, Spectroscopy, Radiometry and Photography from the general area of Physics. From Mathematics, use of both the digital and analog computers. Engineering should provide for Strength of Materials, Properties of Materials, Machine Design, Statics and Kinematics. An often neglected area that is very important is the use of library and other reference facilities.

There can be a great deal of discussion on questions regarding my inclusion of photography, for example, under physics. I don't think such points are important, so long as the material itself is available. In other words, I'd like to have criticisms based on the content or lack of it instead of the classification I've used.

In each of the proposed areas a more detailed description can be provided as a guide to the meaning intended by these rather general terms.

For that purpose the following outline is offered; I have assumed that the individual taking these courses has a bachelor's degree in science or engineering. In a group made up of such persons, some might find a repetition in these courses of some they have already had. For that reason and also because it is generally very stimulating and vitalizing to a class, it would be best if courses were taught by persons who have actual experience and an active interest in pyrotechnics. This probably cannot be arranged in every instance but should be considered a goal to achieve.

Even repeated material, when presented from a fresh viewpoint directly related to the students aims, can be interesting and productive of new thoughts.

The outline is intended to be descriptive, more than definitive.

The following, colored by my own experience, is offered as a starting point for discussion.

#### A. Physics

Assume a reasonable background for the individual; perhaps one full year of University physics.

##### 1. Optics.

- a. General Geometrical Optics as a basis for simple instrument design and operation. 8 hours.
- b. Physical; enough to appreciate the need for physical optics in design of precision equipment & lasers. 8 hours.
- c. Photography - X-ray, still, high speed single and high speed motion pictures. Present the fundamentals, expand to discuss use of these specialized techniques. Demonstrate at ranges.

##### 2. Spectroscopy - This is based on optics, but is really a distinct specialty.

- a. Fundamentals from optics plus atomic and molecular theory. 4 hours.
- b. Visible and Ultraviolet Spectroscopy
  1. Analysis - standard techniques of determining elements. 2 hours.
  2. Spectrophotometry - to teach the methods and their accuracy limitations in determining color and intensity of radiation. 3 hours.
  3. Spectral pyrometry by line reversal, one-two or three "color", relative intensity; emissivity. 3 hours.
- c. Infrared Spectroscopy
  1. Analysis and Structure determination; general foundation plus description of special requirements of transmission and detection in the 1 to 15 micron region.
  2. Determination of molecular species in rocket, jet or flare flames. Application to determination of emissivities and to temperature from vibration-rotation bands. 4 hours.
  3. Radiometry - Total and Spectral Radiometry. Basic apparatus, applications to measurement of energy radiated from source and to seeker systems (i.e., Sidewinder). 4 hours.

## B. Chemistry

Assume a background of general inorganic, inorganic quantitative analysis and general organic chemistry.

1. General Chemistry - good refresher on assumed basic courses. 4 hours.
2. Physical Chemistry
  - a. Reaction Kinetics, 8 hours, simple presentation; prediction of rates, probable reactions.
  - b. Thermochemistry, 4 hours. D.T.A.: T.G.A., Flame Chemistry.
  - c. Chemistry of Propellants, 6 hours.
  - d. Chemistry of Flares, 6 hours.
  - e. Chemistry of Explosives, 6 hours.
  - f. Chemistry of Smokes, 3 hours.

## C. Mathematics

Assume university algebra and integral/differential calculus, differential equations.

1. Chemical calculations, refresher, 2 hours.
2. Use of computer, 6 hours.
  - a. Information storage and retrieval.
  - b. Modelling of propellant strand burning.
  - c. Thermochemical calculations.
  - d. Optical design.
  - e. Ballistics, internal, external.
  - f. Systems analysis.

## D. Library 4 hours.

1. Use of government documents.
2. Library of Congress catalogue system vs. Dewey Decimal.
3. Bibliographic sources, "Citation Index", etc.

## E. Engineering

1. Strength and Properties of materials; emphasis on exotics after

covering the fundamentals, 8 hours.

2. High Energy forming processes - magnetic, explosive, 8 hours.
3. Machine Design Principles, 4 hours, for those who design fuzes for bombs, etc.
4. Mechanics, 4 hours, Dynamics and statics refresher.
5. Reliability

F. Ordnance Laboratory, 24 hours.

1. Safety practices.
2. Use of explosives.
  - a. Demolition.
  - b. Fragmentation (grenades, etc.)
  - c. Separation, explosive bolts.
  - d. Metal forming.
3. Formulation, manufacture and burning of:
  - a. Illuminating flares.
  - b. Signal flares.
  - c. Smokes.
  - d. Flash bombs.
4. High Speed Photography
  - a. Single
  - b. Motion

G. Background Courses

1. Military Pyrotechnics.
  - a. History.
  - b. Requirements, current usage.
  - c. Summary of state-of-the art.
  - d. Future developments.
2. Military Propellants.  
(as in G-1 above)

3. Military Explosives.  
(as in G-1 above)

4. Underwater Ordnance.  
(as in G-1 above)

5. Initiators and Fuzes  
(as in G-1 above)

This is far too much material to cover in anything less than a year, but a choice can be made from this material to be presented in a one-week seminar, or in a concentrated six week course sequence with credit or in various other ways.

As a beginning and with these considerations in mind, it appears that enough can be accomplished toward improving the skills of both newcomers and the worker who has some years of experience to justify a one week seminar. Note the difficulties presented by the diversity of backgrounds anticipated of those who would attend. Those who agree to help present this first seminar should be aware of this problem and present the material accordingly.

Some attention should be given to the desirability of presenting survey lectures that would be of most value to research managers, versus the presentation of areas in depth for the benefit of the laboratory worker. It appears that both needs exist and that a questionnaire may be needed to aid in establishing the proper balance between them in the seminar. Your comments in this area would be most helpful.

A certificate of attendance would be presented to those who attend the entire seminar and text materials would be provided, cost included in the fee.

Some assessment of the financial base to support such a seminar was made, a charge of the order of \$200 - \$300 was felt to be reasonable. This might be reduced if anticipated attendance were of the order of 50 or more. Your opinions on this figure are solicited.

Accommodations in either University dormitories or elsewhere can be provided, with the choice left up to the individual.

With a successful seminar or two of this kind, the development of a formal engineering or science option should follow.

In closing, I must express my sincere and very deep appreciation of the support and encouragement I have received from many people in endeavoring to put ordnance and pyrotechnics on a plane of acceptance which corresponds to that accorded to, say, chemistry, physics and the various engineering disciplines. Many people in this room are much better qualified than I am to do this; I hope they will continue to help. Particular thanks are due to Mr. Bill Cronk, who initiated this reaction, and to Mr. Bernie Douda and the whole Research and Development Department of the Naval Ammunition Depot at Crane who have been outstanding in their support of this seminar. Thank you.



COMPUTER SOLUTION OF PYROTECHNIC  
THERMOCHEMISTRY PROBLEMS

Edward J. Davis  
Thiokol Chemical Corporation  
Reaction Motors Division

While most high speed digital computer programs dealing with high temperature chemically reacting mixtures have been primarily concerned with the calculation of theoretical rocket performance of chemical propellants, almost the entire work involved is in the determination of the equilibrium composition and temperature of the reaction products. Hence, with suitable, and usually minor modification, almost any of the commonly used programs can be adapted to efficiently solve the general problem of computing chemical equilibrium compositions. Successful application in areas remote from that of rocket performance prediction include hazards evaluation, optimization of chemical synthesis processes, and, of course, the theoretical evaluation of pyrotechnic flares.

The equilibrium composition for a reacting mixture at a given temperature is computed by finding that composition which satisfies the mass balance and total pressure constraints as well as satisfying all of the simultaneous equilibria involved. The classical solution has been to list the possible reactions and set up a series of simultaneous nonlinear equations involving element mass balances, equilibrium constants, (for each of the individual equilibria), and total pressure. Obviously, for complex systems, the resulting set of equations becomes unwieldy. Ultimate solution is quite sensitive to initial guesses; convergence is dependent on the selection of major and minor products, and important products tend to be overlooked if the reactants or reaction conditions are unfamiliar.

The free energy minimization method, introduced by White, Johnson and Danzig<sup>(1)</sup> and extended to include condensed phases by Kubert and Stephanov<sup>(2)</sup>, overcame these difficulties, and is widely used today. Basically

the free energy minimization method differs from the classical procedure in that the mathematics are perfectly general with respect to system chemistry. Rather than considering individual equilibria, the distribution of all possible species is established through the mathematical technique of minimizing the system free energy. By including all species which could possibly form, a solution can be achieved which is independent of stoichiometry or pressure and temperature level. Theoretical accuracy is limited only by the completeness and precision of the thermodynamic data. Insensitive to system complexity, the free energy minimization method is ideally adaptable to modern digital computers.

The general mathematical procedure can be outlined quite briefly. By starting with an expression for the free energy of a mixture of assumed composition, the free energy of the unknown equilibrium mixture can be expressed in terms of the assumed mixture and of unknown changes which represent the difference between the assumed initial composition and the final equilibrium composition. This expression, a quadratic approximation, involves the first two terms of a Taylor series. The quadratic approximation to the minimum free energy is then minimized by using the technique of Lagrange multipliers, which enables the simultaneous satisfaction of the mass balance constraint. These manipulations yield a set of linear simultaneous equations equal in number to one more than the total number of elements plus the total number of condensed species. The solution of this set of equations results in a corrected composition which is approaching minimum free energy. By iterating through this procedure until the difference between successive compositions is negligible, a minimum free energy composition is found. When the method is applied to combustion processes and programmed for a high speed digital computer, the addition of a "conservation of enthalpy" constraint enables the automatic convergence to the adiabatic flame temperature.

The classical method has also been modified for use with high speed digital computers. By using a linear set of correction equations to approximate the nonlinear equations defining the problem, a completely general solution can be obtained. While the conditions for equilibrium are given in terms of free energy changes across reactions (equilibrium constants), rather than specifying equilibrium as the minimum of the total free energy of the mixture, the methods have become computationally equivalent. No real advantage can be claimed for either.

To date, by far the greatest success in predicting the combustion properties of pyrotechnic flare compositions has been with the NASA-Lewis program<sup>(3)</sup>. This computer program, selected by the Interagency Chemical Rocket Propulsion Group-Working Group on Performance Standardization as the industry standard, was designed to compute equilibrium compositions for any chemical system for which thermodynamic data exist. However, before relying too heavily on any computer program which is being used outside its intended area of primary application, several questions should be resolved. First, will the program always, or even usually, yield an answer? That is, will the mathematics of the program handle the systems of interest, or is it likely to "hang-up", failing to converge to a solution? Of course, a certain failure rate is expected of any program. The more complex it is, the more ways it can fail. Thermochemistry program failure rates increase sharply as the mass fraction of condensed species in the combustion product mixture increases, and the NASA-Lewis program is no exception. Flare compositions typically produce large quantities of condensed species as combustion products. As a very rough rule of thumb, the percentage of cases which fail can be expected to approximately equal the percentage of total system mass which is present in the condensed phase.

In the event a case does fail, all is not lost. There are several techniques which can be employed to force convergence of failed cases. Convergence criteria can be relaxed, offending species can be removed from consideration, reactant proportions can be changed slightly, etc. Unfortunately, each of these techniques introduces a potential source of error in the results of the calculation. The easiest solution to accomplish, that of omitting offending species, produces the greatest uncertainty in the validity of results. Loosening of convergence criteria will admittedly yield imprecise results, but the magnitude of possible error is at least ascertainable and can often be kept within tolerable limits. When slight changes in ingredient proportions will allow successful program operation, the desired data points can be bracketed, affording an opportunity to gain the requisite information through interpolation.

A second important consideration in program applicability is that of data availability. Are sufficient thermodynamic data available, in a form suitable for use with the program, to accurately describe the systems of

interest? For pyrotechnic flares, the answer is a qualified yes. In the case of ingredient heat of formation data, there is no real problem. Those data which are not available in one of the many published compilations can readily be estimated quite closely. When it comes to thermodynamic data for combustion products, gaps do occur. While the renowned JANAF Thermochemical Tables<sup>(4)</sup> are reasonably comprehensive, they, like earlier compilations, concentrate on those species which are important in hydrocarbon fuel or solid and liquid rocket propellant combustion. Complete sets of data for species not normally encountered in rocket propellant flames are sometimes hard to find. For example, barium and strontium combustion product data are available, but not in a form which is immediately compatible and consistent with the balance of the standard program input data. While it is possible to compute the thermal functions of required combustion species from spectroscopic data or from empirical heat capacity equations, this adds a new dimension of complexity to the task of calculating equilibrium composition. Many computer programs have been developed to provide functional thermal data. Probably the best and most flexible of these is by McBride and Gordon<sup>(5)</sup>.

The importance of using complete thermodynamic data files cannot be overemphasized. One of the most grievous errors that can be committed when performing thermochemical calculations is to inadvertently omit even one moderately abundant species. The consequences can be out of proportion to the crime, with dramatic changes in flame temperature and product composition not uncommon. This can be particularly important in evaluating flares, when a minority of the chemical species may be responsible for the majority of useful radiation emitted. Happily, with some prior knowledge of system characteristics, a simple check for plausibility of results will usually reveal the error.

Still another question needs to be resolved before accepting the program for general use in computing flare properties. Are the limiting assumptions on which the program is based still valid for the types of systems to be evaluated? In general, the basic assumptions are still necessary and correct, but in some instances they are slightly less correct for flares than for rocket engines or other combustion devices. This is so only because flare combustion gases often tend to be heavily laden with condensates. Liquid fuels and rocket propellants normally

produce little or nothing in the way of condensed species, while solid propellants rarely produce as much as twenty five mole percent condensates. On the other hand, flare formulations can yield almost any amount of condensed-phase reaction products when burned.

The computer program assumes that Daltons law of partial pressures applies to all systems considered. It also assumes: that condensates occupy a negligible volume, which holds true until you produce a really overwhelming proportion of condensed species -- and then the case will probably fail for other reasons anyway; that molar enthalpies, entropies and vapor pressures of condensates are independent of pressure -- no problem here at any reasonable pressure; that condensates are immiscible and gases are insoluble in them, which is just one of those things to keep in the back of your mind when interpreting the results; that particles are thermodynamically macroscopic, which is true within the range of interest of flare properties; that homogeneous mixing is attained, which is a function of the flare, not the computer program; and of course the most basic assumption is that complete thermal and chemical equilibrium is attained, which is by definition the ideal theoretical condition a thermochemical equilibrium program is designed to find.

In light of the above assumptions, just how accurate can the results generally be expected to be? If the initial conditions and flare composition have been accurately described, if no important combustion species have been neglected, and if the flare doesn't produce more condensate than gases, thermochemical calculations should be able to reliably predict maximum reaction temperature and species concentrations to within a few percent.

Once the computer program thermal data files have been set up to include all relevant combustion species, the only input data required to run a thermochemical calculation are ingredient elemental empirical formulas and heats of formation, ingredient proportions, and reaction pressure. Any number of ingredients may be input, in any proportions. Ingredient heat of formation should be at the ambient feed temperature, nominally 298.15 degrees Kelvin. Any reaction pressure can be assigned, with one important exception. In a system with condensed products, the assigned pressure must be greater than the sum of the vapor pressures of the condensed species. If the assigned pressure does not exceed the sum of the vapor

pressures by an amount equal to the partial pressures of other species in the gaseous phase, convergence would require negative partial pressures for some species, an impossible condition. The program has a low temperature limit of three hundred degrees Kelvin, and a high limit of six thousand degrees Kelvin, certainly adequate for most purposes.

Typically, between twenty and thirty of the hundreds of candidate combustion species considered will exist in sufficient quantity to appear within the fifth decimal place of the converged composition. For example, a 35% Mg/5% Laminac/60% Sodium Nitrate flare run at sea level pressure and room temperature yielded the following thermochemical data:

Flame temperature, degrees F	5152.
Specific heat, calories/gram degree Kelvin	4.545
Isentropic exponent, gamma	1.083
Average molecular weight	51.763

#### Mole Percents of Products

CO	5.734	CO <sub>2</sub>	2.978
H	1.092	H <sub>2</sub>	0.390
H <sub>2</sub> O	1.505	Mg (gas)	5.682
MgH	0.010	MgOH	0.009
MgO (gas)	1.730	MgO (solid)	38.433
Na (gas)	10.731	Na <sub>2</sub>	0.007
NaH	0.016	NaOH	2.916
NaO	0.819	N	0.001
N <sub>2</sub>	10.787	NO	0.921
O	2.605	O <sub>2</sub>	4.049
OH	1.585		

In a recent study,\* theoretical thermochemical calculations were made, and experimental temperatures were measured in magnesium-Laminac-sodium nitrate flare plumes. A modified version of the NASA-Lewis program produced the theoretical calculations. The results indicated that for those formulations having low equilibrium flame temperatures, there would be no difficulty in using thermocouples to measure temperatures in the plumes. Accordingly, after a method was devised to keep the burning face a constant distance from the thermocouple, when necessary to insure sufficient instrument response time, measurements were taken throughout the plumes of burning flares and maximum temperatures were noted. Pressed flares one inch in diameter by two and one-fourth inches long were burned in the upright position in an inert atmosphere at ambient pressures.

The flare formulations contained 68, 60, and 55 percent magnesium, Laminac was held constant at 5 percent, and the remainder was sodium nitrate. Each of the experiments was repeated several times. For the 68 percent magnesium flares, computed equilibrium temperature was 2306 degrees F and the average maximum plume temperature was 2250 degrees F. Computed equilibrium flame temperature for the 60 percent magnesium flare was 3296 degrees F, while the average maximum plume temperature was 3200 degrees F. For both of these formulations, theoretical and experimental temperatures agree within three percent.

The 55 percent magnesium flare has a theoretical flame temperature of 4668 degrees F, but the average measured temperatures were about 24 percent below this. This large difference between theoretical and experimental data is believed to be a verification of the previous observation (6) that combustion temperature and luminous efficiency for flares of this type drops sharply when flare diameter decreases below three inches at magnesium loadings below about 62 percent.

\*This work was conducted for the United States Air Force, Eglin Air Force Base, Florida, by the Aerospace Research Corporation, Roanoke, Virginia, under contract FO 8635-67-C-0161. The Air Force project engineer in charge of the program was Mr. Larry Moran.

Once experimental data are available, several subsidiary mathematical models which have been developed to extend the utility of the thermochemistry program may be employed. When combined with a reduced enthalpy model, the program will predict the effects of incomplete energy release (combustion). This, in conjunction with a stream tube model, enables the evaluation of variable combustion zones or inhomogeneities. By using a plume mixing model, the effects of burning in air can be studied.

Agreement between experimental data and theoretical predictions is by no means fortuitous. Computerized thermochemical calculations provide the most rapid and efficient means of determining temperature and product composition in the plume of an illuminating flare.

#### REFERENCES

1. White, W. B., Johnson, S. M., Dantsig, G. B., "Chemical Equilibrium in Complex Mixtures," J. Chem. Phys. 28, 751 (1958).
2. Kubert, B. R., Stephanov, S. E., "Extension to Multiphase System of the Rand Method for Determining Equilibrium Compositions," in "Kinetics, Equilibria and Performance of High Temperature Systems," edited by Bahn, G. S., and Zukoski, E. E., Butterworths, London (1960).
3. Selegnie, F. J., Gordon, S., "A General IBM 7040 or 7090 Computer Program for Computation of Chemical Equilibrium Compositions, Rocket Performance, and Chapman-Jouget Detonations," NASA TN-D-1454 (1962).
4. Anon.: JANAF Thermochemical Tables. The Dow Chemical Co., Midland, Mich. (1960 to 1968).
5. McBride, B. J., Gordon, S., "Fortran IV Program for Calculation of Thermodynamic Data," NASA TN D-4097 (1967).
6. Douda, E. E., "25 Million Candle Cast Flare, Diameter and Binder Study," RDTR No. 105, Vol. I and II, U. S. Naval Ammunition Depot, Crane, Indiana (1968).

MATHEMATICAL SIMULATION MODELS

Jerry L. Kemp  
U. S. Naval Ammunition Depot  
Crane, Indiana

## MATHEMATICAL SIMULATION MODELS

### I. INTRODUCTION

The purpose of this paper is to emphasize the need for determining requirements for sub-systems by evaluating the effect that sub-systems have on total system performance and the need for using computer simulation models for this evaluation.

While reading through the reference material, I was impressed by the expression of the concepts of simulation by Hillier and Lieberman in their book "Introduction to Operations Research" Holden-Day, Inc. 1967. By way of introduction, I would like to quote a few brief paragraphs from the introduction to their chapter on simulation, page 439.

I quote,

"The technique of simulation has long been an important tool of the designer, whether he be simulating airplane flight in a wind tunnel, simulating plant layouts with scale models of machines, or simulating lines of communication with an organization chart. With the advent of the high-speed digital computer with which to conduct simulated experiments, this technique also has become increasingly important to the operations researcher. Thus, simulation has become an experimental arm of operations research.

The emphasis in the preceding chapters was on formulating and solving mathematical models which represent real systems. One of the main strengths of this approach is that it abstracts the essence of the problem and reveals its underlying structure, thereby providing

insight into the cause-and-effect relationships within the system. Therefore, if it is possible to construct a mathematical model that is both a reasonable idealization of the problem and amenable to solution, this analytical approach usually is superior to simulation. However, many problems are so complex that they cannot be solved analytically. Thus, even though it tends to be a relatively expensive procedure, simulation often provides the only practical approach to a problem.

Within operations research, simulation typically also involves the construction of a model which is largely mathematical in nature. Rather than directly describing the over-all behavior of the system, the simulation model describes the operation of the system in terms of individual events of the individual components of the system. In particular, the system is divided into elements whose behavior can be predicted, at least in terms of probability distributions, for each of the various possible states of the system and its inputs. The interrelationships between the elements also are built into the model. Thus, simulation provides a means of dividing the model-building job into smaller component parts (where it may be possible to formulate each of these parts by methods described in other chapters), and then combining these parts in their natural order and allowing the computer to present the effect of their interaction on each other. After constructing the model, it is then activated (by generating input data) in order to simulate the actual operation of the system and record its aggregate behavior. By repeating this

for the various alternative design configurations and comparing their performances, one can identify the most promising configurations. Because of statistical error, it is impossible to guarantee that the configuration yielding the best simulated performance is indeed the optimal one, but it should be at least near-optimal if the simulated experiment was designed properly.

Thus, simulation typically is nothing more or less than the technique of performing sampling experiments on the model of the system. The experiments are done on the model rather than on the real system itself only because the latter would be too inconvenient, expensive, and time-consuming. Otherwise, simulated experiments should be viewed as virtually indistinguishable from ordinary statistical experiments, so that they also should be based upon sound statistical theory. Even though simulated experiments usually are executed on a digital computer, this is only because of the vast amount of calculating required, rather than any inherent relationship."

## II. SUB-SYSTEM VS TOTAL SYSTEM

In this discussion, there are two words that I intend to refer to frequently, sub-system and total system. By my definition, a sub-system is equipment (conceptual or real) that performs some function. The total system may contain many sub-systems and involves man, man-machine interfaces and interactions, tactics and operational environment. For example, our fighters and attack aircraft employ decoy flares to countermeasure certain enemy threats. The sub-system, that we would be primarily concerned with, is the decoy flare and

the total system is the friendly aircraft (including the decoy flare), the enemy threat, the tactics of each and the operational environment.

### III. SUB-SYSTEMS

Many technical studies are concerned with relating the sub-system performance as a function of parameter changes within the sub-system. For example, such a study might try to relate the change in flare intensity as a function of changes in particle size of an ingredient of the flare. This is an "inside look" at the sub-system. Another example of an "inside look" would be an investigation to determine the effect of atmospheric pressure on flare intensity.

NAD Crane has developed several computer programs in this category, of which, four of them may be of interest to this conference. These four are as follows:

A. Two dimensional flight—drag proportional to the square of velocity, uses a numerical integration technique. We use this program for simulation of canister and parachute flights.

B. Optimum ignition altitude—determines the ignition altitude for a single parachute flare so as to maximize the integral of area that is illuminated to some specified minimum level over the burning time of the flare.

C. Illumination contours—multiple flares—computes lumens/ft<sup>2</sup> for grid points on the ground.

D. Parachute deployment program—computes snatch force, filling time, force during filling time, maximum opening shock, time of maximum opening shock, and total deployment time of a parachute-flare

system for various input parameters of the system. Also, for fixed fall distance and fixed burning rate of the flare system, the size of a particular chute is determined that maximizes the length of the candle that can be placed with the chute in a given size container.

These "inside look" studies, which might be called systems engineering or systems analysis, are essential and their importance cannot be overemphasized.

#### IV. TOTAL SYSTEMS

However, the area that needs more technical effort is relating sub-system performance to the effectiveness of the total system. Using the decoy flare example, this outside look would examine the effect of flare intensity upon the friendly aircraft's ability to successfully decoy the enemy threat.

Another example of the total system's evaluation would be to determine the relationship of an illuminating flare's intensity and the probability of detecting a target. A better objective might be to relate flare intensity and the probability of destroying a target. Some people call this approach operations research or operations analysis. Regardless of the name of the game, the elements of the game are sub-systems, men, tactics, environmental factors, their interfaces and interaction; and the purpose of the game is to objectively establish sub-system requirements.

Some examples of current work in total systems are as follows:

A. Decoy flare—Naval Research Laboratory has developed this computer program and conducted analysis using the computer results.

B. Enemy Ground Fire Detector-Locator for Helicopters—this computer program has been developed by Systems Research Corporation of Washington, D. C. in conjunction with Naval Research Laboratory and NAD Crane. This problem concerns helicopter troop transport operations. Usually the transports are lightly armed and must depend on escort helicopter gunships to defeat the enemy threat. The transports must detect and locate the enemy threat then transmit this information to the gunship. The total systems simulation will establish equipment requirements in the form of probability of detection, location accuracy, and response time.

NAD Crane first became involved in this problem while examining the accuracy requirements for placement by the troop transport of a smoke marker which would assist the gunship in locating the target.

C. Illuminating Flare Mathematical Model—NAD Crane is beginning work in this area. The elements of this problem are as follows:

1. Source-illuminating flare, intensity versus wavelength
2. Transmission medium
3. Target size and reflectance
4. Sensor
5. Relative positions in space versus time
6. Environmental effects

The measure of effectiveness of this total system will be the probability of detecting a ground target. Various combinations of sources and sensors could be evaluated by this model. The model

would also allow changes in tactics to be evaluated.

#### V. GENERAL COMMENTS ON SIMULATION MODELS

A. They require quantitative expression—omit philosophy.

B. The cost of programming is sometimes high—this will be off-set by obtaining inexpensive computer experimental runs over many environmental conditions and parameter values.

C. Wide ranges of environmental conditions are difficult to obtain for real world experiments. Compresses time.

D. Avoid or at least minimize reprogramming costs by putting model in parametric form. For example, in the illuminating flare mathematical model the target size and reflectance would not be fixed within the program but could be assigned parameter values which would be input data to the computer.

MEASUREMENT OF ILLUMINATION-SOURCE-RELATED CHARACTERISTICS  
OF THE CYANOGEN-OXYGEN-BORON TRICHLORIDE FLAME SYSTEM

Robert L. Tischer and Karl Scheller  
Chemistry Research Laboratory  
Aerospace Research Laboratories  
Wright-Patterson AFB, Ohio

MEASUREMENT OF ILLUMINATION-SOURCE-RELATED CHARACTERISTICS  
OF THE CYANOGEN-OXYGEN-BORON TRICHLORIDE FLAME SYSTEM

Robert L. Tischer and Karl Scheller  
Chemistry Research Laboratory  
Aerospace Research Laboratories, Wright-Patterson AFB, Ohio

Abstract

The luminous efficiency for the premixed flame of the cyanogen-oxygen-boron trichloride system is reported over a range of compositions and burner sizes. The maximum efficiency measured was 33,668 cd-sec/gm. This exceeds the value of 24,366 cd-sec/gm previously determined by the authors for the diffusion flame of this system. The composition yielding the maximum efficiency was found to be nearly the same for both types of flames. The efficiency is found to increase with burner diameter, rapidly at first, then more slowly. Results of computations of the theoretical adiabatic flame temperature and equilibrium composition are also reported over the entire range of compositions and their relation to the experimental data is discussed. Spectra for selected flame compositions are presented.

Introduction

As previously reported by the authors<sup>1</sup> the diffusion flame of cyanogen-oxygen-boron trichloride is among the most efficient luminous sources. The study of this system was extended to include premixed flames in the hope of realizing higher efficiencies and of gaining a better understanding of the mechanism. In the following we present the results to date of this effort.

Experimental

The cyanogen gas was obtained in cylinders from two suppliers, the Matheson Co., Inc. and Air Products and Chemicals, Inc., and was used as received. The oxygen was aviator grade, dried by passing through a column of Drierite (anhydrous calcium sulfate). The boron trichloride, technical grade, was obtained from the Matheson Co., Inc. and it too was used as received.

The gases were metered using rotameters and fed to the burner, a National high intensity hand torch. The boron trichloride was combined with the oxygen flow prior to admission to the torch. In this way the mixing of the boron trichloride with the cyanogen was delayed until the last possible moment. Previous tests had indicated that these two gases react upon mixing, producing a white powder on the walls of the containing equipment.

This observation is supported by the work of Apple and Wartik.<sup>2</sup>

Nozzle tips having various diameter orifices were made by drilling the standard OX-3 nozzle supplied with the torch. Five diameters were tested: 1.68 mm, 2.38 mm, 4.76 mm, 6.35 mm, and 7.94 mm.

The luminous intensities were measured using an Edgerton, Germeshausen and Grier 580 Radiometer. The spectral response of this instrument is filter-corrected to conform with the standard luminosity response and calibrated at the factory. A flat-black vee-shaped light trap was placed behind the flame to minimize reflection into the meter. The experimental intensity values were divided by the mass flow rate to obtain the luminous efficiencies reported herein.

Theoretical adiabatic flame temperatures and equilibrium compositions were calculated on an IBM 7094 digital computer using a program made available to us by NASA.<sup>3,4</sup> Mixture compositions were specified in terms of the following parameters:

$$R = 100 \left[ \frac{C_2N_2}{C_2N_2 + O_2} \right]$$

and

$$D = 100 \left[ \frac{BCl_3}{C_2N_2 + O_2 + BCl_3} \right].$$

Spectra of the various flames were taken using a Jarrell-Ash Model 82-000 grating monochromator, Ebert mounting, 0.5 m focal length. The 1180 grooves per mm grating, blazed for 5000 Å, had a 52 mm by 52 mm ruled area. The detector was an EMI 62568 13-stage photomultiplier-tube, end-on, S-13 response. The wavelength scale of the spectrometer was checked using a mercury penlight and was found to be accurate within 2 Å.

The optical system between the flame and the entrance slit consisted of an  $f/2.8$  achromat, focal length 7.8 cm, and an  $f/1.2$  quartz plano-convex lens with a focal length of 5 cm. This combination was arranged such that an enlarged image of the test section of the flame was focused on the collimating mirror, which also served as the limiting aperture. The achromat was placed as close as physically possible to the entrance slit. As pointed out in Harrison, Lord, and Loofbourow<sup>5</sup> this arrangement fills the collimator with light and provides even illumination of the slit over its entire area insofar as is practicable. The test section at the flame position was less than 1 mm by 1 mm. This provided for a good local sample of radiation.

The calibration of the spectrometer in terms of spectral steradiancy was performed in the following manner. With the detector removed, the mercury penlight was placed at the exit slit of the monochromator. A tungsten ribbon filament lamp, General Electric Company type 30A/6V/T24, calibrated by the National Bureau of Standards for brightness temperature at 653 mμ as a function of lamp current, was positioned at the test section such that the image of the exit slit was focused on the lamp filament at the notch. For a more complete description of the lamp, proper usage, and its calibration by NBS, the interested reader is referred to the paper by Kostowsky.<sup>6</sup>

The power supply for the calibrated lamp consisted of a bank of automobile batteries wired in parallel to produce a 12-volt output. Since the current required to operate the lamp was high (data were taken at 26, 33, and 39 amperes) current regulation was obtained by dropping the potential across two 1-ohm resistors rated for 31.6 amperes each. These dropping resistors were wired in parallel. The remainder of the circuit consisted of the tungsten lamp, a knife switch, and a precision 0.001 ohm shunt all wired in series with the batteries and dropping resistors. The current was determined by measuring the potential drop across the 0.001 ohm shunt. With the potentiometer available, the voltage, and hence the current, could be measured to two decimal places.

Calibration data were obtained by scanning the spectrum at 500 Å per min and simultaneously measuring the potential across the shunt. The slit width, slit height and the potential across the photomultiplier were all held constant throughout calibration and use.

These data were then processed to obtain the calibration constant,  $C_\lambda$ , as follows. We can write

$$R_\lambda = K \int_{\lambda_1}^{\lambda_2} N_{\lambda,T}^0 \epsilon_{\lambda,T} \sin^2 \theta d\lambda + R_{bg}, \quad (1)$$

where  $R_\lambda$  = the response of the instrument, i.e., recorder output, volts;

$N_{\lambda,T}^0$  = spectral steradiancy of a blackbody at wavelength  $\lambda$  and temperature  $T$ , watts/cm<sup>2</sup>-ster-mμ;

$\epsilon_{\lambda,T}$  = emissivity of tungsten at wavelength  $\lambda$  and temperature  $T$ ;

$\Omega$  = solid angle subtended by the system, steradians;

$h$  = slit height, mm;

$S$  = slit width, microns;

$\tau$  = transmissivity of the optical system;

$K$  = instrument response function, volts/watt;

$R_{bg}$  = instrument background (dark current, etc.).

We define

$$c_{\lambda} = KSh\tau. \quad (2)$$

In order to obtain values for  $N_{\lambda,T}^0$  at wavelengths other than 653  $\mu$ , use was made of the relation

$$C_1 \lambda^{-5} \left[ \exp(C_2/\lambda T_B) - 1 \right]^{-1} = \epsilon_{\lambda,T} \tau_{\lambda} C_1 \lambda^{-5} \left[ \exp(C_2/\lambda T) - 1 \right]^{-1} \quad (3)$$

where  $C_1$  = first radiation constant,  $1.1909 \times 10^{16}$  watts/ster-cm<sup>2</sup>;

$C_2$  = second radiation constant,  $1.43879 \times 10^7$   $\mu$ -deg K;

$T_B$  = brightness temperature,  $^{\circ}$ K

$T$  = tungsten filament temperature,  $^{\circ}$ K

$\tau_{\lambda}$  = transmissivity of tungsten envelope

$\lambda$  = wavelength,  $\mu$ .

The emissivity of tungsten is given by Larrabee<sup>7</sup> as

$$\epsilon_{\lambda,T} = 0.6075 - 0.3000\lambda - 0.3265 \times 10^{-4}T + 0.5900 \times 10^{-4}\lambda T, \quad (0.350\mu < \lambda < 0.450\mu); \quad (4)$$

$$\epsilon_{\lambda,T} = 0.4655 + 0.01558\lambda + 0.2675 \times 10^{-4}T - 0.7305 \times 10^{-4}\lambda T, \quad (0.450\mu < \lambda < 0.680\mu); \quad (5)$$

$$\epsilon_{\lambda,T} = 0.6552 - 0.2633\lambda - 0.7333 \times 10^{-4}T + 0.7417 \times 10^{-4}\lambda T, \quad (0.680\mu < \lambda < 0.800\mu). \quad (6)$$

Equations 3 and 5 were used in an iteration routine to determine the value of  $T$ . The transmissivity of the lamp envelope was

assumed to be 0.92.

The iteration proceeded as follows. First a value for brightness temperature was calculated from the potentiometer measurement. Then, since the filament temperature is always considerably higher than the brightness temperature, an initial estimate of the filament temperature was obtained by adding a constant to the brightness temperature. This estimate of the filament temperature was inserted into (5) together with the proper value of  $\lambda$  (653 m $\mu$ ) to obtain a value for  $\epsilon_{\lambda,T}$ . This was inserted into (3) to calculate  $T$ . If the estimated and calculated values of  $T$  did not agree to within 1° the calculated value was inserted into (5) and the process repeated.

The calibration constant,  $C_{\lambda}$ , is given by

$$C_{\lambda} = \frac{R_{\lambda} - R_{bg}}{S \int_{\lambda_1}^{\lambda_2} N_{\lambda,T}^0 \epsilon_{\lambda,T} d\lambda} \quad (7)$$

The wavelength limits indicated in (7) were taken to be  $\lambda \pm d\lambda/2$ . The plate factor and the slit width were used to determine  $d\lambda$ ,

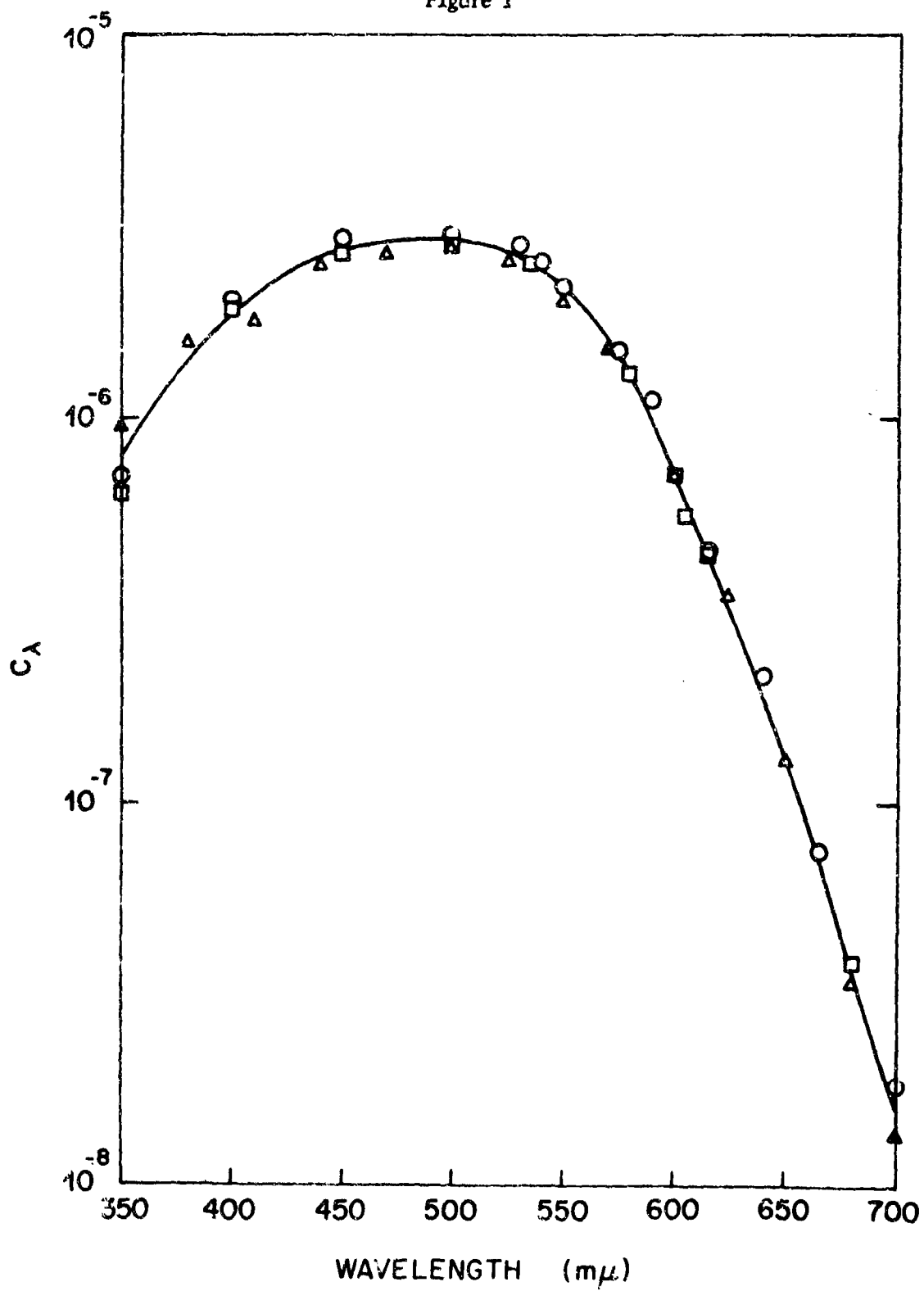
$$d\lambda = \text{plate factor} \times \text{slit width}. \quad (8)$$

The integral was evaluated by calculating values at  $\lambda_1$  and  $\lambda_2$ , obtaining their arithmetic average, and multiplying by  $d\lambda$ . The calibration results are shown in Figure 1.

This procedure was necessary since the brightness temperature is a function of wavelength. It is also worth pointing out that it would have been preferable to extend the calibration to 250 m $\mu$ , the reason being the possibility of overlapping of the first and second orders of the grating. This was not done for two reasons. First, the emissivity data of Larrabee do not extend to these lower wavelengths. Secondly, the transmissivity of the glass envelope begins falling off rapidly below 350 m $\mu$ . Since a cut-off filter was not available, the only recourse was to take the spectra down to 2500 Å and locate possible overlaps in the region of interest by inspection. None were found.

All spectra were taken 1.5 inches above the burner nozzle, well within the mantle area of the flames. The 2.38 mm nozzle size was selected to give well-behaved laminar flames. The slit height used was 7 mm and the slit width 40 microns. The spectral steradiancies obtained represent average values over a wavelength interval of 0.67 Å.

Figure 1



## Results and Discussion

To furnish a basis for comparison, initially an examination was made of the cyanogen-oxygen flame on the 1.68 mm nozzle. In Figure 2 the luminous efficiency of this system is shown as a function of the percentage of cyanogen in the mixture. The curve is similar to that reported by Stokes, et al.<sup>8</sup> with the exception of the appearance of the second peak which apparently was not observed by them. Some understanding of this rather unusual relationship between luminosity and composition may be gained by consideration of Figures 3 and 4.

In Figure 3, the computed equilibrium mole fractions for the various species have been plotted as a function of the percentage cyanogen in the original gases. The NASA program used lists all the chemical species considered and prints out the mole fractions for those whose value exceeds  $5 \times 10^{-6}$ . In the interests of clarity, the graph was restricted to species with a maximum mole fraction greater than  $10^{-4}$ . The most important minor species omitted under this constraint was  $C_2O(g)$  which attained a maximum value of  $9.3 \times 10^{-6}$  at  $R = 56$ . It is of interest to note the high concentrations of the free radicals, particularly the oxygen atom, and the large changes taking place as a function of composition at the stoichiometric and near-stoichiometric compositions. In particular one should observe the rise in the mole fraction of CN followed closely by that of the  $C_2$  free radical. Both of these reach a maximum at a composition of 55% cyanogen, then fall in a linear fashion that is related to the rise in the mole fraction of solid carbon, which does not begin to appear until after  $R = 56$ . Molecular radiation from CN and  $C_2$  molecules as well as continuum radiation was observed in the spectrum of the cyanogen-oxygen diffusion flame. Cyanogen is seen to appear in the product distribution on the rich side.

In Figure 4 the theoretical adiabatic flame temperature has been plotted as a function of composition. It is interesting to note the close correspondence between this curve and the graph for the mole fraction of nitrogen atom in Figure 3. The temperature plot indicates that the extremely high value generally quoted for the cyanogen-oxygen flame is quite sensitive to composition. The rapid rise in temperature is seen to be brought about by the fall in the mole fraction of oxygen atoms which is only partially offset by the increase in the numbers of nitrogen atoms. The formation of the free radicals,  $C_1$ , CN, and  $C_2$  causes the temperature to fall as rapidly as it rose until the condensation of carbon begins to act as a stabilizing factor.

An explanation may now be advanced for the trend of luminous efficiencies depicted in Figure 2. As the CN and  $C_2$  free radicals begin to build up the amount of light produced by the flame increases. The presence of CN in the product gases is indicated

Figure 2

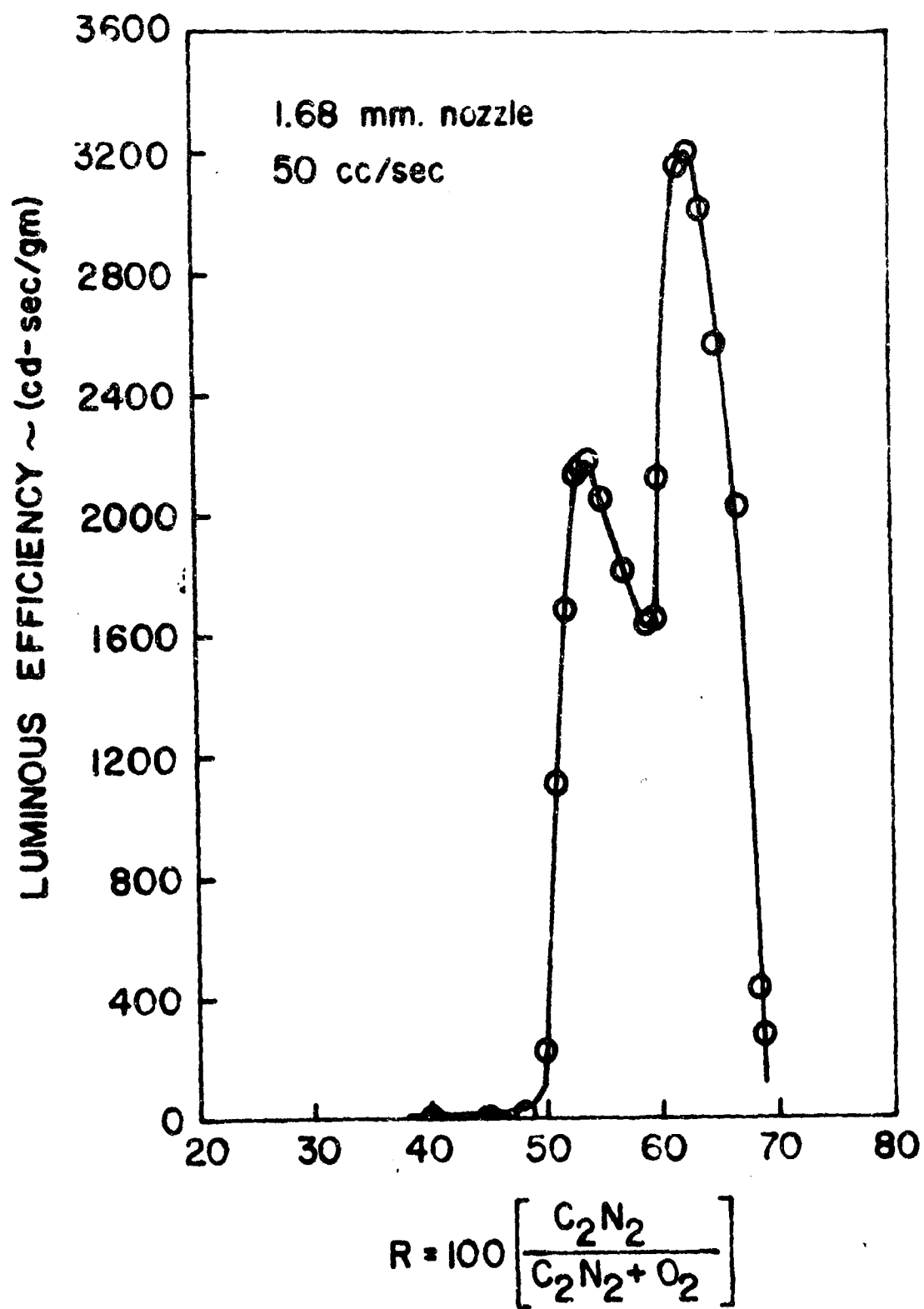


Figure 3

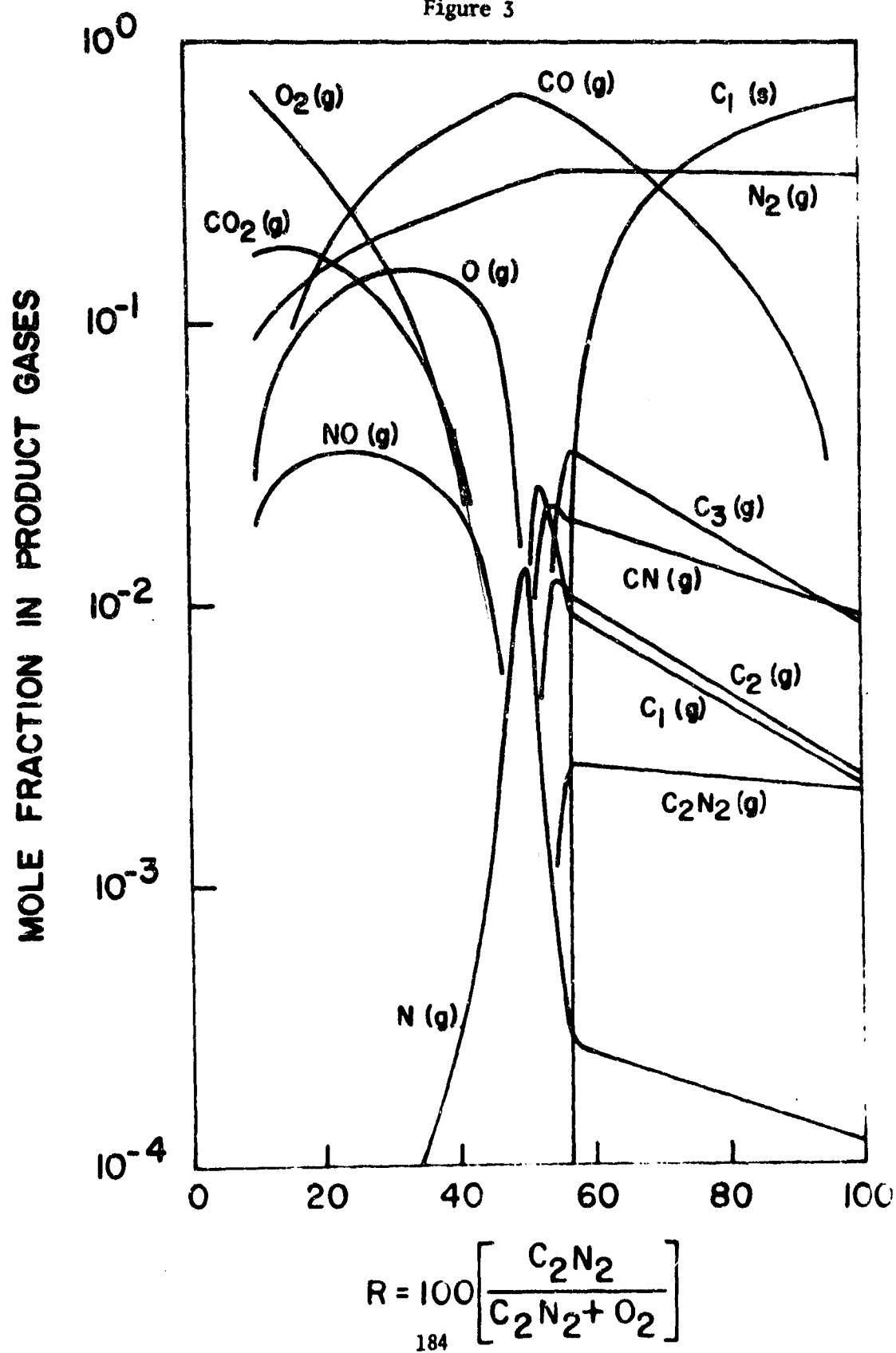
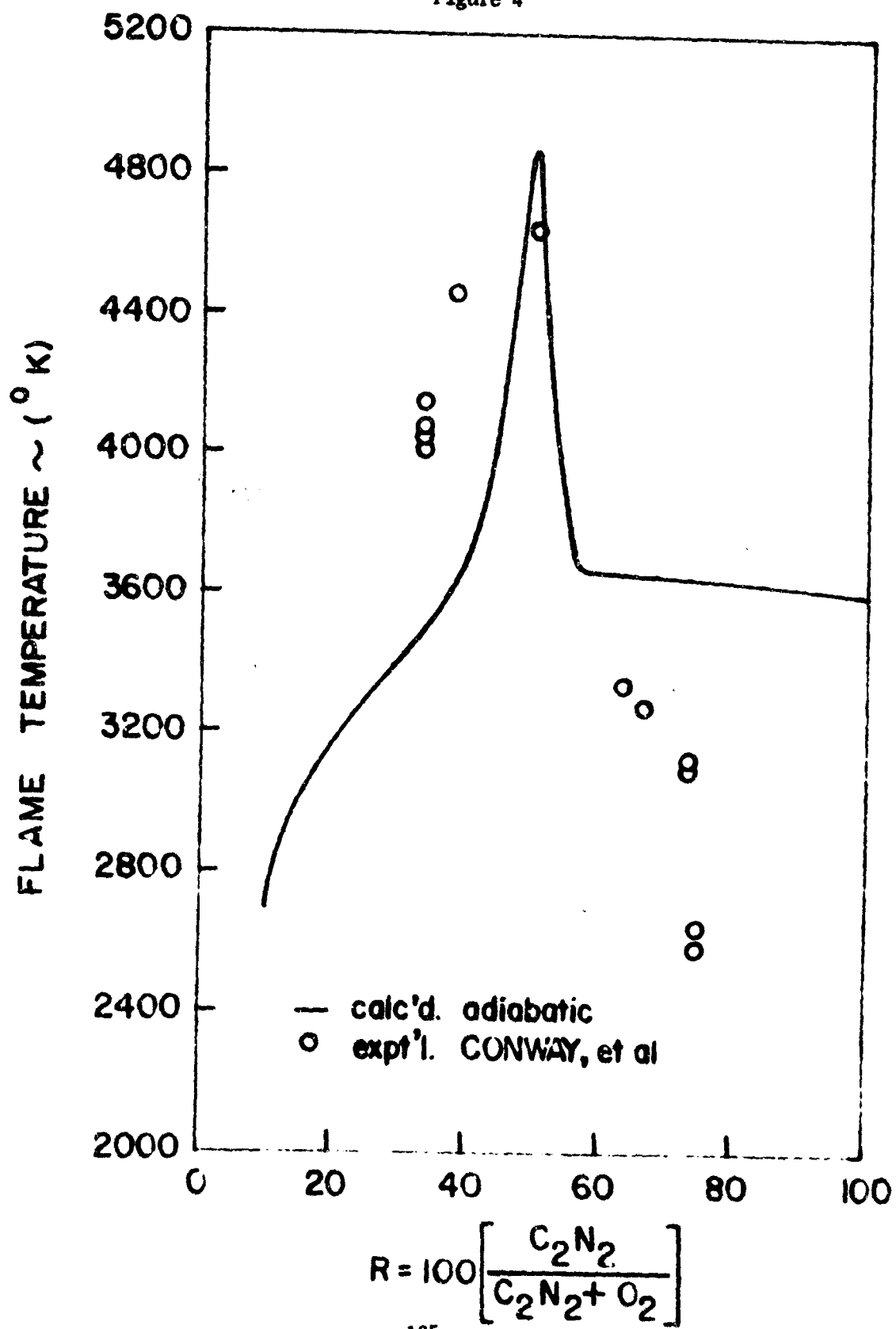
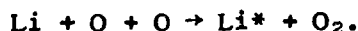


Figure 4



by a pink region just outside the reaction zone for flames a little on the lean side. These free radicals continue to increase in concentration as the flame becomes rich, apparently at a rate great enough to offset the effect of the declining temperature, until they reach their peak values at 55% cyanogen. At still richer compositions the light output falls due to declining numbers of emitters and decreasing temperature until offset by the increasing quantity of solid carbon which reverses the trend. Again an increase in luminous output is observed until the cooling caused by the radiative transport balances the increasing concentration leading to a second peak.

The foregoing supposition is supported in part by the experimentally determined temperatures of Conway, et al.<sup>9</sup> plotted as circles in Figure 4. It is seen that the temperatures are declining rapidly on the rich side ( $R > 50$ ). This may be attributed to the loss of energy by radiative transport which, of course, results in reduced actual flame temperatures as is well known. As regards the anomalously high values reported on the lean side, we note that these occur in a region of very high oxygen atom concentration as shown in Figure 3. Their experimental determination involved the use of lithium in a modified line-reversal technique. Hence, these values may be indicative of the formation of excited lithium via the reaction



The formation of carbon as a product was detected when operating on the rich side. The first indication was the change in color of the mantle top to orange. Conway and Grosse<sup>10</sup> also noted the orange tipped plume and the sensitive nature of the flame in the stoichiometric region. At concentrations of 62% and greater of cyanogen, the formation of long soft black strings of carbon which floated about slowly in the air was observed. This seems to contradict the statement by Gaydon and Wolfhard<sup>11</sup> that "cyanogen will not give any carbon formation at all in either diffusion or premixed flames of normal size", but the discrepancy may very well only be apparent since we do not know whether they have looked at these richer mixtures.

Further credence for the foregoing interpretation is furnished by spectra obtained for selected flame compositions. In Figure 5 is shown the spectrum for the flame containing 63.5% of cyanogen. The major feature in this case is the continuum as would be expected for a flame producing copious quantities of carbon. Also in evidence are bands corresponding to transitions in the violet system of CN at 421.6  $\mu$  (0,1), 388.3  $\mu$  (0,0), and 359.0  $\mu$  (1,0).

The spectrum of the flame containing 55% cyanogen is presented in Figure 6. Prominent bands corresponding to transitions

Figure 5

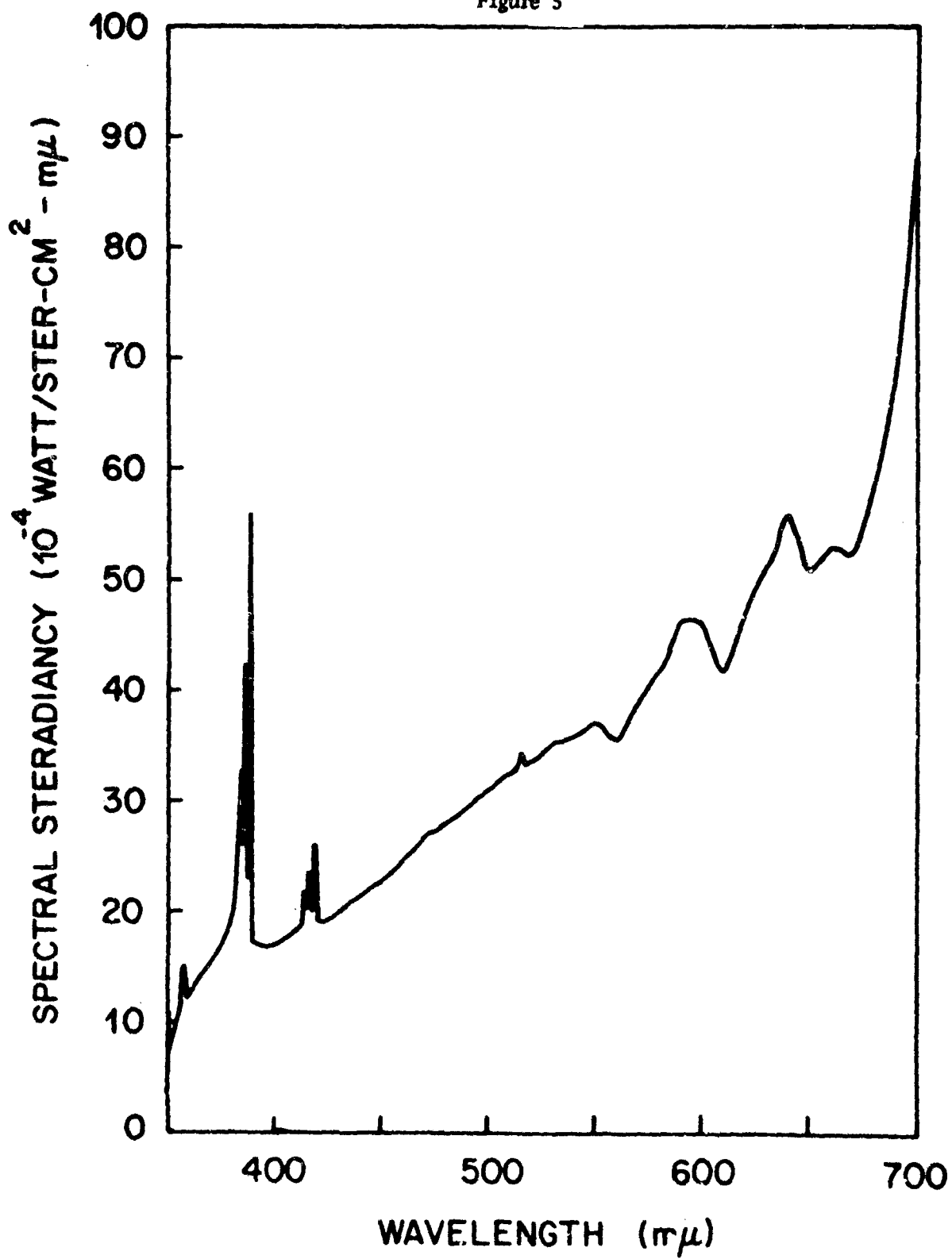
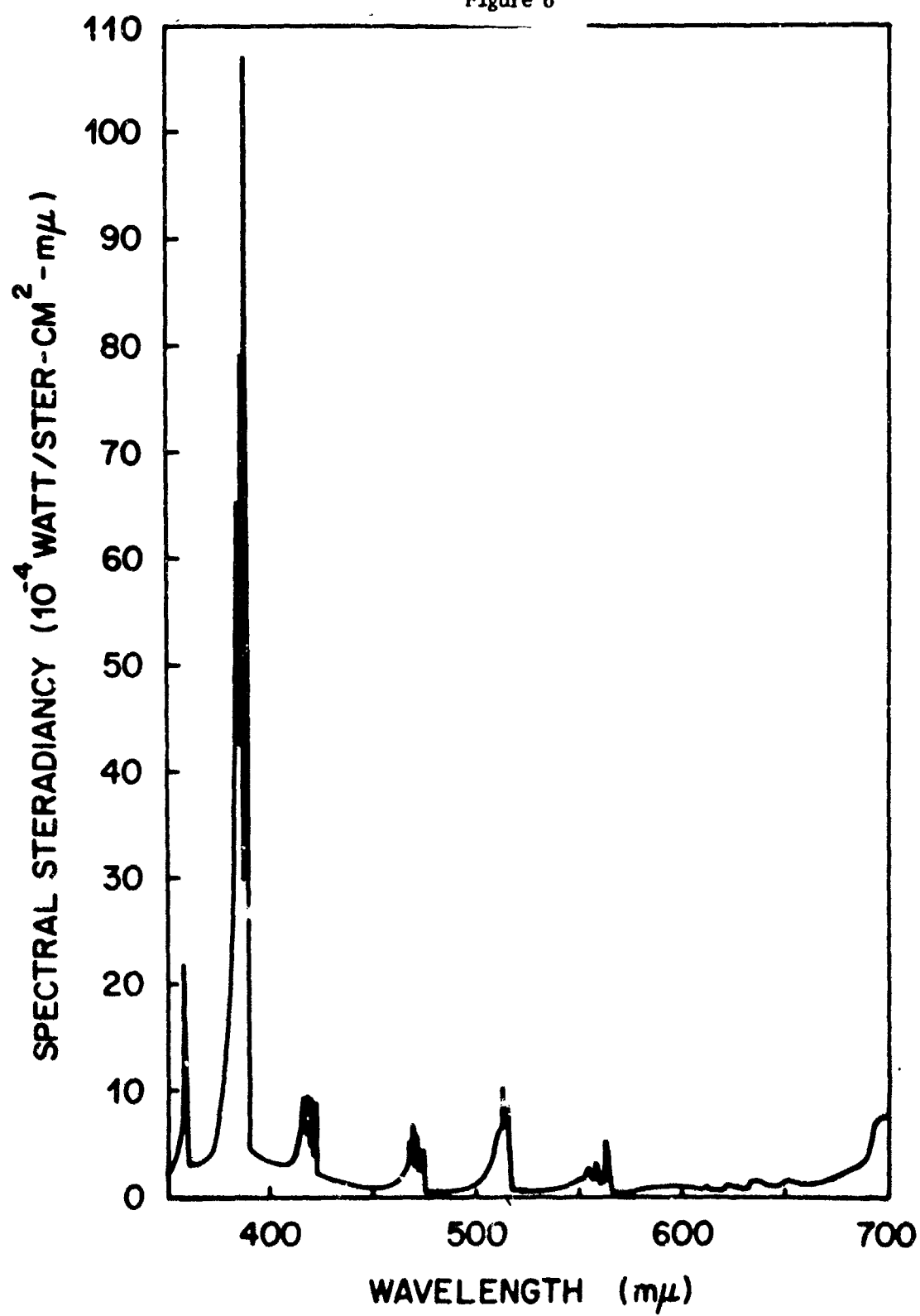


Figure 6



in the Swan system of  $C_2$  are observed at 619.1  $m\mu$  (0,2), 563.6  $m\mu$  (0,1), 516.5  $m\mu$  (0,0), and 473.7  $m\mu$  (1,0). Bands corresponding to the (0,1), (0,0), and (1,0) transitions in the violet system of CN are quite evident. This particular composition was selected in order to determine if the  $C_3$  bands could be detected. If they are present, they do not constitute a major feature.

Contrasted to the previous two compositions the flame containing 43% cyanogen is a very weak radiator. This is borne out by the spectrum of this flame, shown in Figure 7. It should be noted that the ordinate in this case is smaller by a factor of  $10^{-2}$  than those of the two preceding figures.

A sample of the black solid material presumed to be carbon was collected and sent for analysis. The results showed 85.17% carbon, 0.98% nitrogen, 12.11% oxygen, and 2.05% hydrogen. Since hydrogen was not a reactant, this is taken to indicate the presence of adsorbed water. The low value for nitrogen indicates that, while the solid material may contain some CN, the polymer is definitely primarily one of carbon and not paracyanogen.

Turning now to the cyanogen-oxygen-boron trichloride system, Figure 8 presents all the luminous efficiencies that could be measured on the 1.68 mm nozzle for constant volumetric flow rates. It is important to take the data at constant volumetric flow rates for a given nozzle since the efficiency is a function of this parameter as shown in Figure 9. The change in efficiency with volumetric flow rate is considered to be due primarily to the influence of the latter on the resulting plume geometry. While air entrainment certainly must occur, its effect for the 55% composition shown in Figure 9 would be to decrease the luminous efficiency at small D-values as shown by the data of Figure 10. Because of their geometry, air entrainment was not thought to be a problem in the diffusion flames studied earlier by the authors.

Returning to Figure 8, flashback and blowoff considerations limited the compositions that could be studied on this burner size at a constant volumetric flow rate. However, it is seen that the efficiency is increasing as the percentage of cyanogen in the base flame is reduced.

In Figure 10 are shown the efficiencies measured on a 2.38 mm nozzle as a function of cyanogen-content for various fixed amounts of boron trichloride. One observes that as the amount of boron trichloride is increased, the peak at 55% cyanogen gradually disappears. A reason for this behavior is offered by Figure 11 in which the variation of the concentration of some of the significant flame species with cyanogen-content is illustrated for the case  $D = 7.50$ , which is taken as typical. Upon examination of

Figure 7

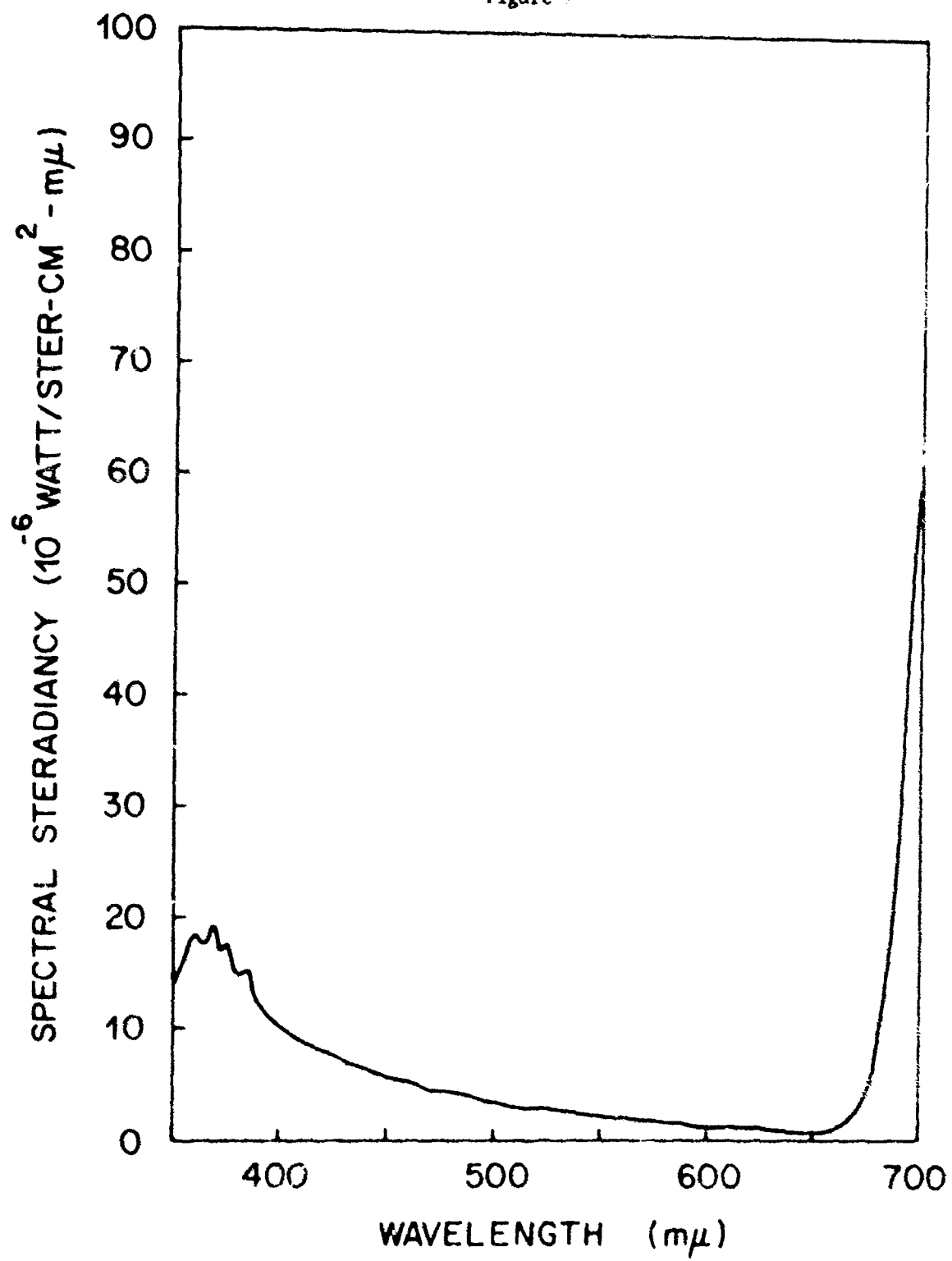


Figure 8

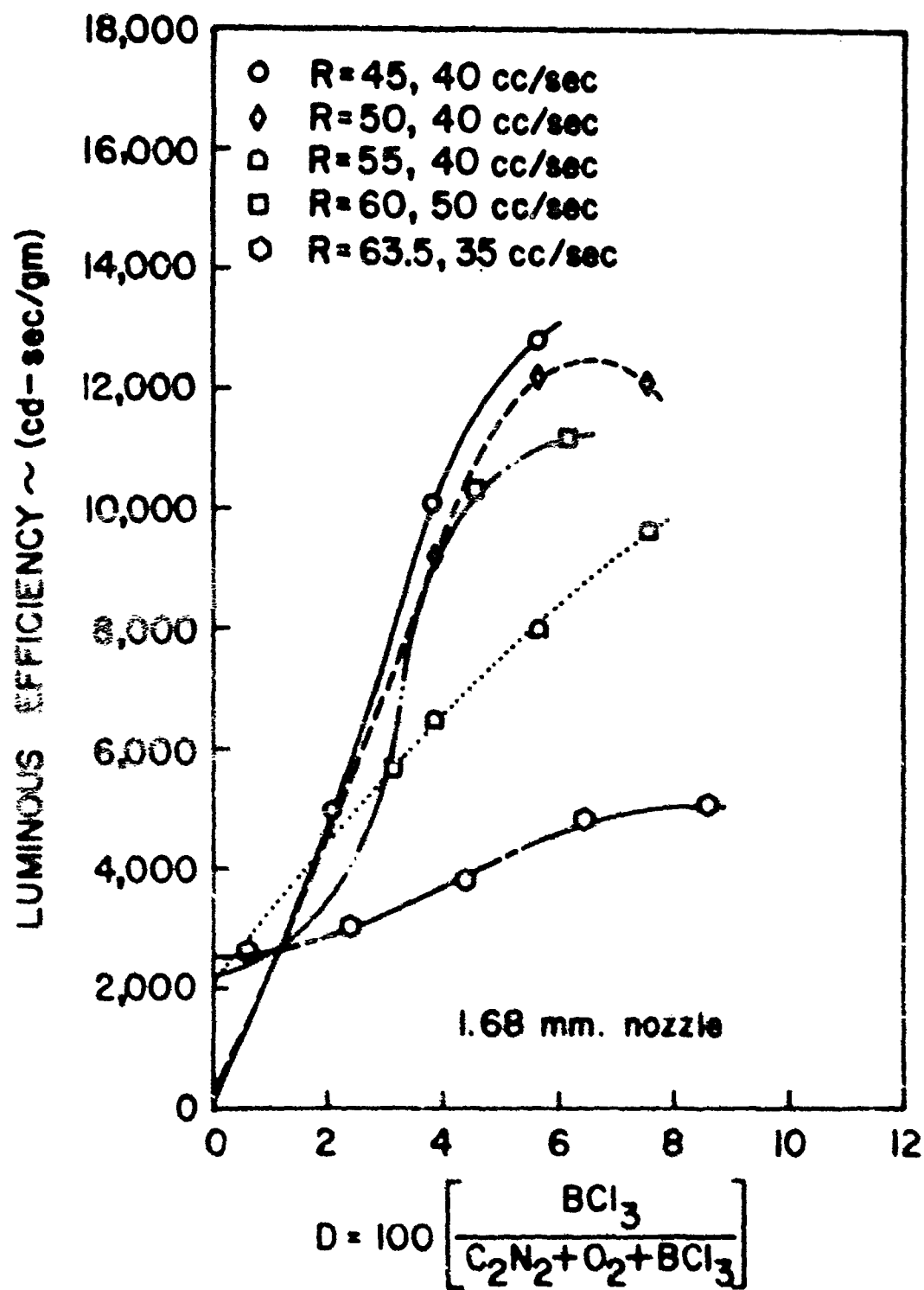


Figure 9

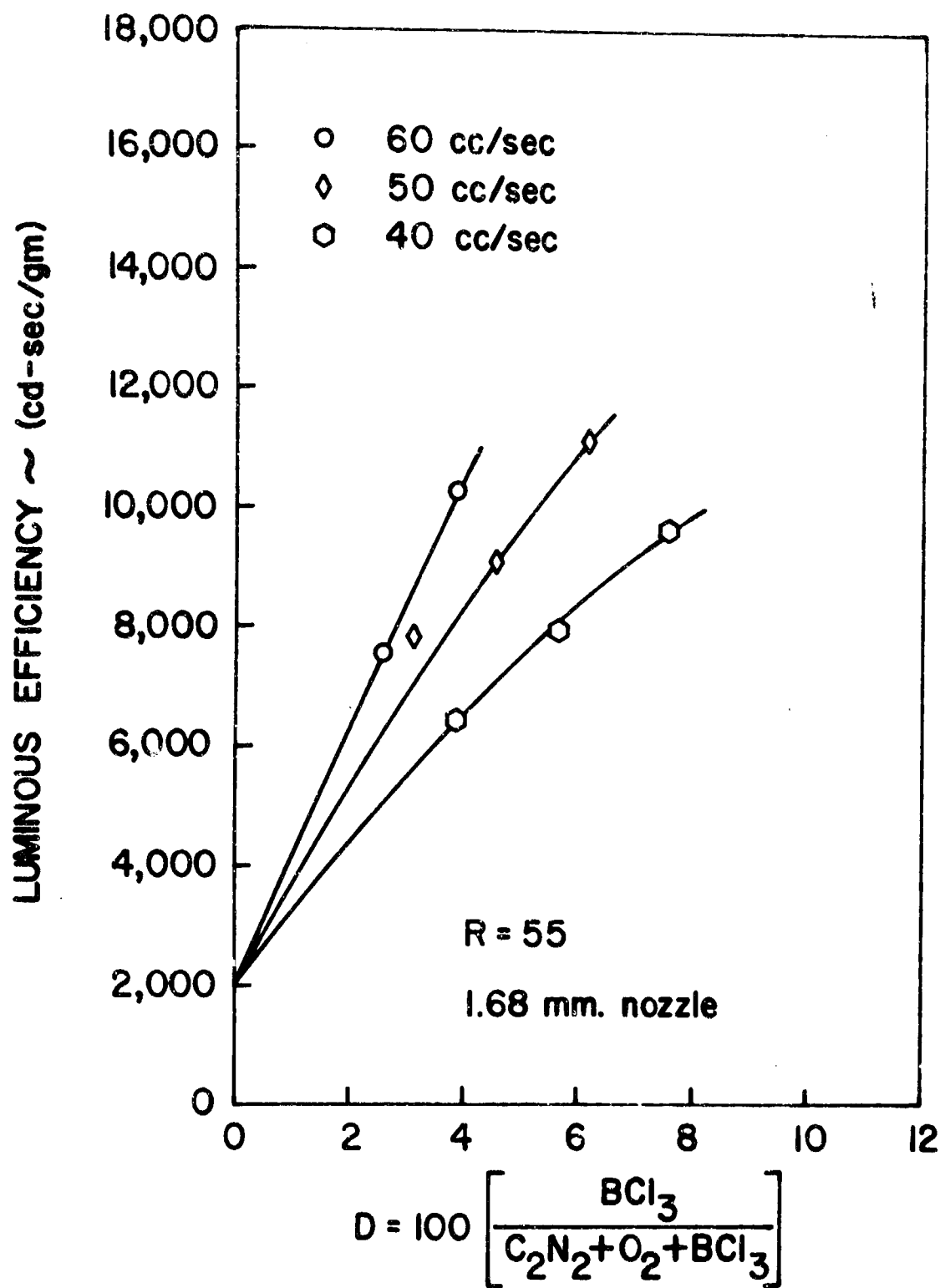
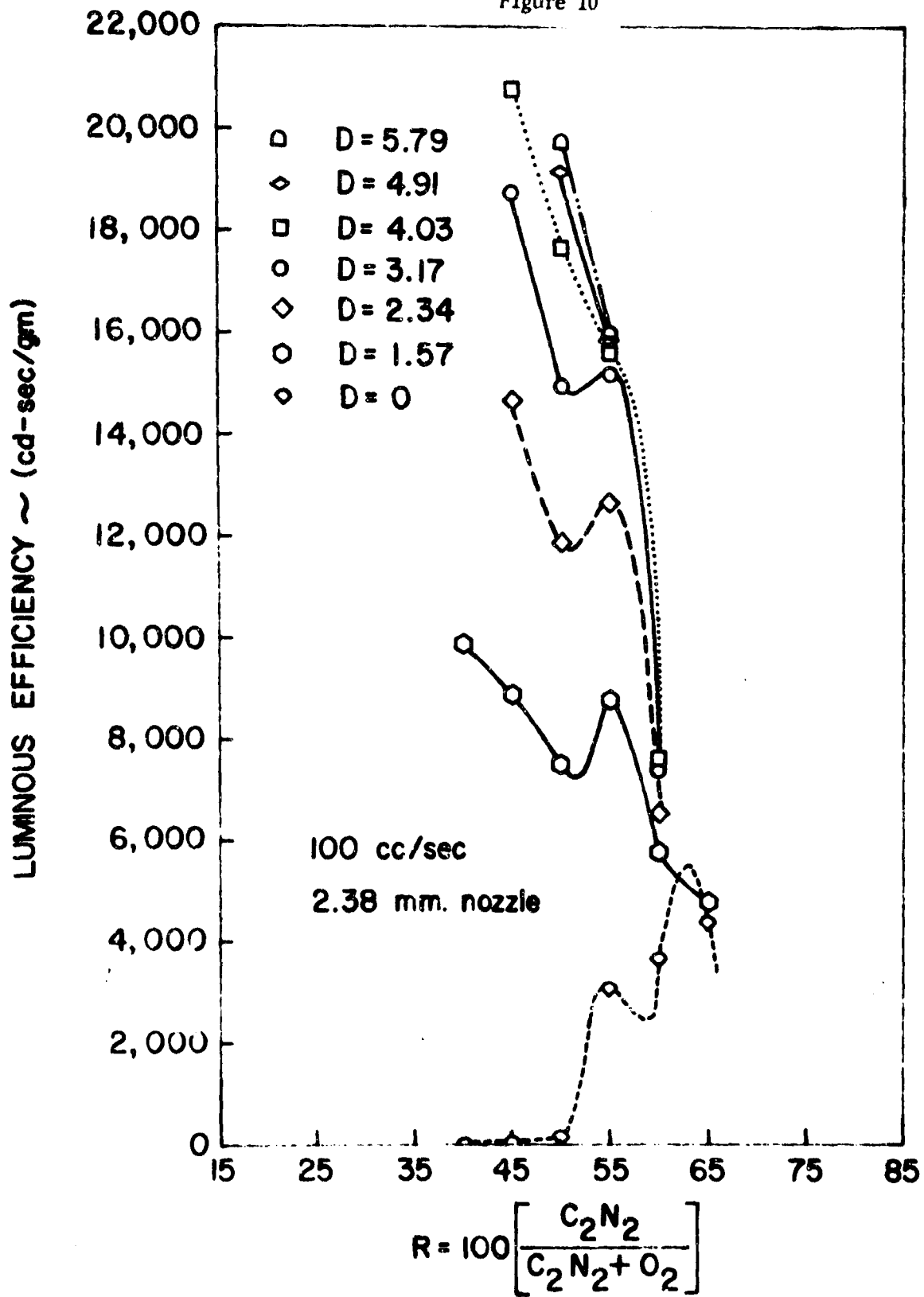


Figure 10



these plots, one will note that the CN and  $C_2$  free radicals and solid carbon all appear in mixtures of lower cyanogen-content than was the case for the flame without additive. Indeed, examination of the computed results shows that as the amount of boron trichloride is increased, all three of these products make their appearance in flames of progressively lower cyanogen-content. Stated in another way---as D increases, the curves of mole fraction vs. R for CN,  $C_2$ , and solid carbon all shift to the left. This simply reflects the fact that the boron is competing for the oxygen.

The mole fractions of the major products of combustion, as well as many minor ones, are not plotted in Figure 11 in an attempt (albeit unsuccessful) to reduce clutter. The graphs of oxygen, carbon monoxide, carbon dioxide, and nitrogen all have the same form as in Figure 3. The mole fraction of nitrogen atom is reduced about two orders of magnitude at its peak value. Boron nitride forms only to a small extent (of the order  $1.5 \times 10^{-4}$ ) on the rich side.

Of those species appearing in Figure 11 one notices a decrease in the mole fraction of oxygen atom relative to that in the parent cyanogen-oxygen flame; the appearance of a BO curve similar in shape to that of nitrogen atom; the relationship of the curves for  $BO_2$ ,  $B_2O_3(g)$ ,  $BOCl$ , and  $Cl$ ; and the fact that the mole fraction of NO is about the same as in the flame without boron trichloride.

Figure 11 also shows that the concentration of  $BO_2$  in these flames can reach values commensurate with those attained by CN and  $C_2$  in the cases previously considered. However, as the spectrum in Figure 12 indicates, while the spectral steradiancy is of the same order of magnitude it is much more broad-band than that of CN or  $C_2$  and hence is a much more effective luminous radiator. It should also be borne in mind that the adiabatic flame temperatures associated with the CN and  $C_2$  radiation is considerably higher.

The temperature curve corresponding to the particular composition under discussion is shown in Figure 13. The most noticeable feature is the disappearance of the large temperature spike at the  $R = 50$  point. The peak temperature occurs at lower R-values as D is increased. This can be seen by examining Table 1.

The data of Figure 10 still did not permit us to determine the maximum efficiency. However, by lowering the volumetric flow rate for the 2.38 mm nozzle to 45 cc/sec the data of Figure 14 were obtained. Plotting the data in this manner permits the determination of trends for R and D simultaneously and independently of each other.

The presence of a maximum in the luminous efficiency as the

Figure 11

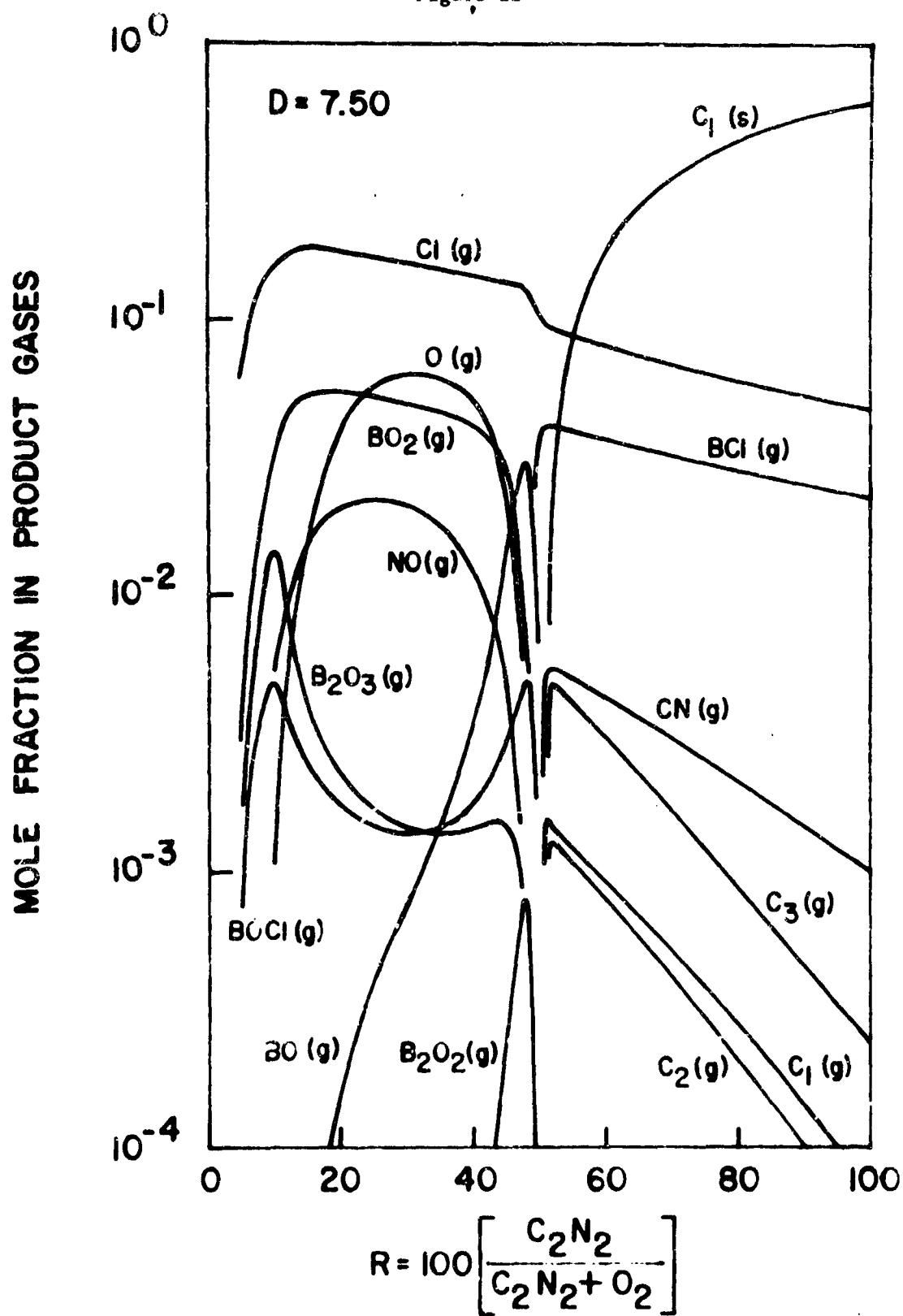


Figure 12

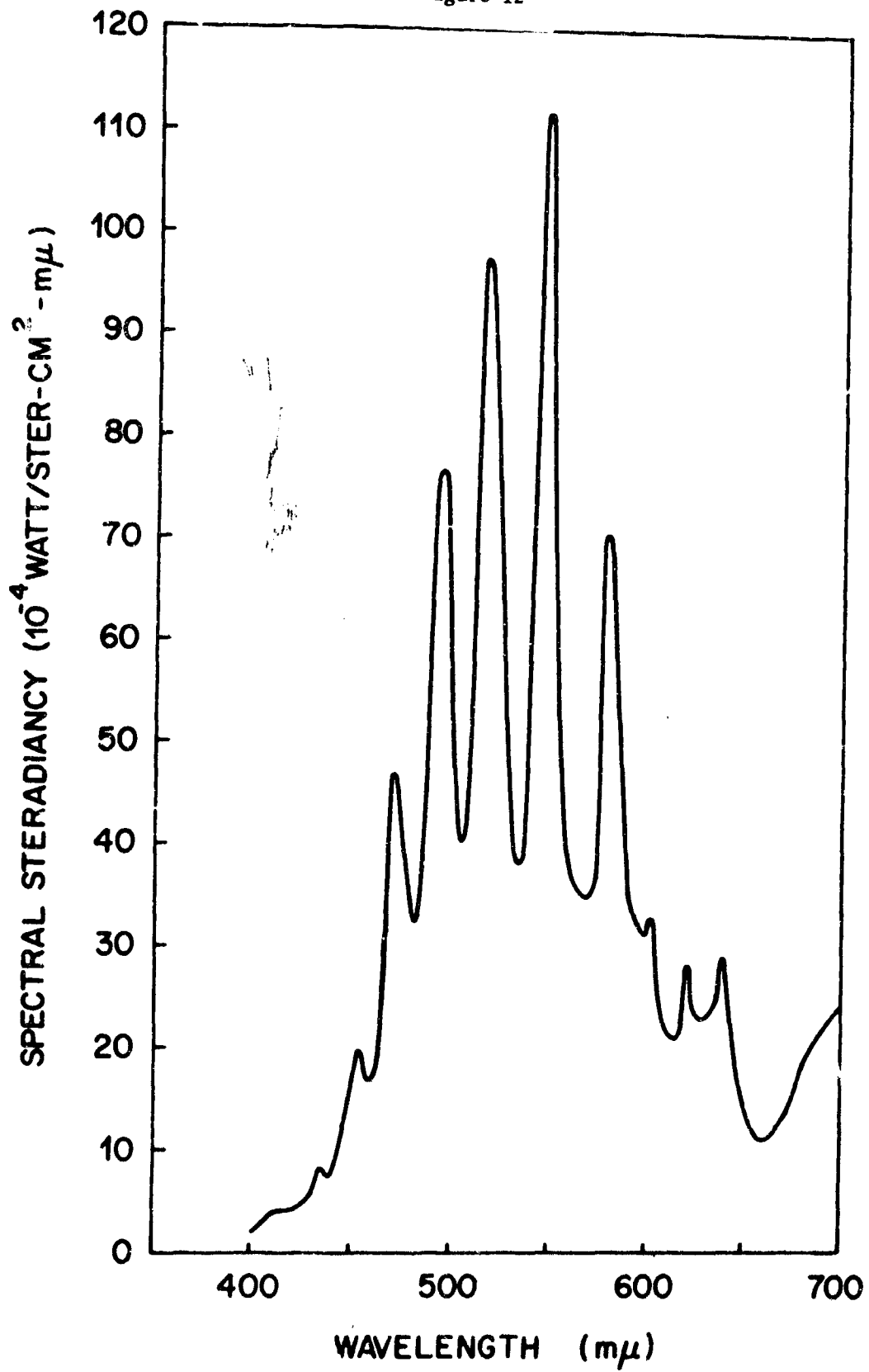


Table 1

Calculated Adiabatic Flame Temperature as a Function of the Composition Parameters R and D

D	R													
	30	35	38	40	41	42	43	44	45	46	47	48	49	50
0.00	3407	3528	3619	3698	3747	3807	3881	3978	4105	4265	4448	4634	4796	4858
2.34	3340	3456	3539	3609	3651	3701	3760	3833	3922	4033	4167	4318	4445	4424
4.91	3262	3372	3446	3506	3541	3582	3628	3683	3746	3817	3897	3986	4021	3917
7.50	3177	3279	3343	3392	3420	3451	3486	3524	3563	3599	3621	3618	3599	3570
9.18	3118	3214	3270	3310	3332	3355	3381	3406	3429	3440	3429	3401	3372	3341
11.00	3051	3138	3182	3210	3224	3238	3251	3263	3271	3267	3243	3202	3152	3086
13.00	2973	3046	3074	3084	3087	3089	3092	3097	3101	3092	3057	3005	2949	2894
15.00	2850	2944	2949	2940	2934	2928	2927	2932	2937	2922	2888	2852	2820	2790

197

Table 2

Calculated Equilibrium Mole Fraction  $\text{BO}_2$  in Product Gases as a Function of the Composition Parameters R and D

D	R														
	30	35	38	40	41	42	43	44	45	46	47	48	49	50	
0.00															
2.34	.01675	.01545	.01449	.01361	.01302	.01225	.01120	.00973	.00770	.00521	.00276	.00104	.00022		
4.91	.03403	.03157	.02977	.02818	.02714	.02581	.02403	.02157	.01815	.01366	.00838	.00326	.00034		
7.50	.04967	.04622	.04362	.04133	.03984	.03797	.03547	.03200	.02708	.02030	.01157	.00272	.00022		
9.18	.05843	.05430	.05102	.04805	.04609	.04360	.04025	.03553	.02871	.01926	.00821	.00153	.00019		
11.00	.06621	.06108	.05658	.05225	.04932	.04552	.04043	.03336	.02377	.01250	.00374	.00078	.00011		
13.00	.07203	.06498	.05790	.05072	.04592	.04001	.03271	.02382	.01382	.00521	.00130	.00029	.00004		
15.00	.07406	.06237	.05139	.04114	.03482	.02795	.02060	.01290	.00572	.00159	.00041	.00010	.00002		

Figure 13

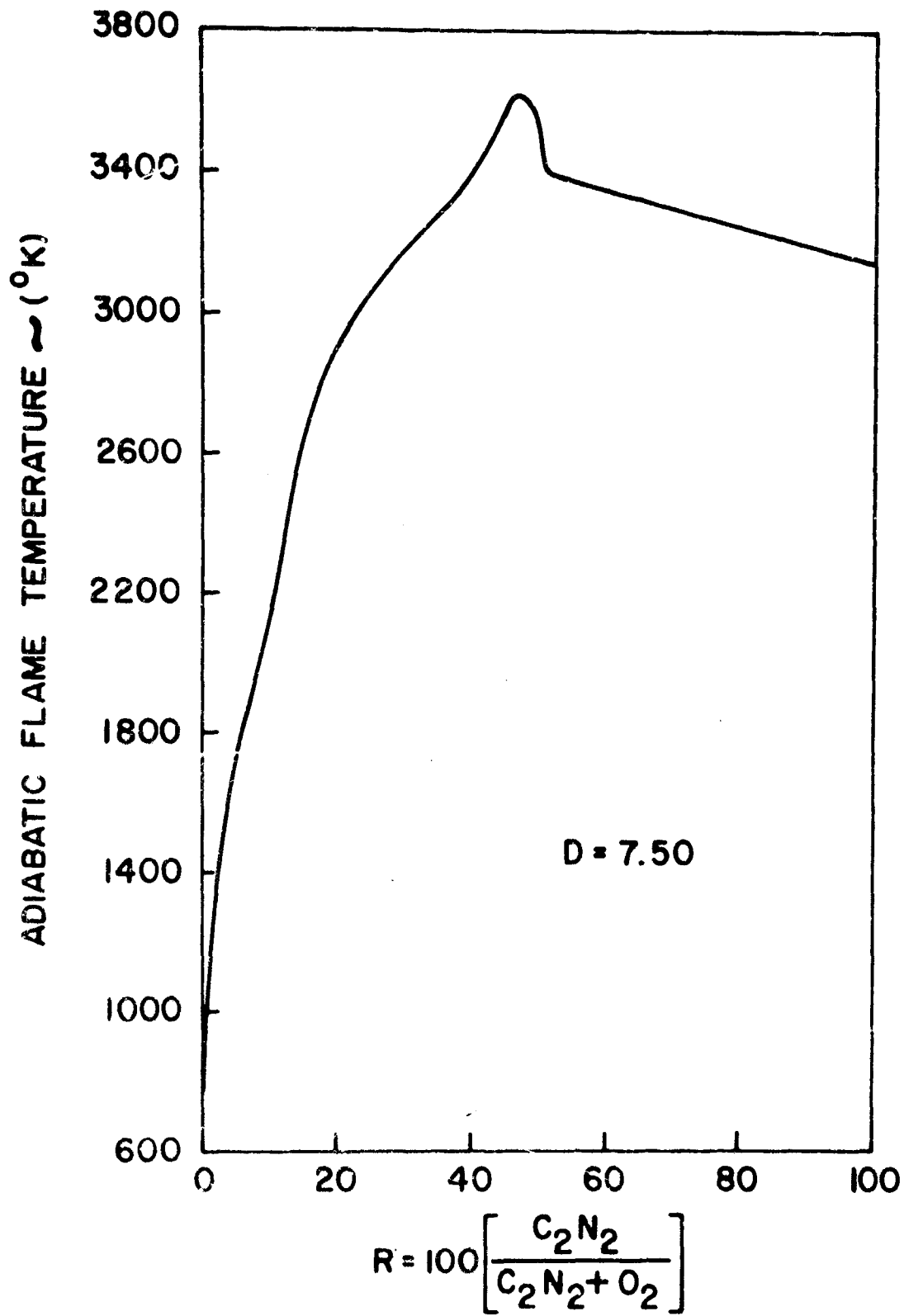
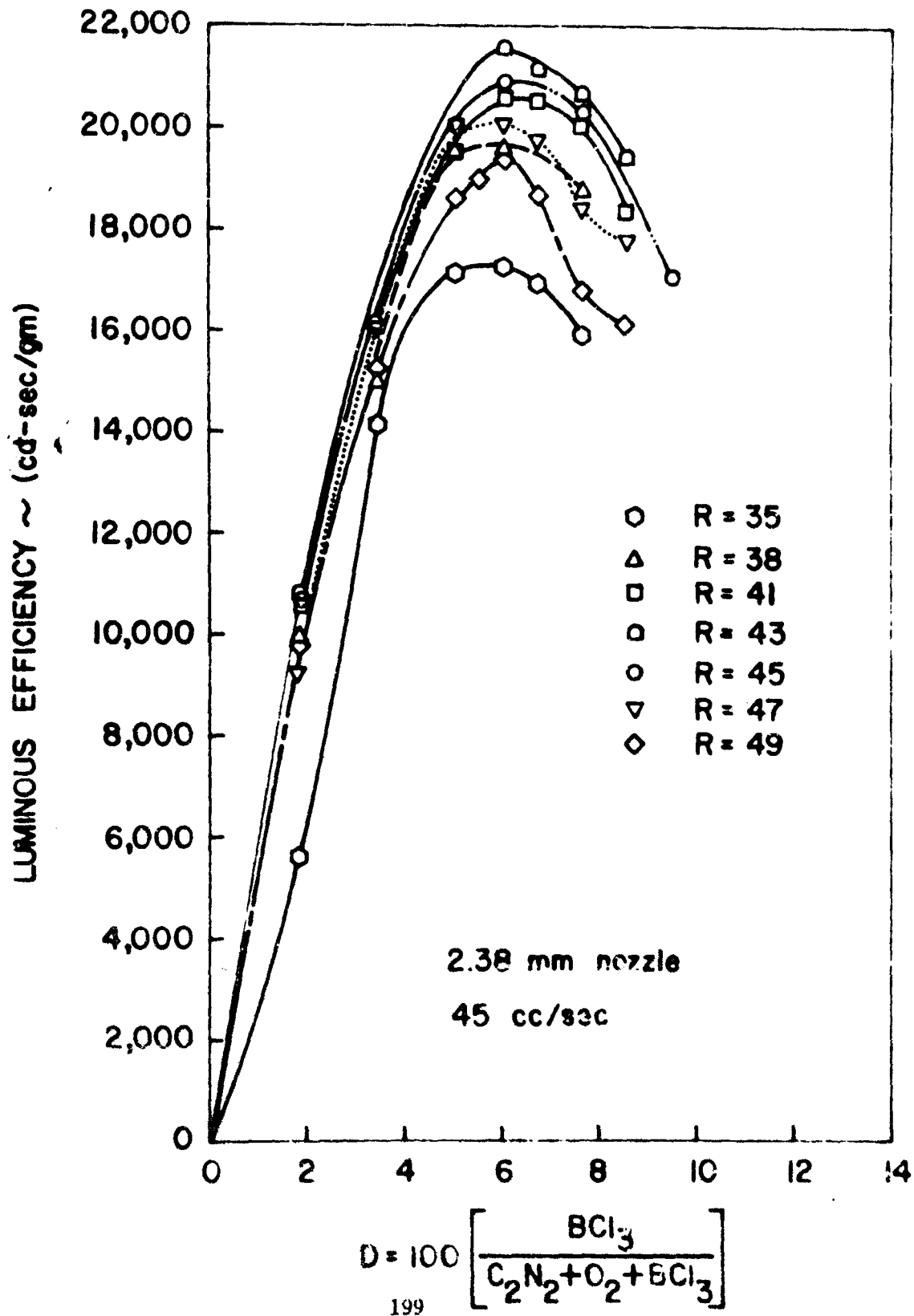


Figure 14



boron trichloride content is increased for constant  $R$  is expected on theoretical grounds. In Table 2 are listed calculated values for the mole fraction of  $\text{BO}_2$  in the product gases. Data from this table are plotted in Figure 15. Similarly, data from Table 1 are plotted in Figure 16. We see that as  $D$  increases at constant  $R$  the temperature decreases monotonically. The increase in the mole fraction of  $\text{BO}_2$  occurring simultaneously can thus be expected to lead to a maximum in the light emitted by this molecular species since the light emission is a function of temperature, concentration, and geometry and the geometry remains essentially constant.

The study was extended to various larger-sized burners with the results shown in Figure 17. In this figure the maximum value of the efficiency measured for each burner size is displayed. Insofar as was practical the attempt was made to keep the bulk average velocity constant. However, as the burner diameter was increased it was found necessary to increase the velocity to prevent flashback. Thus the velocity for the 2.38 mm nozzle was 1077 cm/sec while the value for the 7.94 mm nozzle was 1326 cm/sec. Nevertheless one can still arrive at the general conclusion that the efficiency will not be improved much by any further increase in burner diameter. This is doubtless related to the increase of optical density with burner diameter.

It was also observed that as the burner diameter increased, the value of  $R$  at the maximum decreased, finally appearing to stabilize at  $R = 38$  for the large burners. The explanation for this phenomenon probably lies in the effect of air entrainment. As the burner diameter increases, the entrained air represents a smaller fraction of the total gas and its effect naturally becomes less important.

The effect of hydrogen on the results was investigated by studying the effect of hydrogen gas and hydrogen cyanide gas on the computed values for the  $R = 40$ ,  $D = 7.50$  flame. It was found that the addition of either of these materials resulted in both lower adiabatic flame temperature and lower mole fraction  $\text{BO}_2$ . However, for the amounts which might be present in the reactant materials, the effect would be small indeed. If anything, the efficiencies studied would be a little higher and the burning velocities lower.

The present results for the premixed flame show that, at least for the particular cases studied, the luminous efficiency of the premixed flame is higher than that of the diffusion flame. It is a curious fact though, that both types of flames yielded their maximum efficiencies at approximately the same composition. It is tempting to speculate whether variation of the geometry and/or flow rates could cause the diffusion flame to become more efficient than the premixed one due to its ability to superpose

Figure 15

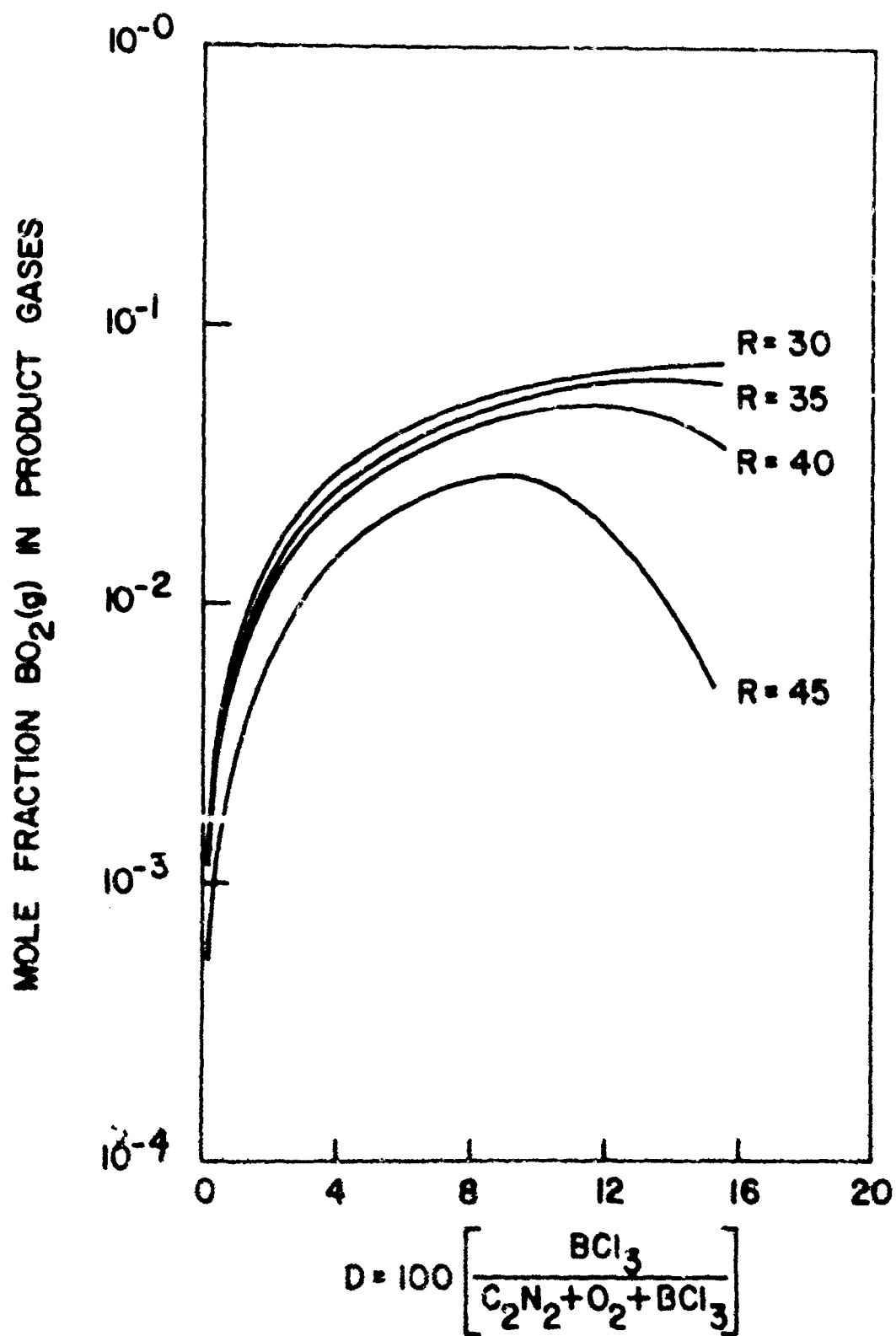


Figure 16

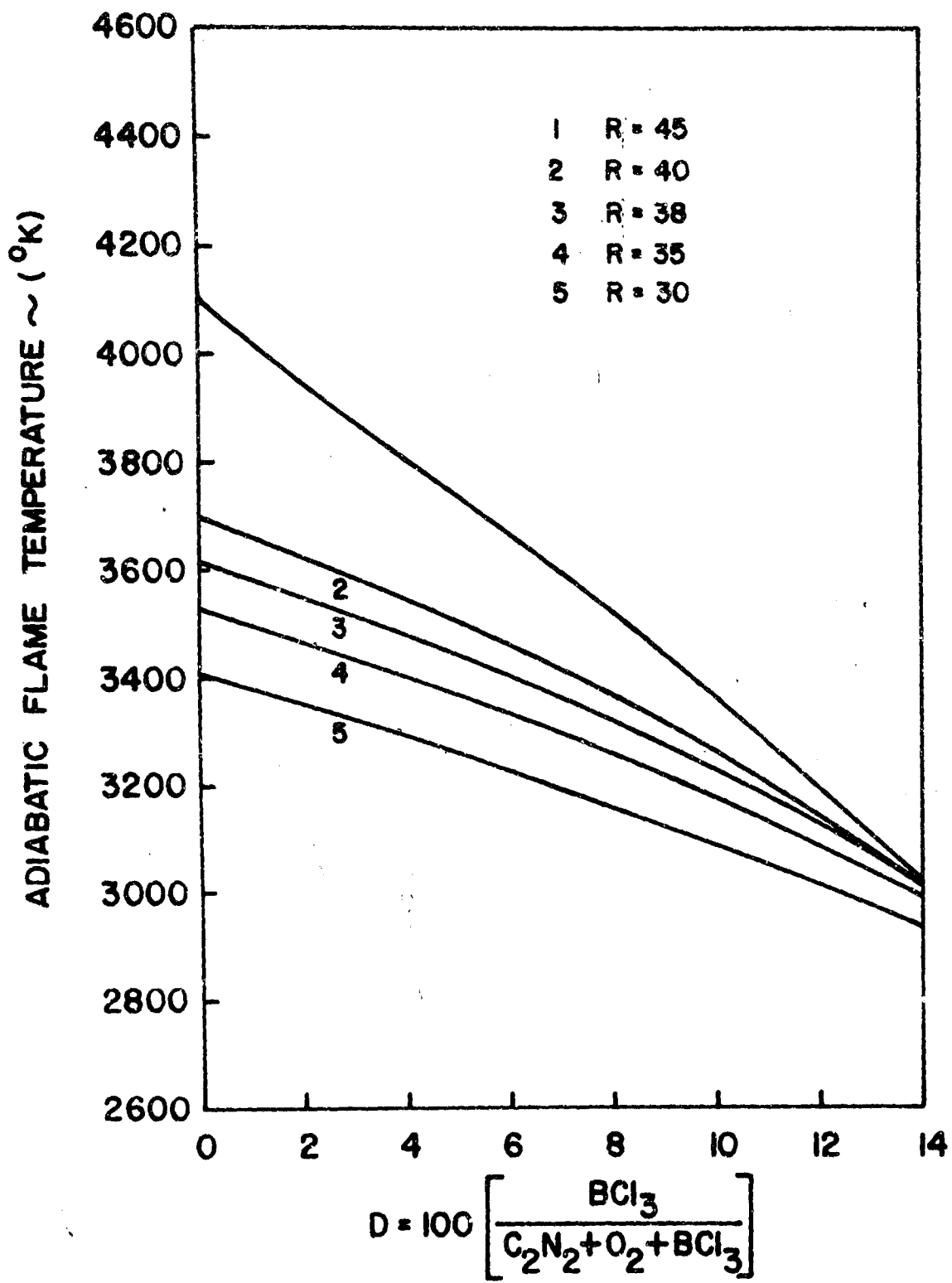
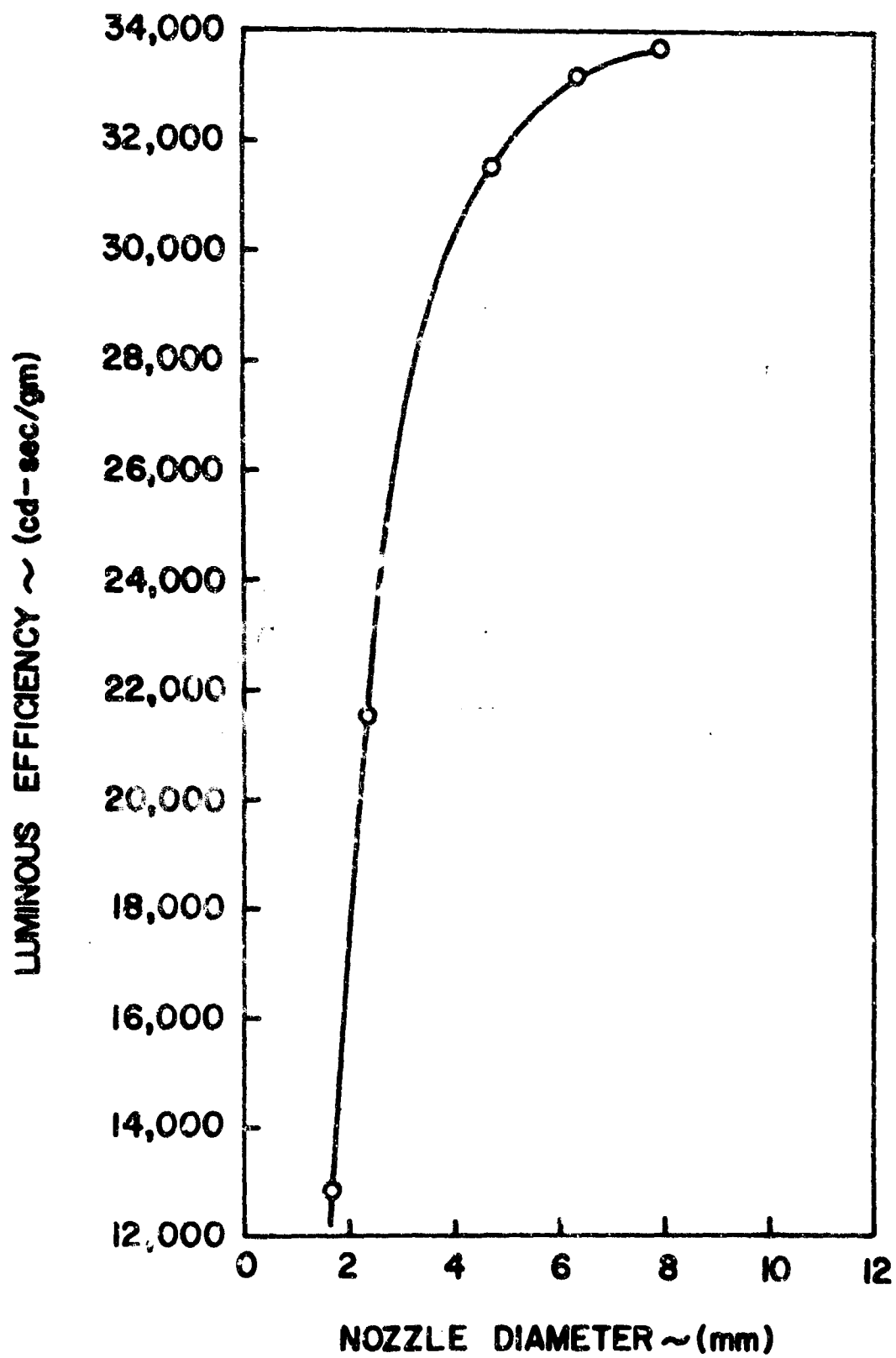


Figure 17



the  $\text{BO}_2$ , CN,  $\text{C}_2$ , and continuum radiation into one effective source.

### Conclusions

1. The flame of cyanogen and oxygen appears to have three distinct compositional regimes with respect to its luminosity. There is an essentially non-luminous flame on the lean side. This is followed by a luminous region having its peak output for the flame containing 55% cyanogen, which appears to involve only banded radiation from the CN and  $\text{C}_2$  free radicals. As the cyanogen-content is increased further a second luminous regime is encountered characterized by continuum radiation produced by solid carbon.

2. Premixed cyanogen-oxygen flames produce solid carbon for compositions containing more than 60% cyanogen. This result is of interest with respect to theories concerned with carbon formation in flames.

3. The maximum luminous efficiency for the cyanogen-oxygen-boron trichloride flame system measured during this work is 33,668 cd-sec/gm at 5.85% boron trichloride in a base flame of 38% cyanogen. ( $R = 38$ ,  $D = 5.85$ .)

4. Luminous efficiency increased with increasing burner diameter, rapidly at first, then more slowly.

5. The composition yielding the maximum efficiency is found to be nearly the same for the premixed flames studied here as for the diffusion flames studied previously.

### References

1. Tischer, Robert L. and Karl Scheller, "The Luminous Characteristics of Cyanogen-Oxygen-Boron Trichloride Diffusion Flames", Combustion and Flame (in press).
2. Apple, E. F. and Thomas Wartik, "The Reaction of Cyanogen with Diboron Tetrachloride and with Boron Halides", JACS, 80, 6158-61 (1958).
3. Gordon, Sanford and Frank J. Zeleznik, NASA TN D-1454, October 1962.
4. Ibid., NASA TN D-1737, October 1963.
5. Harrison, George R., Richard C. Lord and John R. Loofbouroow, "Practical Spectroscopy", p. 118, p. 128, Prentice-Hall, Inc., (1948).

6. Kostowsky, H. J. and R. D. Lee, "Theory and Methods of Optical Pyrometry", National Bureau of Standards Monograph 41, March, 1962, 28p.
7. Larrabee, Robert D, "Spectral Emissivity of Tungsten", J. Am. Opt. Soc. 49, 619-625 (1959).
8. Stokes, Charles S., Robert P. M. Werner, William F. R. Smith, and Joseph A. Cahill, "Premixed Flames of Cyanogen and the Endothermic Oxides of Nitrogen and the Premixed, Preheated Oxy-Cyanogen Flame", AFOSR TN 58-810, Astia Doc. AD202355, 24p., September, 1958.
9. Conway, J. B., R. H. Wilson, Jr., and A. V. Grosse, "The Temperature of the Cyanogen-Oxygen Flame", JACS, 75, 499 (1953).
10. Conway, J. B. and A. V. Grosse, "The Cyanogen-Oxygen Flame Under Pressure", JACS, 80, 2972-76 (1958).
11. Gaydon, A. G. and H. G. Wolfhard, "Flames, Their Structure, Radiation and Temperature", p. 177, p. 186, p. 198, Chapman and Hall, Ltd., (1960).

### List of Figures

- Figure 1. The calibration constant  $C_\lambda$  for the spectrometer system as a function of wavelength.
- Figure 2. Luminous efficiency as a function of cyanogen percentage for the premixed cyanogen-oxygen flame.
- Figure 3. Equilibrium composition of the product gases as a function of cyanogen percentage for the adiabatic premixed cyanogen-oxygen flame.
- Figure 4. Flame temperature as a function of cyanogen percentage for the premixed cyanogen-oxygen flame.
- Figure 5. Spectrum of mantle gases of the premixed cyanogen-oxygen flame, 63.5% cyanogen.
- Figure 6. Spectrum of mantle gases of the premixed cyanogen-oxygen flame, 55% cyanogen.
- Figure 7. Spectrum of mantle gases of the premixed cyanogen-oxygen flame, 43% cyanogen.
- Figure 8. The effect of boron trichloride percentage on the luminous efficiency of the premixed cyanogen-oxygen-boron trichloride flame for fixed cyanogen-oxygen ratios at fixed volumetric flow rates.
- Figure 9. Effect of the volumetric flow rate on the luminous efficiency of a premixed cyanogen-oxygen-boron trichloride flame.
- Figure 10. Effect of boron trichloride addition on the luminous efficiency of premixed cyanogen-oxygen-boron trichloride flames.
- Figure 11. Equilibrium composition of the product gases as a function of the cyanogen-oxygen ratio for a premixed cyanogen-oxygen-boron trichloride flame containing 7.5% boron trichloride.
- Figure 12. Spectrum of the mantle gases of the premixed cyanogen-oxygen-boron trichloride flame, 6.07% boron trichloride added to a cyanogen-oxygen flame containing 43% cyanogen.
- Figure 13. Adiabatic flame temperature as a function of the cyanogen-oxygen ratio for a typical premixed flame of cyanogen-oxygen-boron trichloride containing 7.5% boron trichloride.

- Figure 14. Luminous efficiency as a function of percentage boron trichloride for fixed cyanogen-oxygen ratios at a fixed volumetric flow rate.
- Figure 15. Variation of equilibrium mole fraction of  $\text{BO}_2$  in the product gases of a premixed cyanogen-oxygen-boron trichloride flame as a function of percentage boron trichloride at fixed cyanogen-oxygen ratios.
- Figure 16. Variation of adiabatic flame temperature of a premixed cyanogen-oxygen-boron trichloride flame as a function of percentage boron trichloride at fixed cyanogen-oxygen ratios.
- Figure 17. Maximum measured luminous efficiency of premixed cyanogen-oxygen-boron trichloride flames as a function of nozzle diameter.

ULTRASONIC ENHANCEMENT OF PYROTECHNIC PROCESSING:  
PRESSING, EXTRUSION, CASTING

Richard Pheasant and C. Dana McKinney  
(Technidyne Incorporated, West Chester, Pennsylvania)

ULTRASONIC ENHANCEMENT OF PYROTECHNIC PROCESSING:  
PRESSING, EXTRUSION, CASTING

Richard Pheasant and C. Dana McKinney  
(Technidyne Incorporated, West Chester, Pennsylvania)

Presentation at Denver Pyrotechnics Seminar  
Estes Park, Colorado, August 12-16, 1968

Perhaps many of you are familiar with the slippery feel of metal surfaces that are excited to ultrasonic frequencies. This "lubricating" effect of ultrasonic vibration on solid surfaces has been known for some time, and is often used to advantage in assembly operations such as bolt-tightening and interference-fitting.

Less well known is the friction-reducing effect of ultrasonic energy on finely divided solids. Many of the problems in powder compaction are due to particle-to-particle friction, bridging of particles, and friction between particles and container or die walls. Some years ago Technidyne undertook investigations in the application of ultrasonics to powder forming processes -- ceramics and powder metallurgy -- finding in all instances that the force required to obtain a given degree of compaction is significantly reduced, and the compacted powder is more uniform and free from residual stresses. When the powders are wetted, as in extrusion, casting and some types of pressing, the effects of ultrasonics may be even more pronounced, and it has been possible to substantially reduce the amounts of additive liquids, lubricants and binders from normal values with resulting process economies.

Generally, the application of ultrasonics has resulted in improvements as follows:

1. Greater uniformity of compact.
2. Higher density.
3. Improved structural integrity.
4. Fewer increments needed, in incremental loading.
5. Reduced compressive force, or temperature.
6. Increased processing rates.
7. Formula modification to eliminate or reduce additives which are non-functional after processing or costly in processing.
8. Improved case-bonding.

There have also been other improvements, such as improved fill of mold or die, reduction of elastic rebound, reduced processing temperature, more rapid cure, improved bonding, increase in content of most desirable ingredient, and lack of need to process further for size or finish.

These investigations have been extended into the processing of pyrotechnics, propellants and explosives. Initially there was concern that ultrasonics would initiate combustion or detonation, but a very substantial amount of experience, without incident, argues strongly that there is little such risk (though we continue to run sensitivity tests, for safety, on each new composition).

I will not go into theory supporting these observations; it is covered in some detail in the reports in the bibliography. And I shall mention only briefly the considerations necessary for the efficient coupling of ultrasonic energy into particulate systems that are being subjected to pressure, heat, or other processing conditions.

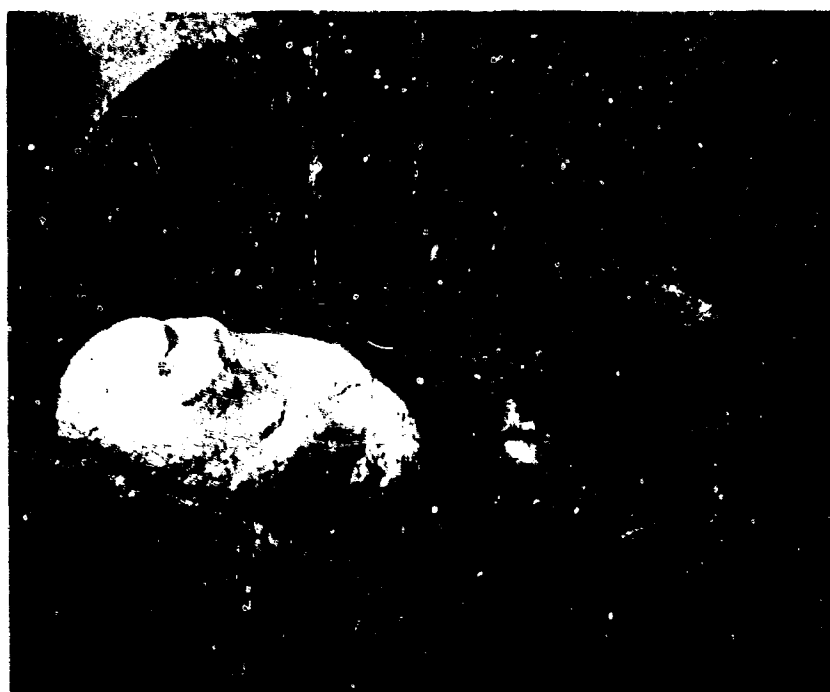
In order to deliver effective levels of ultrasonic energy to an area where it does useful work it is necessary to design the over-all waveguide system, from transducer to working hardware, according to acoustic principles and in such a manner as to provide for natural resonance (as in a tuning fork). It is also necessary to isolate the acoustic system from the mass of the rest of the equipment. With specially designed, force-insensitive waveguide mounting systems, punches and dies loaded to 80 tons have been ultrasonically activated without significant power loss or frequency shift.

Recent improvements in energy-converting equipment -- the use of solid-state electronic frequency converters instead of electron-tube circuits, and ceramic piezoelectric transducers to replace magnetostrictive nickel types -- have resulted in a several-fold efficiency increase in the generation of ultrasonic power. Hence, the equipment for applying ultrasonics is much more compact and much less costly than it was only a few years ago.

I have a few slides which illustrate typical effects and data from several of the ultrasonic investigations.

Slide 1

The first is from our ceramic extrusion work and shows the extent to which the liquid (water) content can be reduced to give comparable extrusion under ultrasonic energy.



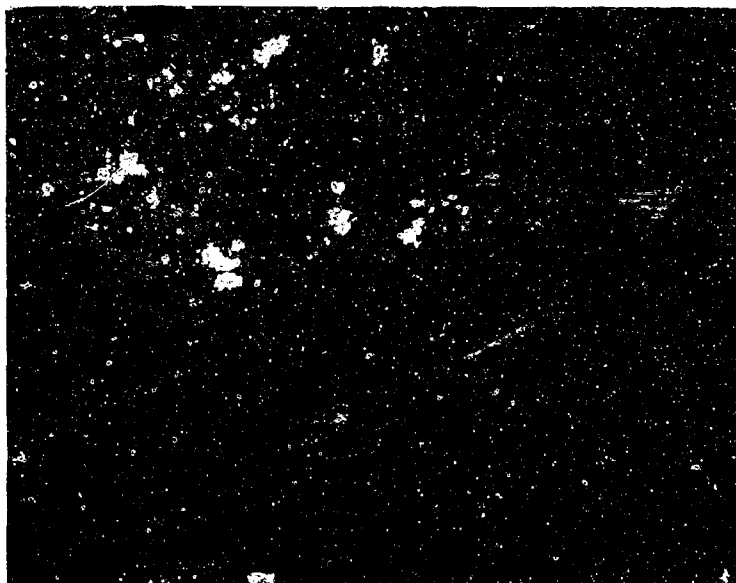
Slide 2

This shows the stiffness of a ceramic paste which can be slip-cast with ultrasonic energy, though not otherwise.



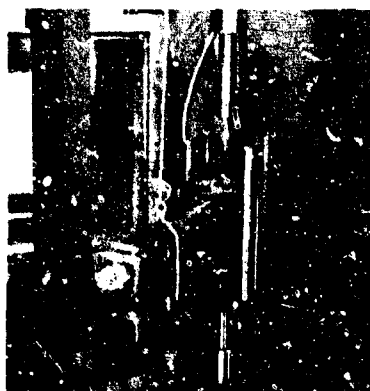
Slide 3

This shows, on the right, the complete mold filling of the slip from the previous slide, when cast with ultrasonics. In the middle is the same slip, cast with low-frequency (sonic) vibration. On the left is the amount that will flow in by itself.



Slide 4

This is the ultrasonic array used to press pyrotechnic smoke mix. In this program two modes of ultrasonic activation were evaluated: Die activation, shown here, and ram activation, shown in the next slide.



Slide 5

With the L/D ratio of the M-18 canister (about 2:1), either mode of ultrasonic activation was effective in improving uniformity and density. With ultrasonic ram activation, it was possible to load in one increment, rather than three without ultrasonics. Higher L/D ratios favor die activation, which can be extended indefinitely in constant cross-section geometry.



We have recently finished the first stage of an investigation in the extrusion of a fluorocarbon-base solid propellant, under Navy sponsorship.

The ultimate objectives are improvements in production, such as increased extrusion rate, higher and more uniform density, and dimensional control of as-extruded material, to eliminate machining to size.

Slide 6

This slide shows extrusion conditions. Ultrasonic power was at different levels to 1500 watts input, at 15 kHz.

CONDITIONS

--Extrusion Ratio            7.1  
--Temperature                195-205°F  
--Pressure                    2270-3180 psig  
--Ultrasonic Power        0-1500 Watts

---

Slide 7

This shows the effect of ultrasonics on extrusion rate at three different pressures, with an inert propellant.

EXTRUSION RATE  
INERT PROPELLANT

Ultrasonic Power (Watts)	Extrusion Pressure (psig)		
	2725	2950	3175
0	5.2* 1.00	13.0* 1.00	11.6* 1.00
1000	7.6* 1.46	7.6* 0.58	16.8* 1.45
1500	7.8* 1.50	13.4* 1.03	18.4* 1.59

\* in/min. The other number in each box is the ratio between the first number and the corresponding zero-power control.

Slide 8

The same conditions with live propellant show an even greater ultrasonic effect.

EXTRUSION RATE  
LIVE PL-6301

Ultrasonic Power (Watts)	Extrusion Pressure (psig)		
	2500	2725	2950
0	3.6* 1.00	5.9* 1.00	13.0* 1.00
1000	10.1* 2.81	15.2* 2.58	25.8* 1.98
1500	13.0* 3.61	20.2* 3.42	23.5* 1.81

\* in/min. The other number in each box is the ratio between the first number and the corresponding zero-power control.

Slide 9

In the inert propellant extrusions, blocks of two colors were alternated so that interface phenomena could be observed. Note that the non-ultrasonic control was incompletely bonded. The ultrasonic interfaces were perfectly bonded and more symmetrical in geometric shape.



Slide 10

These are the benefits demonstrated in the first stage. In the second, now underway, we expect to demonstrate acceptable as-extruded shape, and to work out design parameters for production equipment.

SIGNIFICANT RESULTS

- 250 to 300 Percent Increase in Rate
  - Less Density Variation
  - Better Interface Between Propellant Blocks
-

We are also investigating the benefits to be obtained by ultrasonics in the pressing of delay trains. The principal objective here is to reduce variance in burn time, but we also are looking at increased density, reduced pressure with equal density, and reduced number of increments.

Slide 11

This shows the ultrasonically activated pneumatic press (28 kHz axial punch) and the aluminum delay housing. All pressings were made with 100 watts power input to the magnetostrictive transducer.



Slide 12

This is some very preliminary data, with a boron/barium chromate mix. It covers only one ultrasonic power level and does not go into reduced increments. It clearly indicates, however, increased compaction with ultrasonics under normal pressure, and the possible pressure reduction with ultrasonics for the same degree of compaction. The number of replicates is, unfortunately, not sufficient to show any conclusions about burning time. Additional data is being obtained and will be available at some time in the future.

ULTRASONIC PRESSING OF DELAY COLUMNS

Composition: Boron 3.5 parts  
Barium Chromate 96.5 parts  
Super Floss 5.0 parts

Column diameter: 0.24 inch  
Five-increment loading, total 1.5 g.  
No. of replicates: 5

---

Ultrasonic Power, watts		0	100	100
Pressure, 1000 psi		45	45	39.5
Delay Column Length	Ave.	0.666	0.624	0.660
Inches	Range	0.036	0.096	0.014
Burning Time	Ave.	2.54	2.62	2.46
Seconds	Range	0.25*	0.30	0.25

---

\* range of 4 only -- one was missed.

Other projects currently started, but which have not yet produced data which may be included here, are

1. Pressing long-burning delay trains (Navy).
2. Pressing illuminating flares (Army and Navy).

Additional early applications are

1. Casting and curing of double-base propellant.
2. Casting of flares and smoke mixes.
3. Extrusion of flares and smoke mixes.
4. Casting or pressing of red phosphorus with explosive.

A preliminary investigation has also been carried out in melt-casting of an explosive (octol).

In summary, the application of ultrasonic energy to pyrotechnic compaction and forming processes offers a general easing of the necessary physical conditions, an extension of the range of composition variables, faster processing, more uniform and better bonded compacts, higher densities, and greater product reliability. Not all of these can be obtained simultaneously in most cases, but conditions can be directed toward the most desirable combination of effects.

### BIBLIOGRAPHY

1. McKinney, C. D., Jr., and D. J. Smith, "Investigation of the Feasibility of Ultrasonic Enhancement of Fluorocarbon-Based Propellant Extrusion." Technidyne Incorporated Research Report No. 68-7 under Contract NO0174-68-C-0045 for Naval Ordnance Station, Indian Head, Maryland, February 1968. Further work in process under P. O. NO0174-68-C-0506.
2. McKinney, C. D., Jr., "Ultrasonic Enhancement of Explosives Melt Casting." Technidyne Incorporated Research Report No. 67-57 under Contract DAAA21-67-C-0504 for Picatinny Arsenal, Dover, New Jersey, In Process.
3. McKinney, C. D., R. F. Parkhurst, and W. B. Tarpley, "Feasibility of Ultrasonic Deaeration and Compaction of Pyrotechnic Powders." Technidyne Incorporated Final Report No. 66-77 under Contract DA-18-035-AMC-367(A) for Edgewood Arsenal, Maryland, July 1967.
4. Tarpley, W. B., K. H. Yocum, and R. Pheasant, "Ultrasonic Extrusion: Reduction in Vehicle and Plasticizer Requirements for Non-Clay Ceramics." NYO-10006, Aeroprojects Incorporated, AEC Contract AT(30-1)-1836, November 1961.
5. McKinney, C. D., Jr., W. B. Tarpley, and R. S. Winchester, "Applications of Ultrasonic Energy to Pyrometallurgical and Pyrochemical Processing of Nuclear Materials." Aeroprojects Incorporated Topical Report NYO-2581 under Contract No. AT(30-1)-1836 for Atomic Energy Commission, April 1961.
6. Tarpley, W. B., and H. Kartluke, "Ultrasonic Hot Pressing of Metals and Ceramics." Aeroprojects Incorporated, Topical Report NYO-10007 under Contract No. AT(30-1)-1836 Task 2 for Atomic Energy Commission, December 1961.
7. McKinney, C. D., Jr., W. B. Tarpley, and F. H. Gaskins, "Ultrasonic Casting of Ceramic and Cermet Slips." Aeroprojects Incorporated, Topical Report NYO-9586 under Contract No. AT(30-1)-1836 for Atomic Energy Commission, November 1961.
8. Thomas, J. G., and J. B. Jones, "Application of Ultrasonic Vibration to the Compaction of Metal Powders." Aeroprojects Incorporated, Final Report NYO-7921 under Contract AT(30-1)-1836 for Atomic Energy Commission, June 1958.

9. Tarpley, W. B., and R. Pheasant, "Ultrasonic Filling of Tubular Cladding with Ceramic Fuel Powders." Aeroprojects Incorporated, Topical Report NYO-9587 under Contract AT(30-1)-1836 for Atomic Energy Commission, November 1961.
10. Tarpley, W. B., and H. Kartluke, "Application of Ultrasonic Vibration to Cold Pressing of Ceramic Pellets." Aeroprojects Incorporated, Topical Report NYO-10005 under Contract No. AT(30-1)-1836 for Atomic Energy Commission, November 1961.
11. Ellarn, H., Military and Civilian Pyrotechnics. Chemical Publishing Company, Inc., New York, 1968.
12. Technidyne Incorporated, "Ultrasonic Compaction of Delay Element Compositions in NOS Test Housings." Contract NO0174-68-C-0442 for Naval Ordnance Station, Indian Head, Maryland. Program in Process.



CHARACTERIZATION AND CHEMICAL REACTIVITY

William Ripley  
U. S. Naval Ammunition Depot  
Crane, Indiana

## CHARACTERIZATION AND CHEMICAL REACTIVITY

by  
William Ripley

1. Although chemicals used in pyrotechnic compositions are purchased under appropriate military specifications, which are supposed to control the chemical and physical properties so that a degree of consistency can be expected in the performance of the composition, many practical pyrotechnicians are convinced from experience that unpredictable variations occasionally appear in the performance characteristics of these chemical components. These variations are difficult to document for several reasons. For one thing, military specifications do not usually require a performance test to determine the reactivity of the components, but instead assume that if the chemical and particle size requirements are met, then the reaction characteristics will be acceptable. Secondly, variations are often subtle and may only occasionally become pronounced enough to cause serious performance changes. Since there are usually no laboratory control tests available to measure reactivity, except the quality control tests that are run on the finished units, it is difficult to determine whether the process, the chemical components, or the hardware is the source of the failure. If the chemical components are suspected, chemical analysis and particle size determination may be rerun on each component. However, the materials may very well pass the tests, although one of the materials is actually the source of trouble, since the specifications tests do not necessarily reveal reactivity variations.

2. Military specifications for chemical components used in pyrotechnic compositions are necessarily compromises between a set of ideal properties and the practical limitations of commercial manufacturing processes. Certainly, the more rigorous the requirements the more expensive is the process needed to meet them. Furthermore, the "ideal properties" of a material depend upon its use and indeed may not always be understood. The April 1968 edition of Metal Progress was devoted to a special report entitled: "Characterization - Industry's Most Urgent Materials Problem . . . ." It is the thesis of this special report that most materials are so poorly characterized that consumers cannot tell manufacturers precisely what properties they require. What are the ideal properties of lead dioxide when it is used as a component in one of the starter compositions? They are not really known. Consequently, certain "reasonable" or minimum requirements are established for purity, contaminants, and particle size that are a compromise between what the pyrotechnician thinks he needs to make a composition with predictable performance and what the manufacturer can make at an acceptable price. There is, of course, a good deal of looseness in this arrangement. Variations in the chemical components inevitably appear and, consequently, so do variations in the performance of the final pyrotechnic item. The variations in the components may at times be so gross that the component fails to meet the specification requirements. On the other hand the component may meet the specification requirement and still introduce an undesirable variation in the performance of the composition. At best, formula changes must be made to compensate for the variation;

at worse, the material may be unusable.

3. One way out of this situation is to prescribe additional requirements for the material over and above the general specification requirements. Besides increasing the cost of the material, or running into procurement problems at any cost, the "additional requirements" needed again may not be known.

4. Another approach could be the development of a performance test for the material. In such a test the reactivity of the material would be evaluated. Since the reactivity of the material - that is, the ease and rapidity with which the material interacts with other materials - depends upon the totality of all physical and chemical properties, the effect of variations in the material could be seen even if the causes were not known.

5. This is the approach that has been used in the study of various chemical materials which are used in current pyrotechnic compositions. Variations in the behavior of such materials as lead dioxide, red phosphorus, magnesium, and sodium nitrate have been suspected from time to time, but no hard data are available to support this suspicion. Consequently, an investigation of the reactivity, as well as some of the chemical and physical properties, of these materials has been undertaken. This paper is concerned with the study of lead dioxide.

#### OBJECTIVES

1. The present investigation has had six principal objectives:
  - a. To find laboratory methods of measuring the reactivity, or the reaction rate, of lead dioxide and ultimately of other

pyrotechnic chemicals.

b. To compare and correlate when possible reactivity results obtained from different methods of determining reactivity.

c. To investigate a quantitative relationship between the average particle size, the surface area, and the reactivity of lead dioxide.

d. To determine which method of measuring the particle size is more valid in predicting the reactivity of lead dioxide.

e. To determine if other factors besides the average particle size or surface area affect the reactivity of lead dioxide.

f. To determine the variations in reactivity that exist in lead dioxide currently used in production, and in lead dioxide from different sources.

#### EXPERIMENTAL RESULTS

##### 1. Determination of the reactivity of lead dioxide

a. A laboratory test method for determining the reactivity, or the reaction rate, of a solid material like lead dioxide must necessarily be a destructive test. The lead dioxide is attacked by some chemical agent, and in the process of the ensuing reaction, the lead dioxide is destroyed. The rate at which the lead dioxide is destroyed is somehow measured and recorded, and this rate is assumed to be related to the reactivity of the lead dioxide.

b. Since the lead dioxide must react with another substance, three general modes of reaction are possible: the lead dioxide can react with a gas, with a liquid, or with a solid. While all three of these modes are currently under study, this report is mainly concerned with a study of the reaction of solid lead dioxide with a

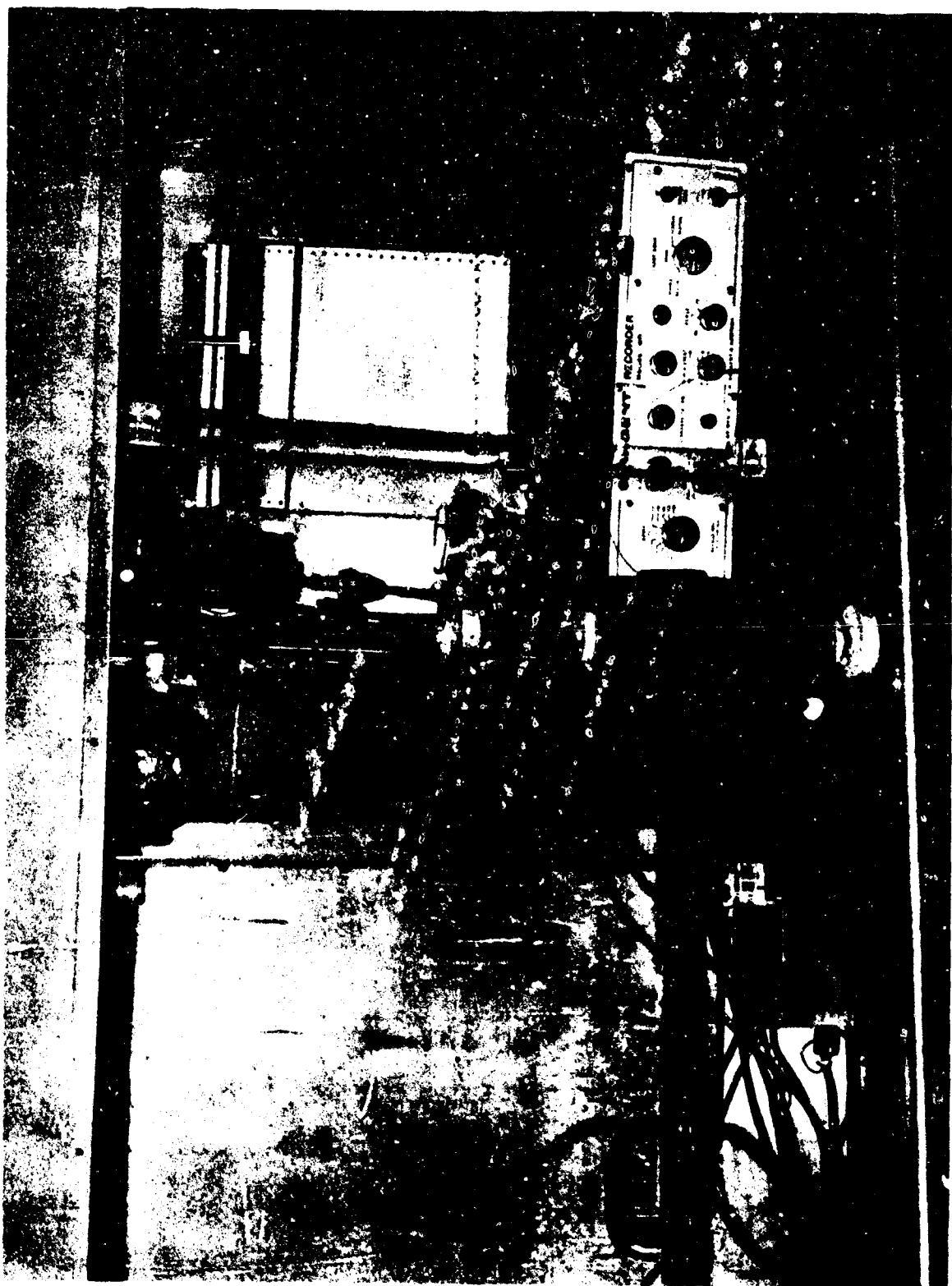
liquid reactant, and with the burning characteristics of certain solid-solid systems.

c. Lead dioxide is dissolved by many liquid chemical reagents. If we obtain a temperature-time curve of the reaction between lead dioxide and some liquid reactant under isothermal conditions, two requirements must be satisfied in choosing a reactant: sufficient heat must be generated and the reaction must not proceed either too rapidly or too slowly. Reactions with hydrogen peroxide and hydrochloric acid proved to be too rapid, while the reaction with oxalic acid was slow and developed little heat. A reagent was finally developed, based on an alcoholic solution of oxalic and hydrochloric acids, which gave a satisfactory time-temperature curve. The apparatus used, which is basically a rate calorimeter, is shown in Figure 1.

d. Commercial lead dioxide specimens were obtained from five different manufacturers. In order to study the relationship between the particle size and the reactivity, the five specimens were fractionated by sedimentation and liquid elutriation. Separation using distilled water was relatively easy on the large particle specimens, but on the small particle specimens separation was difficult at best. This difficulty in obtaining relatively coarse and fine fractions indicates a limited particle size distribution as well as the limits of the fractionating technique itself.

e. All of these curves reveal the rate at which heat is generated when lead dioxide reacts with an excess of alcoholic oxalic acid-hydrochloric acid reagent. Temperature is indicated on the Y coordinate and time on the X coordinate. Figure 2 shows the reaction rate curves of the five lead dioxide specimens plotted on the same scale.

FIGURE 1 Rate Calorimetry Apparatus for  
the Determination of the  
Reactivity of Lead Dioxide



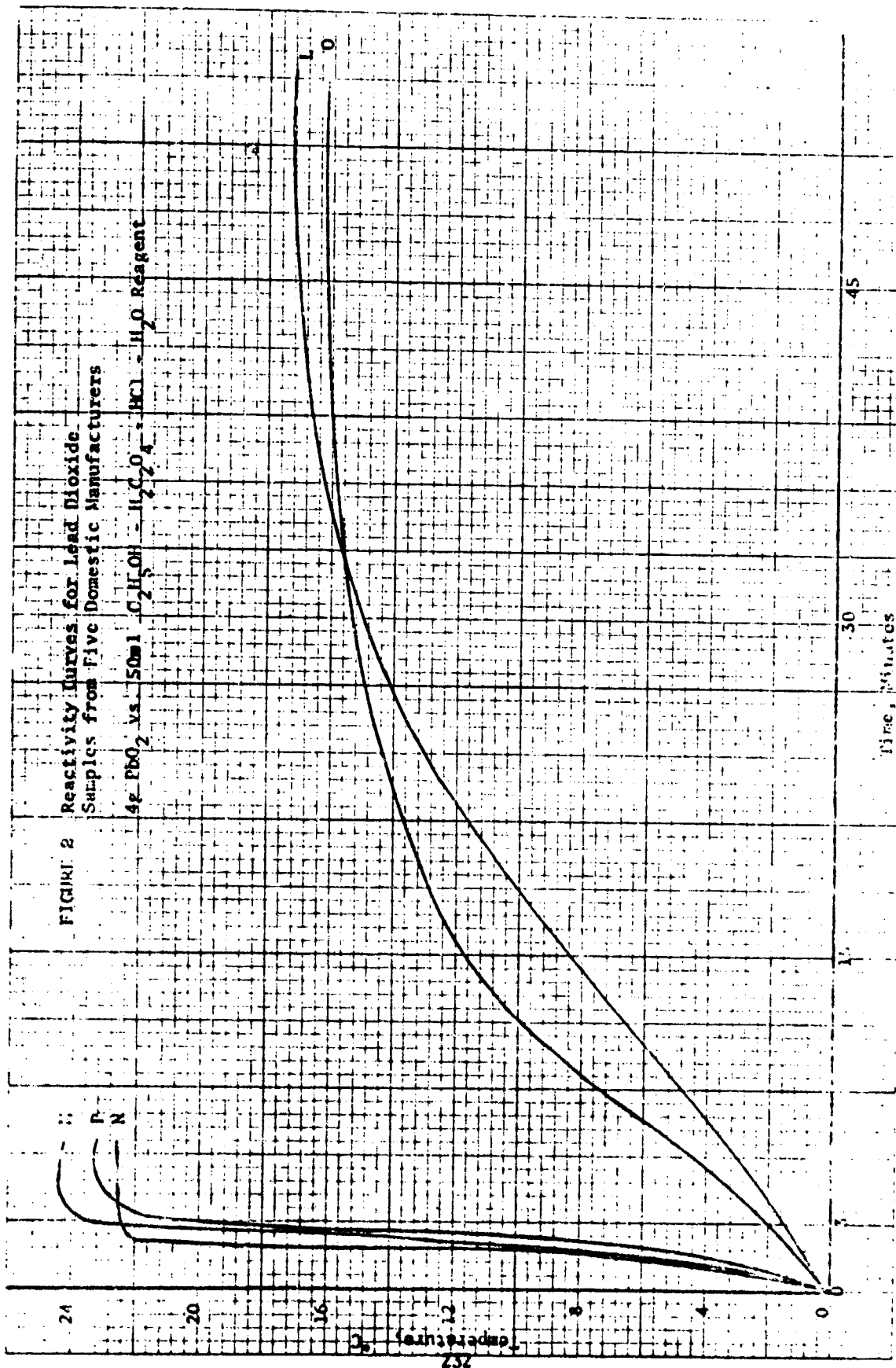
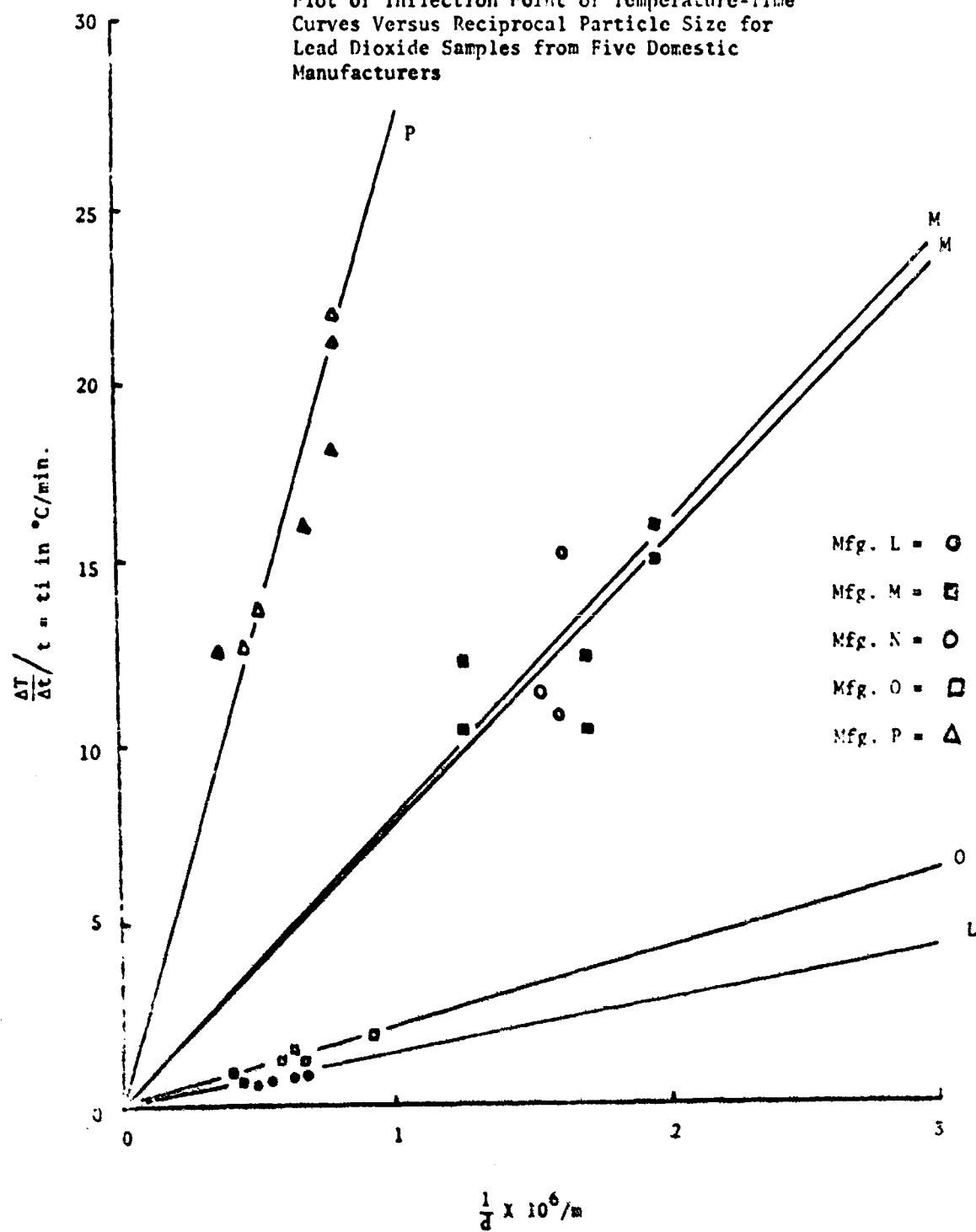


FIGURE 2 Reactivity Curves for Lead Dioxide Samples from Five Domestic Manufacturers

f. The temperature-time curves obtained from exothermic reaction of lead dioxide with alcoholic oxalic acid-hydrochloric acid solution are sigmoid type curves. This type curve is characteristic of autocatalytic reactions, although it has not been definitely demonstrated that the reaction is in fact autocatalytic. The inflection point of each curve has been chosen to characterize the reaction rate of the individual sample, since at this point the rates of the two competing processes - autocatalysis which increases the rate process versus depletion of lead dioxide which slows the rate process - are at equilibrium. The rate of reaction at the inflection point is expressed as the value of the slope at that point. When the values obtained for the slope at the inflection point are plotted against the reciprocal particle diameter for each of the lead dioxide parent specimens and its fractions, linear relationships are obtained. The individual slopes for each of the five lead dioxide specimens obtained from U. S. Manufacturers are shown in Figure 3. The wide range of values for the different slopes is an indication of the variations in the reactivity of the different lead dioxide specimens. For example, lead dioxide samples furnished by Manufacturer L and Manufacturer P have comparable particle sizes (although different surface areas) and yet they stand at the opposite extremes in terms of reactivity. The reaction rate of the specimen from Manufacturer P is in the range of 19 times as fast as that of Manufacturer L. Moreover, the heat energy released from the different specimens is not the same. The temperature rise shown by the peak height of the curve is about 50% greater for specimens M, N, and P than for specimens L and O, necessitating that they be recorded on a

FIGURE 3

Plot of Inflection Point of Temperature-Time  
Curves Versus Reciprocal Particle Size for  
Lead Dioxide Samples from Five Domestic  
Manufacturers



higher millivolt range and at a faster chart speed. A higher heat of reaction indicates a different internal energy and therefore a different composition or structure. The linear plots shown for each of the lead dioxide specimens in Figure 3 can be represented by the equation:

$$\left. \frac{dT}{dt} \right|_{t=t_1} = \frac{K}{d}$$

Where  $t_1$  equals the lapsed time at the point of inflection,  $\frac{dT}{dt}$  equals the rate of temperature increase,  $d$  equals the average particle diameter, and  $K$  equals a proportionality constant. Values for  $K$  are shown in Table I.

## 2. Particle size

a. The average particle size of the five parent lead dioxide samples was determined by the air permeability method using the Fisher Sub Sieve Sizer. Values are shown in Table II.

b. The surface area of the lead dioxide samples was studied by the nitrogen adsorption method. A Muntz-Orr Surface Area - Pore Volume Analyser, Model MIC-103, shown in Figure 4, was used.

c. A comparison of the specific surface area,  $S_g$ , and the average particle diameter for five parent samples of lead dioxide and four fractions of one of the parent samples (Sample O) is shown in Table III. Inconsistencies between values for the APS and values for the surface area are evident: e.g., the APS of Sample L is 2.15  $\mu$  with a surface area of .69  $m^2/g$ , while the APS of Sample P is 2.10  $\mu$  and the surface area is 3.72  $m^2/g$ . Also it can be seen in

TABLE 1

Values for the Reaction Rate Constant K  
 in the Equation  $\frac{\Delta T}{\Delta t} \bigg|_{t=t_i} = K/d$

Manufacturer	K
L	$1.40 \times 10^{-6} \text{ }^{\circ}\text{C-m/min.}$
M	$7.75 \times 10^{-6} \text{ }^{\circ}\text{C-m/min.}$
N	$7.70 \times 10^{-6} \text{ }^{\circ}\text{C-m/min.}$
O	$2.10 \times 10^{-6} \text{ }^{\circ}\text{C-m/min.}$
P	$26.90 \times 10^{-6} \text{ }^{\circ}\text{C-m/min.}$
Q	$0.45 \times 10^{-6} \text{ }^{\circ}\text{C-m/min.}$

TABLE II  
Comparison of Reactivity and Various Property  
Values for 13 Lead Dioxide Samples  
From Six Domestic Manufacturers

Lead Dioxide Source and Sample	Average Particle Diameter, Microns	Absolute Density, g/cc	Apparent Density, g/cc	Purity, %	Heat of Reaction, cal/g	Pressure time curve values			Delay Burning rates, °C - m/min.	Reactivity, $K \times 10^{-6}$
						$t_p$	$t_{max}$	$t_{max}$		
Manufacturer L Sample #1 Sample #2	2.0	9.28	2.63	94.3	369.9	61	7.4	5.5	4.57	1.40
	1.65		2.17	94.8	370.1	53	6.36	5.96	3.89	
Manufacturer M Sample #1 Sample #2 Sample #3	0.51	7.86	1.38	92.2	358.0	52	7.8	7.4	5.18	7.75
	0.52		1.41	89.7	364.4	58	8.2	6.4	5.06	
	0.6		1.44			61	8.0	6.0		
Manufacturer N Sample #1 Sample #2 Sample #3 Sample #4	0.32	6.82	1.43	89.4	360.1	50	8.7	9.1	4.85	7.70 10.3
	0.52	7.91	1.38	79.5	353.3	64	8.6	5.36	4.82	
	0.66	8.00	1.36	85.1	357.4	66	8.6	4.8	4.27	
	0.59	7.70	1.92	96.3	360.4	41	7.3	10.5	5.19	
Manufacturer O Sample #1	1.5	7.99	2.85	95.9	372.4	68	7.9	4.0	5.18	2.10
Manufacturer P Sample #1 Sample #2	2.38	7.92	2.26	95.9	360.7	59	7.5	6.2	2.97	26.9
	1.20		1.68			63	7.1	5.1		
Manufacturer Q Sample #1 Sample #2	0.46	8.89	1.72		370.0	49	6.6	7.2	5.13	0.45
	0.21					49	6.1	6.9	4.22	

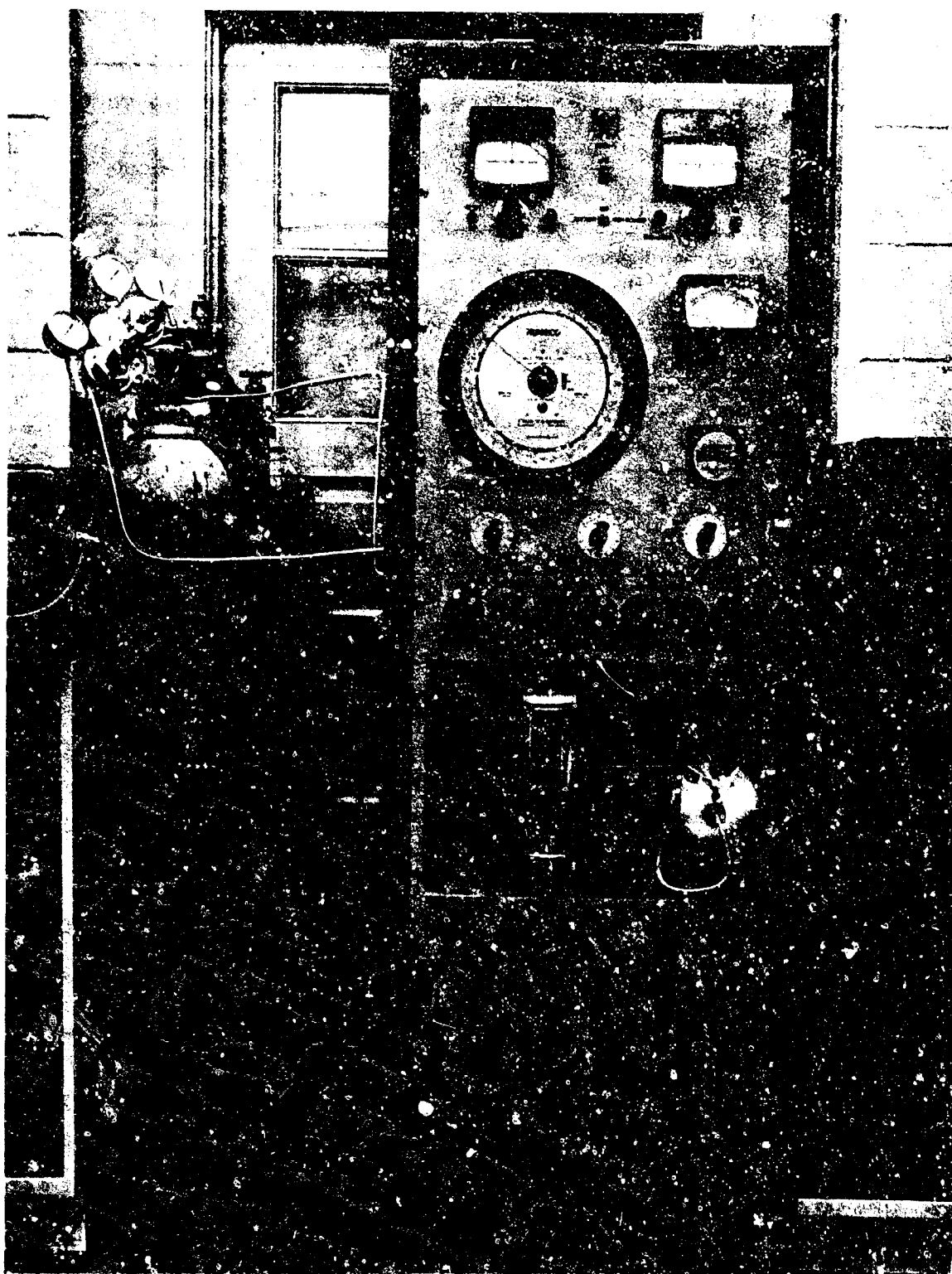


FIGURE 4 Numisco--Orr Pore Volume--  
Surface Area Analyzer for  
the Determination of Specific  
Surface Area

TABLE III

THE RELATIONSHIP BETWEEN THE AVERAGE PARTICLE DIAMETER, THE SURFACE AREA  
AND THE REACTIVITY OF LEAD DIOXIDE FROM FIVE DOMESTIC MANUFACTURERS

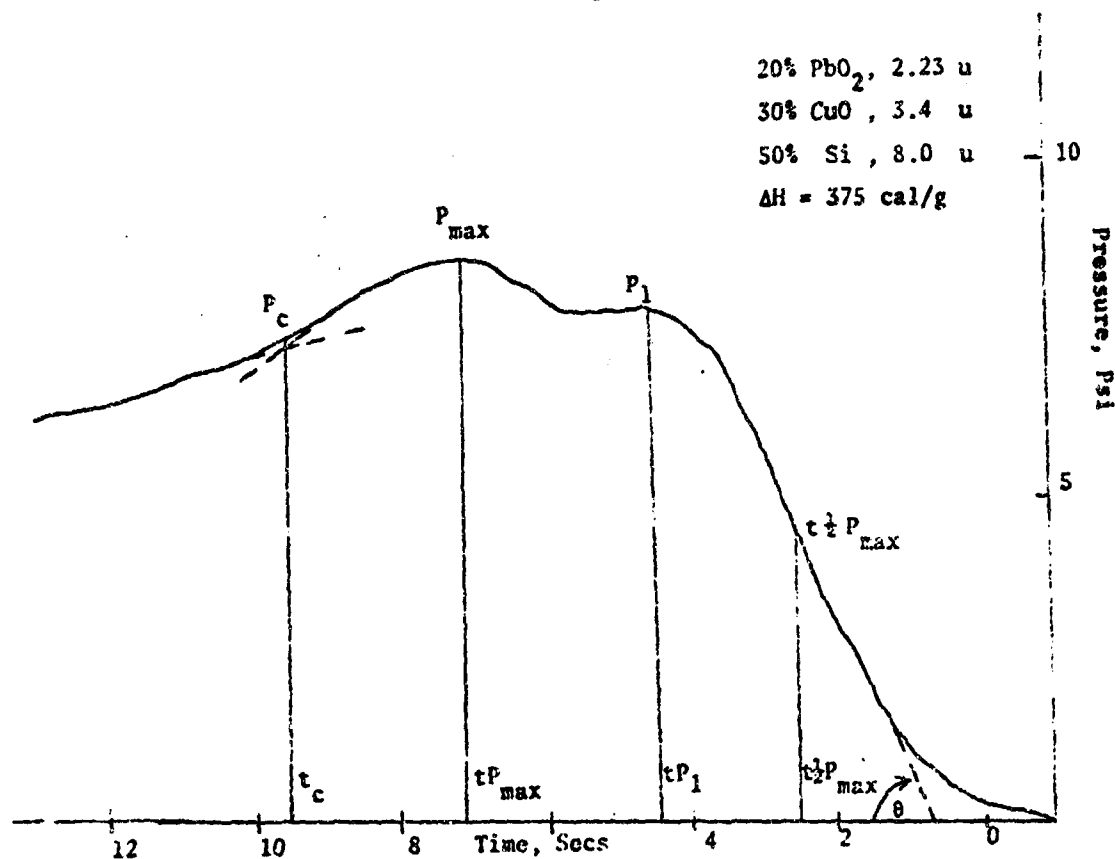
Sample	Average Particle Diameter, Microns	Specific Surface Area, S <sub>g</sub> , m <sup>2</sup> /g	Computed Surface Area, $S = \frac{6V}{d}$ , m <sup>2</sup> /g	Reactivity Constant $K \times 10^{-6}$ , °C-m/m
Manufacturer L	2.15	0.59 0.60	.30	1.40
Manufacturer M	0.60	4.94 4.94	1.27	7.75
Manufacturer N-3	0.60	4.38 4.33	1.25	7.70
Manufacturer O				
Parent	1.85	0.96 0.97	.36	2.10
Fraction 1	2.55	0.66 0.67		
Fraction 2	1.76	0.94 1.00		
Fraction 3	1.55	1.14 1.09		
Fraction 4	1.20	1.52 1.49		
Manufacturer P	2.38	3.71 3.73	.32	26.9

Figure 2 that the two groups of lead dioxide samples are determined by their surface areas and not their average particle diameters. Obviously, this is an instance in which the average particle diameter is not a function of surface area and where the surface area is the true property that relates to the reactivity.

### 3. Burning characteristics exhibited by pressure-time curves

a. Since late 1963 the performance of the 2L-3C-3S starter composition used in the Mk 25 and Mk 58 Marine Location Markers has been evaluated on the basis of its pressure-time curve. This pressure-time curve is obtained by combusting 12 grams of the starter composition in a closed vessel which is equipped with a transducer and a recorder. The apparatus and the procedure have been described in RDTR No. 41. Based on this study an acceptable range of burning characteristics for the Mk 25 Mod 2 starter composition was determined. Figure 5 shows the pressure-time curve for a typical starter composition obtained during that study. Three properties of the curve were used to characterize the burning performance of the composition. The burning rate,  $\theta$ , is obtained by finding the angle of the slope of the curve at  $t_{\frac{1}{2}P_{max}}$ , that is, the time at which one-half of the maximum pressure is attained. The accepted range for the angle  $\theta$  was chosen on the basis of experience to be  $55^\circ$  to  $68^\circ$ . The maximum pressure,  $P_{max}$ , was assigned a value of 6.75-9.65 psi. The time required for the pressure to reach its maximum value,  $t_{P_{max}}$ , was assigned a range of 6.1-7.9 seconds. Again, there was no inner necessity about these performance requirements. They were selected as reasonable values based on the performance of a great number of production batches tested over several months. While this

FIGURE 5 A Pressure-Time Curve of  
A Typical Mk 25 Mod 2  
Starter Composition



- $t \frac{1}{2} P_{\max} = 2.75 \text{ secs}$  = the time at which one half of the maximum pressure is attained.
- $\theta = 64^\circ$  = the slope of the curve at  $t \frac{1}{2} P_{\max}$ .
- $tP_1 = 5 \text{ secs}$  = time to the first peak, in the event there is more than one peak.
- $tP_{\max} = 7.38 \text{ secs}$  = time to the maximum pressure peak.
- $P_{\max} = 8.5 \text{ psi}$  = maximum pressure in psi.
- $P_c = 7.2 \text{ psi}$  = pressure at which the normal cooling curve of the system is established.
- $\Delta P = 1.3 \text{ psi}$  = the difference between  $P_{\max}$  and  $P_c$ .
- $\Delta H = 375 \text{ cal/g}$  = the heat of reaction. This value is not derived from the pressure-time curve, but from calorimetric determinations. It is included with the other data for convenient reference.
- $t_c = 10.5 \text{ secs}$  = time until normal cooling curve is established.

method was useful in evaluating the burning characteristics of the starter composition, no rigorous analysis of the significance of the pressure-time curve was performed at that time, or has been performed since. And although various factors which affect the pressure-time curve--composition, particle size, moisture, contaminants, crystalline modifications--were investigated, undesirable variations that eluded explanation have continued to appear from time to time.

b. Although the problem of a standard oxidizer and a standard fuel has not yet been solved to the satisfaction of everyone, some reproducible variations can be found among starter compositions made with the same silicon and cupric oxide but with different specimens of lead dioxide. Table II shows the values for the burning characteristics of a total of 13 specimens from six manufacturers along with other physical and chemical characteristics.

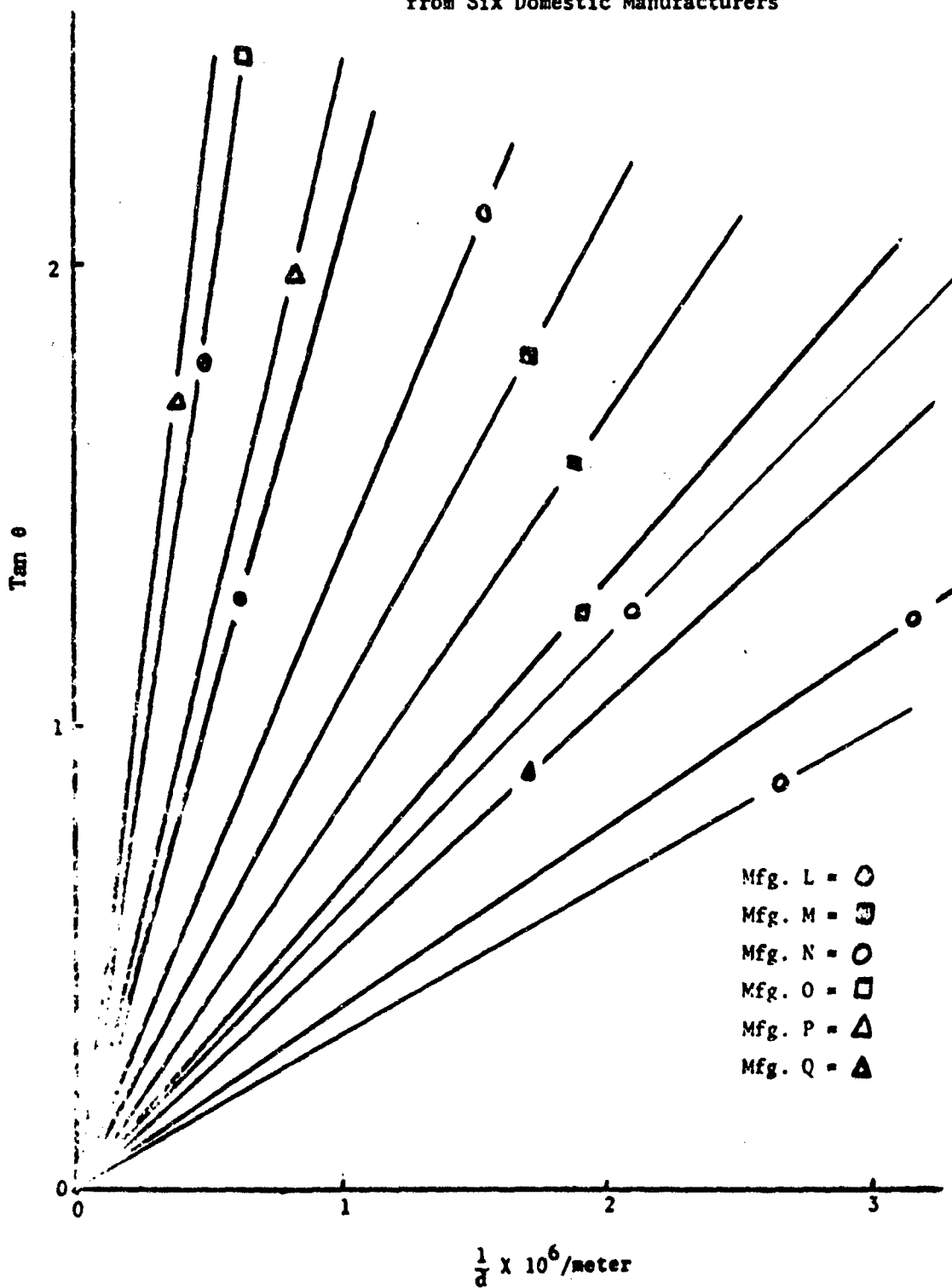
c. Altogether, this data presents a baffling picture of contradictions and inconsistencies. While the pressure-time curves obtained on a single specimen are fairly reproducible, there are still some individual runs that are far beyond the norm, indicating that variations do exist in the procedure itself. However, any attempt to relate the physical and chemical properties of lead dioxide that were investigated during the course of this work to the burning characteristics shown by the pressure-time curves appears to be futile. Take particle size, for example: there is no discernible correlation between the tangent of  $\theta$  and the reciprocal of the average particle diameter. Inspection of Table II will show that specimens with small average particle diameters are sometimes relatively fast burning and sometimes relatively slow burning. The smallest specimen with an APS

of 0.38u is comparable in burning rate with specimens having APS values of 0.51u and 1.65u. This lack of pattern or trend is all too clearly shown by the scatter of points in Figure 6, where  $\tan \theta$  is plotted versus the reciprocal of the average particle diameter. Nor is there any discernable correlation between the absolute density or the apparent density and the burning rate. Specimen L-1 with the highest absolute density has the high value for the angle  $\theta$  of  $61^\circ$ ; but specimen Q with the second highest absolute density has one of the lowest values for the angle  $\theta$ ,  $42^\circ$ . This same lack of correlation also exists between the apparent density and the burning rate. Nor is there any obvious relationship between the purity and the burning rate. Sample N-2 assayed 79.5%  $\text{PbO}_2$ , which is about 15% below the minimum specification requirement of 95%. Yet it burns relatively fast -  $\theta$  is  $64^\circ$  and the maximum pressure is 8.6 psi - while the two slowest burning samples have purities above 96%. All this indicates that some other factor or group of factors outside those considered in this investigation determine the burning rate. This data also suggests that the military specification requirements of lead dioxide have little or no correlation with the burning characteristics of the starter composition of which the lead dioxide is an important component.

#### 4. Burning rate of delay bodies

a. The inconclusiveness of the pressure-time curve study made it desirable to investigate further the burning rate of solid-solid lead dioxide compositions. Consequently, it was decided that the burning time of delay bodies which normally utilize a lead

FIGURE 6 Pressure-Time Curve Slope of  
2L-3C-5S Starter Composition  
Versus the Reciprocal Particle  
Size for 13 Lead Dioxide Samples  
from Six Domestic Manufacturers



dioxide composition should be investigated.

b. The burning rate in grams per second of ten lead dioxide specimens from five U. S. manufacturers is shown in Table IV. Also the weight of composition that could be pressed into the 1" x 1/4" I. D. aluminum delay body is shown, as well as the burning time per inch. It can be seen that the burning rate varies from 2.97 g/sec for specimen P to 5.19 g/sec for specimen N-4. It is of passing interest to note that this specimen with the fastest burning rate in a delay composition exhibited the slowest burning rate on the pressure-time curve. Furthermore, it can be seen that the weight of the delay composition which could be pressed into the body varies from 3.850 grams for Specimen L to 3.000 grams for specimen N-1. Thus, it would appear that there is a correlation between the average particle diameter, the apparent density, and the absolute density of the lead dioxide specimens, and the loaded density of the composition.

c. Figure 7 shows the plot of the burning rate in g/sec versus the reciprocal of the product of the absolute density and the average particle diameter. Figure 8 shows the plot of the burning rate in g/sec versus the reciprocal of the product of the apparent density and the average particle diameter. Figure 9 shows the plot of the burning rate in g/sec versus the reciprocal of the average particle diameter multiplied by the sum of the reciprocals of the apparent density and the absolute density. The fact that the wide differences shown in Figure 7 become much less pronounced in Figure 9 indicates that the difference in burning rates of the various lead dioxide-boron delay compositions depends almost entirely upon the

TABLE IV

## Burning Characteristics of Boron-Lead Dioxide Delay Rods

Lead Dioxide Sample Source	Average Particle Diameter, of $PbO_2$ , g/cc	Apparent Density of $PbO_2$ , g/cc	Absolute Density of $PbO_2$ , g/cc	Weight of Composition per inch, grams	Average Burning Time, sec/inch	Burning Rate, g/sec
Manufacturer L Sample #1	2.0	2.63	9.28	3.85	0.843	4.57
Sample #2	1.65	2.17	-	3.85	0.989	3.89
Manufacturer M Sample #1	0.51	1.38	7.86	3.25	0.628	5.18
Sample #2	0.52	1.41	-	3.25	0.643	5.06
Sample #3	0.6	1.44	-	3.25	-	-
Manufacturer N Sample #1	0.32	1.43	6.82	3.00	0.619	4.85
Sample #2	0.52	1.38	7.91	3.25	0.676	4.82
Sample #3	0.66	1.35	8.00	3.25	0.761	4.27
Sample #4	0.59	1.92	7.70	3.25	0.626	5.19
Manufacturer O Sample #1	1.5	2.83	7.99	3.45	0.66	5.18
Manufacturer P Sample #1	2.38	2.26	7.92	3.386	1.140	2.97
Sample #2	1.20	1.68	-	3.386	-	-
Manufacturer Q Sample #1	0.60	1.72	8.89	-	-	-

FIGURE 7 Plot of Boron - Lead Dioxide Delay  
Burning Rate Versus Reciprocal  
Particle Size Multiplied by Absolute  
Density for Five Lead Dioxide Sources

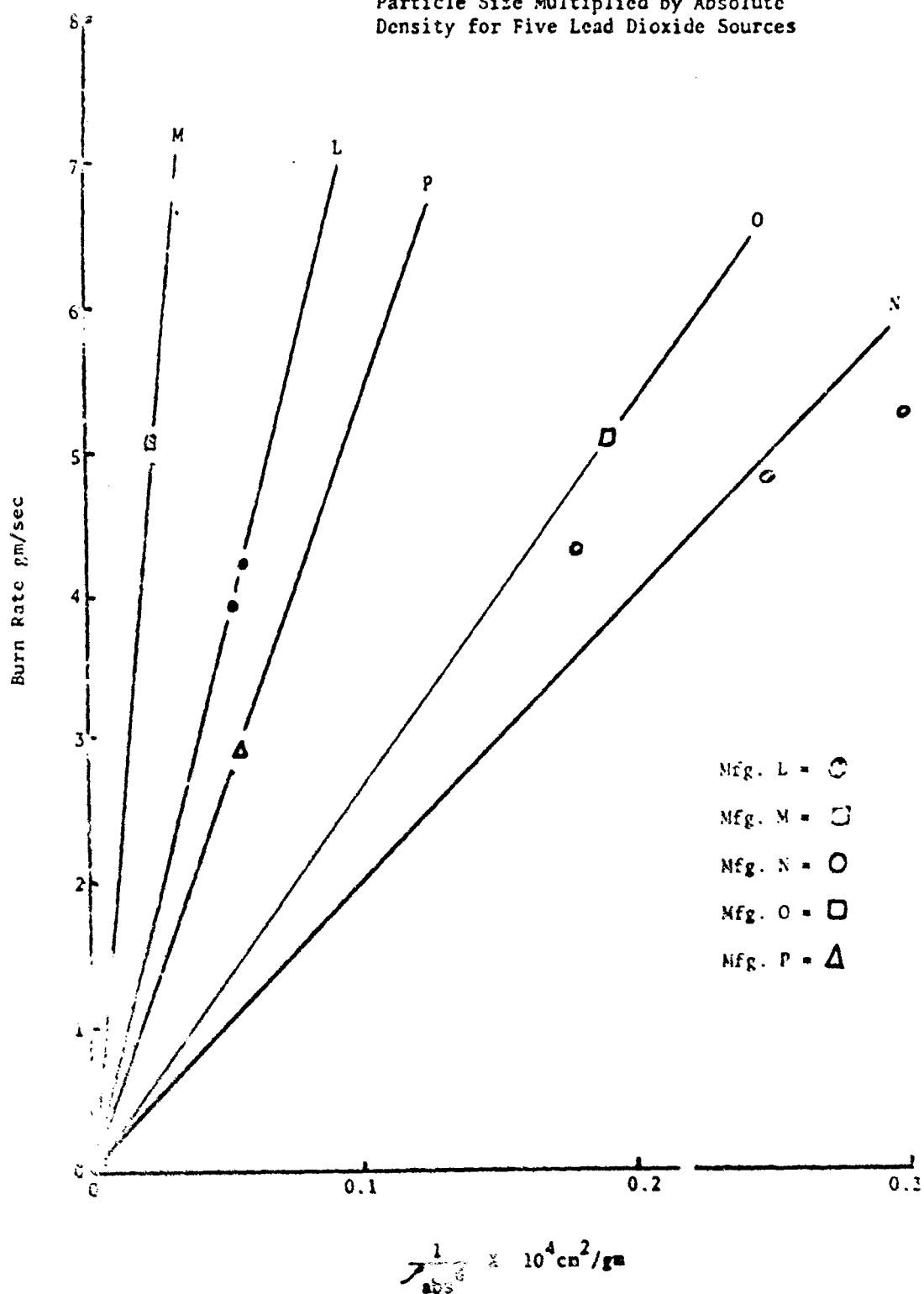


FIGURE 8 Plot of Boron - Lead Dioxide Delay  
Burning Rate Versus Reciprocal  
Particle Size Multiplied by Apparent  
Density for Five Lead Dioxide Sources

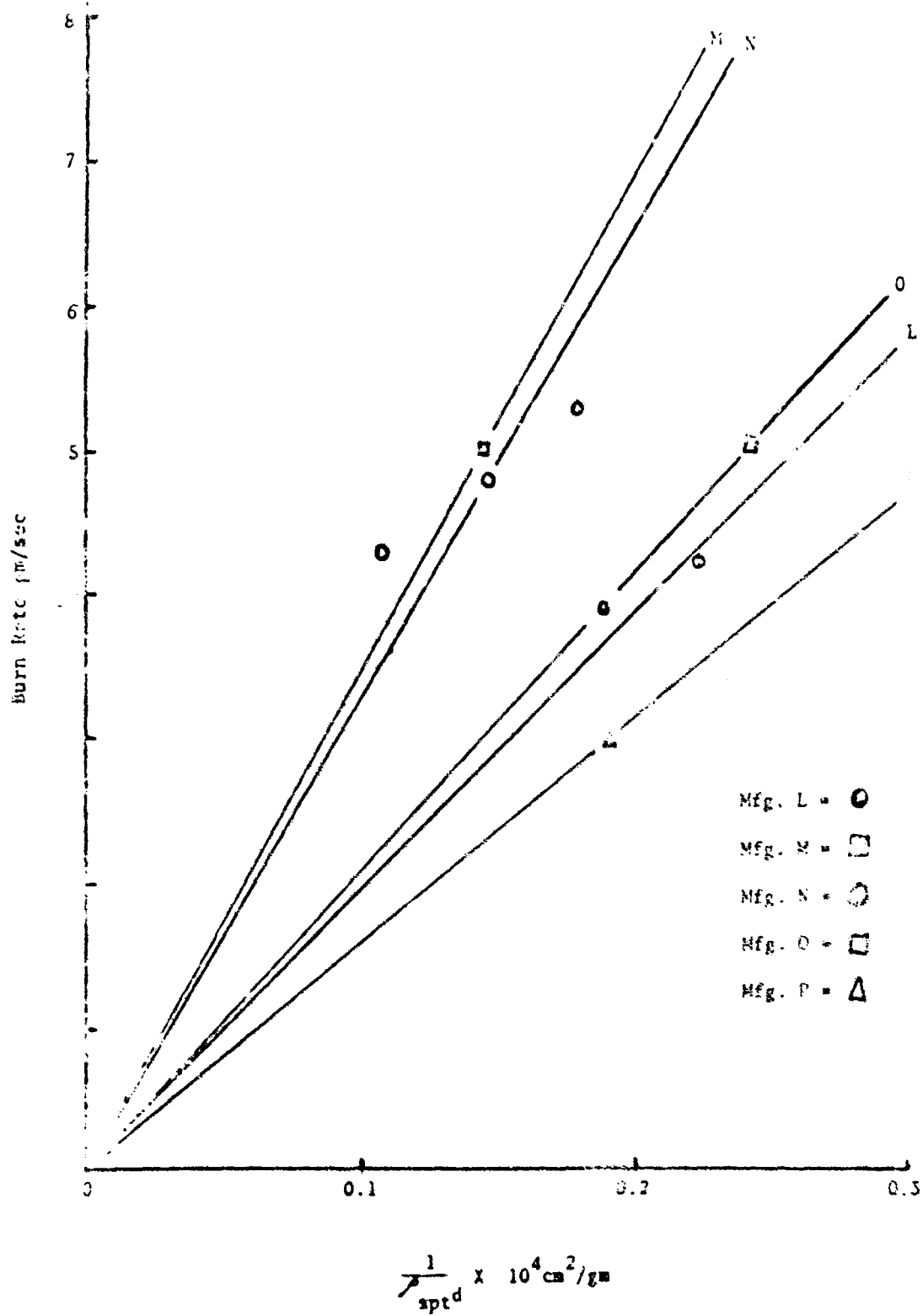
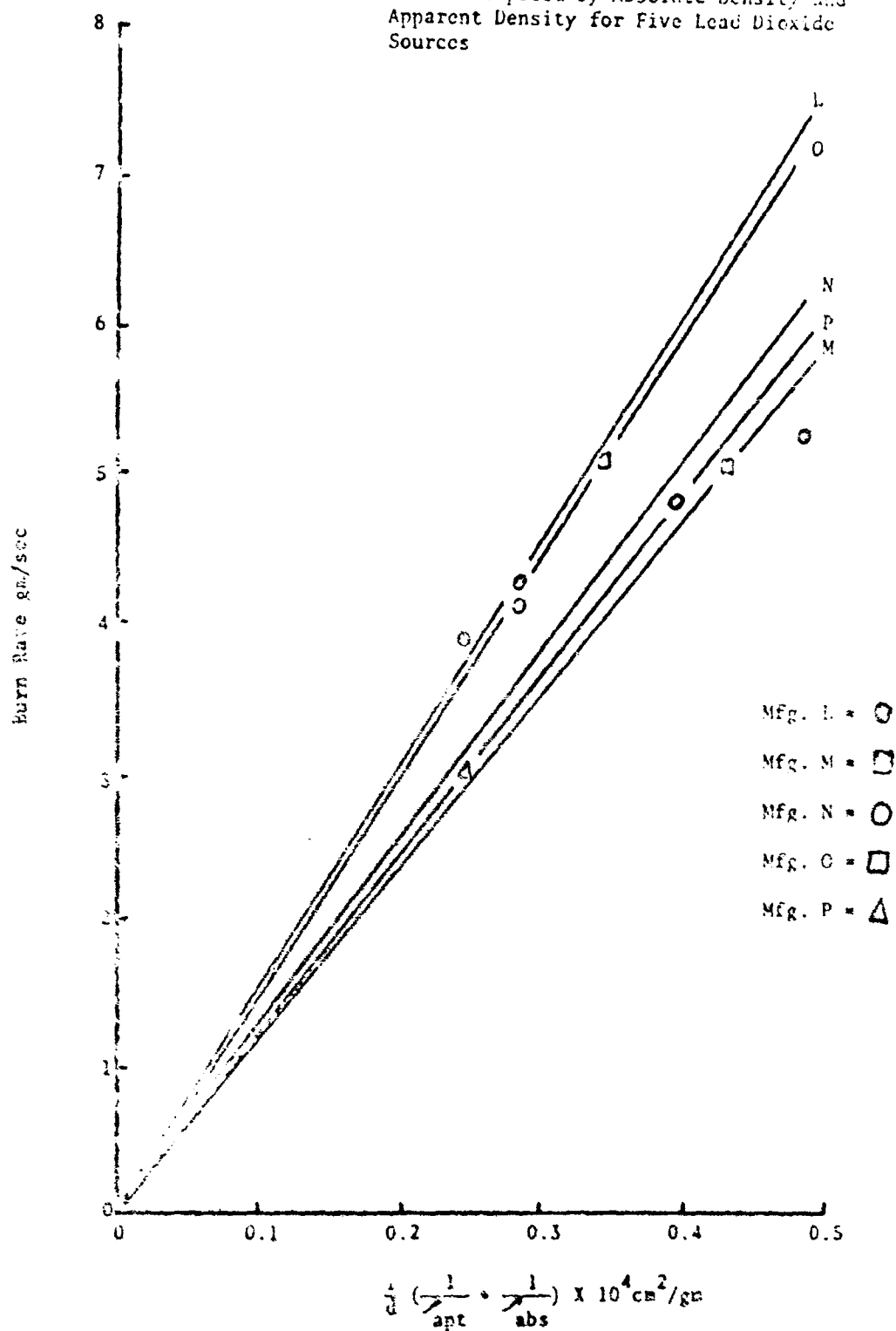


FIGURE 9 Plot of Koron - Lead Dioxide Delay  
burning Rate Versus Reciprocal Particle  
Size Multiplied by Absolute Density and  
Apparent Density for Five Lead Dioxide  
Sources



average particle diameter, the apparent density, and the absolute density of the lead dioxide specimen used in the delay composition.

### 5. Calorimetry

a. Calorific values for the heats of reaction of 2L-3C-5S starter compositions made from the various lead dioxide samples obtained from the six domestic manufacturers are shown in Table II. It can be seen that values range from 372.44 cal/g for sample O to 353.34 cal/g for sample N-2. It can be seen from the results given in Table II that large variations in the purity of the lead dioxide used in the starter compositions do not show correspondingly large variations in the calorific value of the compositions. Sample N-2 assays at 79.5%  $\text{PbO}_2$  - 15.5% below the minimum specification requirement - and yet it shows barely a 2% decrease in calorific output from other samples (N-4 and P-1) that assay about 96%  $\text{PbO}_2$ . Moreover, this low purity does not particularly affect the other performance tests in an adverse way: the pressure-time curve is fast and the delay burning rate average. Thus the relation between the performance and the purity is anything but clear. Indications are that factors more important than the  $\text{PbO}_2$  assay dominate the performance of the compositions.

b. Calorific values for the heats of reaction of different ratios of lead dioxide and silicon are shown in Table V. From this table Figure 10 was obtained in which the enthalpy is plotted as a function of the percent of the silicon fuel. The enthalpy,  $q$ , is equal to the heat per mole of available oxidizer; or

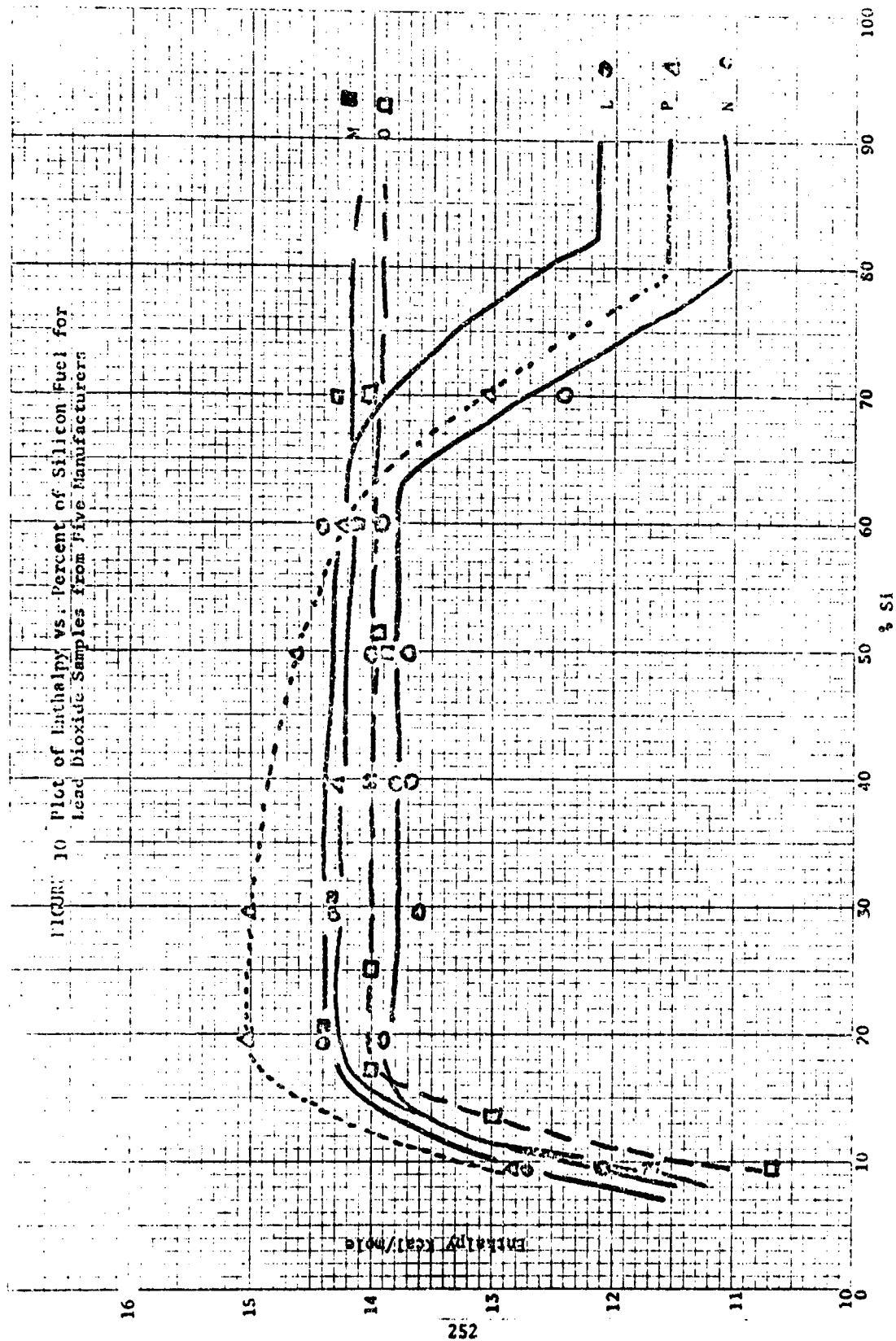
$$q = \frac{\Delta H \times \text{molecular weight of oxidizer}}{\text{weight of composition} \times \text{percent of oxidizer}}$$

TABLE V

CALCULATED VALUES FOR THE HEATS OF REACTION OF DIFFERENT RATIOS OF  
LEAD DIOXIDE AND SILICON

Ratio of PbO <sub>2</sub> to Si:	Heat of Reaction in cal/g				
	Manuf L	Manuf M	Manuf N	Manuf O	Manuf P
9.5 : 0.5				301.1 302.0	
9.0 : 1.0	483.6 480.3	460.8 458.1	446.1 443.3	440.6 441.3	485.4 488.5
8.7 : 1.3				493.1 489.7	
8.5 : 1.5				501.1 500.0	
8.0 : 2.0	483.2 480.4	477.9 468.0	484.9 486.9		500.7 505.7
7.5 : 2.5				441.0 440.0	
7.0 : 3.0	420.7 421.4	395.8 413.2	422.0 423.0		447.0 480.4
6.0 : 4.0	355.9 347.0	341.5 355.6	354.5 359.6		384.3 388.7
5.0 : 5.0	295.3 299.0	291.0 288.9	301.1 297.5	292.0 291.7	311.3 309.8
4.0 : 6.0	241.9 240.1	233.3 231.2	233.3		243.2 230.9
3.0 : 7.0	166.2 172.2	155.9 156.7	183.4 177.7	179.6 179.0	165.8 162.2

FIGURE 10 Plot of Enthalpy vs. Percent of Silicon Fuel for  
Lead Dioxide Samples from Five Manufacturers



where  $\Delta H$  is the calorific value of the fuel-oxidizer combinations shown in Table V. Figure 10 indicates still another way of demonstrating inherent differences in the lead dioxide samples. At the stoichiometric point of about 18% silicon, the enthalpy varies from approximately 13.5 K-cal/mol for sample N to 15.0 K-cal/mol for sample P, a variation of almost 10%.

#### CONCLUSION

1. The study of materials is ultimately the study of the complex interrelationship between properties, composition, structure, and energy state. These are all merely aspects of a larger whole. A substance has certain properties because of its composition, structure, and energy state.

2. Traditionally, substances have been characterized by their chemical composition (based on a partial rather than an ultimate analysis) and by their physical particulate state. In the course of this work we have adopted an alternate approach to the characterization of substances. Substances have been characterized by their behavior under a given set of conditions. If they behave differently, it has been assumed that they are different; if they are different, then some of their measurable properties must be different.

3. Lead dioxide was among the substances chosen for this study because reports on its structure and properties vary and because its behavior as a pyrotechnic component has more than once come under suspicion. Variations in its density from 7.0 to 9.4 g/cc have been reported in the literature and similar variations have been found in this study. The color of commercial lead dioxide varies from red-brown to almost black while its particle size varies from approximately 0.3u

to approximately 2.4u. The particle size distribution, as evidenced by the difficulties encountered in fractionating the powdered material, also varies from sample to sample, with some materials such as sample O showing a considerable range of particle size, while others such as sample N-3 showing almost no range at all. Based on x-ray diffraction patterns, two types of lead dioxide -  $\alpha$ -PbO<sub>2</sub> and  $\beta$ -PbO<sub>2</sub> - have been reported, although all of the samples studied during this investigation were fundamentally  $\beta$ -PbO<sub>2</sub>. Differential thermal analysis indicates that there are two distinct types of decomposition mechanism shown by the various lead dioxide samples, one characterized by three endothermic peaks (Figure 11) and the other characterized by four endothermic peaks (Figure 12). The heat of reaction of 2-3-5 starter composition made from the various lead dioxide samples varies from 372.4 cal/g to 353.3 cal/g. Chemical analysis utilizing the hydrogen peroxide - lead dioxide reaction indicates that the purity of the samples varies from 79.5% PbO<sub>2</sub> to 95.9% PbO<sub>2</sub>. Similarly, the performance and reactivity tests indicate significant differences in the behavior of the various lead dioxide samples.

4. These measurements of properties and performances raise two immediate questions: first, is there any correlation between the various performance tests, e.g., is the same material always the fastest reacting in all of the tests; and secondly, is there any correlation between the properties of the lead dioxide samples and their performance?

5. Figure 2 shows that the temperature-time curves of the lead dioxide samples fall into two distinct groups. The data on specific surface area in Table III shows that these two groups depend upon

FIGURE 11 Typical DTA Thermogram of  
Lead Dioxide from Manufacturer L

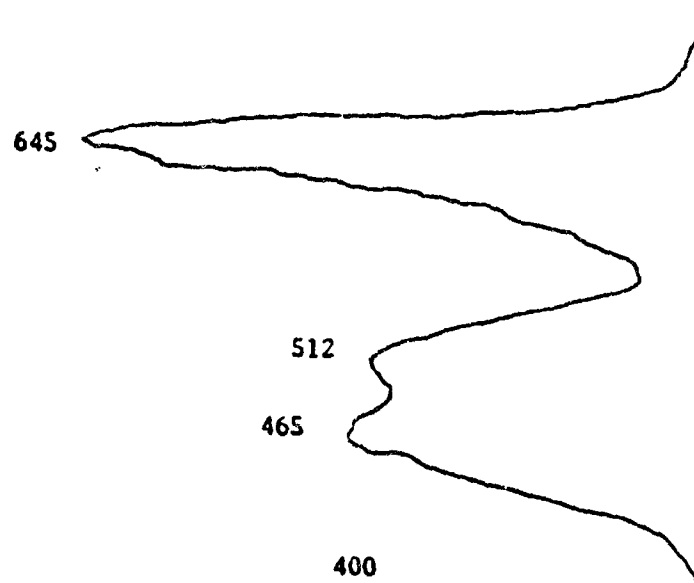
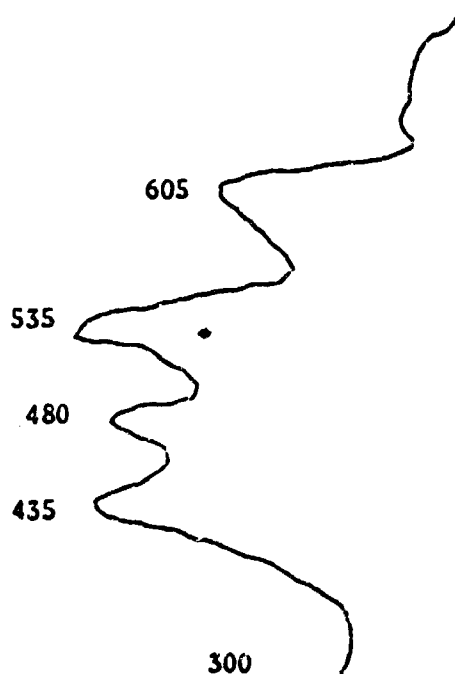


FIGURE 12 Typical DTA Thermogram of Lead  
Dioxide from Manufacturer P

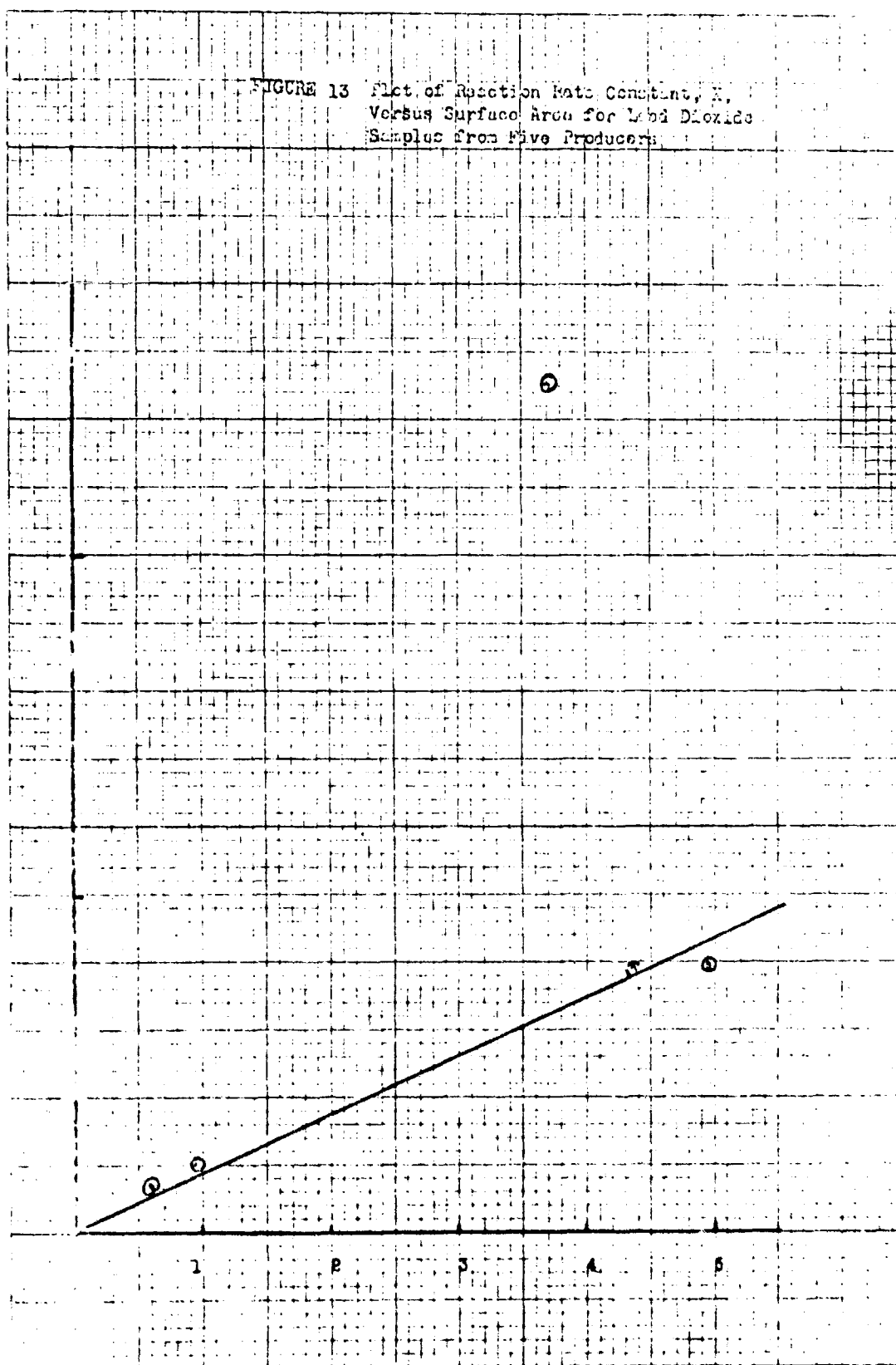


the surface area of the lead dioxide samples. For example, samples L and O which make up the slow reacting group have surface areas of  $0.6 \text{ m}^2/\text{g}$  and  $0.96 \text{ m}^2/\text{g}$  respectively, while samples P, M, and N which make up the fast reacting group have surface areas of  $3.72 \text{ m}^2/\text{g}$ ,  $4.35 \text{ m}^2/\text{g}$ , and  $4.94 \text{ m}^2/\text{g}$  respectively. For four of these samples the reaction rate constant is a linear function of the surface area, as shown in Figure 13. However, sample P does not fit into this linear relationship, indicating that its reaction rate constant is influenced by some other factor in addition to the specific surface area. Moreover, the value of the average particle diameter of sample P,  $2.38\mu$ , is very poorly related to the surface area,  $3.72 \text{ m}^2/\text{g}$ , and to the reaction rate of the sample in a liquid medium. This is an important instance where the apd is entirely misleading as a factor in determining the reactivity, which is in fact related to the surface area. One can only speculate concerning the reason for the large discrepancy between the value given by the Fisher Sub Sieve Sizer and the value given by the Surface Area Meter. The particles apparently have a large internal area and may resemble porous balls.

6. If we turn now to the reaction rates of these five specimens in solid-solid reactions - in this case as components in a delay composition - we find little resemblance between the burning rates and the reactivity rates shown in Table II. In the delay burning rates, sample P is the slowest, and samples M, N, and O are the fastest. Not much resemblance to the clear cut division of groups shown in Figure 2. The slopes of the lines in Figure 6 indicate the order of increasing rate of reaction to be N, O, P, L, M with a loose grouping of N and O as the slowest and M, L, and P as the fastest.

Reaction Rate Constant,  $K$ ,  $0^\circ\text{-m/min}$

FIGURE 13 Plot of Reaction Rate Constant,  $K$ ,  
Versus Surface Area for Lead Dioxide  
Samples from Five Producers



Surface Area,  $\text{m}^2/\text{g}$

In Figure 7 where the burning rate in a delay body is plotted against the reciprocal of the average particle size times the apparent density (instead of the absolute density as in Figure 6) the lines draw together somewhat and the groupings change. Now the order of increasing reaction rates are P, L, O, N, and M, with M and N forming one group and O, L, and P another. However, in Figure 8 where the effects of particle size ( $\frac{1}{d}$ ), absolute density ( $\frac{1}{\rho_{abs}}$ ) and apparent density ( $\frac{1}{\rho_{apt}}$ ) are all taken into account, the lines draw even closer together and the slopes of the lines fall once again into two distinct groups, M, P, and N forming the slower group and O and L the faster group. Two things are remarkable about this. The first is that the samples fall into the same groupings that were shown in the liquid reaction in Figure 2: L and O in one group and N, P, and M in the other. In other words, when the effects of the average particle size, apparent density, and absolute density are normalized - effects that dominate the burning characteristics in a delay - the original groupings based on reactivity in the liquid reagent are restored. The second remarkable thing is that the order of increasing reactivity is almost exactly reversed. Sample L, the slowest in Figure 2, becomes the fastest in Figure 8. In the liquid reaction the order of increasing reaction rates was L, O, N, M, and P; in the delay burning rate the order of decreasing reaction rates is L, O, N, P, and M.

7. If this is indeed true, as it certainly seems to be, it suggests a number of interesting possibilities. It indicates differences of "reactivity" exist over and above differences in purity,

particle size, or surface area. It indicates that the reactivity differences may be covered over and obscured because one test is responsive to one set of factors while a second test may be responsive to a second set of factors. And it indicates that differences in reactivity can be seen in different types of tests in which the reaction rate of a series of samples may be reversed.

8. The reactivity results shown in Figure 2, in which powdered lead dioxide reacts with a liquid reagent in which it is suspended, are almost exactly reversed in Figure 8, in which lead dioxide is mixed with boron (and a viton binder) and pressed into a delay composition. And furthermore, the order and magnitude of the reactivities of the five lead dioxide samples undergo changes from Figure 6 to Figure 7 and finally to Figure 8. We have already suggested an explanation for this second phenomenon. The delay burning rate is largely dependent on properties that affect the packing density--the particle size, the absolute density, and the apparent density. On the other hand, the reaction rate of lead dioxide in acid solution is largely dependent on the surface area and little affected by the packing density. So we see that factors that may heavily affect the rate of reaction in one set of conditions may have little effect on the rate of reaction in another set of conditions. And indeed the properties that cause lead dioxide to react rapidly in solution--that is, the particle size and more directly the surface area--cause it to react more slowly in a delay composition. This is because large particles with a small particle size range do not pack closely in a delay composition, and the increased porosity that results causes the composition to propagate the flame front through it more rapidly.

9. Pressure-time curves are routinely obtained on starter compositions used in the Mk 25 and the Mk 28 Marine Location Markers. The starter composition contains lead dioxide in varying proportions--usually 20% by weight--and the lead dioxide is a key component since it largely controls the ignitability and burning rate of the composition. The effect of formula changes on the pressure-time curves has already been studied in RDTR No. 41. However, continued variations in the same formula have not been satisfactorily explained. In the present study, it has been shown that lead dioxide specimens from different manufacturers, used in otherwise identical formulas, give a wide range of pressure-time performance curves. This only confirms what was already suspected. The problem will no doubt continue. Moreover, it must be said that the significance of the pressure-time curve is not well understood. This difficulty is compounded by the fact that there appears to be no correlation between the form of the pressure-time curve and the physical and chemical properties of lead dioxide studied in this investigation. Considerable differences in purity and average particle size, upon which the military specification is based, appear to have no directly discernable relationship with the form of the pressure-time curve. This problem is currently under study.

10. Besides the poor correlation between  $\text{PbO}_2$  purity and the pressure-time curve--Table II indicates that sample N-2 has a purity of only 79.5%  $\text{PbO}_2$  and yet it has a fast pressure-time curve--there is generally also a poor correlation between  $\text{PbO}_2$  purity and the heat of reaction of the starter compositions. For example, sample N-3 has a purity of 85.1%  $\text{PbO}_2$  and a calorific value of 357.4 cal/g;

sample N-4 has a purity of 96.3%  $\text{PbO}_2$  and a calorific value of 360.4 cal/g. This would not appear to be consistent and would indicate that the evaluation of the chemical purity has little relation with the actual oxidizing power of the lead dioxide in a pyrotechnic composition.

NOVEL PYROTECHNIC COMPOSITIONS FOR SCREENING SMOKES\*

George A. Lane, W. Arthur Smith and Erwin M. Jankowiak

The Dow Chemical Company  
Midland, Michigan

\* This work was supported by the Air Force Armament Laboratory (ATOC), Eglin Air Force Base, Florida.

## NOVEL PYROTECHNIC COMPOSITIONS FOR SCREENING SMOKES\*

George A. Lane, W. Arthur Smith, and Erwin M. Jankowiak

The Dow Chemical Company  
Midland, Michigan

### ABSTRACT

Exploratory studies have been conducted on pyrotechnic screening smokes. A chamber has been constructed for evaluating screening smokes by both a visual target technique and a light attenuation technique. Using  $TiCl_4$  (FM) smoke agent, these methods have been studied and standardized. Nearly exact agreement in total obscuring power (TOP) values between the two techniques has been obtained.

Chemical smokes, consisting of boron oxide, boron nitride, silicon dioxide, and pyrotechnic oil fogs, were studied. Relative humidity was found to have a pronounced effect on the obscuring power of nearly all the smoke agents investigated.

Boron oxide smokes generated from boron - lithium perchlorate mixtures are superior in TOP to the FM standard. A satisfactory boron nitride smoke could not be generated from the mixtures investigated. The best silicon dioxide smoke was generated from a silicon-lithium perchlorate composition. A major part of the obscuring power is due to the presence of lithium chloride in the smoke. Good obscuration can be attained only if good combustion is achieved. To do this, it is necessary to use fine particle silicon. Pyrotechnic oil fogs are superior in TOP to FM below 50% relative humidity, but inferior under more humid conditions.

### I. INTRODUCTION

The purpose of this research was to study a number of promising smoke-generating formulations designed to produce a non-toxic, non-corrosive smoke of maximum obscuration and maximum persistence.

---

\*This work was supported by The Air Force Armament Laboratory (ATCC), Eglin Air Force Base, Florida.

The ideal screening smoke will have the following properties:

- (a) Non toxic
- (b) Non-corrosive
- (c) Great persistence of smoke
- (d) High cloud reflectivity
- (e) Particle diameter about 0.6-0.7 $\mu$
- (f) Low index of refraction
- (g) Ability to react with or absorb moisture from the air

Since oil smokes are known to meet the requirements of a non-toxic, non-corrosive, and persistent smoke, research was performed to improve their application and overcome their shortcomings. An exploratory program to develop new types of smoke based on boron oxide, boron nitride, and silicon dioxide was carried out. Optimization and evaluation of total obscuring power (TOP) for the various formulations were carried out in a specially designed smoke chamber. Studies of safety, compatibility, and stability were performed on promising smoke formulations.

## II. STANDARD SMOKES AND MEASURING TECHNIQUES

### A. TECHNIQUE

A horizontal cylindrical steel tank, eight feet in diameter and twenty-eight feet long, was equipped as a smoke chamber. Three mixing fans are located at equal distances apart along one side of the chamber. Two rows of lights (16 lights in all, 60 watts each) are mounted running the length of the chamber. A visual target, installed on a track, is positioned to move the length of the smoke chamber. The tank is fitted with an airtight door and ports for visual and optical measurements. A floodlight is mounted inside the chamber in line with a collimator and external photocell assembly. Ventilation is accomplished by two overhead ports and an external exhaust fan. The inside of the tank is painted black.

Experimentally, the smoke unit is functioned at about the center of the tank. The fans are then turned on to stir the smoke in the chamber to uniformity, and left on through the balance of the test. Three minutes after operation of the smoke unit, light attenuation measurements are started, and a minute later visual obscuration tests are begun. Measurements are taken at five-minute intervals. The data at the point of minimum light transmission and maximum target obscuration are taken as representative for the smoke unit.

Titanium tetrachloride (FM) smoke was selected as a standard for this research, since it is convenient to use and less corrosive to the chamber and associated equipment than a standard smoke such as FS. This material is readily hydrolyzed by atmospheric moisture to a dense white smoke. Problems in disseminating were encountered initially. Evaporative techniques reported in previous literature were found inefficient;  $TiCl_4$  gums at the surface of the liquid preventing further evaporation. Work with atomizers was hindered by gumming at the tip of the nozzle. Finally, a DeVilbiss paint sprayer operated by dry nitrogen gave reproducible results with a minimal amount of difficulty.

In order to determine the efficiency and smoke yield of experimental formulations, an aerosol sampling technique was employed. Smoke particles were collected on membrane filter pads by means of vacuum air-sampling; 9.5-liter air samples were taken at one-minute intervals.

Titanium, boron, boron oxide, and boron nitride were analyzed photometrically. Chlorine determinations were made by the Volhard titration technique, and by coulometric titration. Silicon analyses were performed by X-ray fluorescence. Lithium was determined by flame photometry.

## B. THEORY

Evaluation of the screening ability of smokes is based on a figure of merit, the total obscuring power (TOP). TOP is the area in square feet that can be obscured by a pound of smoke formulation.

By using the light attenuation apparatus and the target device, two independent methods of obtaining TOP are available. In the target method, a known smoke agent concentration is introduced in the tank, and the obscuration distance is measured by varying the distance from the target to observer. In the light transmission method, the distance is held constant, the amount of smoke agent is varied, and the concentration required for obscuration is determined, usually by an extrapolation technique. Thus, by utilizing the photocell system, movable visual target, and overhead lights, a procedure was developed whereby all smoke clouds could be evaluated.

Use of the light transmission method of evaluating obscuring power is based on the Beer-Lambert relationship:

$$I = I_0 e^{-\epsilon c l} \quad (1)$$

where  $I$  is the observed light intensity,  $I_0$  is the initial

intensity without smoke,  $c$  is the concentration of smoke,  $l$  is the path length, and  $e$  is the scattering or extinction coefficient.

TOP is defined as:

$$TOP = \frac{1}{C^* l^*} \quad (2)$$

where  $l^*$  is the fixed distance to the photolamp and  $C^*$  is the concentration of smoke agent required for obscuration. The asterisk refers to obscuration conditions.

At this point it should be noted that  $c$  in Equation (1) refers to the actual concentration of smoke in the chamber, while  $C$  in the TOP Equation (2) is the weight of the smoke-producing agent or formulation used, divided by the chamber volume. These two concentrations are proportional to each other,

$$c = yC \quad (3)$$

where  $y$  is the yield of the smoke agent or smoke formulation (weight of aerosol produced per unit weight of smoke generating composition). Yield is supposedly a constant for a liquid agent such as FM, but can vary with munition size for solid formulations.

Combining Equations (1), (2), and (3), we obtain the total obscuring power:

$$TOP = \frac{-ey}{\ln I^*/I_0} \quad (4)$$

where  $I^*$  is the transmitted light intensity under obscuration conditions. Researchers at Denver Research Institute (1) adopted a value of 0.0125 for  $I^*/I_0$  at the obscuration point, based on physiological studies concerned with the discrimination capability of the human eye.

Introducing this criterion into Equation (4) gives:

$$TOP = \frac{\ln \frac{I}{I_0}}{\ln 0.0125 C l^*} \quad (5)$$

For a ten-gram smoke munition in the Dow chamber, this becomes

$$TOP = -6620 \log \frac{I}{I_0} \quad (6)$$

This relationship can then be used to determine TOP for each functioning of a smoke unit. However, care must be taken that measurements are performed on a dilute smoke cloud for which particle coalescence is minimal, since Equation (6) is only valid for such a smoke.

## C. RESULTS

### 1. Effect of Relative Humidity

It was expected that humidity has an influence on TOP (2). Using  $\text{TiCl}_4$ , a pronounced humidity effect was immediately observed. It also soon became apparent that the measured TOP is a function of relative humidity (R.H.), rather than absolute humidity.

The values found are exceptionally high, in comparison with previously reported TOP values for  $\text{TiCl}_4$ . Several explanations are offered. Atomization of  $\text{TiCl}_4$  is a more reproducible and efficient method of dissemination than the evaporative techniques used in some studies. Secondly, few reported TOP values for  $\text{TiCl}_4$  are accompanied by relative humidity data. Denver Research Institute (1) reports a value of 3900 for  $\text{TiCl}_4$  (FM) at 60% relative humidity, in good agreement with the data reported in Figure 1. A lower TOP value of 2050 (humidity not specified) reported by DRI for  $\text{TiCl}_4$  smoke is consistent with a relative humidity below 30%, more characteristic of the climate in Denver than the 30-90% humidity range of Dow's tests at Midland.

### 2. Smoke Concentration Effects

In order to determine the range of sample size necessary to give a dilute enough smoke for accurate TOP determination by the light transmission method, measurements were taken for five-, ten-, and fifteen-gram samples of  $\text{TiCl}_4$ .

Plots of  $\log \frac{I}{I_0}$  as a function of the weight of  $\text{TiCl}_4$  disseminated showed a good linear relationship for five- and ten-gram samples, but deviations for the fifteen-gram charges.

As a result the ten-gram sample size was selected for subsequent use in determining TOP by the light transmission method.

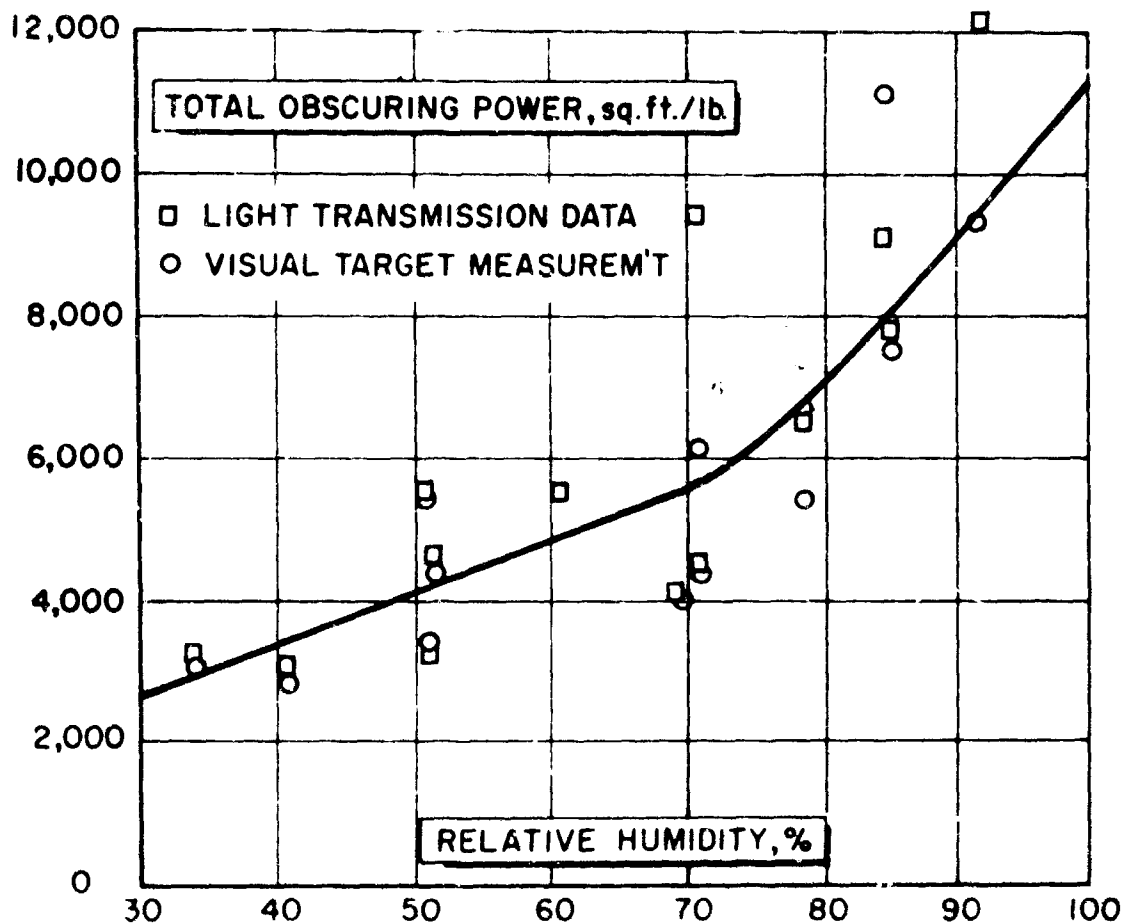


Fig. 1 - Variation of TOP with Percent Relative Humidity for 10-Gram  $\text{TiCl}_4$  Smoke

### 3. TOP Values

The agreement between TOP values obtained by the visual target and light transmission approaches is excellent, as shown in Figure 1. Some of the scatter of data is due to poor relative humidity measurements taken at the onset of this work. The technique used has been upgraded to obtain more accurate readings in subsequent work. Nevertheless, the agreement between the two independent measuring techniques is unexpectedly good, and results in a high level of confidence in the data generated.

### 4. Specific Obscuration

Up to this point TOP has served as a practical measurement to evaluate the obscuring potential of a smoke material. However, it must also be taken into account that, when ten grams of smoke agent material is used in the various experiments, ten grams of smoke is not necessarily generated. Analyses of the titanium and chlorine in the smoke cloud from  $TiCl_4$  agent indicate less than 100% conversion of  $TiCl_4$  to the smoke cloud. From a practical standpoint, the weight of material needed to produce a smoke cloud of a certain density is important. However, a true evaluation of the obscuring ability of the actual aerosol smoke species is not revealed in the TOP value.

Therefore, a new value, designated as specific obscuration ( $O_s$ ), is proposed. It is obtained by using the actual weight of material in the smoke cloud, obtained through analysis of material collected from the cloud. This value should give an indication of the ability of the chemical species involved to obscure.  $O_s$  is defined as:

$$O_s = \frac{\text{Volume of Tank (ft.}^3\text{)}}{\text{Wt. of Aerosol Smoke (lb.)} \times \text{Obscuring Distance (ft.)}}$$

TOP may be obtained from  $O_s$  by multiplying by the yield of the munition:

$$TOP = yO_s$$

$O_s$  must be determined for various relative humidities, since the same weight of material disseminated has been shown to have varying obscuring capability over a range of relative humidities. It should be noted that the weight of aerosolized smoke does not include the weight of any unreacted water vapor taken up by the smoke. Therefore,  $O_s$  will have a higher value for hygroscopic smokes.

TiCl<sub>4</sub> presents a certain amount of difficulty in this calculation, since the identity of the smoke species is not definitely known and there are probably more than one kind. Utilizing the titanium and chlorine analyses, the weight of the smoke species was calculated by assuming that the smoke consists of a mixture of compounds with titanium bonded to oxide, chloride, and oxychloride groups. For convenience, the chlorine content in the smoke was calculated on the basis of TiCl<sub>4</sub>, and the excess titanium not bonded to chlorine was calculated as TiO<sub>2</sub>. Table I shows the titanium and chlorine analyses, the calculated weight of the nominal smoke species, and the O<sub>s</sub> at various relative humidities. Significantly greater obscuration is attained at elevated relative humidities. The major value of O<sub>s</sub> is that it may be used to indicate the obscuring power of a smoke species even though the yield of the munition is low and TOP values are low.

Table I  
Specific Obscuration for 10-Gram Samples of TiCl<sub>4</sub>  
at Various Relative Humidities

<u>Ti</u> <u>g.</u>	<u>Cl</u> <u>g.</u>	<u>TiO<sub>2</sub></u> <u>g.</u>	<u>TiCl<sub>4</sub></u> <u>g.</u>	<u>Relative</u> <u>Humidity</u> <u>%</u>	<u>O<sub>s</sub></u> <u>ft. <sup>2</sup>/lb.</u>
2.345	1.399	3.12	1.892	34	6,460
2.43	0.734	3.64	0.982	41	6,140
1.475	0.955	1.92	1.278	59	12,610
1.735	1.303	2.16	1.743	71	11,340
1.56	0.912	2.08	1.220	79	17,340
1.845	1.129	2.445	1.512	92	24,250

### III. DEVELOPMENT AND EVALUATION OF EXPERIMENTAL SMOKE AGENTS

#### A. BORON OXIDE SMOKES

Table II shows the relative smoke-producing capabilities of several boron-containing fuels assuming 100% conversion to boron oxide.

Table II  
Relative Smoke Producing Potential of  
Boron-Containing Fuels

<u>Boron-Containing Fuel</u>	<u>Theoretical Yield of B<sub>2</sub>O<sub>3</sub> g./g. fuel</u>
Boron	3.23
Decaborane, B <sub>10</sub> H <sub>14</sub>	2.85
Boron Carbide, B <sub>4</sub> C	2.51
Trimethoxyboroxine (TMB)	0.60
Methyl Borate	0.33
Triethylborane	0.36

Since the highest potential of boron oxide is available from elemental boron, decaborane, and boron carbide, the greatest research emphasis was placed on these boron-rich fuels. Experiments were also conducted on the organic boron compounds, however.

#### 1. Decaborane Fuel

To generate an obscuring cloud of boron oxide smoke, study of decaborane-fueled formulations was undertaken. Sodium, potassium, and ammonium nitrate oxidizers formulated with varying percentages of decaborane generated moderate smoke clouds. The best cloud generated from a decaborane system resulted from a 65:35 mix of decaborane and guanidine nitrate. Analysis of the smoke showed the major constituent to be boron oxide with minor amounts of elemental boron and boron nitride. Ten-gram formulations consisting of 65% decaborane and 35% guanidine nitrate have an average conversion of decaborane to boron oxide of 60%; this corresponds to a yield of 108% of boron oxide on the total weight of the formulation.

Visual and optical measurements were conducted in the smoke chamber to evaluate boron oxide smoke. The data are presented in Figure 2 which shows the variation with relative humidity for a ten-gram munition composed of 65% decaborane - 35% guanidine nitrate. There is excellent agreement between the light transmission and visual target data. Relative humidity has a strong influence on the obscuring ability of this smoke. Below about 80% R.H. it is superior to TiCl<sub>4</sub> in obscuration.

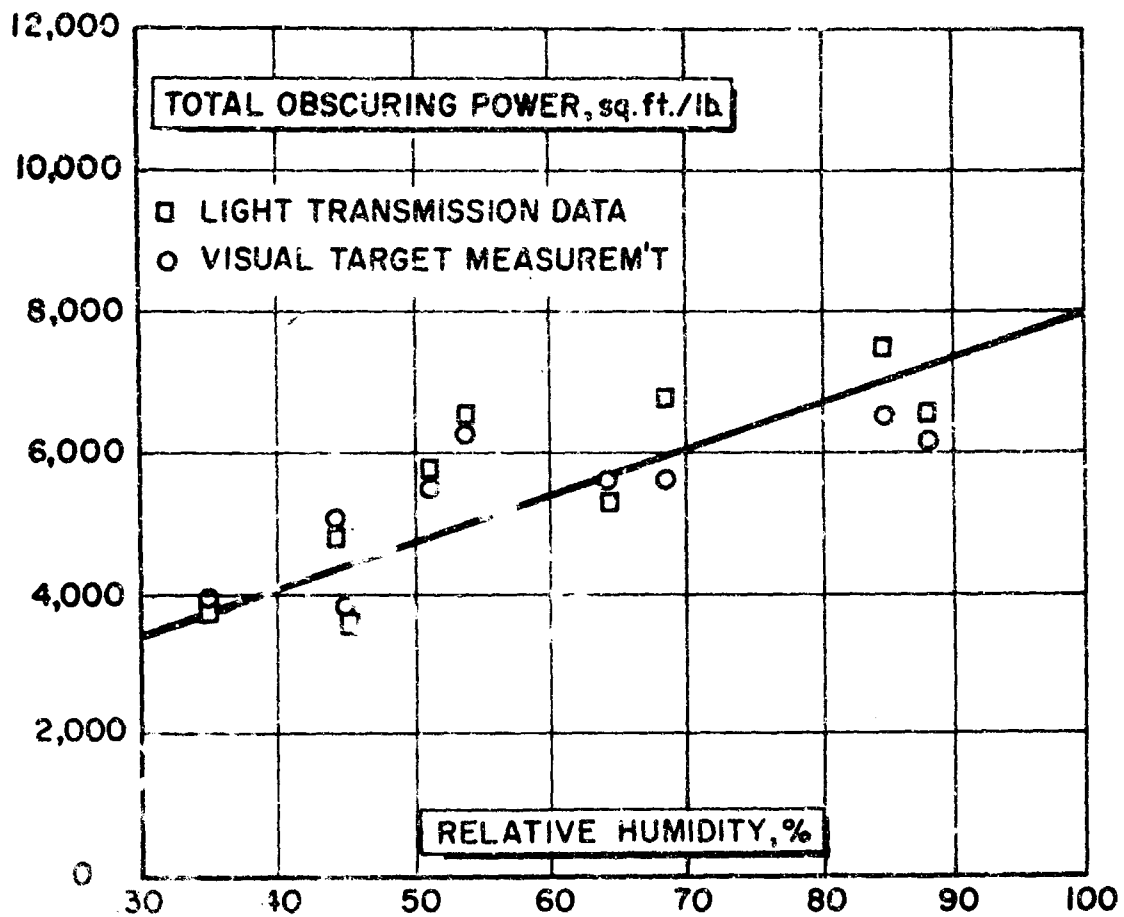


Fig. 2 - Variation of TOP with Percent Relative Humidity  
for 10-Gram Munitions Composed of 65%  
Decaborane - 35% Guanidine Nitrate

## 2. Organic Boron Fuels

Since decaborane is too expensive to be considered for an operational system, alternate fuel sources were sought. Alkyl borates, boroxines, and alkyl boranes were studied. Trimethoxyboroxine (TMB) and methyl borate were chosen for evaluation because of their availability and lower cost. TMB and methyl borate were atomized in the same apparatus used to disseminate  $TiCl_4$ . Neither of these liquids was readily hydrolyzed by atmospheric moisture to generate smoke clouds.

Triethylborane, a pyrophoric liquid, was disseminated using the DeVilbiss paint sprayer and a chamber designed to contain the liquid under nitrogen. The liquid flamed in air, generating a thin cloud. TOP values of 1326 and 1820  $ft.^2/lb.$  were obtained at 58% and 93% relative humidity. The reaction gave 58% efficiency and 21% yield. Triethylborane, containing only 11% boron, has limited potential for generating boron oxide smoke when compared to boron and boron carbide fueled formulations.

## 3. Elemental Boron Fuel

Studies were initiated on smoke compositions based on powdered boron as the fuel. A mix of 60% boron - 40% lithium perchlorate gave outstanding performance, exceeding the decaborane composition in obscuring power.

The effect of relative humidity for ten-gram munitions composed of 60% boron and 40% lithium perchlorate is shown in Figure 3. TOP data for the visual target measurements agree with those obtained using light transmission data.

Since it is possible in this system for lithium chloride smoke to be generated, work was undertaken to determine the amount of this compound present in the smoke evolved from the 60% boron - 40% lithium perchlorate formulation. Analyses indicated the presence of approximately 8% by weight lithium chloride in the smoke, based on the lithium content. Chloride analyses were lower than expected, indicating that species such as lithium oxide or lithium hydroxide may be present.

Ten grams of the 60% boron - 40% lithium perchlorate formulation theoretically can yield 1.59 g. of lithium chloride. Thus, approximately half of the potentially available salt is accounted for in the smoke cloud.

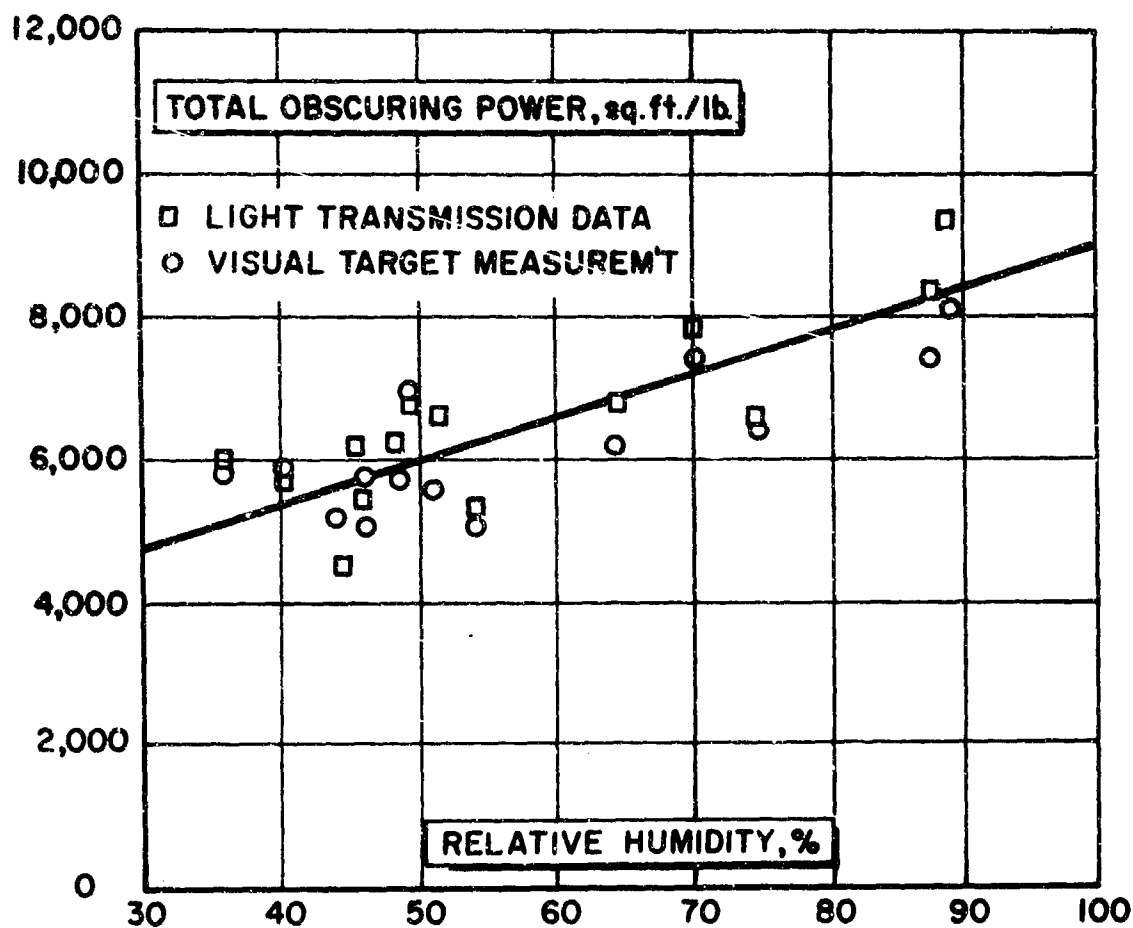


Fig. 3 - Variation of TOP with Relative Humidity  
for 10-Gram Munitions Composed of  
60% Boron - 40% Lithium Perchlorate

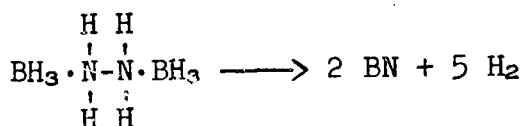
It was assumed, as an approximation, that  $B_2O_3$  has the same obscuring properties, whether produced from the boron - lithium perchlorate formulation or the decaborane - guanidinium nitrate mix. Specific obscuration values were then calculated for lithium chloride smoke itself. At 100% relative humidity, a value of 24,000 ft.<sup>2</sup>/lb. was derived, comparable to that of FM smoke.

#### 4. Boron Carbide Fuel

A 30:70 mix of boron carbide and lithium perchlorate generated a good cloud of smoke. Figure 4 shows TOP (using light transmission data) as a function of relative humidity for ten-gram munitions of this composition. No attempt was made to analyze this smoke for LiCl.

#### P. BORON NITRIDE SMOKES

Attempts were made to disseminate boron nitride. Hydrazine bisborane (HBB), a white powder, was studied initially. On ignition of neat HBB pressed into a munition can, little smoke was produced, but there was much light, flame, and ash.



Combination of nitrogen-rich and boron-rich compounds was next investigated. Polytaz, the pseudoplastic pyrolysis product of triaminoguanidinium azide, and dekazene [ $B_{10}H_{12}(NH_3)_2$ ] were mixed to form a tough waxy composition. On ignition, it gave little smoke and negligible obscuration. Similar results were obtained for a solution of bis-hydrazinium perhydrodecaborate ( $H_2D$ ),  $B_{10}H_{12}(N_2H_4)_2$ , in hydrazine.

From the results obtained on boron nitride smokes, it would appear that BN formation occurs in the solid phase, rather than after boron-containing and nitrogen-containing moieties are vaporized. This is supported by the observation that nearly all the BN product remains in the munition can or is scattered on the floor of the tank beneath the can.

#### C. SILICON DIOXIDE SMOKES

Research was initiated on producing  $SiO_2$  smoke from pyrotechnics. Table III shows the theoretical yield of  $SiO_2$  available from various fuels.

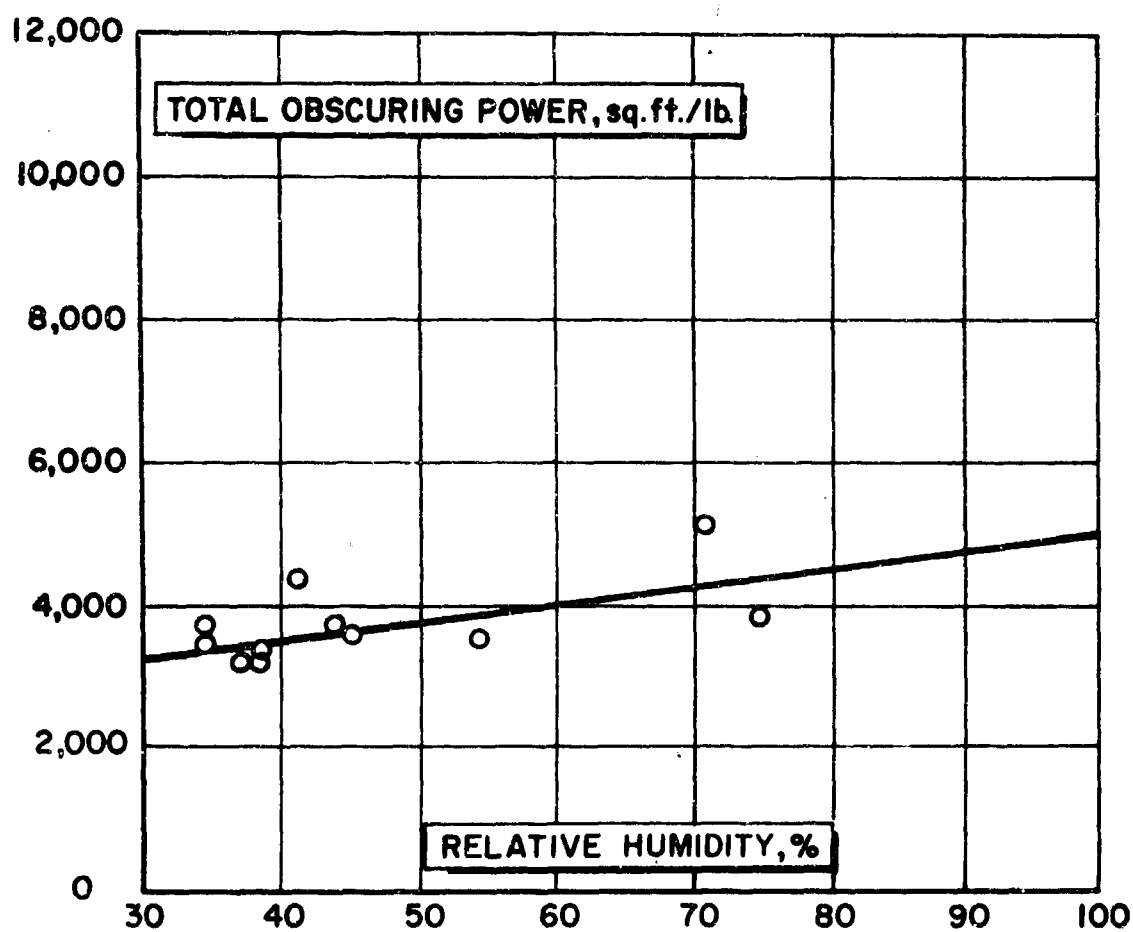


Fig. 4 - Variation of TOP (Light Transmission Method) with Relative Humidity for 10-Gram Munitions Composed of 30% Boron Carbide - 70% Lithium Perchlorate

Table III

Relative Smoke Producing Potential of  
Silicon-Containing Fuels

<u>Silicon-Containing Fuel</u>	<u>Theoretical Yield of SiO<sub>2</sub></u> <u>g./g. fuel</u>
Silicon	2.14
Silicon carbide, SiC	1.50
Hexamethyldisilane, (CH <sub>3</sub> ) <sub>6</sub> Si <sub>2</sub>	0.82
Hexamethyldisiloxane, (CH <sub>3</sub> ) <sub>6</sub> Si <sub>2</sub> O	0.74

Most of the research effort has involved silicon and silicon carbide fuels, but some work was done on organic silicon compounds.

1. Organic Silicon Fuels

Hexamethyldisilane (HMDS) was prepared and distilled to a pure product. It was absorbed on a synthetic silicate powder (Micro-Cel E), formulated with a solid oxidizer such as sodium, potassium, or ammonium nitrate, and pressed into a munition. On ignition there was some smoke but mostly a bright flame.

Because of the poor results obtained with alkylsilane composition, other silicon-containing fuels were investigated.

2. Elemental Silicon Fuels

Formulation development efforts were concentrated on silicon compositions, using various oxidizers. The most encouraging results were shown by smoke munitions consisting of elemental silicon and lithium perchlorate. A pyrotechnic mix consisting of the stoichiometric ratio, 35% elemental silicon and 65% lithium perchlorate, is the best composition developed to date for the production of silicon dioxide smoke. The pressed grain ignites without the use of a first-fire and a substantial cloud is generated. As detailed later, analysis of the smoke shows considerable lithium chloride along with the silicon dioxide. Lithium chloride is a hygroscopic salt which contributes significantly to the obscuration of the cloud.

Figure 5 shows TOP data as a function of relative humidity for 10-gram munitions composed of 35% Si - 65% lithium perchlorate. The low TOP values obtained are due to the very low efficiency of combustion of the elemental silicon, 14%. A sample of the residual slag from this composition was analyzed by X-ray fluorescence and found to consist of 44% by weight of silicon. This is consistent with the low efficiency of the 35% silicon - 65% lithium perchlorate formulation.

#### a. Fine Particle Size Silicon

The most encouraging results were obtained when a series of munitions was fired using varying particle size silicon powder. Mesh sizes of 200 (74  $\mu$ ) and 400 (37  $\mu$ ) were used. Significantly less light transmission was found when smaller particle size silicon was used.

An attempt was made to prepare a finer particle size silicon powder. "As received" silicon powder, which is approximately 200-300 mesh, was agitated with ceramic balls for two hours on a paint shaker. By inspection with a microscope most of the treated material appeared to be a few microns in size. The treated silicon powder was free flowing and easily passed a 400 mesh screen.

The fine powder was formulated and fired in a metal canister. It burned twice as fast as the untreated powder and analysis of the smoke showed a substantial increase in efficiency of combustion. The efficiency and yield were 47% and 35%, respectively. At 100% relative humidity, a TOP value of approximately 6600 ft.<sup>2</sup>/lb. was attained.

#### b. Fiberglass Canister

A continuing problem was the combustion and melting of the one-ounce steel munition can which is used with the ten-gram 35% silicon - 65% lithium perchlorate formulation. Upon functioning of the munition, the can becomes cherry red and the side and bottom burn out. Uneven burning and a loss of pressure are consequences. An epoxy-reinforced fiberglass canister was tried, and considerable improvement in the smoke cloud was noted.

Using the 35% silicon - 65% lithium perchlorate formulation a series of firings employing both fiberglass and metal canisters was made over a range of relative humidities. The size of the fiberglass canister approximated the dimensions of the metal canister. Upon combustion the fiberglass canister showed remarkably little deterioration except for char of the organic constituents. Metal canisters nearly always disintegrated.

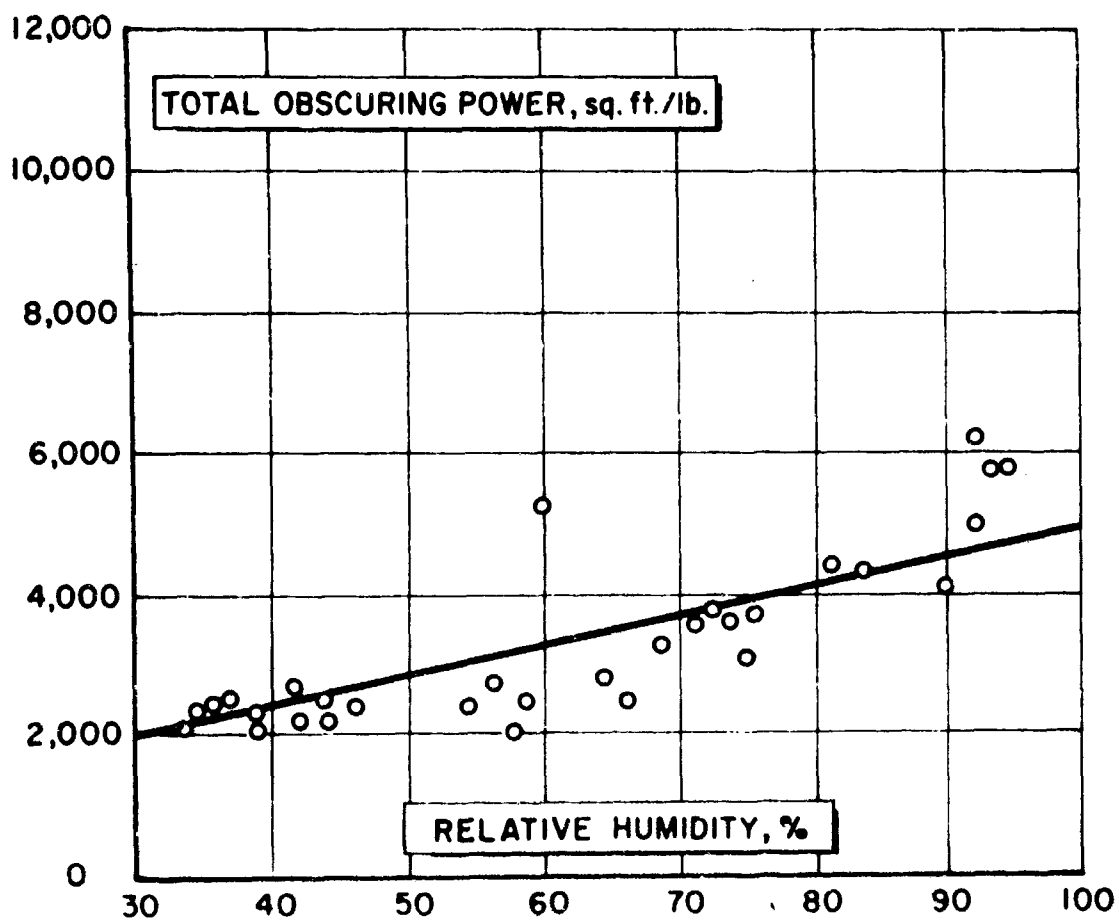


Fig. 5 - Variation of TOP (Light Transmission Method) with Relative Humidity for 10-Gram Munitions Composed of 35% Silicon - 65% Lithium Perchlorate Fired in Metal Canisters

Munitions fired in fiberglass consistently gave higher TOP values than the identical formulation fired in metal canisters. Analytical data confirm an increase in efficiency and yield. Using the fiberglass canister an average efficiency of 27% was obtained. This is marked improvement over 14% efficiency for metal canisters. Figure 6 shows the variation of TOP with relative humidity for munitions fired in fiberglass canisters.

The metal canister appears responsible for a loss in the efficiency of combustion. It is believed that when the metal munition can is used, some of the oxidizer reacts with the container, and is not available to oxidize silicon. The resultant loss in efficiency leads to a lower TOP, compared with the fiberglass munitions. Some of the increase in TOP for fiberglass containers also may result from volatilization of components of the bonding resin in the case. A sample of the smoke obtained using the fiberglass canister was gray in color, indicating the presence of carbon, whereas smoke samples taken when the metal canister was used were white. It is believed, however, that the carbon produced contributes little to the obscuration.

A limited amount of work was done with fine particle size silicon prepared by grinding in a paint shaker. Formulations based on the fine powder were fired in a fiberglass canister at 100% relative humidity. An efficiency and yield of 43% and 32%, respectively, and a TOP value of approximately 7900 ft.<sup>2</sup>/lb. were obtained.

Thus, by using fine particle size silicon powder and employing a fiberglass canister, significant increases both in combustion efficiency and TOP have been achieved for silicon dioxide smoke compositions. They have been shown superior to FM smoke at ordinary humidity levels by the most recent test results.

#### c. Lithium Chloride as a Smoke Constituent

As previously mentioned, analytical investigation of the smoke from silicon-lithium perchlorate compositions revealed substantial amounts of lithium chloride. As much as 75% of the total lithium chloride available from the lithium perchlorate oxidizer was accounted for in the smoke cloud. Lithium chloride is hygroscopic, has a low index of refraction, and should be a very effective smoke screening material.

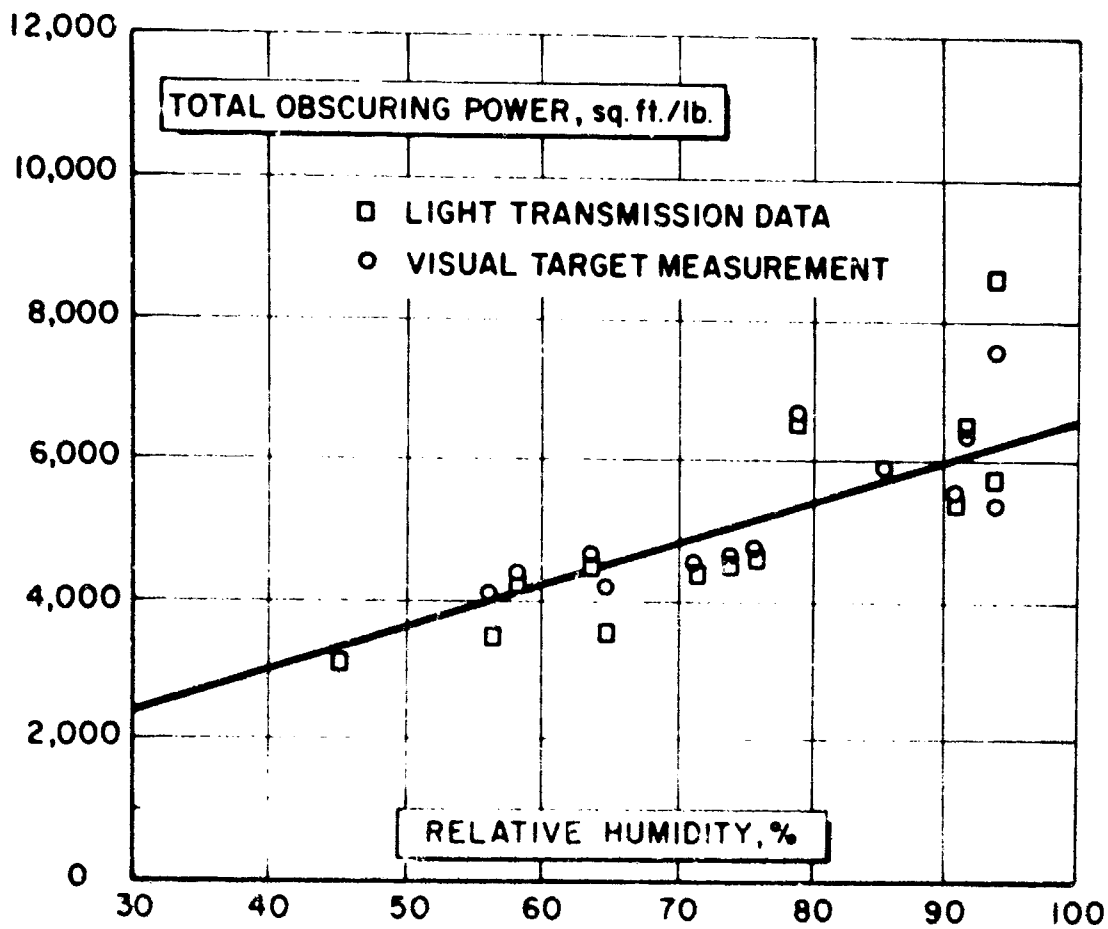


Fig. 6 - Variation of TOP with Relative Humidity for 10-Gram Munitions Composed of 35% Silicon 40% Lithium Perchlorate Fired in a Fiberglass Canister

Table IV shows the data obtained for the different particle sizes of silicon and the different canister materials. The yield of  $\text{SiO}_2$ , as previously discussed, changes dramatically. The  $\text{LiCl}$  yield, however, is nearly constant.

Table IV

Effect of Silicon Particle Size and Canister Material on Combustion and Smoke Obscuration

	<u><math>\text{SiO}_2</math></u>		<u><math>\text{LiCl}</math></u>		<u>TOP<sup>a</sup></u> ft. <sup>2</sup> /lb.	<u>O<sub>s</sub><sup>a</sup></u> ft. <sup>2</sup> /lb.
	Eff. Yield	Eff. Yield	Eff. Yield	Eff. Yield		
"As Received" Silicon Powder	Ave. %	Ave. %	Ave. %	Ave. %		
Metal canister	13.8	10.4	69.3	17.5	5,000	17,950
Fiberglass canister	27.0	20.2	72.1	18.7	6,500	16,700
<u>Fine Silicon powder</u>						
Metal canister	46.8	35.0	75.5	19.6	6,500	12,000
Fiberglass canister	42.8	32.1	68.7	17.8	7,880	15,750

<sup>a</sup>Relative humidity, 100%

Since the data in Table IV show a wide range of yields of  $\text{SiO}_2$ , it is possible to calculate approximate  $\text{O}_s$  values for the separate species. At 100% relative humidity a value of 13,000 ft.<sup>2</sup>/lb. was obtained for  $\text{SiO}_2$  and 21,000 ft.<sup>2</sup>/lb. for  $\text{LiCl}$ . The latter figure is in agreement with the value of 24,000 ft.<sup>2</sup>/lb. obtained for  $\text{LiCl}$  in boron-fueled mixtures.

From these data it appears that at 100% R.H.  $\text{LiCl}$  is superior to  $\text{SiO}_2$  as an obscuring smoke species. Both  $\text{LiCl}$  and  $\text{SiO}_2$  have higher  $\text{O}_s$  values than  $\text{Fe}_2\text{O}_3$ . For Si- $\text{LiClO}_4$  composition, only about 25% of the obscuration can be attributed to  $\text{SiO}_2$  and the balance to  $\text{LiCl}$ , if coarse Si and a metal canister is used. This increases to about 40% for a fiberglass canister, and to about 50% for fine particle Si in a fiberglass case.

### 3. Silicon Carbide Fuel

Silicon carbide was studied as a potential fuel for the generation of  $\text{SiO}_2$  smoke. Various systems were investigated involving nitrate and chlorate oxidizers, but poor results were obtained. Progress was made in systems containing lithium perchlorate as oxidizer. The best SiC-containing formulation developed to date consists of 55% SiC and 45%  $\text{LiClO}_4$ . This system has demonstrated 9% efficiency and 1.4% yield. A typical TOP value at 50% relative humidity was 1470  $\text{ft}^2/\text{lb}$ .

A sample of 1.0  $\mu$  silicon carbide powder was obtained and investigated as a smoke fuel. This fine size material was formulated into the optimized formulation of 55% silicon carbide - 45% lithium perchlorate. A small improvement in combustion over that of the coarser material was evident. The burning rate of the fine material was markedly faster than that of the coarse material.

### D. PYROTECHNIC DISSEMINATION OF OIL SMOKES

Pyrotechnic dissemination techniques for producing an oil fog involve the development of heat from the reaction of a pyrotechnic mix, which causes the vaporization of a relatively low boiling fog oil, followed by condensation to fog particles capable of obscuration. Experiments have involved the use of an intimate mix of oil and pyrotechnic components. The high efficiency pyrotechnic dissemination system utilized in this work is based on a nitrogen-rich fuel, thiourea, formulated with  $\text{KClO}_3$  oxidizer to obtain combustion rates and temperatures conducive to the production of effective obscuring smokes.

Initial studies revealed several difficulties: (i) physical instability of the grain, (ii) flaming during combustion, and (iii) poor performance reproducibility. Formulations containing low viscosity oils tended to undergo segregation and separation of the solids ( $\text{KClO}_3$  and thiourea), leading to improper combustion and low obscuration. To overcome this, gelation of low viscosity oils and the use of high temperature greases were investigated.

Flaming during combustion destroys the smoke agent and gives diminished obscuration. It was found that proper exhaust vent dimensions, correct oxidizer-fuel ratios, and proper oil concentrations control flaming and flashing.

Poor reproducibility in the performance of identical formulations was evident in wide variations of combustion times and obscuration of the fog generated. This difficulty

was attributed to agglomeration of the oxidizer. The addition of 3% by weight of  $\text{MgCO}_3$  as an anti-caking agent to the  $\text{KClO}_3$  alleviated the problem.

### 1. Fog Oil Gelation

To overcome solids separation in formulations with low viscosity oils, a polyethylene (PE) of melt index 28, Dow experimental product QX-3936.1, was employed as a gellant. Several grades and types of oils were studied for gel formulation. Utilizing identical formulation methods of preparation, and a constant oil to PE ratio, the relative obscuration of varying molecular weight oils was studied. The data indicate an inverse relationship between obscuring power and molecular weight of the oil. Increased cloud persistence parallels the improved obscuration. Table V gives the characteristics of one of the better obscuring formulation containing PE-gelled Neutral No. 75.

The polyethylene gelling agent QX-3936.1 appears to possess the required properties of chemical compatibility with the fog-oil, efficiency in gelation, non-toxicity, and non-corrosiveness. Pending extended surveillance testing, the gelled formulation appears physically stable in processing, as well as in ambient and elevated temperature storage.

The gelation procedure involves premixing of the paraffinic oil (Neutral No. 75) with QX-3936.1 in a ratio of 6.63:1, heating to 200-210°C. with vigorous stirring, and cooling to room temperature with continued stirring. The softening point of this self-supporting gel is approximately 85-95°C.

### 2. High Temperature Grease

The use as a fog oil agent of a high viscosity, high temperature grease, Darina A-X, was investigated. One advantage would be the simplification of processing through elimination of the gelation step. The maximum obscuration attained was 3700 ft.<sup>2</sup>/lb. (visual target) for 30-gram munitions of the formulation shown in Table VI. Three-week surveillance data also indicated favorable stability.

### 3. Curable Polymer-Based Systems

The grease and gelled oil systems previously described have the physical consistency of petrolatum. For many smoke applications more rigid or rubbery properties would be desirable. Therefore, work was initiated on compositions containing a curable polymeric fuel based on the epoxy resin glycerin diglycidyl ether (GDGE).

Table V

Characteristics of an Obscuring Formulation  
Containing PE-Gelled Neutral No. 75 Oil

<u>Ingredients, %</u>	<u>Formulation</u> <u>No. 97</u>
Thiourea	10.3
KClO <sub>3</sub>	34.1
NaHCO <sub>3</sub>	10.3
Neutral 75 Oil	43.4
QX-3936.1	6.6
<u>Properties</u>	
Consistency	Petrolatum-like
Weight, g.	30.0
Height, in.	1.25
Diameter, in.	1.25
<u>Ignition</u>	Immediate
<u>Combustion</u>	
Time, sec.	102
Rate, in./sec.	0.012
<u>Flaming</u>	None
<u>Cloud</u>	
Light trans. %	0.80
TOP, ft. <sup>2</sup> /lb. (visual target)	3,900
<u>Abbr. Surveillance</u>	Self-supporting 48 hrs. @ 72°C.

Initial attempts to prepare solid cured grains were hindered by incompatibility of the oil with the cured polymeric binder. Darina A-X grease and PE-gelled No. 75 oil, however, were found to improve markedly the physical compatibility of the fog agent with the polymeric binder. The maximum gelled oil loading is limited to 40-43%. Above this level, incompatibility of the oil with the binder system is evident.

Table VI  
Properties of Obscuring Formulation Containing  
Darina A-X Grease

<u>Ingredients, %</u>	<u>Formulation</u> <u>No. 160</u>
Thiourea	9.3
KClO <sub>3</sub>	30.7
NaHCO <sub>3</sub>	
Darina A-X	60.0
KClO <sub>3</sub> /thiourea	3.30:1
<u>Grain Size, grams</u>	30.0
<u>Exhaust Hole</u>	
Diam., in.	15/64
<u>Combustion,</u>	
Time, sec.	62
Rate, in./sec.	0.020
<u>Flaming</u>	None
<u>Cloud</u>	
Light trans., %	1.0
TOP, ft. <sup>2</sup> /lb. (Visual target)	3,700

Although only a brief study was made of polymer-based white smoke compositions, promising results were obtained. No TOP measurements were performed, but visual observations were favorable.

#### IV. SUMMARY

Figure 7 shows the measured TOP as a function of relative humidity for the smoke agents studied in this program. Of the novel smoke formulations developed, the 60% boron - 40% lithium perchlorate mix has given the highest TOP values over a wide range of humidity conditions. Decaborane-fueled

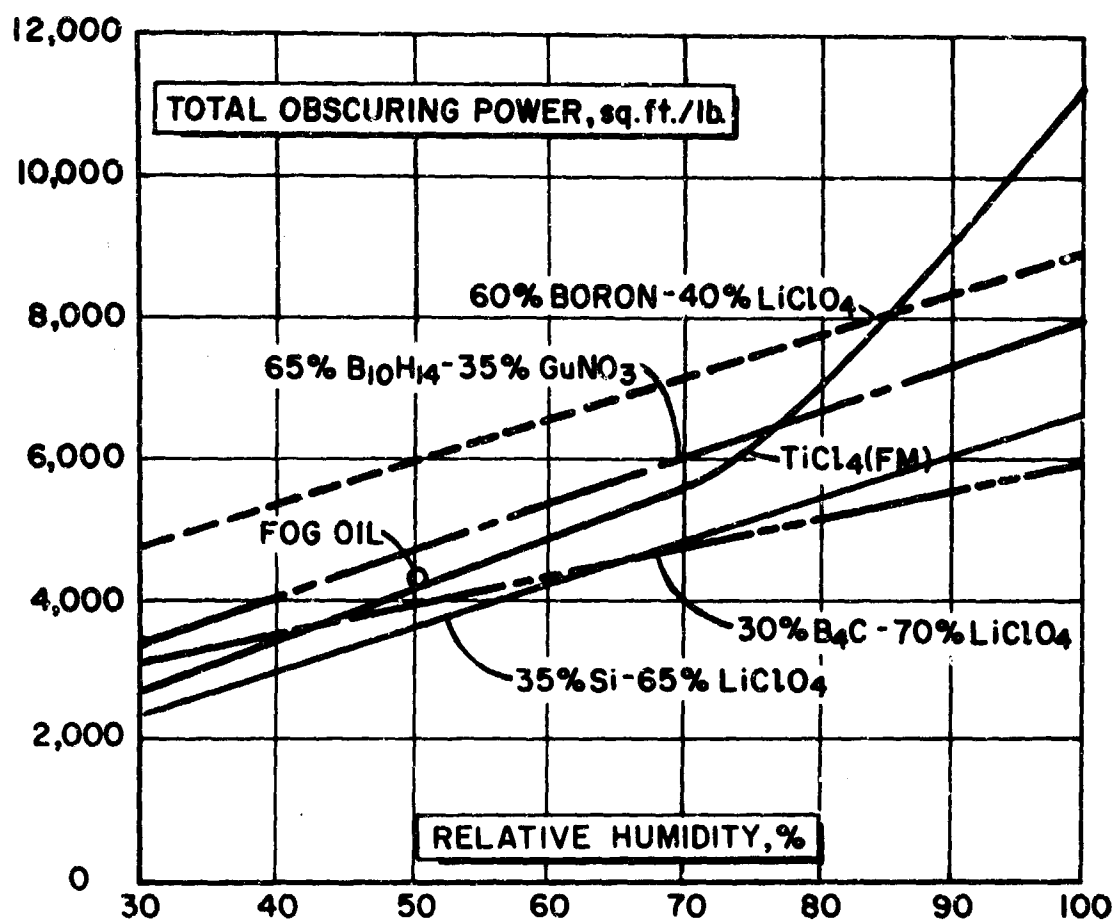


Fig. 7 - Variation of TOP with Relative Humidity for Smoke Formulations Studied

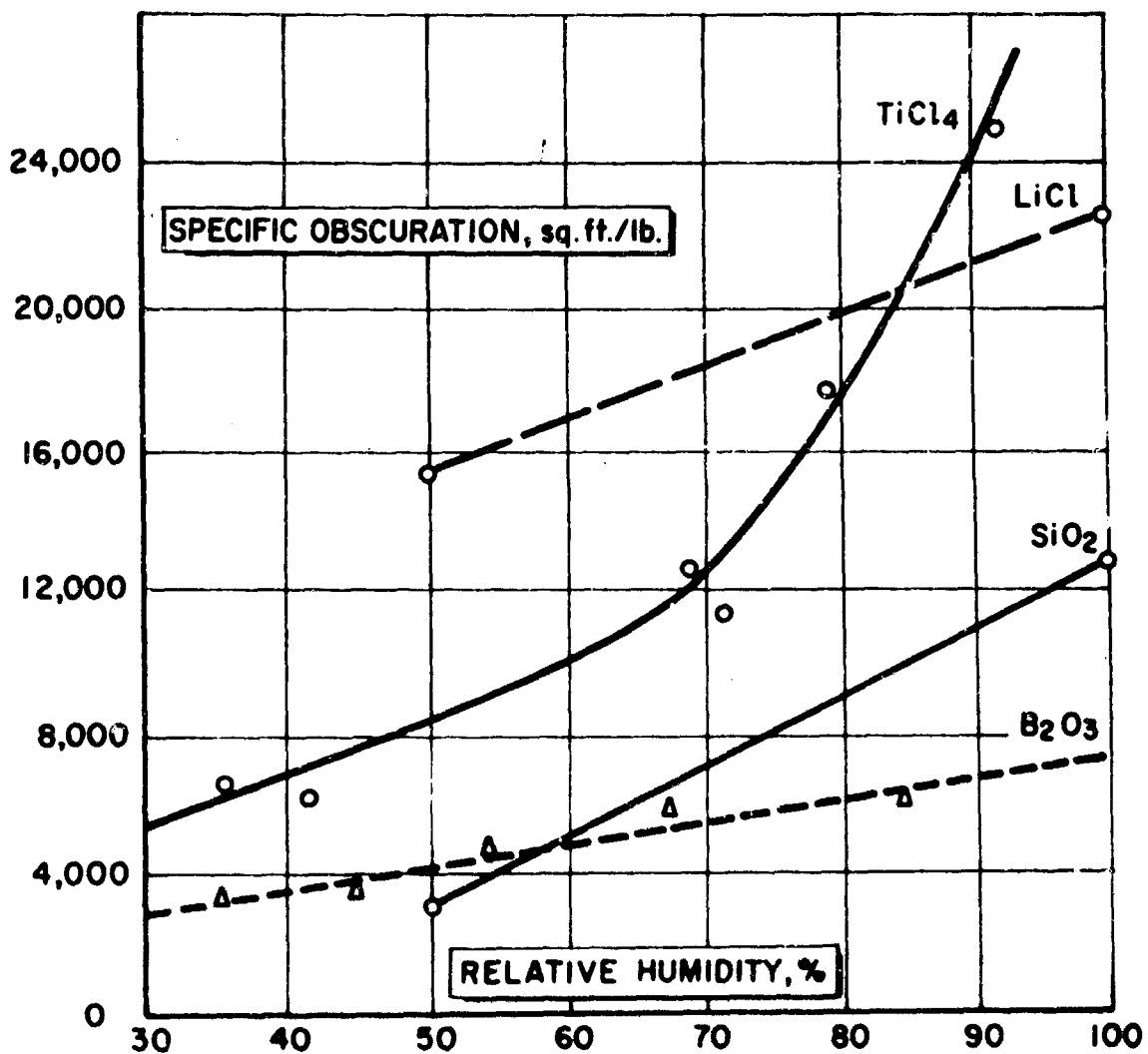


Fig. 8 - Specific Obscuration of Smoke Materials as a Function of Relative Humidity

compositions are next in effectiveness, followed by the silicon-fueled and the boron carbide-based formulations. The data given for silicon formulations were obtained using as received Si powder and fiberglass munition cases. Higher TOP values are obtained when fine ground Si is employed. Pyrotechnic fog oil compositions are intermediate between decaborane and silicon formulations at 50% R.H. However, very little change in TOP is expected with relative humidity for these smoke compositions. The standard FM smoke is approximately equivalent to the boron carbide composition in the 30-60% R.H. range, and superior above 60% R.H.

On the basis of specific obscuration, which ranks smoke agents in the order of extrapolated potential rather than demonstrated effectiveness, there is a different outlook, as shown in Figure 8. Lithium chloride ranks highest in obscuration, followed by FM smoke,  $\text{SiO}_2$ , and then  $\text{B}_2\text{O}_3$  smoke. Using these data, it is possible to predict the TOP of the various experimental formulations, assuming 100% conversion of ingredients to smoke species. At 100% R.H., one would predict:

- 11,200 ft.<sup>2</sup>/lb. for 30%  $\text{B}_4\text{C}$ -70%  $\text{LiClO}_4$ ,
- 13,000 ft.<sup>2</sup>/lb. for 65%  $\text{B}_{10}\text{H}_{14}$  - 35%  $\text{GaNO}_3$ ,
- 15,500 ft.<sup>2</sup>/lb. for 60% B-40%  $\text{LiClO}_4$ ,
- 14,500 ft.<sup>2</sup>/lb. for 55%  $\text{SiC}$ -45%  $\text{LiClO}_4$ , and
- 15,200 ft.<sup>2</sup>/lb. for 35% Si-65%  $\text{LiClO}_4$ .

The safety and surveillance aspects of these compositions must also be considered. The 60% boron - 40% lithium perchlorate system is the only one found to be sensitive to spark. The impact sensitivity is not prohibitive. Its fast burning rate and the tendency of the smoke to pillar would limit its use, and all attempts to overcome this have degraded the smoke. This system has shown stability over a twelve-week surveillance period at both ambient and elevated temperatures.

The 30% boron carbide - 70% lithium perchlorate formulation is not sensitive to spark, and its impact sensitivity is not troublesome. The silicon formulation is not stable in extended surveillance testing, probably because of reaction of the oxidizer with moisture.

The gelled Neutral 75 oil formulated with  $\text{KClO}_3$  - thio-urea pyromix is the most promising fog-oil generator. It is not sensitive to electrostatic spark below 18.75 joules (which is the limit of the instrument capacity). The formulation has an acceptable sensitivity to impact. The system also exhibits advantages over the other compositions studied in its burning time. Munitions could be designed to produce a continuous fog over a long time period. No surveillance work has been done on this system.

#### V. REFERENCES

1. Report Nr. 6, Contract Nr. DA-18-035-AMC-127A, "A new Smoke Screening Chemical for Use in Aerial Smoke Tanks," W. H. McLain and R. W. Evans, December 1965, Denver Research Institute.
2. "Screening Smokes," CDRL Special Publication 1-42, L. Finklestein, June 1964.



HEATS OF REACTION PLOTS AS DESIGN CRITERIA FOR  
PYROTECHNIC REACTIONS

Dr. Joseph H. McLain

## HEATS OF REACTION PLOTS AS DESIGN CRITERIA FOR

### PYROTECHNIC REACTIONS

DR. JOSEPH H. MC LAIN

The self propagating exothermic reaction between solids has not been widely studied and in some respects this is surprising from a theoretical as well as practical point of view. It would seem to offer unique opportunities to study accurately the propagation of combustion because the reactions (at least some of them) are relatively slow and reproducible inasmuch as long range diffusion and convection effects are generally negligible.<sup>(1)</sup> As a practical matter the study is important in the design of delay mixes, flare mixes, propellant and igniter mixes.

Even the recent burgeoning of interest in solid state chemistry continues to omit and neglect this interesting area of solid reactivity.<sup>(2)(3)(4)</sup> Possibly this is because there has been very little in the open literature about these reactions.<sup>(5)</sup> Some noticeable and important exceptions are Spice and Staveley,<sup>(5)</sup> Hill et al.<sup>(6)</sup>

In fact this article owes a great deal to these contributions particularly those of Spice and Staveley, and it is hoped that the ideas put forward by them and extended by this work will increase the interest in the theory of these reactions.

### Experimental

#### PbO<sub>2</sub> - Si System

PbO<sub>2</sub> was "Baker Analyzed" Reagent grade with an assay of 99.2% PbO<sub>2</sub>.

Silicon was Belmont Smelting and Refining Co. of approximately 5μ average particle size.

Mixing was done in distilled water by means of a Waring Blender. The mixture was sucked dry on a Buchner and the oven dried filter cake was screened through a 50 mesh screen six times.

A Parr Bomb calorimeter previously calibrated was used for the heats of reaction by the hot wire method.

In accordance more or less with the treatment by Spice and Staveley it is possible to use experimental heats of reaction to choose between possible reactions.

Their method was to calculate Q (the amount of heat given off by that weight of a mixture that contains one mole of oxidizer. A plot of Q versus the % reductant was then made for a given binary

system. Eleven of their systems were found to be Class I systems,\* i.e. where  $Q$  continues to increase as the reducing agent content is increased up to that composition where the reducing agent uses up all the oxidizing agent. This point should correspond to the stoichiometric composition. Also it is at this point that  $\Delta H$ , the heat evolved per gram of mixture should be a maximum.

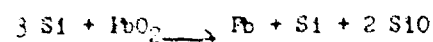
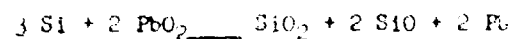
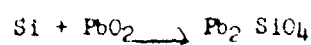
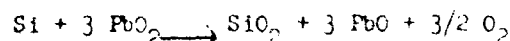
From these plots and calculation of  $Q$  for postulated reactions certain conclusions were obtained as to the chemical nature of the products and what the reaction was on which stoichiometry should be based.

Another method of differentiation between possible reactions is the use of  $\Delta H$  versus % reductant.

An example of this is the  $PbO_2$  - Si System, and can best be explained by Figure 1 in which heats of reaction calculated from heats of formation data for various candidate reactions corresponding to a given percentage of silicon is shown by the solid line. The experimental heats of reaction from calorimetric measurements are shown by the dotted line.

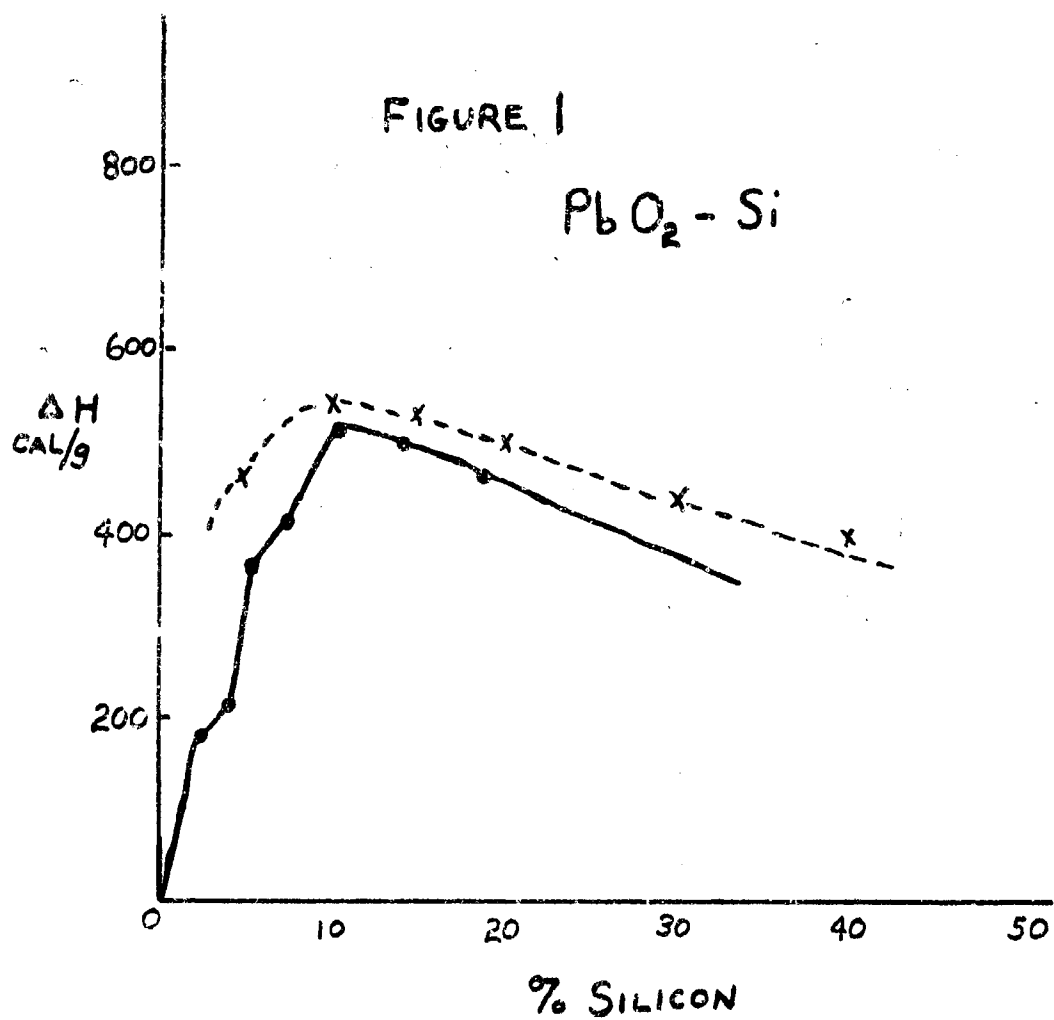
As can be seen the maximum  $\Delta H$  (experimental) which should correspond to the stoichiometric reaction occurs at approximately 10% silicon as does the theoretical  $\Delta H$  calculated for the expected reaction  $PbO_2 + Si \rightarrow Pb + SiO_2$ .

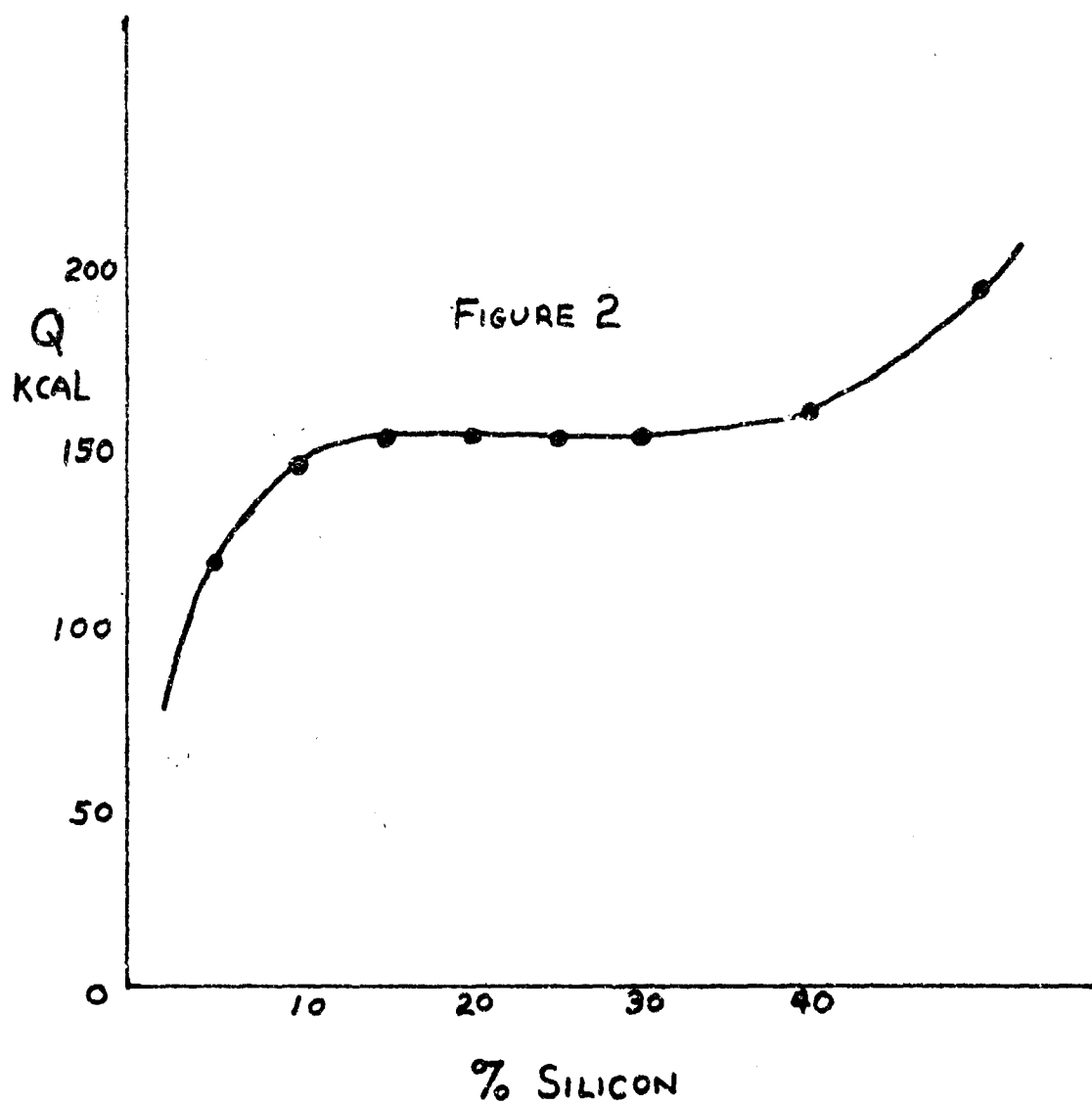
The other equations postulated and used for the calculation of the theoretical  $\Delta H$  curve were:



It is interesting to note that in this particular system  $Q$  plotted versus % silicon does not reach a constant value as shown by Figure 2 and therefore does not conform to the Spice & Staveley criterion for Class I systems or there may be more than one reaction operative over the burning range. But in the 3 to 30% silicon range the  $Q$  plot shows that there is probably only one reaction but at a slightly higher (approximately 15% silicon).

\*Class I systems are those in which  $Q$  rises to a constant value with increasing proportion of reducing agent which indicates quite strongly that there is only one reaction operating in this range of composition.





Further insight as to the nature of the operative reaction may be obtained by rates of burning versus % reductant, inasmuch as if the same reaction is operative within the range of compositions with which we are concerned it is just that percentage composition that gives a maximum  $\Delta H$  that should give a maximum rate of burning. Unfortunately the data on burning rates for the  $PbO_2$  - Si system are in centimeters per second rather than grams per second. This makes quite a difference especially when there is a wide separation in densities of the oxidizing and reducing agents such as is the case in this system.

#### RATE OF BURNING, HEAT OF REACTION AND

##### NATURE OF REACTION

The application of burning rate and heat of reaction data on the determination of stoichiometry can best be described by using the data on the B-BaCrO<sub>4</sub> system taken from Table 5-16, page 5-37 of the source referenced below.<sup>(7)</sup> The applicable data are contained in Table 1.

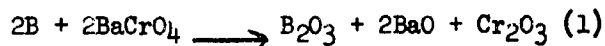
A plot of burning rate,  $Q$  and  $\Delta H$  versus % boron is shown as Figure 3.

#### Discussion of Results

##### Stoichiometry

It has been the usual practice in delay train technology to start development of a given mix by going to the intuitively stoichiometric mix and then varying of the % reductant to reach the envelope desired for the munition. One of the standards mixes involving B and BaCrO<sub>4</sub> is a 5-95 B-BaCrO<sub>4</sub> (see Table 5-14, page 5-35 of reference (7).)

This would be "stoichiometric" for the following reaction which calculates to be



just slightly over 4% boron.

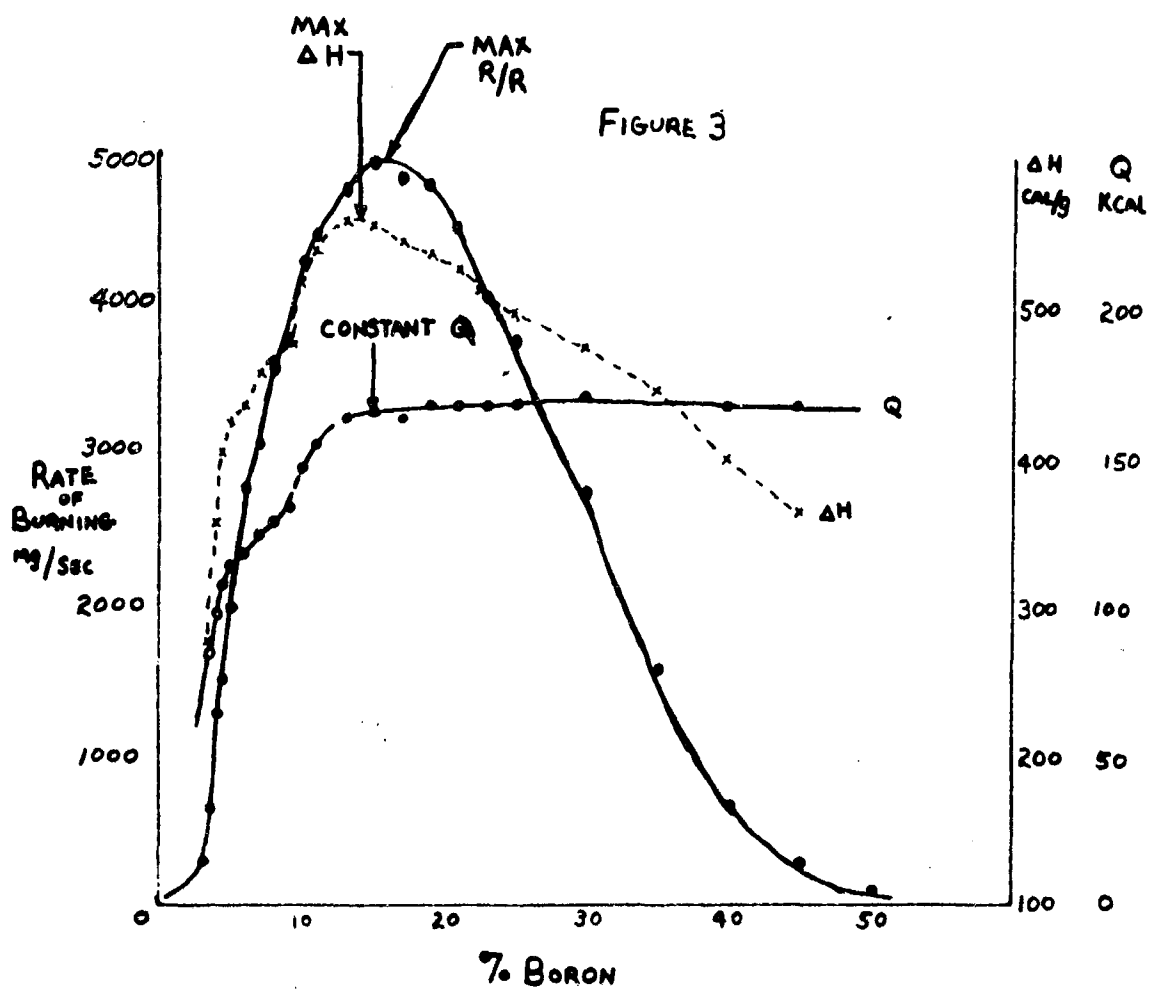
Yet it is obvious that from the  $Q$ ,  $\Delta H$  and burning rates as plotted in Figure 3 that the stoichiometric percentage composition for the system is somewhere about 15%.

TABLE I

<u>% Boron</u>	<u><math>\Delta H</math> cal./g</u>	<u>Q kcal</u>	<u>Burning Time Sec.</u>	<u>Charge Weight Mg</u>	<u>Burning Rate mg/sec.</u>
3.0	Incomplete react		7.56	2130	282
3.5	278	68.7	3.54	2150	608
4.0	354	93.0	1.72	2140	1245
4.5	400	106	1.44	2125	1475
5.0	420	112	1.09	2130	1956
6.0	431*	116	0.767	2110	2750
7.0	453	123	0.653	2000	3060
8.0	462	127	0.560	2000	3570
9.0	474	132	0.539	2000	3720
10.0	515	145	0.465	1975	4250
11.0	536	152	0.432	1925	4450
13.0	556	162	0.397	1900	4820
15.0	551	164	0.382	1875	4910
17.0	543	161	0.375	1800	4800
19.0	535	167	0.366	1750	4790
21.0	526	168	0.375	1685	4500
23.0	503	165	0.407	1650	4050
25.0	497	168	0.433	1625	3750
30.0	473	171	0.574	1611	2820
35.0	446	173	0.965	1500	1555
40.0	399	168	2.19	1430	653
45.0	364	168	5.25+	1360	259
50.0	Incomplete react		14.5 +	1290	89

\*Reported as 231 but data obtained in this laboratory makes it apparent that this is a typographical error.

+Two rounds not ignited.



The calculated percentage for the following equation



is slightly more than 14.5%.

Although equation (2) is somewhat surprising to most chemists perhaps this is because we have conditioned to a world in which the 25°C conditions for stability play too large a role. If we are interested in what goes on in the combustion zone, that is the operating reaction we should be conditioned to stabilities at flame temperatures of the order of 3000°C.<sup>(10)</sup> As a matter of fact, BO has been found in the combustion zone of burning propellants to which boron has been added.

#### Burning Rates

As can be seen from figures (2) and (j) the maximum rate of burning as well as the maximum experimental  $\Delta H$  is somewhat to the right (higher reductant content) than theoretical. Of some twenty other delay systems for which I have made similar plots, this has been found to be true to a greater or lesser degree. This displacement is generally greater if the reducing agent is a metal such as iron, antimony or manganese, which points toward the effect of heat transfer in columnar burning inasmuch as the metals are much better heat conductors than the non-metallic oxidizers provided the mechanism of propagation is basically one of heat transfer as proposed by Spice and Staveley and Hill.

This postulate is supported by other experimental evidence.

(1) Smaller the heats of reaction in cal/g the more to the right of theoretical.

(2) The slope of the R/B curve prior to theoretical maximum is always much steeper than it is after the maximum which can be explained by regarding the first portion of the curve as one in which the excess oxidizer is acting as a better heat insulator than the excess reductant in the after portion of the curve.

#### Practical Application to Delay Systems

Once a system has been studied in detail such as the B - BaCrO<sub>4</sub> system used above it is fairly obvious that its optimum performance requires the stoichiometric composition in that it will be more easily ignitable and will propagate more readily with less chance for duds.

However, sometimes design requirements require that the burning rate be slower than the 2.07 inches per second that corresponds to the maximum rate of burning. It may be required that only one inch of delay train can be used and that the delay time be one second. It has been traditional for design engineers to go to the R/B curve and choose the lower percentage reductant mix which will give in theory the desired rate: for the system under discussion 6% boron. Although there is an alternative available on the far side of the maximum 30% boron, which should be equally applicable. I have never seen the latter

alternative used. In most other systems than B -  $\text{BaCrO}_4$ , the higher reductant alternative should be more desirable in that mixing problems and departures from homogeneity should give less effect on delay times because the slope is not so steep.

The B-  $\text{BaCrO}_4$  system was selected, however, to point out that neither of the alternatives posed is in reality the proper selection. Any "gasless" delay system should be used at its optimum or stoichiometric because it is there and only there that there is a plateau and departures from homogeneity or slight differences in new lots of chemicals make but a very slight change in the burning rate.

But the question is -- how does one get the desired delay time? The answer is of course, nothing new to the art -- add an inert (to the chemical reaction) ingredient which will serve as a heat sink such as kaolin, infusorial earth, super floss, et al. As said before, this is not new and has been done many times before. The converse of this, i.e. adding one or two percent of powdered copper or silver to get increased rate of burning has never been tried to my knowledge in the "gasless" mix area. Metallic strand inserts in propellant grains have been used but the mechanisms are quite different.

The consequences of this "rule" of application would be that stoichiometric mixes of any given system would always be used within a certain envelope of delay times that would be determined by experiment and in most cases should not exceed 5% of inert additive. If the design criteria are such as to demand more delay per inch than can be allowed with this system then another and naturally slower burning system should be used at its predetermined (by experiment) stoichiometric composition.

#### Mechanism

I have mentioned previously that delay mixes that have good conductors as reducing agents have their maximum burning rates well to the right of the stoichiometric point. Such is the case with D16 delay mix. ( $\text{Mn}$ ,  $\text{PbCrO}_4$ ,  $\text{BaCrO}_4$ ),<sup>(8)</sup> and with the high percentage iron mixes used by Hill and Cottrell.<sup>(1)</sup>

Attempts to treat the illuminating flare mix ( $\text{Mg}$ ,  $\text{NaNO}_3$ , Laminoc) which also has a high metallic content from data obtained at N.A.D. Crane<sup>(9)</sup> gave an exact agreement between maximum rate of burning and the  $Q$  inflection point at 50% magnesium. I was forced to conclude that the heat conductance mechanism did not hold in this system but that the energy for propagation of burning must be delivered to the next zone by some other mechanism such as radiative transfer. Some previous studies on this mix had led to the same conclusions.

It does show the mix to be a Class I and that the stoichiometric point is 58% magnesium. Thus the magnesium percentage should not be varied to get various burning times as is the general practice in flare mixes as well as delay mixes, but a composition should be determined and used with necessary inert additives.

FOOTNOTES

1. Hill, R. A. W. and Cottrell, T. L. "Studies of the Combustion Waves in Solids", Fourth Symposium (International) on Combustion, The Williams and Wilkins Co., Baltimore, Md., 1963.
2. Garner, W. E. "Chemistry of the Solid State", Butterworths, 1955.
3. Hannoy, N. B. "Solid State Chemistry", Prentice-Hall, 1967.
4. Galway, A. "Chemistry of Solids", Science Paperbacks, Chapman-Hall, 1967.
5. Spice, J. E. and Staveley, L. A. K., J. Soc. Chem. Ind. 68 348-55 (1949).
6. Hill, R. A. W., Proc. Roy. Soc. A 226 455-71 (1954).
7. Engineering Design Handbook, Military Pyrotechnic Series, Part One, Theory and Application. AMCP 706-185, Headquarters, U. S. Army Material Command, April, 1967.  
  
These data were originally part of the Picatinny Arsenal Technical Report 2477 by B. Werbel and S. Lopatin. Picatinny Arsenal, Dover, N. J. 1958.
8. Comyn, R. H. DOFL Report 22-576, Harry Diamond Laboratories, Washington, D.C., 1957.
9. Johnson, D. M. Pvt. communication.
10. Coppeno, P., Smoes, S. and Drowart, J.; T. F. S. 64 630 (1968).



**SLURRIES ARE SAFER**

by

**R.D. SHEELINE and J. J. VROLYK**

**Presented at the Pyrotechnics Seminar**

**August 12 - 16, 1968**

**at the**

**University of Denver**

**\* Rocketdyne, A Division of North American Rockwell, Inc.,  
Canoga Park, Calif.**

## SLURRIES ARE SAFER

Rocketdyne's Safe, Low Viscosity, Low Shear Stress  
Quickmix\* Process may Replace Conventional Mixing.

Early in 1956, a group of Research personnel at Rocketdyne, a Division of North American Aviation, Inc., conducted a brainstorming session to eliminate the hazard inherent in processing solid propellants. As a basic premise it was stated that a simple propellant could be made by combining a granule of oxidizer and a droplet of fuel-binder. "How," they were asked, "can this be safely accomplished on a production scale?"

From this session came the concept that grew into Quickmix: First, separate the solid particles from each other so that there is considerable space between them. Do the same with binder droplets. Then bring these suspensions together continuously to produce an intimate mixture.

Nine years and several million dollars later Quickmix has evolved into a continuous process that is both simple and sophisticated, applicable for production of pyrotechnics, high explosives and commercial compositions as well as propellants. It is the only known method which keeps explosive ingredients in non-propagating form during manufacture.

Several types of vehicles were considered for suspending the ingredients. Gases were rejected for several reasons, relatively high hazard and difficulty of accurately controlling and metering of flow being the prime considerations. Liquid carriers have a significant safety advantage in that dilute suspensions of hazardous ingredients will not propagate a detonation. With a liquid carrier the effective viscosity of mixing is reduced several magnitudes along with similar reductions

---

\*North American Aviation, Inc. Trademark.

in mixing time, friction and shear stresses on the materials being mixed. Because they are incompressible, liquid carriers provide a means of simple and accurate flow control.

Since its conception, the process has been steadily improved, each improvement resulting in further simplification of its operation. Today, the moving machinery in the process consists only of centrifugal pumps and continuous feeders.

The basic Quickmix process is covered by U.S. patent number 3,022,149 dated February 20, 1962. It was initially conceived and developed under a Rocketdyne-funded program. Additional company funds were continually expended on this program and there have been contracts from all three Department of Defense Services. Currently, the Naval Propellant Plant, Indian Head, Maryland, is completing the architect and engineering design phase for a high energy propellant production plant.

Rocketdyne maintains a flexible Quickmix Research Plant for process development and for preparation of various materials in experimental quantities. The Research Plant can produce mixes in quantities ranging from a few pounds to several hundred pounds at rates ranging from a few hundred to several thousand pounds per hour.

One of the features of the Quickmix process is its ability to reach steady state conditions in two or three minutes and to be easily shut down and cleaned out. This feature makes it feasible to use the same equipment in the research plant as is used in a production plant. The research plant is run only long enough to obtain the experimental quantities desired. Similarly, short runs in a production plant can be used for development-scale quantities, eliminating most scale-up problems. Figure 1 is a sketch of the Rocketdyne Quickmix Research Plant. It should help visualize the process described below.

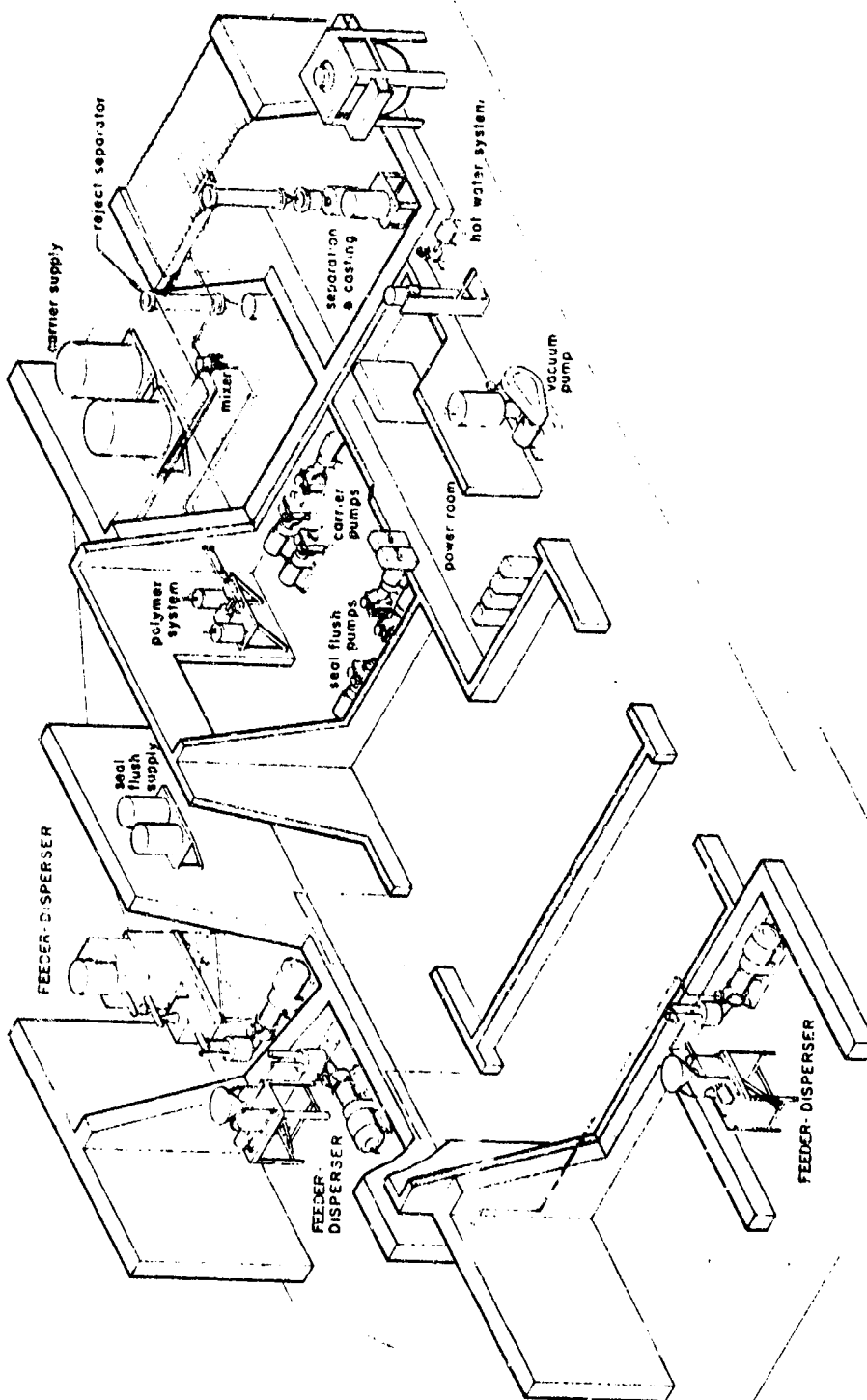


Figure 1. Rocketdyne Quickmix Research Plant

### The Continuous Process

The basic Quickmix continuous process is quite flexible, as shown by its ability to manufacture pyrotechnics, smoke compositions, and high explosives as well as propellants. The flow diagram shown in Figure 2 is a typical example of how the continuous Quickmix process operates. Since most ordnance compositions contain an oxidizer, two separate solids dispersion systems are shown. This allows the oxidizer and fuel components to be kept separate while they are in the dry powder stage.

In the first dispersion system there may be one or more feeders continuously metering fuel-type solid ingredients into the disperser hopper. In disperser system number 2, several granulations of oxidizer can each separately be fed. The recycling liquid carrier is also added continuously to the disperser hopper and the slurry formed enters a centrifugal pump whose output is split so that most is recirculated back to the tank to provide a very high degree of agitation. The remainder of the pump output goes downstream to a jet mixer where it is joined by the output of the second disperser.

The binder ingredients are fed through positive displacement metering pumps. The jet mixer has no moving parts and a sectional view is shown in Figure 3. The slurries from each disperser enter the mixer as indicated and swirl around at high velocities at the center section. The liquid ingredients are jetted into this highly turbulent area through small holes. There are no moving parts in this mixer and it is small enough to be easily held in one hand.

The product slurry then travels to the separator, a small tank where the transition from turbulent to laminar flow permits the product to drop out. The product is withdrawn from the bottom of the separator tank and dried if necessary. Normally, there is approximately one percent carrier (before drying) remaining in the product at this point and a typical operation for castable compositions is to vacuum cast the

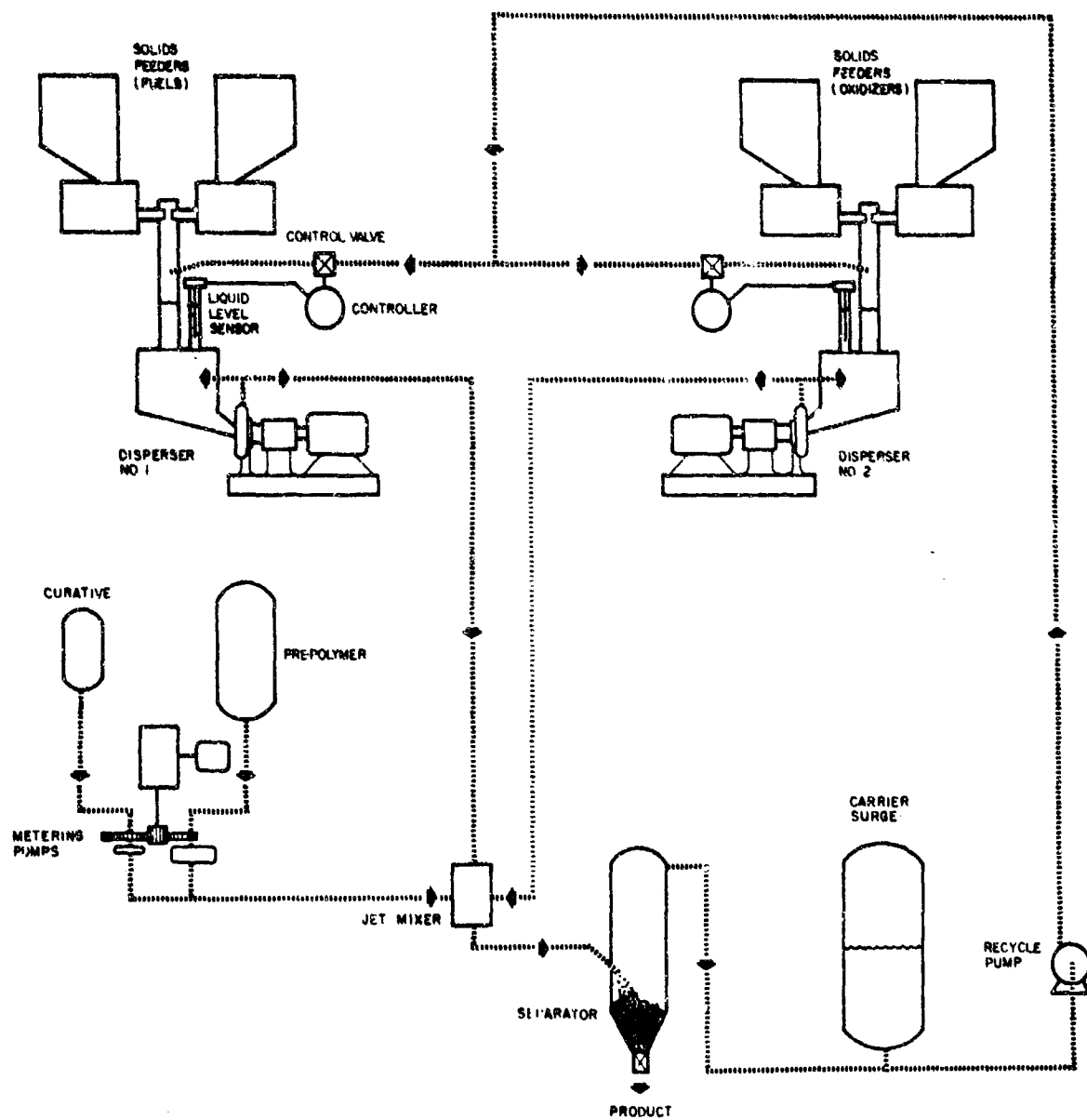


Figure 2. Basic Quick-mix Continuous Process

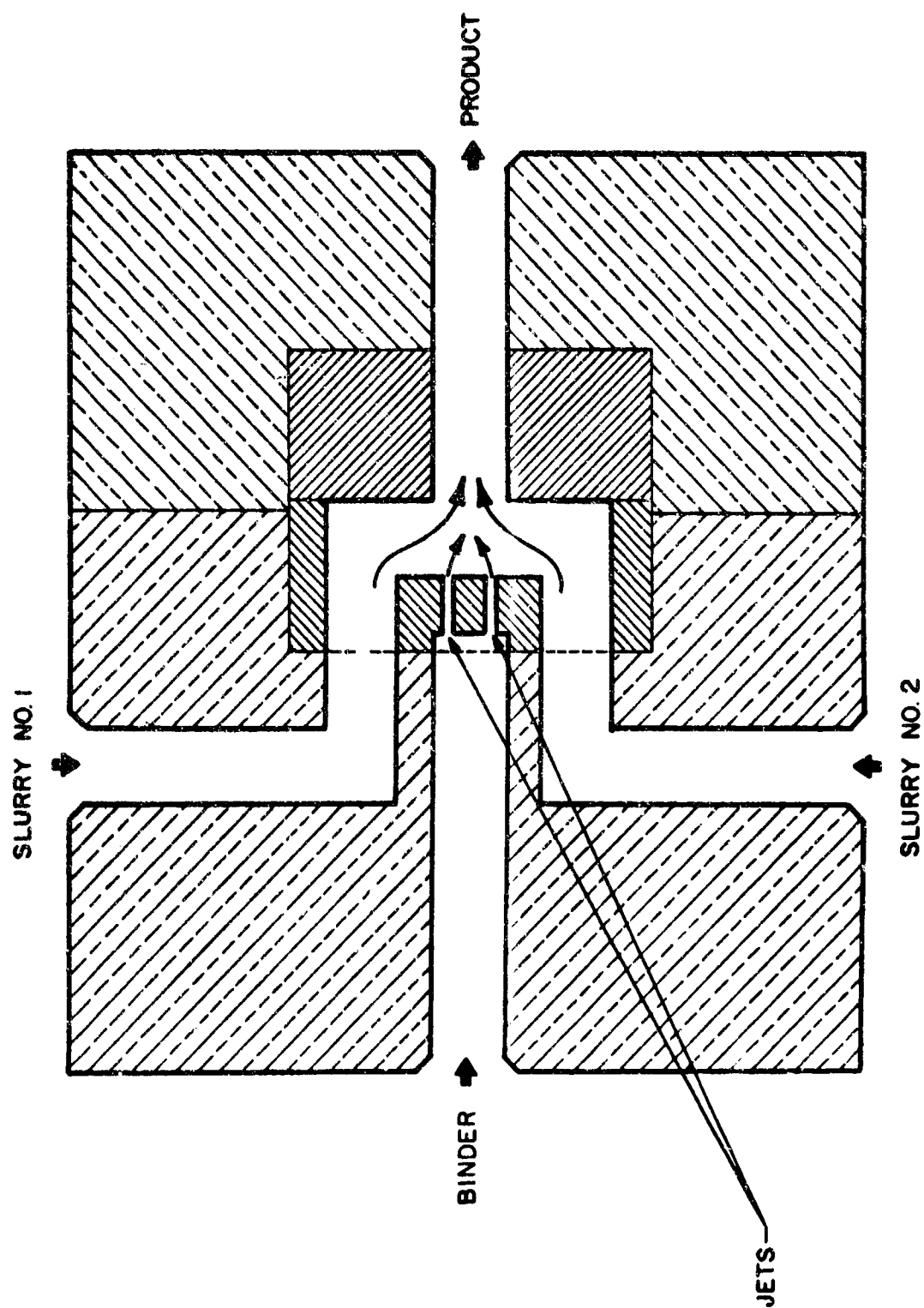


Figure 3. Jet Mixer

mix directly into its final container. The vacuum casting operation is essentially the same as that used in the final steps of conventional solid propellant processing. Total volatiles (carrier plus other volatile materials) after vacuum casting usually range between 0.05 percent and 0.3 percent.

Clear carrier overflows from the top of the separator and is recycled back to the dispersion systems. This closes the carrier loop and it can be seen that the carrier acts much like a liquid belt, picking up solids in the dispersers, liquid ingredients in the mixer, dropping them off in the separator and then returning for the next load.

#### Dispersion System

The initial dispersion concept involved the use of flow control valves, slurry flow meters, and closed loop controls. Through an analog computer study it was found that the basic process is remarkably stable under flowing conditions. In fact, the stability of the system is far greater than can be obtained under any type of closed loop metering and valving arrangements. As a result of this study the control of flows has been greatly simplified.

The solids dispersion system in Figure 4 shows the only flow control now used. This is the control valve on the recycle carrier entering the disperser. This valve is operated through a liquid level sensor and keeps the volume of slurry in the disperser constant.

The disperser hopper is designed to attenuate feeder errors. Most feeders show cyclic variations occurring several times a minute and the hopper is sized to reduce these variations to a point where they are not measurable in the final product. The dispersers will not attenuate low frequency feeder performance cycles, and, under certain conditions, it may be desirable to monitor feeders by conventional instrumentation to discern indications of long-term drift and correct the feeder output.

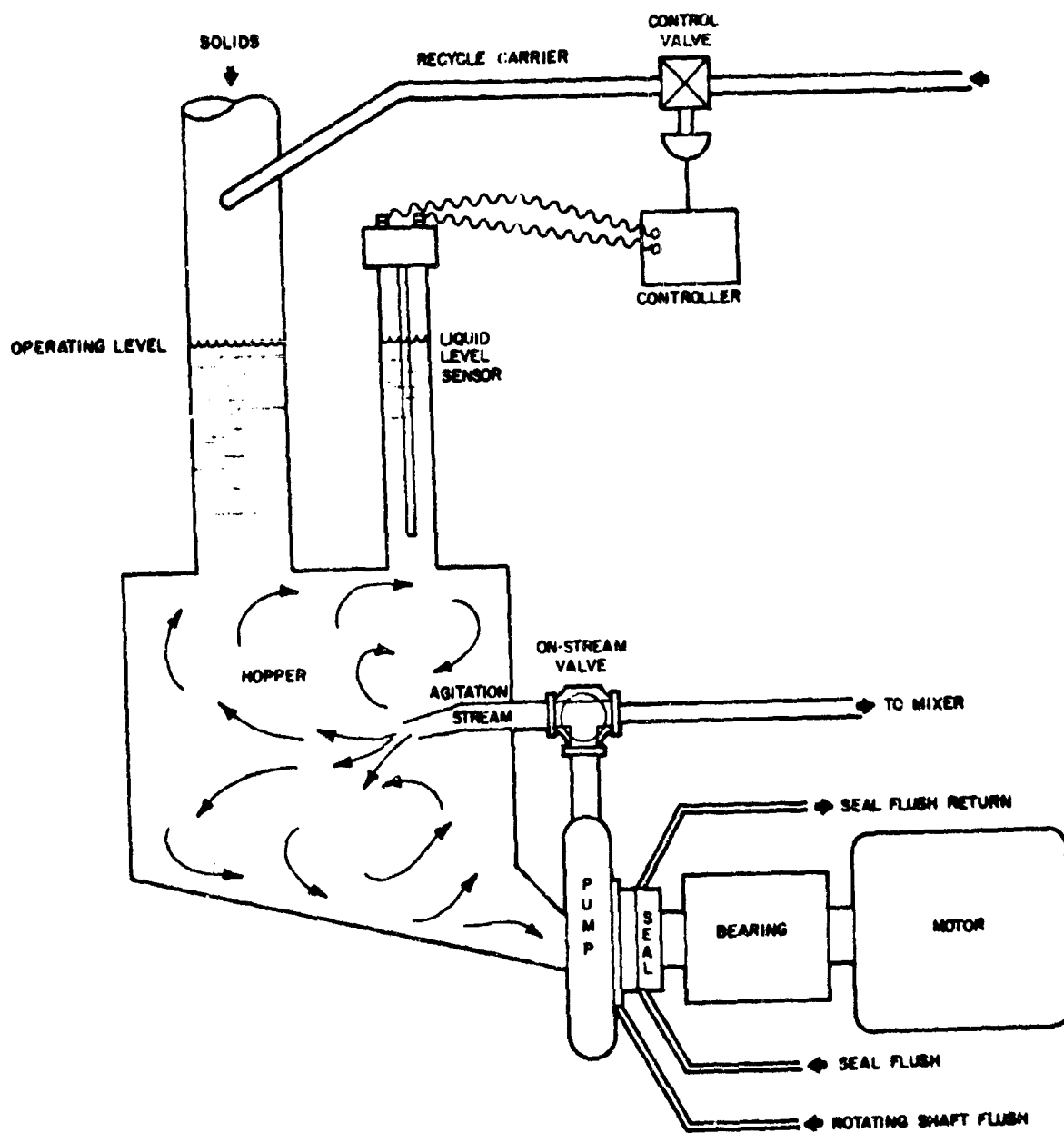


Figure 4. Solids Dispersion System

From the safety standpoint, the disperser pumps are modified to provide a continuous flush of clear carrier entering just in front of the seal and flowing along the rotating shaft toward the impeller to insure that no hazardous solids particles can enter this area. As a further safety feature, a double mechanical seal may be used. This seal is operated under relatively high pressure using clean carrier as the seal flush. If any leakage occurs in the seal, clear carrier will flow into the pump rather than hazardous slurries flowing toward the seal. Where very hazardous ingredients are involved a control system can be designed which will immediately start a shut-down sequence should the rotating shaft flush or seal flush fail.

#### Composition Errors Less Than $\pm 0.1$ Percent

The analog computer analysis of the process, mentioned above, showed the process dynamic stability to be extraordinarily high, and the degree of accuracy and precision of the product was recognized as primarily a function of feeder performance. When a requirement arose for composition control within  $\pm 0.1$  percent, Rocketdyne designed a feeder which met these requirements, since no commercial feeder provides this degree of uniformity. The details of this feeder are described in the adjoining

The feeder operates on a time-allocation principle of weighing small increments of ingredients and varying the time for adding each increment to the process so that the time is exactly proportional to the increment weight. With this feeder it is possible to operate and control the Quickmix process so that the product's uniformity will be within a range of  $\pm 0.1$  percent. However, the feeder is capable of being used with other continuous processes and should find a number of industrial applications.

A feasibility study has been made which showed that the principle of the Rocketdyne dry solid feeder could also be used to safely weight hazardous liquid or solid ingredients while they are wet. For example, an explosive

such as IMX could be delivered wet with the carrier, handled and weighed in carrier instead of in air, greatly reducing the probability of an accidental explosion.

#### Quick Start and Stop

The process is started by first filling the system with carrier, then dropping the carrier level slightly in the disperser hoppers by closing the carrier control valves. The onstream valves are turned so that the pump outputs completely recirculate to the hoppers. Since the hopper volumes are known and the operating concentrations of the slurries are known, solids are fed into the hopper through the feeders for a readily calculated preset time (usually about one minute), then the carrier control valves are opened to bring the slurries up to the operating levels. Almost immediately the on-stream valves are opened and the liquid binder components feed systems are started. Steady state operating conditions are achieved shortly after the clear carrier in the lines from the on-stream valves to the separator has been replaced with slurry.

Shut down and cleanout can be accomplished simply by shutting off the feeders and shifting the mixer output from the on-stream separator to the reject separator. Cleanout can be speeded up by closing the carrier control valves until the disperser hoppers are nearly empty, then filling and emptying each hopper several times. About five such cycles results in a quite clean plant. Product has to be cleaned only from the bottom of the separators and from any drying equipment, such as that used for vacuum casting. A flush with warm water and a detergent frequently is a quick and safe way to perform this cleaning operation.

### Carrier-Product Separation

In an operating plant, two separators normally are used. The first is for the reject material from the initial minutes of operation. Later it is used during cleanout. Flow is redirected from this reject separator to the on-stream separator approximately two minutes after startup.

Recycle of the carrier occurs automatically without any controls. The surge tank shown in Figure 2 is sized to hold approximately twice the amount of carrier necessary to fill the empty system. Once the system is filled and the carrier is recycling, the overflow from the separator is essentially equal to the carrier flowing into the dispersers. When product is being made, the surge tank makes up for the carrier lost with the product. In a 500 pound per hour plant, at a loss rate of 1 percent, this amounts to only 5 pounds per hour.

### Production Rate

Production rate range in any given Quickmix plant is limited primarily by the range of feeder outputs. Line sizes are relatively small for a production plant. For example, for a nominal 500 pound per hour plant, one-quarter inch to one-half inch OD tubing is used. For a 5,000 pound per hour plant, tubing sizes will range from three-quarters of an inch to one and one-half inches. For a 50,000 pound per hour plant, two or three inch diameter tubing would be used. The same size pumps probably could be used for a 500 pound per hour or 5,000 pound per hour plant, although a larger size would be necessary for a 50,000 pound per hour plant.

## Safety

Not only are small amounts of material in process at any time, but the dilute slurries used have been shown to be relatively safe to handle. To test for propagation of detonation by slurries of explosives in carriers, a rotating tube test, Figure 5, was used. Here a two inch diameter tube, eighteen inches in length, was rotated to maintain the solids under test in suspension. A "Composition C" high explosive charge, shaped as a cone, was detonated while the ingredients were suspended. A witness plate attached to the far end of the tube was used to determine whether the detonation propagated through the slurry. Typical results, Table I, showed that under conditions of the test 20 percent and even 30 percent slurries would not propagate a detonation. Similar results were obtained with 20 percent slurries of mixed ingredients in the proportion used in several propellant compositions. One exception to the data shown was a lot of ball powder which appeared to be very sensitive. Even this would not propagate a detonation under proper conditions of dilution and tube size. The PNC, IMX and ball powder also did not propagate a detonation as slurries in rotating containers simulating the size and shape of the disperser hoppers.

Additional tests were made to simulate what might occur should power fail. A tank similar in size to a disperser tank was filled with slurry and allowed to settle. The same types of ingredients used in the rotating tube tests were used. When an igniter placed in the bottom of the tank, under the settled ingredients, was set off, there was no indication of any transition from burning to detonation, even when the ingredients were high explosives such as IMX. As expected, however, it was found that settled slurries of explosive ingredients could be detonated if initiated by a detonating charge such as that used on the two inch diameter tubes. Overall, this is a significant improvement in safety when compared to the hazards involved in conventional mixing.

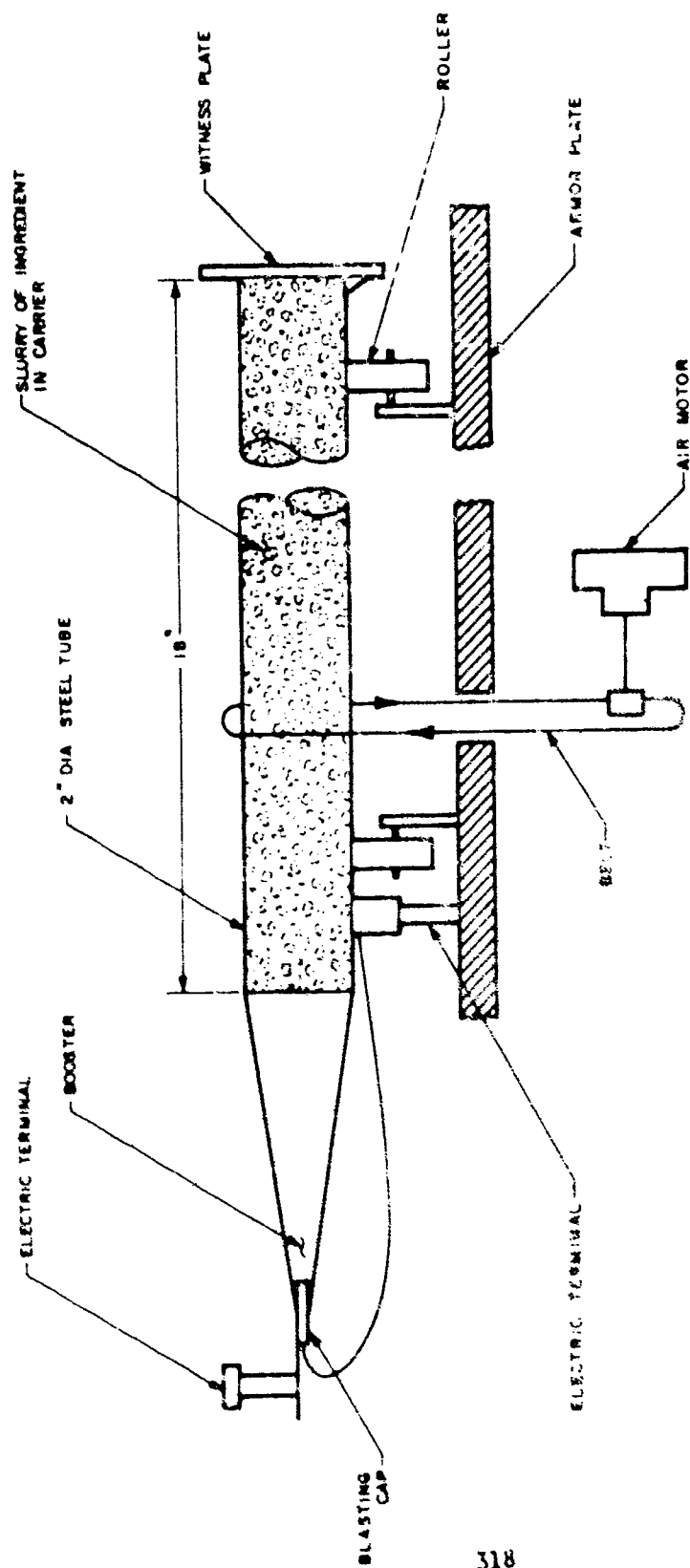


Figure 5. Propagation of Detonation Test

# SLURRY DETONATION PROPAGATION

## 2 Inch Diameter Rotating Stainless Steel Tubing

Ingredient	Wt-%	Number of Tests	Results
PNC	20	6	Non-Propagating
BMX, 25 Micron	20	6	Non-Propagating
BMX, 25 Micron	30	1	Non-Propagating
BMX, 10 Micron	30	1	Non-Propagating
BMX, 60 Micron	30	1	Non-Propagating
BMX, 200 Micron	30	1	Non-Propagating
Fluid Ball Coating Powder "A"	20	6	Non-Propagating
$\text{NH}_4\text{ClO}_4$	20	5	Non-Propagating

TABLE 1

A point frequently raised regarding the safety of the Quickmix process relates to the possibility of ignition of the carrier itself. Heptane is a typical carrier. What is not usually realized is that its flash point is approximately 75 F higher than the usual run of gasoline. The probability of accidental vapor ignition using heptane in the Quickmix process is less than the probability of an accidental fire while your car tank is being filled at the corner gasoline station. However, sensible precautions are taken in the design and operation of a Quickmix plant. Carrier vapor is relatively dense and if any leaks it will flow toward the floor. Good ventilation of the floor area is used and inexpensive vapor detectors can be obtained to detect traces of vapor. The plant itself is designed to be as leak tight as possible and the few carrier surfaces involved are blanketed with inert gas. All equipment is connected to a common ground. Specially designed safety couplings are used for tubing which permit inspection for leaks at a glance. Inspection can readily be made while carriers are being circulated through the plant and before any hazardous materials are fed into the system.

The plant is so designed that it can be completely automated. For processing of highly hazardous ingredients, a control system can be designed which will sense the important operating parameters of the process, automatically stop the plant if any potentially hazardous condition develops, or shift the product to the reject separator if out-of-specification conditions occur. Should there be a power failure, the plant could be automatically emptied of its contents by a flush of water from a pressurized tank.

#### Economics

As the Quickmix process developed, it became apparent that it had many economical attributes. Its features economically affected a large segment of the manufacturing procedure. For example, incoming lots of ingredients could be larger and could be shipped and received in large

bulk containers, perhaps up to 5000 pounds, which would serve as auxiliary feeder hoppers. This avoids much of the incoming costs relating to testing, handling and weighing. Pre-blending, with its separate weighings and extra handling, can be eliminated. Within-plant transport of weighted, blended, or mixed ingredients and return of their containers is eliminated. Mixer operation is eliminated, reject rates should be reduced and the number of quality control tests would be expected to be reduced significantly.

Control of the Quickmix process comes before the fact rather than after, as is usually the case. With Quickmix a continuous record of ingredient input and recycle carrier flowrates gives complete information as to what the product composition will be a minute or two later. Any "out of specification" product can be discerned beforehand and either sent to the reject separator until the error is corrected, or the plant can be stopped at the discretion of the operator.

Aside from the materials and product handling crew, a Quickmix plant can be designed for operation by one man (although a stand-by assistant is considered to be good policy) whether its output rate is 100 pounds an hour or 100,000 pounds an hour. Small additional costs are incurred with Quickmix in that a small amount of carrier is usually lost during operation and a small amount of an inert gas is required to blanket carrier surfaces.

In the manufacture of many ordnance items, the charge is finally shaped by a pressing operation. Some work has been completed which indicates that non-flowing mixes can be cast into place by leaving some carrier in the product until casting is accomplished. Relatively high density castings can be achieved by applying vibration before removing the carrier. Elimination of the pressing operation would effect a considerable cost saving.

A number of economic studies have been made showing that overall savings related to Quickmix will range from approximately 15 cents a pound to about \$1.00 per pound depending on the application.

The equipment cost for a manually operated plant suitable for producing pyrotechnics or conventional composite propellants with a product uniformity of  $\pm 0.5$  percent would probably run between \$100,000 and \$200,000. Where a higher degree of composition control, or where hazardous ingredients are being handled, costs would increase in proportion to the increased uniformity required and the degree of automation and remoteness needed for safety.

#### Carrier-Ingredient Relationships

Ideally the carrier and all ingredients in the mixture should be mutually insoluble. However, this generally is not the case and when the Quickmix process was first conceived this was considered to be a potential major problem. Through experience with a wide number of different types of ingredients, it has been found that solubility problems usually can be overcome. The solubility of concern is the solubility under the steady-state conditions of the process. For example, a cross-linking agent which was quite soluble in the carrier was found to dissolve only to the extent of 0.2 percent during the operation of the process. If more than 0.2 percent were initially dissolved in the carrier, the value would eventually work down to 0.2 percent under the conditions of operation, more agent appearing in the product than was being fed. Another example is the use of a polyester-styrene binder. While styrene is extremely soluble in heptane, under the steady-state conditions of the process approximately 5 percent styrene added to the heptane minimized further extraction of styrene from the polyester-styrene mixture. In general, by proper adjustment of the quantity of soluble ingredient dissolved in the carrier, most solubility problems can be overcome.

Removal of the final traces of carrier from the product is a function of carrier solubility in the product. The worst condition encountered in our processing experience has been with a binder material that dissolved 40 percent carrier. In this case the product had to be vacuum cast twice to reduce the total volatiles below 0.3 percent.

#### Summary

There appears to be no known mixing method as safe as Quickmix for the processing of hazardous mixtures. It has realistic economics and can provide a high degree of uniformity and product control, even to the point where composition is controlled with more accuracy and precision than would be expected from usual chemical analyses. The simplicity of the process permits direct and relatively inexpensive control by open-loop monitoring.

Its high production rate capabilities with small equipment and its ability to quickly start and stop make it feasible to build a mobile plant. With such a plant it would be economical to load large solid rocket boosters at the launch site at rates of the order of 100,000 pounds an hour, moving the plant away from the site as soon as the booster was loaded.

High viscosity, high shear mixing methods may eventually yield to this safe, economical and simple system.

**APPENDIX**

**A NEW COMPUTERIZED CONTINUOUS FEEDER**

## A NEW COMPUTERIZED CONTINUOUS FEEDER\*

### ABSTRACT

This paper describes a new materials feeder that operates on a "time-allocation" basis. To provide the desired weight flowrate, an increment of material is weighed electronically, then a computer determines the waiting period before the material is delivered. The ratio of weight to time is maintained constant, and is the feedrate set into the computer. New electronic techniques provide greater precision and accuracy than previously obtainable; accuracy is better than  $\pm 0.1$  percent.

The advantages gained in the areas of economy, safety, accuracy, and flexibility are pointed out. Speculations are made regarding its use in areas where weigh-feeding has heretofore been considered impossible. Accuracies realized in actual use as part of the Quickmix process are given, along with a brief discussion of the electronic computer and weigh transducer.

### TIME-ALLOCATION PRINCIPLE

The following is a description of the time-allocation principle for establishing a net average mass flowrate of a material.

An arbitrary starting point in time is established. An approximate quantity of a material is placed in a small container and weighed electronically. An electronic computer then determines the length of a waiting period as measured from the arbitrary starting point in time before the material is delivered as output, or "dumped" from the container

---

\*Patent # 3,261,415.

(Fig. 1 and 2). Accordingly, time allotted for each delivery of material is made directly proportional to the weight of material delivered during that time. The ratio of the weight of material to the time allotted is thus held constant and is the feedrate. A typical waiting period is approximately 10 to 12 seconds for each quantity of nominal size to be delivered; thus, 2 pounds of material delivered each 12 seconds corresponds to a feedrate of 600 pounds per hour. For the smallest individual quantities of material, the time increment might be as short as 6 seconds, and as long as 18 seconds corresponding to the largest quantity of material. The feedrate can be easily changed of course by changing the programming of the computer. A feeder based on this principle is shown in Fig. 3 and 4. This machine will be described in detail later.

The above principle is in contrast to previous material feeder schemes which utilize an expressed or implied constant time interval during which a precise quantity of material must be delivered. Since the time interval is constant, the quantity handled each time must be precisely the same. This is not the case for the time-allocation type feeder. At first, this simple difference may seem rather trivial, but upon close examination, a number of advantages become obvious.

#### ADVANTAGES

Consider the simple sequence of operations illustrated in Fig. 5a. A lumpy material is ground into a powder in a mill and fed to a conventional weigh feeder. Assume high accuracy is required, so that the material must be ground into a fine powder, otherwise the conventional feeder will not operate properly. Subsequently, the material is fed to a reaction tank or some such portion of a process where it might be brought into a

FEED RATE,  $\dot{w} = \Delta W_1 / \Delta T_1 = \Delta W_2 / \Delta T_2 = \Delta W_3 / \Delta T_3 = \Delta W_n / \Delta T_n$  LBS / HR

INDEPENDENT VARIABLE:  $\Delta W$

DEPENDENT VARIABLE:  $\Delta T$

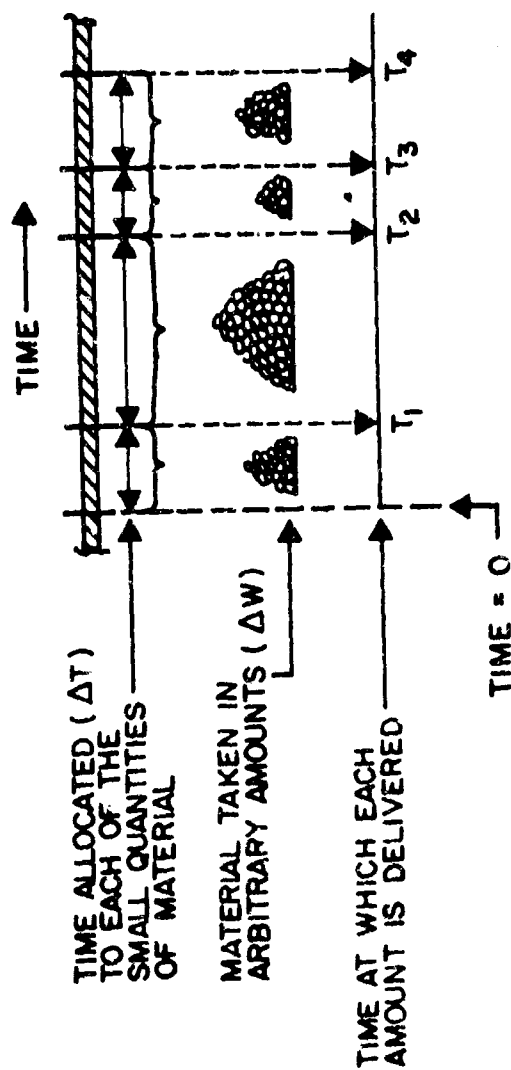


Figure 1. Time-Allocation Principle for Material Feeding

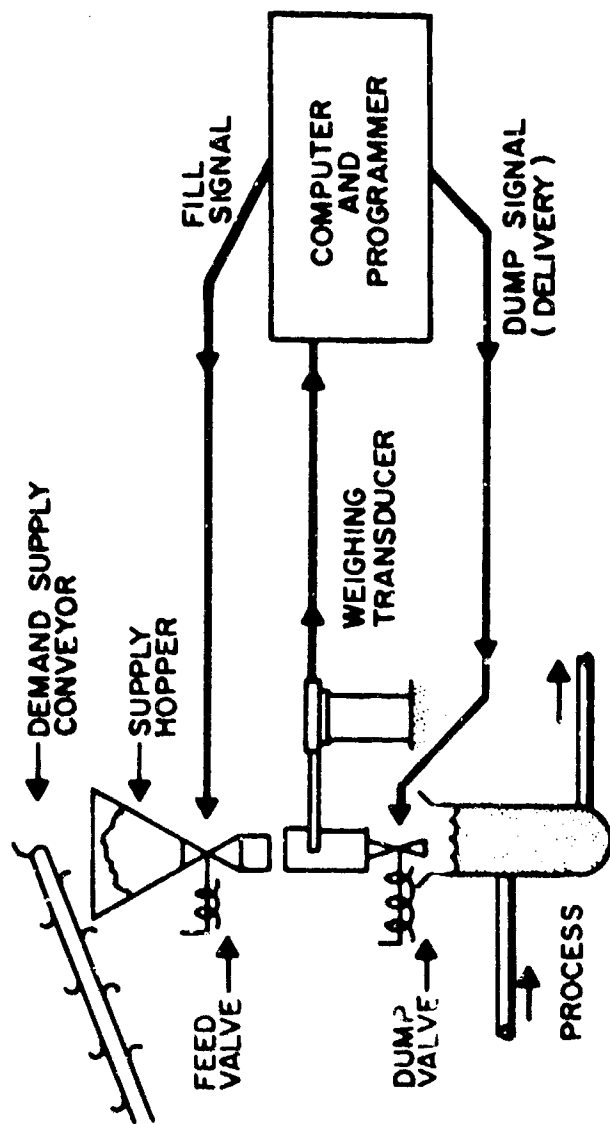


Figure 2. Simplified Schematic of Time-Allocation Feeder

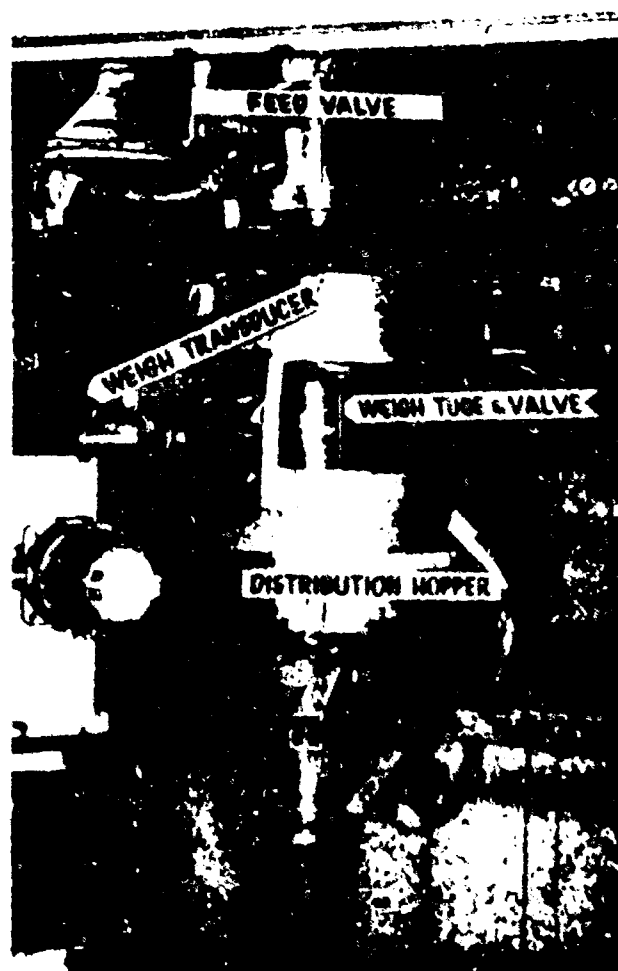
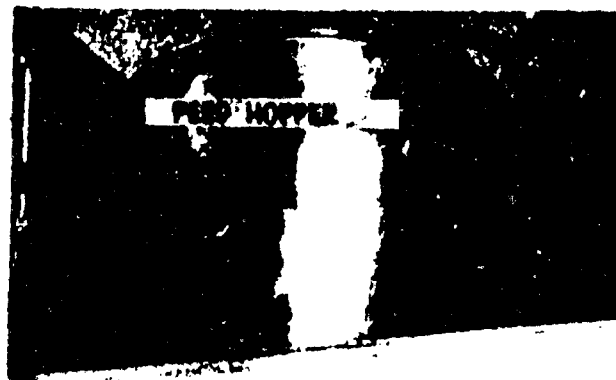


Figure 3. Computerized Feeder



Figure 4. Feeder computer-controller  
330

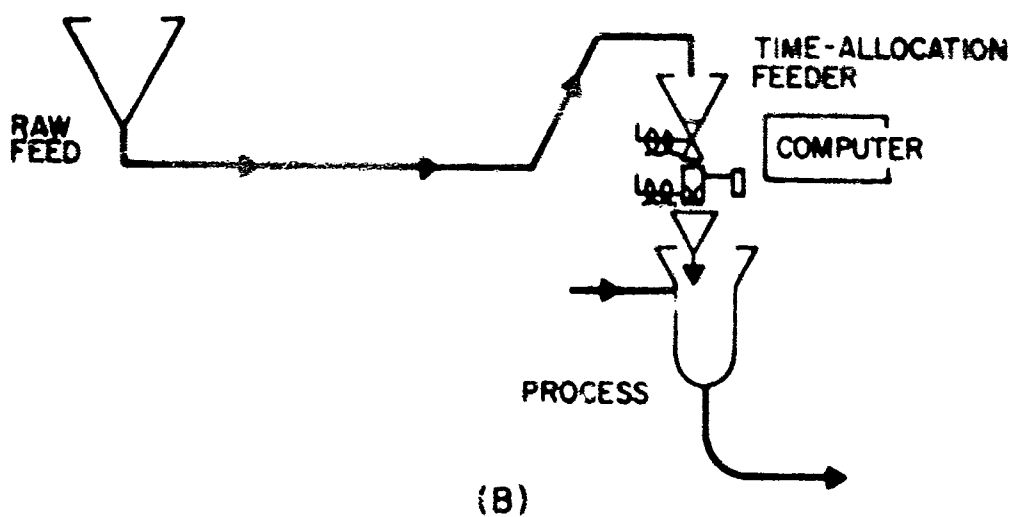
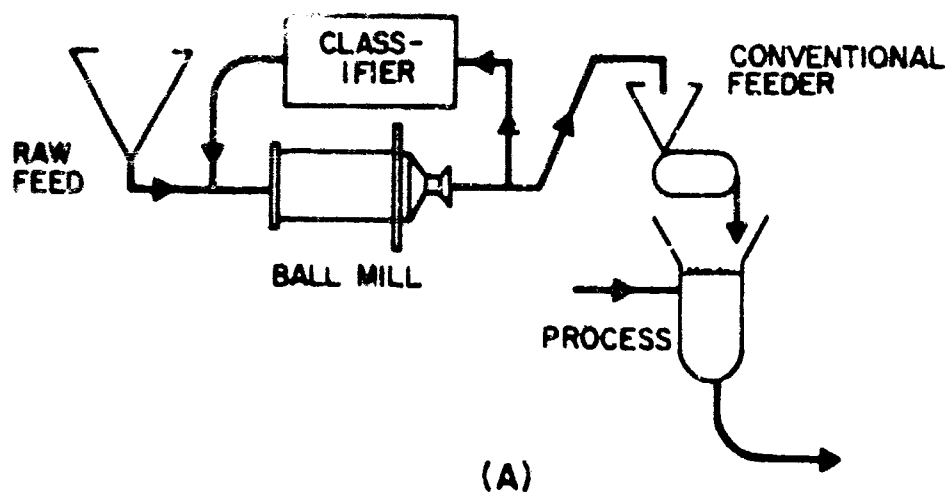


Figure 5. Possible Elimination of a Grinding Operation

solution. With a time-allocation feeder, the grinding operation might be entirely eliminated in that the reaction tank might just as easily accept the lumpy material as the finely ground material. This is illustrated in Fig. 5b. An obvious economic gain may be possible by eliminating the need for the mill.

An extension of this is to consider the case where the material to be fed is of such a character that it is usually not even considered for possible weigh feeding. Viscous and sticky materials are in such a category. Bread dough or chunks of roofing tar might be good examples. Highly dusty materials can be "lumped" and then fed by a time-allocation type feeder. This lumping does not need to be carefully done as would be required for a conventional feeder, but would permit use of fairly large chunks of a fairly wide range of sizes.

Only a brief study has been made of the possible areas where full advantage can be made of the unique characteristics of the time-allocation feeder. Further study in this area might be profitable.

The present feeder was actually built for the feeding of explosives. A highly shock-sensitive material which could not be ground up had to be fed into a process (Quickmix) at a very precise rate. Thus, chunks of material had to be fed at an average rate to an accuracy of better than 1/10 of 1 percent.

The attributes mentioned above become overwhelmingly favorable when combined with the requirement for very high accuracy, i.e., between 0.01 and 0.1 percent. The basic reason for the high feedrate accuracies attainable is the fact that the material is weighed under "quiet" conditions, i.e., no material is being added to, or subtracted from, the

container during the time a particular sample is being weighed. No mechanisms or material need be in motion during the short interval when the actual weight determination takes place. The feeder actually weighs the container just before and just after the material is dumped into the weighing container. The difference in the container weight is thus taken as the weight of the material delivered during that interval. This automatically eliminates many sources of error inherent in conventional, continuous-weigh feeders.

Since no mechanical weigh-arms, knife-edges, or servoloops are employed, design considerations of the mechanical portion of the feeder can be focused upon idealizing the material-handling aspects. For instance, when sensitive high explosives must be accurately fed into a process, safety rather than accuracy considerations can dictate the design. Gentle handling of portions of arbitrary size can be made the prime consideration with only minimum restrictions being placed upon the design by the mechanism essential to the feedrate measuring function.

#### APPLICATION OF NEW PRINCIPLE

A feeder developed by Rocketdyne is composed of three sections: (1) mechanical or material handling, (2) electronic or computer-controller, and (3) the weigh transducer which connects the electronic section with the mechanical by converting weight into an electronic signal.

#### MECHANICAL OR MATERIAL-HANDLING SECTION

The mechanical section of the feeder (Fig. 6) evolved from the basic requirements of safety, accuracy, precision, reliability, and versatility and, as a result, is designed to handle dry solids gently so that

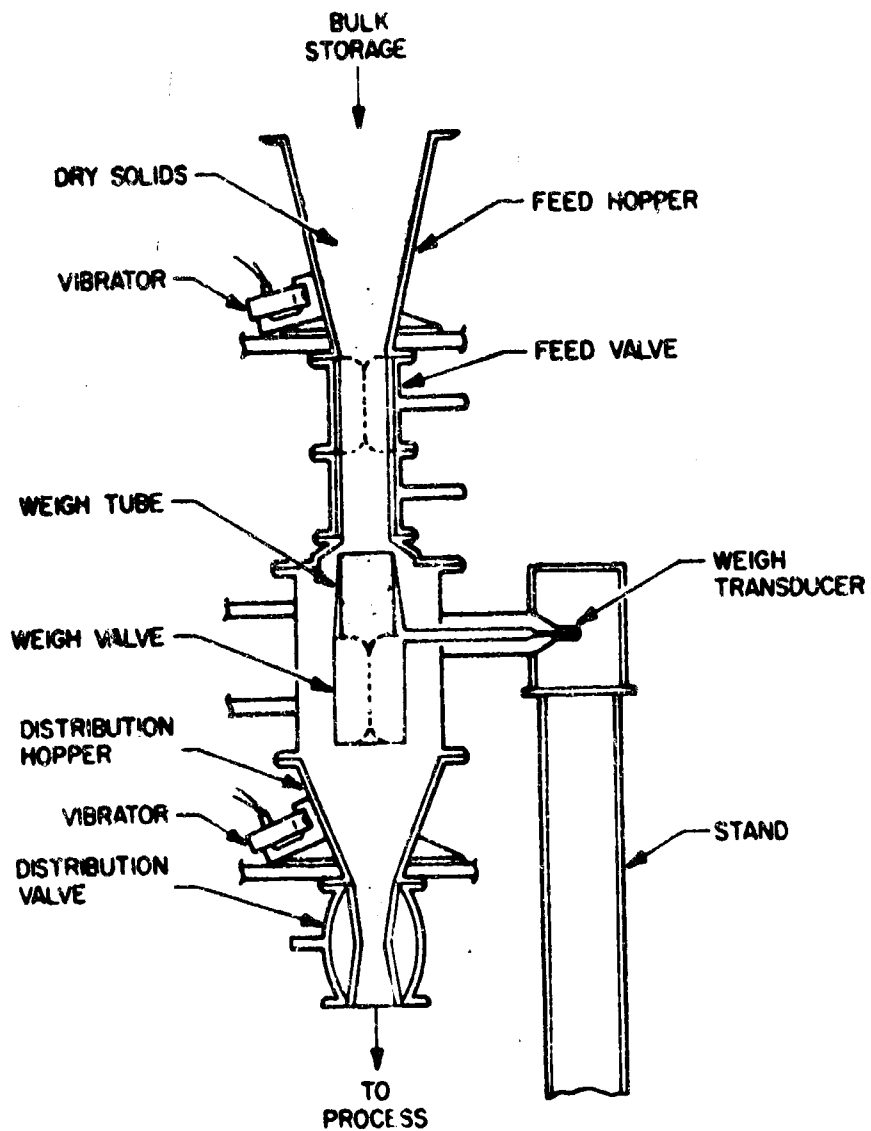


Figure 6. Dry Solids Feeder

it can be used for feeding explosive materials which are sensitive to friction or impact. The design concept of the operation of the mechanical section is described in the following paragraph.

Dry solids are supplied to the feed hopper and an increment of dry solids flows through the feed valve, each time it is opened, and then into the weigh valve. The increment is weighed by the weigh transducer, and the resulting signal is fed into the computer-controller, which computes the correct opening time of the weigh valve. At the time determined by the computer-controller, a signal is sent to a solenoid valve which actuates and causes the weigh valve to open. The increment of dry solids then flows into the distribution hopper and from there into the process. The cycle is then repeated and results in a precise weight-per-unit-time feedrate.

#### Materials Handling

The size and shape of the feed hopper are based on flowability tests performed on the materials or like materials currently anticipated for feeding. A controllable vibrator is mounted on the outside of the feed hopper and actuated by a solenoid valve controlled by the computer-controller. The computer-controller controls the time of vibration as to length and relationship to the feed or fill time. This is a preset value dependent upon the material being fed. Past experimentation has established vibration as a critical parameter (duration, frequency, and amplitude) in the feeding of certain dry solids. Special vibration mounts are used to isolate the feed hopper vibrations from the weigh valve system and to make more effective use of the vibrator.

The top cover of the feed hopper has provision for a bulk dry solids supply inlet, sized to fit a commercial vibrating screen. In addition, inlets are provided for: water deluge, carbon dioxide for fire extinguishing, nitrogen for pressurizing or blanketing, and a level probe for indication and control to the bulk dry solids supply.

#### Feed Valve

Safety, through gentle handling of friction and impact-sensitive dry solids, was the primary design consideration in the development of a feed valve. A "pinch" or "squeeze" valve design was evolved which proved to be gentle acting, reliable, simple, and easily maintained.

As shown in Fig. 7, the feed valve is basically a flexible tube, housed in a metal cylinder in such a way that when pneumatic or hydraulic pressure is applied, the flexible tube closes and when the pressure is released, the tube is opened. The pressure is applied through the use of a solenoid valve actuated by a signal from the computer-controller. The signal from the computer-controller controls the open time of the feed valve and is a factor in controlling nominal increment size which must be consistent within the range of the computer-controller for precise feeding. An early prototype valve with a neoprene rubber liner was tested to 69,000 cycles without sign of failure. There were indications of some slight permanent set, but after a certain point was reached this did not increase.

A second valve in series with the main feed valve is used as a safety or alternate feed valve. It is actuated only in case of failure of the main feed valve system.

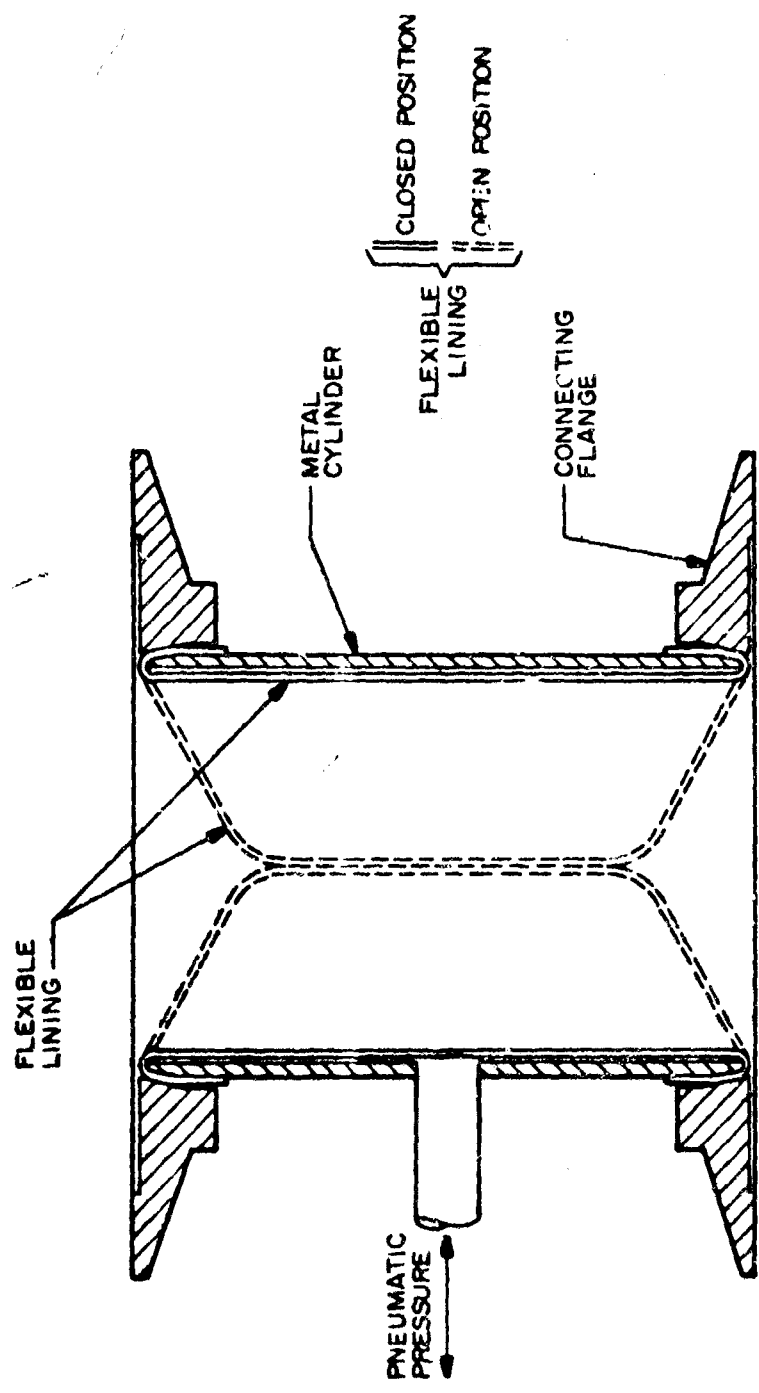


Figure 7. Feed Valve

### Weigh Valve

The weigh valve design is similar to the feed valve except that it must be lightweight, or increment weight accuracy will suffer. While the signal to operate the feed valve will remain constant, as to duration and position in the cycle, the signal to operate the weigh valve is dependent upon the weight of the increment in the valve at the time. The weigh valve opening signal is in exact time proportion to the increment weight.

### Weigh Transducer

The weigh transducer is the connecting link between the computer-controller and the material-handling section. It is, in effect, the heart of the feeder. Its precision, accuracy, and reliability are major factors in the precision and reliability of the total dry solids feeder. Each increment weight is translated into a precise signal by the transducer and sent to the computer-controller. The computer-controller, in turn, sends a signal to the weigh valve which releases the increment in an exact time so that a precise feedrate is maintained. This signal from the transducer can be recorded or indicated in the control room of a process plant.

To have a higher output signal and a more acceptable signal-to-noise ratio, the transducer design is based on the latest semiconductor-strain gage technology. Data on linearity and temperature effects are illustrated in Fig. 8 and 9. This transducer is designed for a nominal 2-pound increment size. The millivolt output vs temperature curve (Fig. 9) shows that a precision of  $\pm 0.03$  percent may be obtained over the compensated temperature range of 70 to 90 F. A special separate H-beam stand supports the weigh transducer and housing so that it will not be subjected to the

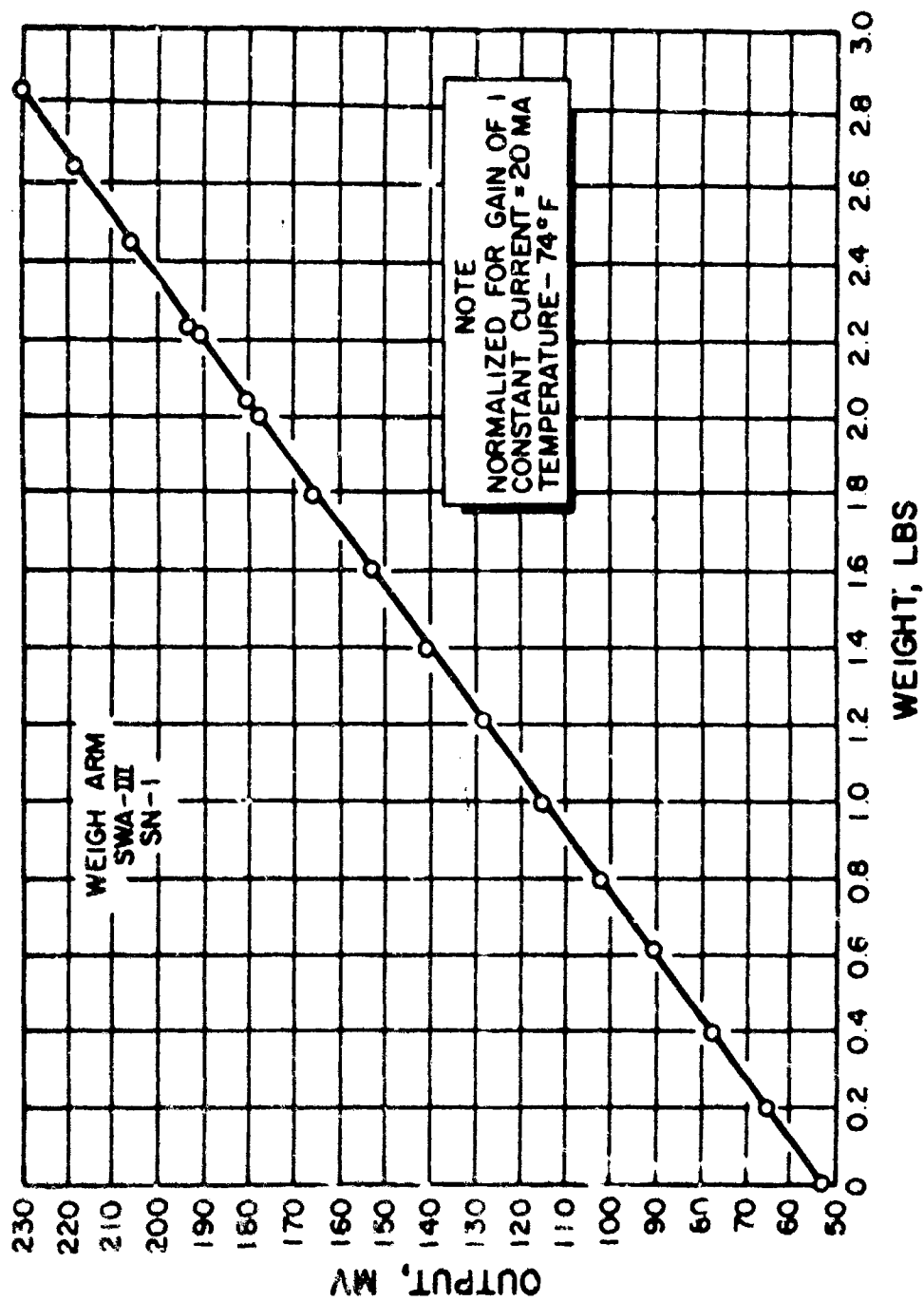


Figure 8. Transducer Millivolt Output vs Applied Weight

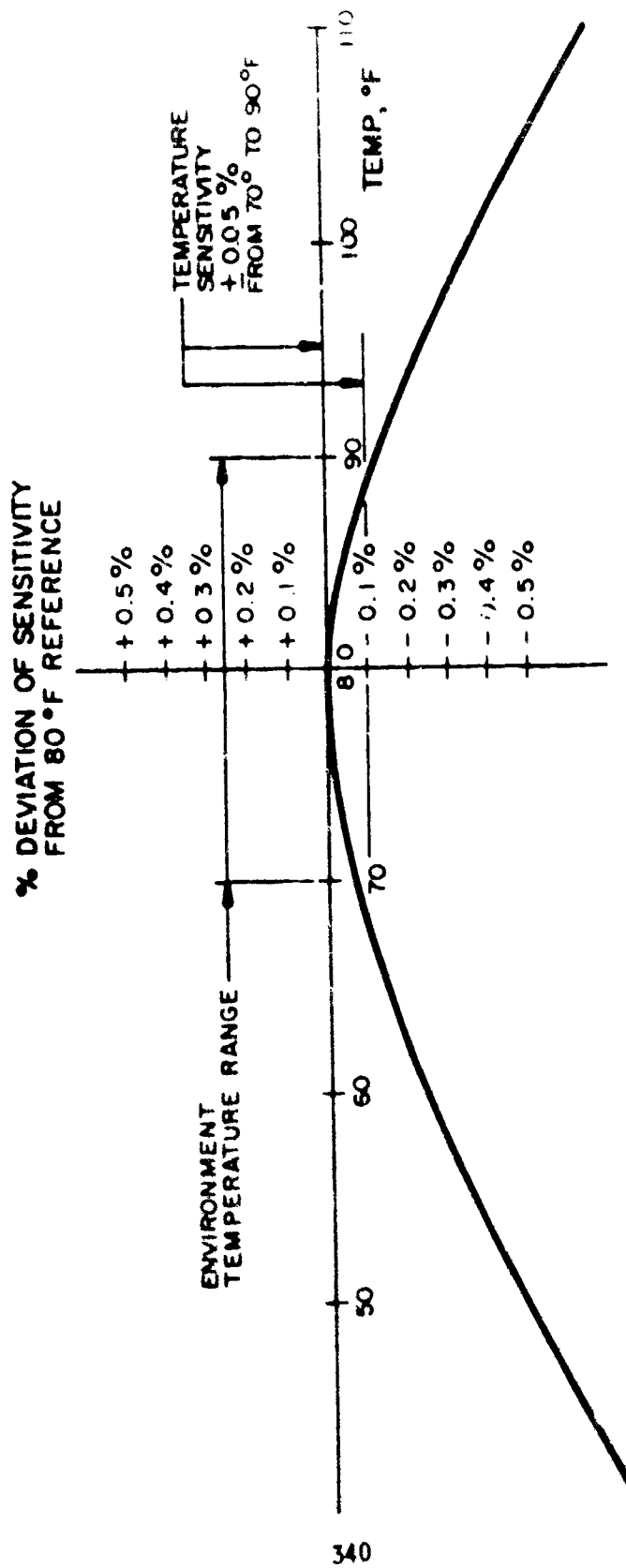


Figure 9. Percent Deviation of Millivolt Output vs Temperature Weight Transducer

vibrations of the material-handling portions. Vibration of the weigh transducer would cause noise to appear on the weigh signal.

#### Distribution Hopper and Control Valve

The distribution hopper is designed to partially smooth out the flow of ingredient from the feeder. The control valve regulates the output of the hopper so that the entire increment flows out just before the next increment is dumped.

The distribution hopper is dustproof, has a vibrator mounted on it, has V-band-type connections where feasible, is mounted on vibration mounts, is easily disassembled for cleaning, has a size and shape compatible with materials expected to be used, and is provided with a capacitance probe to indicate the level of the material. The control valve is used only as a flow restriction and not as an on-off valve except in an emergency.

#### ELECTRONIC COMPUTER-CONTROLLER

An increment of nominal weight is measured out by volume, accurately weighed, and an analog voltage proportional to this weight is generated (Fig. 10). This voltage is then compared with a second analog voltage which is a linear function of time and, at the instant of coincidence, a "weighed-out" signal is generated which subsequently causes the increment of material to be dumped. The incremental dumps are smoothed by the distribution section of the lower hopper and allowed to flow from the feeder at a nearly constant rate into the process which follows the feeder.

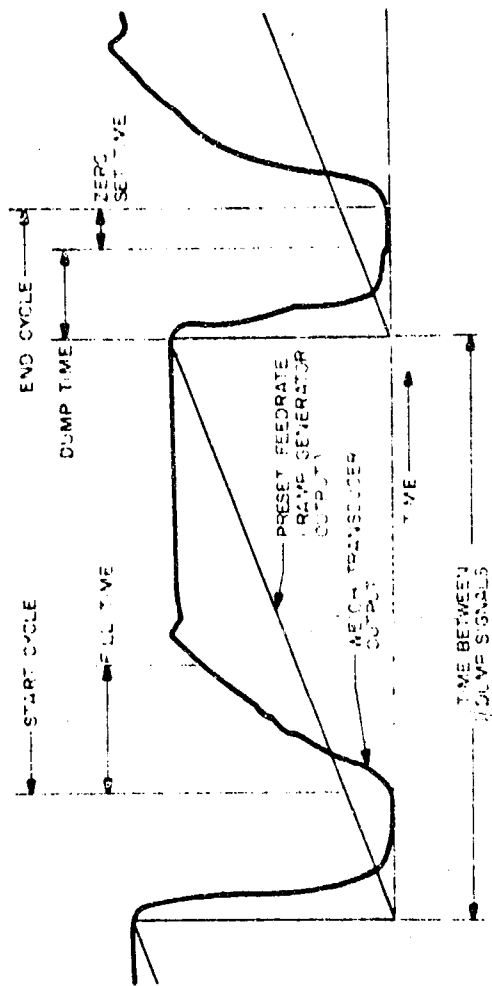


Figure 10. Feeder System Cycle

The comparator output signal generates the start of each cycle of measurement; this signal is sent to a double, solid-state thyatron circuit (Fig. 11) which, via relays, disables the comparator (switch  $S_2$ ), resets the ramp voltage (by momentary activation of switch  $S_3$ ) to zero, and starts the clock of the sequence timer circuit, all within a few milliseconds. The ramp voltage is increasing at its set rate, and a new measuring period is in effect. The sequence timer immediately operates the feeder dump valve and delivers the previously weighed ingredient increment. Upon completion of the dump, the weigh signal input to the comparator is re-zeroed by momentary activation of switch  $S_1$  of the zero memory circuit. This re-zeroing readjusts the computer zero to account for any change in the tare weight due to ingredient hang-up in the weigh bucket by subtracting a voltage proportional to this zero shift from the input voltage of amplifier No. 2. The fill valve is then operated, and a new increment is delivered to the weigh bucket. Since a weigh signal is now available to the comparator, the sequence timer enables the comparator and resets itself. It then waits for the next command from the comparator to end this cycle and begin the next. Two additional signals are available for timing the vibrators installed on the upper and lower hoppers of the feeder.

The sequence timer circuit incorporates a solid-state program timer which puts out four-digit time as a decoded sequence. On the sequence timer panel, the appropriate operation time for each timed function of the system is selected through patch cords and applied to solid-state AND gates which operate high-reliability relays via solid-state relay drivers. This system has extremely high versatility for controlling the feeder and computer functions; it is also capable of easy circuit addition for controlling additional functions if necessary. Allowance has been made in the current design for two additional functions, as required.

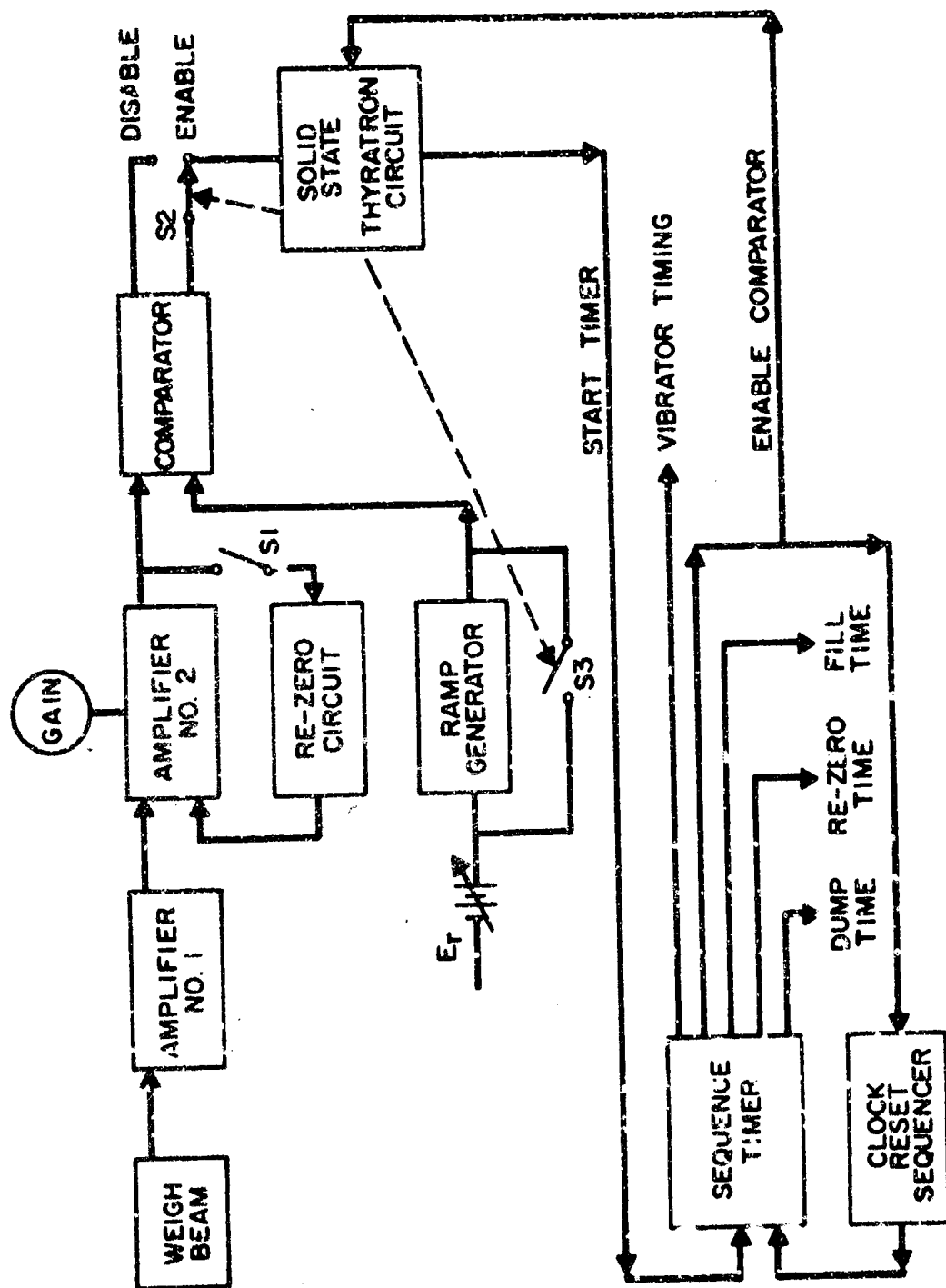


Figure 11. Computer Controller: Simplified Block Diagram

This complete system cycle is listed below and shown in Fig. 10. The advent of the signal from the comparator (time = zero) causes the following events to take place:

1. The ramp generator voltage is brought down to zero and a new ramp starts immediately.

The sequence timer is started.

The dump valve is operated to release the previously weighed increment of material.

The comparator circuit is disabled.

2. The computer is re-zeroed to correct for any change in tare weight.

3. The fill valve is operated to supply a new increment of material to be weighed.

4. The comparator is enabled.

The sequence timer is reset to zero.

5. A weigh period ensues and continues until the ramp signal equals the weigh signal.

6. The comparator output signal causes the system to recycle.

## RESULTS

Tests were devised to evaluate the capability of various portions of the feeder. The electronic computer alone is capable of 0.01-percent accuracy. The portion giving the greatest error is probably the weigh transducer which is slightly temperature sensitive. Data shown in Fig. 12 and 13 represent results obtained by weighing each individual dump of material and simultaneously recording the time assigned by the computer to each corresponding increment of material. Each weight was then divided by each time interval to arrive at a feedrate. The samples were also collected in 25 sample groups and the corresponding time allotted for these 25 samples was measured.

The precision is shown to be  $\pm 0.06$  percent for the series representing 25 integral dumps.

Upon close investigation of the effects of temperature upon various portions of the feeder and upon the limitations of the auxiliary weighing methods used to check the sample weight, it was decided that a nominal  $\pm 0.1$  percent accuracy was probably a conservative figure for the accuracy capability.

Group Number	Sample Number	Individual Dumps			Integrated Dumps		
		Net Weight (pounds)	Cycle Time (seconds)	Feedrate (lb/hr)	Total Net Weight (pounds)	Total Cycle Time (seconds)	Feedrate (lb/hr)
1	5	2.0831	12.4226	603.671	60.35	359.6116	604.152
	10	2.0787	12.3971	603.635			
	15	2.1034	12.5439	603.659			
	20	-----	12.5255	-----			
	25	2.0942	12.4787	604.159			
2	30	2.0986	12.5725	600.911	63.72	379.5548	604.371
	40	2.1169	12.6074	604.474			
	45	2.1301	12.7007	603.775			
	50	2.1319	12.7048	604.090			
	55	2.1191	12.6364	603.713			
3	60	2.1186	12.6290	603.924	65.98	381.2418	604.152
	70	2.1056	12.5586	603.583			
	75	2.1535	12.8310	604.209			
	80	2.1380	12.7335	604.453			
	85	2.1387	12.7467	604.025			
4	90	2.1006	12.5262	603.698	64.51	384.4606	604.057
	100	2.1998	13.1107	604.025			
	105	2.1694	12.9340	603.809			
	110	2.1804	13.0164	603.035			
	115	2.1418	12.7837	603.147			
5	120	2.1076	12.5630	603.945	64.30	383.1747	604.111
	130	2.1729	12.9570	603.723			
	135	2.1557	12.8450	604.167			
	140	2.1647	12.9185	603.237			
	145	2.1164	12.6222	603.622			
6	150	2.1279	12.6849	603.902	64.56	384.6763	604.186
	160	2.1669	12.9278	603.416			
	165	2.1517	12.8375	603.398			
	170	2.1561	12.8563	603.748			
	175	2.1429	12.7908	603.124			

Figure 12. Precision Test for Individual and Integrated Dumps

Group Number	Sample Number	Individual Dumps			Integrated Dumps		
		Net Weight (pounds)	Cycle Time (seconds)	Feedrate (lb/hr)	Total Net Weight (pounds)	Total Cycle Time (seconds)	Feedrate (lb/hr)
7	180	2.1369	12.7441	603.639	64.63	385.2900	603.878
	190	2.1806	12.9959	604.049			
	195	2.1824	13.0234	603.271			
	200	2.1559	12.8441	604.265			
	205	2.1731	12.9511	604.054			
8	210	2.1317	12.7048	604.033	64.59	385.0654	603.856
	220	2.1544	12.8475	603.685			
	225	2.1603	12.8790	603.857			
	230	2.1713	12.9457	603.805			
	235	2.1389	12.7529	603.787			
9	240	2.1471	12.8043	603.669	64.66	385.5883	603.691
	250	2.1632	12.9172	602.880			
	255	2.1608	12.9019	602.925			
	260	2.1473	12.8118	603.372			
	265	2.1431	12.7869	603.364			
10	270	2.1577	12.7242	610.468			
	280	2.1228	12.6658	603.363			
		Mean Feedrate = 603.799			Mean Feedrate = 604.050		
		$\frac{\%(\text{Range}/2)}{(\text{Mean})} = \pm 0.80\%$			$\frac{\%(\text{Range}/2)}{(\text{Mean})} = \pm 0.06\%$		

NOTE: Total feed in one hour was 603.77 pounds

Figure 13. Precision Test for Individual and Integrated Dumps

**ULTRASONIC WELD ENCAPSULATION -- HEATLESS, HERMETIC SEALING**

by

**Charles Zglenicki, Picatinny Arsenal, Dover, New Jersey  
Harold L. McKaig, Jr., Aeroprojects Incorporated, West Chester, Penna.**

## ULTRASONIC WELD ENCAPSULATION -- HEATLESS, HERMETIC SEALING

by

Charles Zglenicki, Picatinny Arsenal, Dover, New Jersey  
Harold L. McKaig, Jr., Aeroprojects Incorporated, West Chester, Perma.

The protection of pyrotechnics from environmental degradants has long been an area of packaging effort, and is now of primary concern in Vietnam, where the high humidity and temperatures could cause loss of munitions effectiveness and reliability, such as field-use misfires or failure to detonate.

The overpacking of munitions in sealed shipping containers has reduced the time span of exposure, but overpacking affords no protection to the individual round after the container is opened or damaged. Each round, therefore, should be individually impervious to environment. Efforts to achieve this desired leaktight package have included the use of O-rings, sealants, gaskets, and mechanical crimps. None of these approaches is completely effective because each relies either on synthetic materials, which themselves degrade as a result of exposure to sunlight, temperature, humidity, or solvent vapor, or on mechanical closures, which are dependent upon fit and mating surfaces, and thus difficult and costly.

In recent years ultrasonic welding has been proposed and evaluated and progressively utilized to accomplish hermetic packaging of pyrotechnics. Unlike fusion welding techniques, the ultrasonic process does not involve high temperatures, nor is there electrical current at the weld area, and this method has thus far presented no serious hazard of material detonation or ignition.

Hermetic sealing is reliably and reproducibly obtained with ultrasonics. The closures are usually helium-leak tested to about  $5 \times 10^{-10}$  cubic centimeters of helium per second sensitivity at standard temperature and pressure. Hermeticity is the result of true metallurgical bonding of the joined components, with no need for filler materials, and the bond is as impervious to environment as are the basic container metals.

Ultrasonic welding is straightforward to implement, and in most cases can replace previous sealing techniques with little or no container parts modification. The weld is accomplished by clamping the workpieces between an anvil or holding fixture and a hollow, annular sonotrode tip which is excited torsionally in a plane approximately parallel to the plane of the weldment. Vibratory frequency is usually 15 to 30 kilohertz, depending on the design of the system. The uninterrupted weld perimeter is produced with a single power pulse, of an interval generally less than 0.5 second.

The welds need not be circular; they can be square, elliptical, rectangular, or of irregular geometry, provided the overall length-to-width weld zone ratio does not exceed very roughly 3 to 1. This ratio can be exceeded by using two "hits," or by using a proportioned weld area.

Ultrasonic ring welds have been made between a variety of similar and dissimilar metals, including combinations of aluminum alloys (even the high-strength structural alloys), stainless steel, titanium, copper, brass, Kovar, gold, beryllium, and beryllium copper. Ring weld diameters have ranged from 1/4 inch to about 3 inches. As the ring diameter and/or the weld width (and thus the weld area) is increased, higher power levels are, of course, necessary.

A standard ultrasonic ring welder (as illustrated by the commercial model shown in Figure 1) can be used for a variety of welding applications, requiring only the interchange of appropriate terminal impedance-matching couplers, welding tips, and part-holding fixtures. The flexibility enhances practicability, and therefore the value, of the process for production and "short-run" applications.

A few typical pyrotechnic and explosives container geometries illustrate both the advantages and the flexibility of ultrasonic welding.

The first container, one of the most common types of pyrotechnics, is shown in Figure 2. This assembly is conventionally sealed by installing a gasket between the cover disk and the cup flange and mechanically applying pressure across the seal area via the installation above the disk of a press-fit ring or a threaded ring nut. In contrast, hermetic sealing of this container is accomplished ultrasonically by using only the cup and disk. In the associated ring welding operation, as shown in Figure 3, the pyrotechnic-loaded cup is placed in a positioning fixture, the cover disk is positioned, and a moderate static clamping force is applied concurrently with the short-duration pulse of vibratory energy. The required distribution of force and energy is obtained by maintaining parallelism of the holding fixture face and the plane of the welding tip.

Generally, there is no need for special parts cleaning, and in many cases a leaktight closure can be achieved even when a light dust of the pyrotechnic fill is present at the weld interface.

In another application, a similar package without the extension skirt (Figure 4) was loaded with M-5 propellant, ultrasonically welded, and subjected to degradation testing. For comparison, standard production assemblies incorporating a crimped and plastic-sealed closure

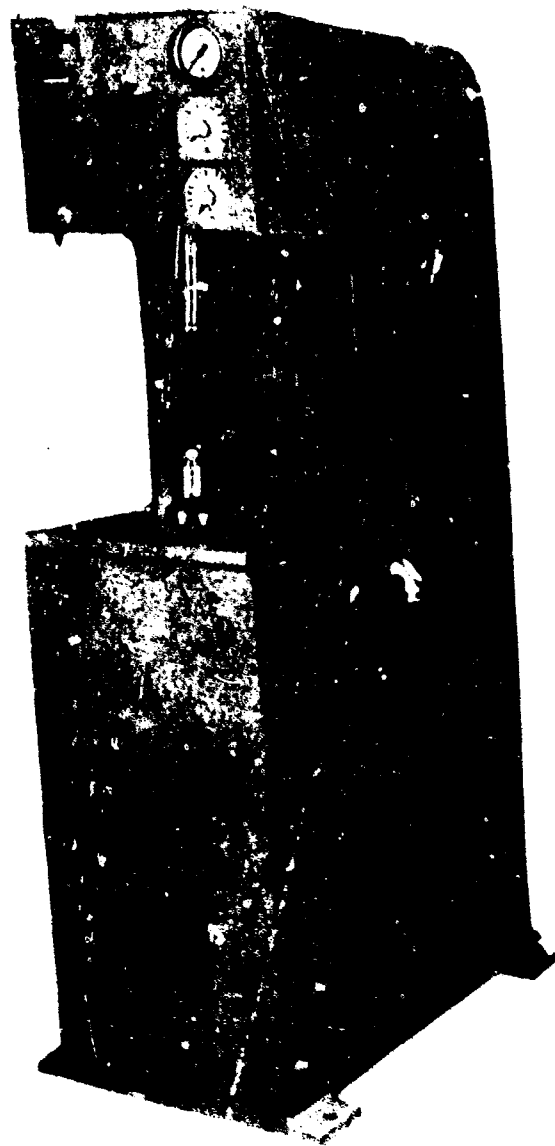


Figure 1

A TYPICAL COMMERCIAL ULTRASONIC RING WELDER

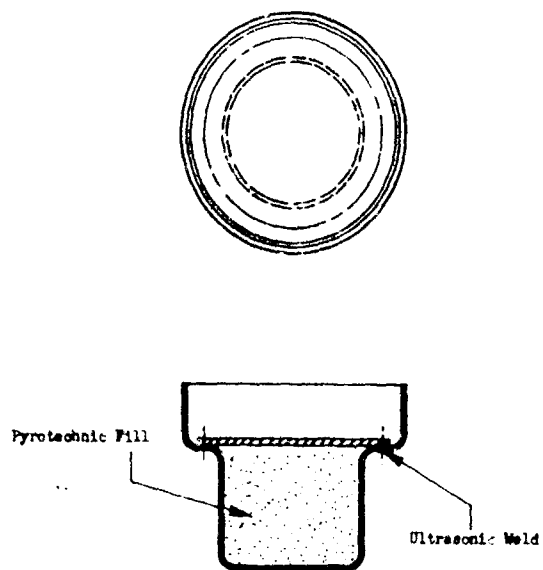


Figure 2  
PYROTECHNICS CONTAINER  
SHOWING AREA OF ULTRASONIC RING WELD

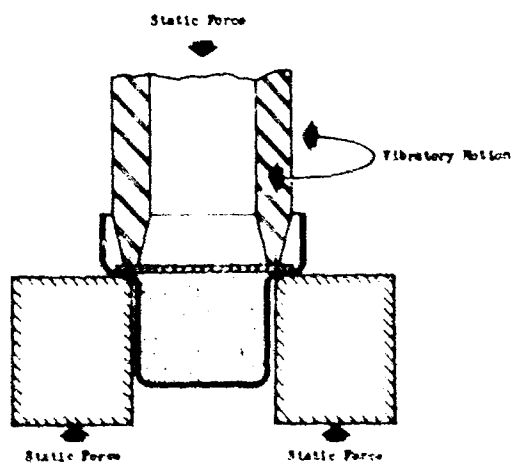


Figure 3  
ULTRASONIC RING WELDING OF CONTAINER CUP AND COVER DISK

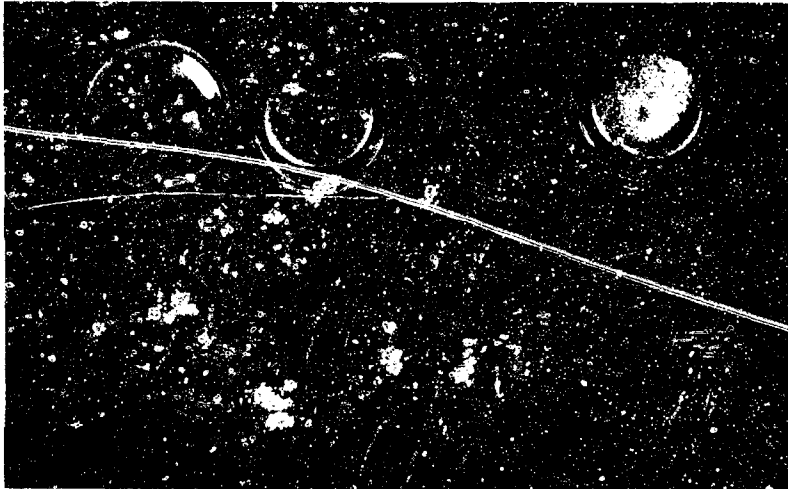


Figure 4

ULTRASONICALLY WELDED STARTER CUPS  
CONTAINING M-5 PROPELLANT

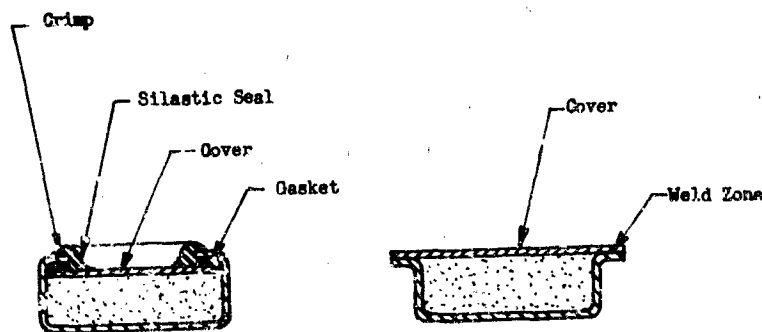


Figure 5

COMPONENTS OF SILASTIC-SEALED VERSUS ULTRASONICALLY WELDED  
PROPELLANT STARTER CUPS

were similarly tested. Quantities of each package were subjected to a week of temperature cycling between  $-65^{\circ}\text{F}$  and  $+165^{\circ}\text{F}$  and a 15-day exposure to a saturated atmosphere of acetone and cyclohexane. The relative quickness and relative force of the lot of M-5 propellant used were established, and the fill of the tested packages was evaluated by closed-bomb techniques. The propellant from the silastic-sealed packages showed zero percent relative quickness and 47 percent relative force at the conclusion of the exposures. Propellant from the ultrasonically welded packages showed no observable loss of either quickness or force at the conclusion of the same exposures.

A third geometry is that of the non-circular propellant package shown in Figure 6. A sample lot of 1100 units was ultrasonically ring welded for process evaluation. These units demonstrated 100 percent reliability and reproducibility.

These ellipse-like containers also used an outwardly flanged lip (approximately 0.025 inch wide) for the weld surface. In other applications, the flange may be undesirable for packing purposes. This is the case with the smoke canister shown in Figure 7; individual canisters are stacked within a cylindrical body, and the number of canisters determines total burning time. Figure 8 shows the method for obtaining a required straight-sided configuration. The impact-extruded aluminum canister was flanged and filled. The punched-sheet cover was welded in place, and the assembly was re-formed by pressing through a ring die. Since the ultrasonic weld does not produce embrittlement or loss of ductility in the parent metals, the weld zone can be re-formed without loss of weld strength or sealing properties.

Containers having relatively heavy walls can be sealed without forming and re-forming. The gas generator shown in Figure 9 incorporates a welded foil cover joined directly to the end of the container wall. The thin foil sealing disk also functions as a rupture disk to fail at a specific internal pressure. A design variation of the same package (Figure 10) resulted in the production of a complete assembly entirely sealed with one weld. The design concept developed for the ultrasonic sealing of this package is shown in Figure 11.

Internal shoulders on machined parts are suitable locations for ultrasonic ring welds, as shown in the Figure 12 canister filled with 65 grams of M-10 propellant. The hermetic seal was completed in 0.5 second, indicating that a production rate of 1500 units per hour is obtainable using essentially standard equipment. Ultrasonic ring welding equipment can be incorporated into automated production lines, and the frequency converter that supplies the high-frequency power can be remotely located as may be necessary.



Figure 6

ELLIPSE-LIKE CONTAINERS  
ULTRASONICALLY RING WELDED

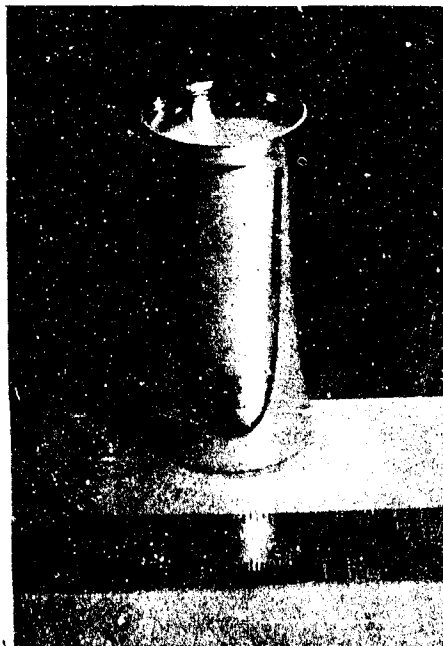


Figure 7

FLANGED SMOKE CANISTER  
RE-FORMED TO STRAIGHT WALL CYLINDER

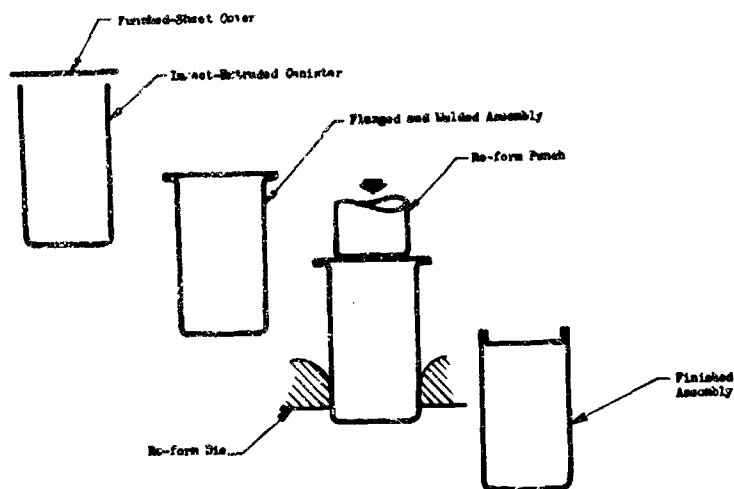


Figure 8

FORMING STEPS FOR ULTRASONICALLY WELDED  
SMOKE CANISTER

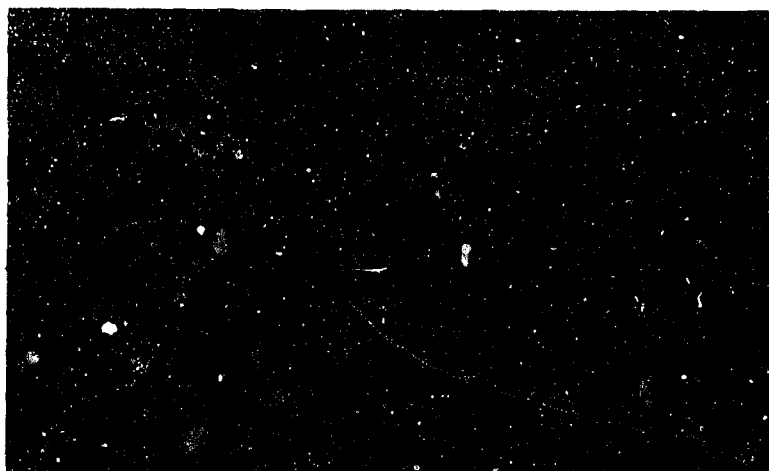


Figure 9

FOIL COVER RING WELDED DIRECTLY TO CONTAINER WALL

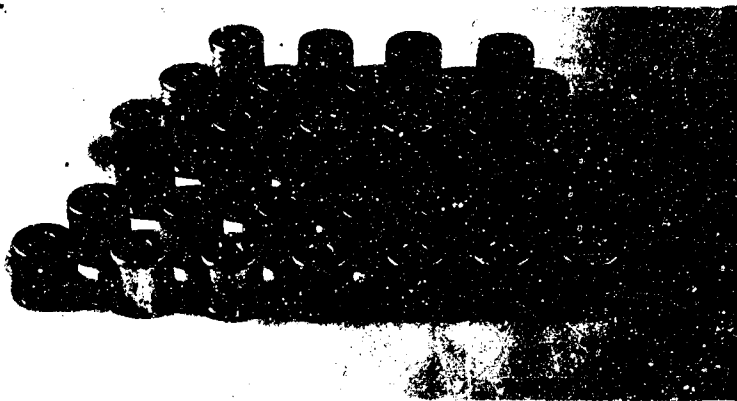


Figure 10  
SINGLE-WELD SEALING OF GAS GENERATOR ASSEMBLY

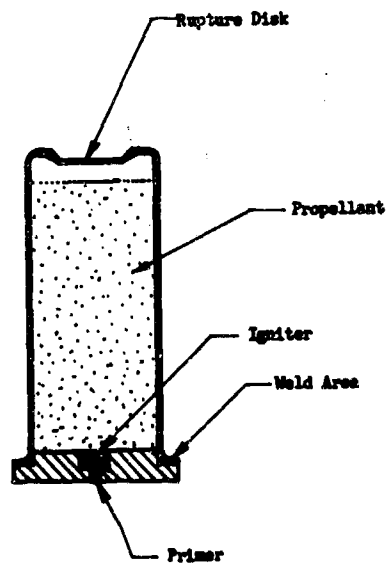


Figure 11  
DESIGN CONCEPT FOR SINGLE-WELD SEALING  
OF GAS GENERATOR ASSEMBLY



Figure 12

RECESSED-SHOULDER WELD SITE

The few package geometries discussed are only a representative cross section of the several dozen specific pyrotechnic assembly geometries investigated, but even from the few examples given, many geometric variations are readily evident for application to packaging problems.

In the course of applications considered to date, ultrasonic welding has been accomplished without incident. In almost all cases, the weld has been in close proximity to many of the common propellants, explosives, and hazardous materials. Figure 13 lists some of these materials and the quantity per package in some of the hermetic applications.

Investigation of materials sensitivity to the conditions of ultrasonic welding has included placing quantities of M-5, Hercules Red Dot, RDX, and HMX directly on the weld zone of two sheets of 0.010-inch-thick aluminum. No ignition occurred. In the case of the Red Dot powder, the large and tenacious flakes could not be reliably dispersed to guarantee a leaktight weld in all cases. However, such heavy concentration at the weld zone should occur only by intentional placement.

The ultrasonic ring-weld seals provide a high degree of reproducibility and reliability. Results from exploratory investigations involving as few as 25 units as well as preproduction runs of more than 5000 assemblies have shown a zero reject rate under standard helium leak testing, generally to a sensitivity of  $1.0 \times 10^{-6}$  cc per second at STP.

Thus, the ultrasonic welding process offers a solution to the problems of protective packaging of pyrotechnics. This hermetic sealing process is now being specified by munitions manufacturers, and production facilities are incorporating ultrasonic welding equipment.

Figure 13  
TABLE OF REPRESENTATIVE REACTIVE MATERIALS  
ENCAPSULATED BY ULTRASONIC WELDING

Material	Quantity (approx.)	Geometry	Material	
			Cover	Container
M-5	9 grains	Right cylinder 0.56" dia x 0.19"	0.003" 3003-H25 Al	0.010" 3003-0 Al
M-9	14 grains	Ellipse-like 1.037" x 0.467" x 21" deep	0.005" 3003-H19 Al	0.010" 3003-0 Al
M-10	65 grams	Right cylinder 1-1/2" dia x 3"	0.006" 3003-H19 Al	Solid 2014-T4 Al
Red Smoke	1/4 lb	Right cylinder 1.2" dia x 2.2"	0.010" 3003-H14 Al	0.020" 1100 Al Impact Extr.
M-5	11 grains	Right cylinder 11/16" dia x 1/8"	0.005" 1100-H14 Al	2014-T4 Machined Part
Hercules Bullseye	2 grains	Flat sheets	0.010" 3003-H14 Al	0.010" 3003-H14 Al
Hercules Red Dot	2 grains	Flat sheets	0.010" 3003-H14 Al	0.010" 3003-H14 Al
Lithium Al Hydride		Right cylinder 1/4" dia x 1/4"	0.005" 1100-H14 Al	0.010" 1100-H14 Al
Magnesium Hydride		Right cylinder 1/4" dia x 1/4"	0.005" 1100-H14 Al	0.010" 1100-H14 Al
Red Fuming Nitric Acid		Tube 0.10" dia x 1/2" long		0.005" 1100-H14 Al
Bromine Trifluoride		Tube 0.10" dia x 1/2" long		0.005" 1100-H14 Al
Nitronium Perchlorate		Hemisphere 1/8" radius	0.005" 1100-H14 Al	0.010" 1100-H14 Al
Lead Azide	2 grains	Right cylinder 0.09" dia x 0.06"	0.002" 3003-H14 Al	Solid 5050 Al
Double Base	14 grains	Right cylinder 3/4" dia x 0.5"	0.005" - 0.010" Al	0.025"-0.035" 5050 Al
Modified RDX	6 grams	Right cylinder 1.0" dia x 1-1/2"	0.060" 5050 Al	0.025" 5050 Al



Pyrotechnics Seminar  
Denver Research Institute  
University of Denver  
Estes Park, Colorado  
12 - 16 August 1968

PRINCIPLES AND APPLICATIONS OF EXPLOSIVE BONDING

W. W. Cavell, J. F. Kowalick, and H. J. Addison, Jr.

Pitman-Dunn Research Laboratories  
Frankford Arsenal  
Philadelphia, Pa. 19137

## INTRODUCTION

In explosive bonding, the energy released during detonation of an explosive is used to establish interatomic bonds between metals. Tests have indicated that the strength of the bonds formed may equal or exceed the strengths of the individual metals involved. More recent work has been reported on the explosive bonding of non-metals<sup>1,2</sup>.

## STUDIES AT FRANKFORD ARSENAL

Explosive bonding investigations at Frankford Arsenal have been concerned with six topics, as indicated in Table I.

Types of Welds. Some of the earliest work reported on the various types of weld configurations which could be obtained and the first published information on the fabrication and properties of explosive seam welds was accomplished at F.A. In this work, seam welds, spot welds, lap joints, area welds, were all demonstrated.

Inspection Techniques. In addition, various inspection techniques were used, including visual and metallographic, radiography, and ultrasonic inspection. We will come back to these techniques later in this paper. This early work is covered by two publications of the ASME and the Welding Journal, respectively<sup>3,4</sup>.

Flat Panels. Later work at F.A. involved the development of procedures for explosively bonding flat Ta-8W-2Hf alloy panels to 4150 steel bars. Results of visual examinations, metallographic surveys, peel tests, hardness and tensile tests were evaluated and would later be applied toward the bonding of refractory liners in steel gun barrels. In this flat panel work, nitroguanidine explosive at a bulk density of 0.4 g/cc was used, in conjunction with 0.05 inch spacing between the tantalum and steel members. This work is reported in reference 5.

TABLE I  
EXPLOSIVE BONDING INVESTIGATIONS AT F.A.

1. Types of Welds
  - a. Seam
  - b. Spot
  - c. Lap
  - d. Area
2. Inspection techniques
  - a. Visual
  - b. Ultrasonic
  - c. Photomicrography
3. Bonding of Flat Panels
  - a. Tantalum to steel
  - b. Nitroguanidine explosive
4. Bonding of Liners in Gun Barrels
  - a. Refractory Liners
  - b. Steel Gun Barrels - 0.50 Cal., 20mm
  - c. Raises serious problems - Materials & Explosive
5. Study of the Explosive Bonding Mechanism
  - a. Instrumentation and Measurement Techniques
6. Related Work
  - a. Explosive Forming of Magazines in Dies
  - b. Explosive Forming of Tubular Members in Dies

Lining of Gun Barrels. The technical objective of the current studies at F.A. is to develop procedures for explosively bonding refractory metal liners in gun barrels. The refractory liners would enable lighter base metals to be substituted for steel gun barrels, with accompanying weight and cost reductions. This would fulfill a major objective of the DOD, that seeks to impart increased transportability, maneuverability, firepower and useful life to weapon systems. In line with this objective, many unsatisfactory attempts have been made to bond refractory alloys to steel structural components by using conventional welding processes. Primary causes for failure are attributable to the inability of conventional welding processes to form strong joints in dissimilar metal combinations and geometries of interest. Quite often weak joints are produced by the formation of brittle intermetallic phases, or the processes are not economically feasible. The E. B. process offers considerable promise for overcoming these problems. As is indicated in Table 1 we are currently interested in two calibers -- caliber 0.50 and 20mm. In general, the complexity of this process decreases with increasing caliber. This is primarily true for two reasons. First, a given liner thickness requires a minimum amount of explosive to accelerate it to the required velocity, so there is a certain minimum interior barrel volume below which bonding will not be obtained. Secondly, the detonation velocity of an explosive decreases with decreases in linear dimension of the explosive charge configuration, eventually reaching a cutoff point where the explosive ceases to propagate. The linear dimension at this out off point is termed the "critical size" of the

explosive. In general, critical size is a function of explosive composition, particle size and density. To date, refractory metal liners (notably tantalum and its alloys) have been metallurgically bonded inside smooth-bore gun steel tubes (0.50 caliber). In addition satisfactory bonds have been obtained inside rifled barrels; however, it has been found that the lands and grooves require some modification - in terms of rounding them off to avoid cutting during liner impact. To date, all specimens have been limited in size to lengths of 4 inches.

Explosive Bonding Mechanism. In a concurrent effort, the Research Institute of the Drexel Institute of Technology has been supported to conduct basic research studies on the explosive bonding mechanism, as it relates to such factors as the nature of the bond interface and criteria for metallurgical bonding. In the short period in which this project has been funded, Drexel has made some significant strides in the areas of dimensional analysis of gross parameters and dynamic measurement techniques<sup>6</sup>.

Related Work. A related area to the work already discussed -- explosive forming -- has, nevertheless, played an important role in understanding explosive welding operations. Two sub-tasks at F.A. are worthy of noting: the explosive re-forming of M-14 Rifle magazines; and the explosive forming of steel tubes in dies<sup>7</sup>.

#### EXPLOSIVE BONDING THEORY

History: For many years, probably since the 1880's when modern high velocity gunnery was first introduced, instances of unintentional explosive bonding had been observed, but not recognized for their potential

importance, when metal projectiles fired at metal targets were occasionally found metallurgically welded to pieces of the target. Visitors to the Ordnance Museum, Aberdeen Proving Ground, Maryland can view an exhibit of such a projectile welded to a target plate that the projectile was intended to penetrate. During the 1880's Professor Charles E. Munroe discovered the Munroe or shaped-charge effect which was intensely studied and used in designing ammunition for armor-defeating purposes during World War II <sup>8</sup>.

Although the pertaining principle of both shaped charge ammunition and explosive bonding is the same -- namely the "Munroe Effect" in which there is formation of a high velocity jet between impacting surfaces - the jet is used to achieve directly opposite end-effects. Shaped charge ammunition uses the jet to increase the total target depth penetration or maximum destruction attainable per unit weight of explosive. On the other hand, explosive bonding uses the jet to achieve metallurgical bonding of two materials. Explosive bonding was probably first recognized for its full potential when explosive forming investigators during the 1950's observed that the metal blanks being explosively formed sometimes became welded or metallurgically bonded to the metal dies. From examination and study of these random accidental instances, explosive bonding has grown to the point where it is currently a useful and practical metals bonding technology. Several domestic and foreign research papers on explosive bonding, illustrating the current world-wide interest in this new technology, were recently presented at the First International Conference of the Center for High Energy Forming held at Estes Park Colorado on 19-23 June 1967. This conference was sponsored by two agencies of the Department of Defense, namely the U.S. Army Materials Research Agency and Advanced Research Projects Agency.

Criteria for a Metallurgical Bond. Two criteria must be satisfied in any welding process, namely (1) all surfaces to be joined must be free of surface films consisting of oxides, nitrides or adsorbed gases that are inevitably present and (2) the atoms of the pure materials to be joined must be brought into such close contact that inter-atomic forces can act as a bonding force. These criteria are satisfied in explosive bonding by the formation of a "jet" consisting of surface material from both metals to be joined. This jet, which is identical with the shaped charge "jets" of interest during World War II era, contains all the unwanted surface impurities, and permits the pure metals to come together under the propelling action of the extremely high-pressure (up to 4,000,000 psi) explosive gases as shown in Figure 1. In addition to these two criteria which apply to all types of welding, two more criteria for explosive bonding have been established; first, in bonding parallel surfaces, the detonation velocity of the explosive should be about equal to (and preferably slightly less than) the lower acoustic velocity of the two metals to be joined. This criterion has resulted in a currently intensive search for explosives having low velocities of detonation and having explosion products that produce no deleterious effects on metal surfaces. To date, explosives with detonation velocities as low as 1000 meters per second have been used in explosive bonding studies. Secondly, the impacting velocity of the plate must exceed some critical velocity which is necessary to plastically deform the parent (base) metal. Table II shows explosive used in the studies at Frankford Arsenal.

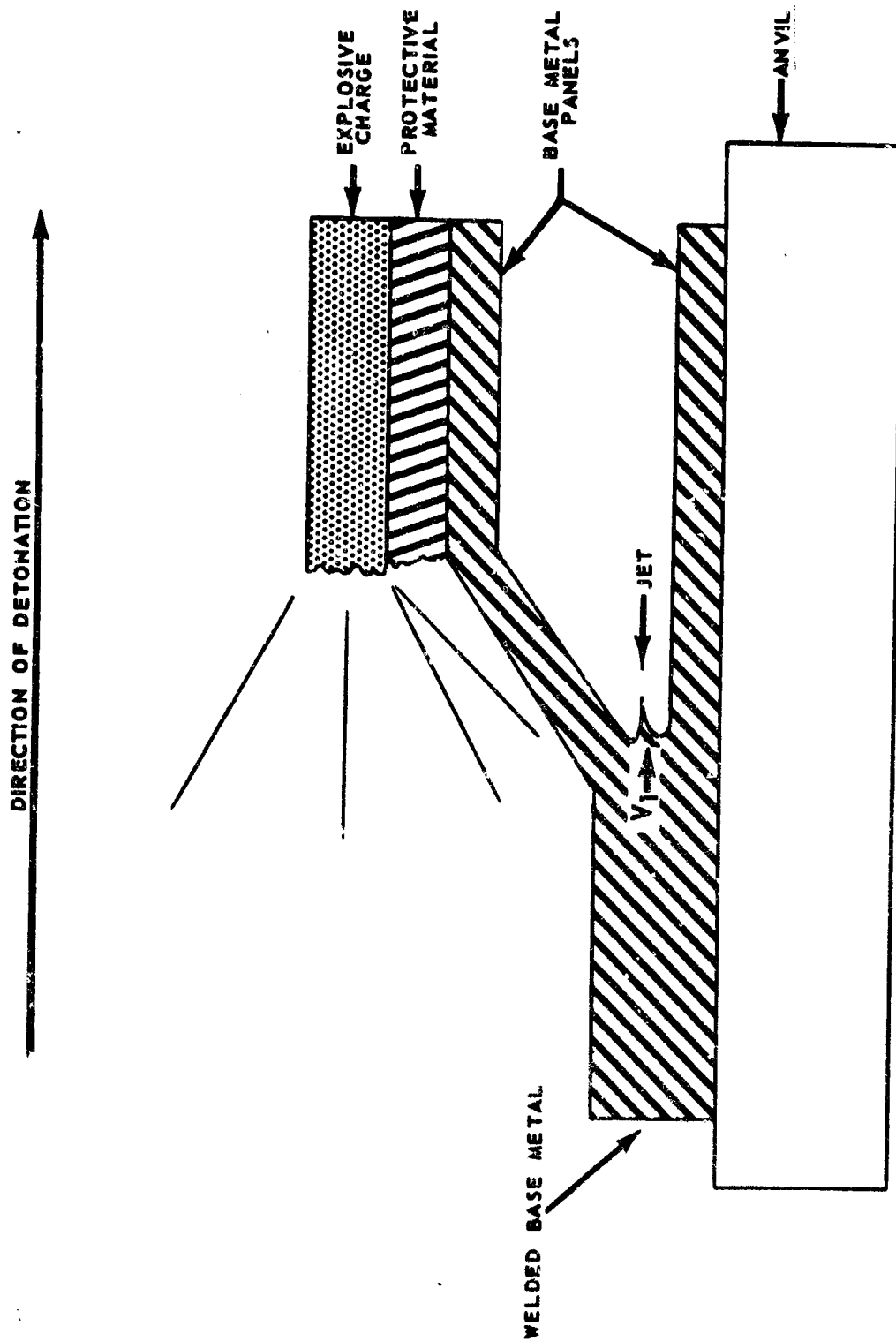


FIGURE 1. ILLUSTRATION OF JETTING IN EXPLOSIVE BONDING

TABLE II

EXPLOSIVES USED IN EXPLOSIVE BONDING STUDIES AT FRANKFORD ARSENAL

High Velocity

PETN

PDX

EL-506A\*

Tetryl

Primacord\*\*

Medium Velocity

Low Density PETN

Nitroguanidine

Dynamite

\* Proprietary sheet explosive made by E. I. du Pont de Nemours and Co., Inc.

\*\* Proprietary cord explosive made by Ensign-Bickford Company

Appearance of the Interface. While three general types of bonded zones have been recognized (classified as to the micro-appearance of the bonded interface) only one type appears to be useful in practice. Here, the demarcation line between the bonded materials has the appearance of a periodic Sine wave, with a lapping over at the top of the wave crests in the form of "fish-hooks" shown in Figure 2. Close examination of the demarcation line area usually reveals the coarse crystalline structure of the base materials (at some distance from the actual bonded zone), a much finer crystalline deformation structure within the bonded zone, and pockets of a cast recrystallized structure actually in the demarcation area.

In an effort to explain the wave-formation process, previous investigators have resorted to various ingenious models and experimental techniques. Abrahamson<sup>9</sup> studied an analogue system which consisted of a moving, silicone-putty base material deformed by the action of a (water) jet which penetrated the putty at an angle. From this relatively crude model, photographic evidence of periodic wave formation in the silicone putty was collected, and a qualitative wave-formation model proposed. Crossland<sup>10</sup> modified, qualitatively refined and experimentally confirmed this model by direct and metallographic observation through the use of galvanic platings on the surface of both base materials. Similar plating experiments were carried out by Cowan et al<sup>11</sup> in a more quantitative fashion; and by Rosensteel<sup>12</sup> chiefly for the purpose of avoiding undesirable brittle intermetallic compound formation.



FIGURE 2. EXPLOSIVE BOND OF ALUMINUM TO STEEL USING  
NITROGUANIDINE

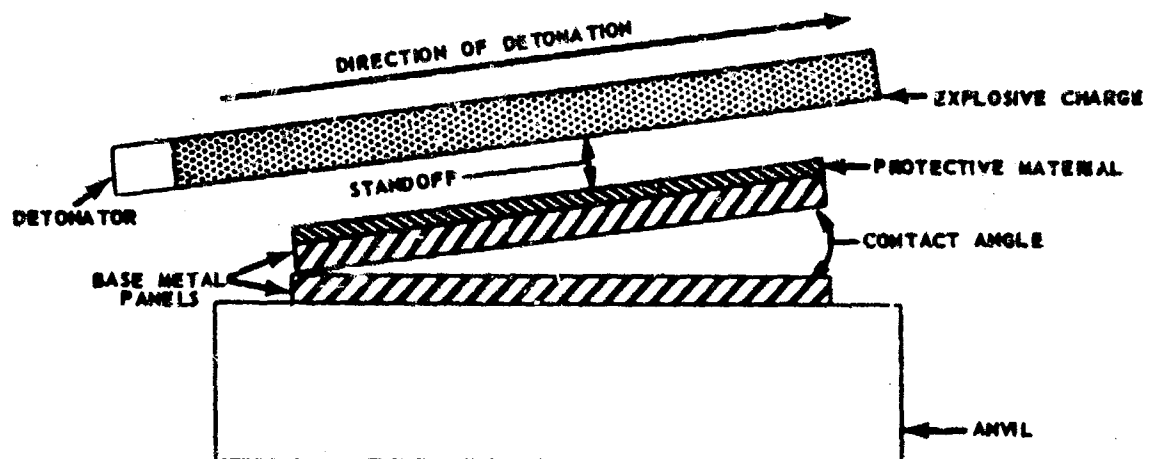
In addition, Cowan gathered experimental evidence of the existence of a metal jet formed during the explosive bonding process and cited this jet formation as a corollary criterion for explosive bonding.

For the explosive bonding process, it has been found that close control of all material parameters (including those of the explosive) must be maintained in order to avoid severe side effects, such as severe deformation and surface damage to the cladding (flyer) plate; the formation of a relatively large proportion of brittle, intermetallic compounding at the bond interface; and the damaging effects to the bonds formed of any high energy shock waves reflected from free surfaces of the base material.

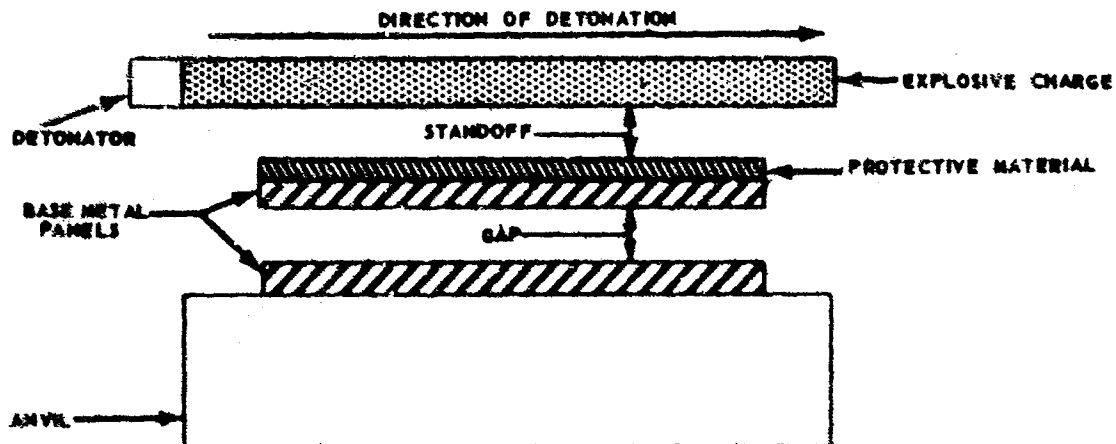
#### EXPLOSIVE BONDING TECHNOLOGY

Geometrical Configurations. Explosive bonding generally is accomplished with one of the two techniques illustrated in Figure 3. The most obvious dissimilarity between the two setups is the positioning of the panels to be bonded. The top panel, (Figure 3A) is placed at an angle to the bottom member. This angle is sometimes known as the "contact angle" and consequently the method has been called the "angular" technique. In Figure 3B the members are parallel to each other. The panels may be either in contact or a predetermined distance apart. This technique has been called the "gap" technique due to the gap or spacing between the panels.

The setups also are similar in several respects. The panels are located between an explosive charge and an anvil with the bottom panel resting on the anvil. The anvil removes excessive energy from the weld region, preventing the bond from being torn apart after it is formed.



A. ANGULAR TECHNIQUE



B. GAP TECHNIQUE

FIGURE 3. EXPLOSIVE BONDING SETUPS

The purpose of the protective material, which is not necessary for some explosive charges, is to prevent pitting or gouging of the panels. Protective materials have been made from many substances including rubber, masking tape, wood, and plastics.

Variations of the above techniques also are employed. The gap technique in Figure 3B, for example, lends itself with slight modification to the cladding of hollow cylinders such as gun barrels. In order to bond a liner to the interior surface of a hollow cylinder, the explosive may be placed inside the liner and a die positioned outside the cylinder. The die serves as an energy sink and aide in maintaining the exterior dimensions of the cylinder. Conversely, the outer surface of a hollow cylinder may be clad with tubing by placing the explosive around the exterior of the tubing and a mandrel inside the cylinder to prevent it from buckling. In these examples, an appropriate spacing would exist between the cylinder and liner or tube that would serve as the gap. Tubing or pipe may be joined to itself with these techniques.

Important Parameters. In an attempt to relate these process parameters, Carpenter and Wittman<sup>13</sup> derived an empirical relationship (which, it is claimed, is applicable for good bonding) between the explosive charge mass per unit area  $L$ , and certain material properties and geometric factors which may be incorporated into the term  $\frac{gpc^2}{d}$ , where:

$\sigma$  = yield strength of cladding plate

$p$  = density of the cladding plate

$t$  = thickness of the cladding plate

$d$  = gap distance between the base materials, using the gap technique

$\theta$  = dynamic collision angle

This relationship may be generally expressed as:

$$L = \frac{\sigma p t}{d} \theta^2$$

It is to be noted that this relationship is not dimensionally consistent. However, it appears that it is satisfied over an appreciable range of material properties and gap distances for a specified explosive. In a more recent investigation by Hay and Kowalick<sup>14</sup>, dimensional analysis has been used to relate the process parameters by the relation:

$$L = \frac{\sigma p t}{E d} \theta^2$$

where  $E$  is the elastic modulus of the base material, and the other parameters are as defined above. This relationship is dimensionally consistent and appears to satisfy available data on explosive welding (see Figure 4).

Types of Welds and Joints. Essentially three types of welds have been accomplished with the explosive bonding process. These are seam welds, spot welds and wide area welds more commonly known as claddings. The greatest application for the process, thus far, has been associated with cladding applications in which the lower member, for example, a steel plate, has been overlaid with a thin sheet of another alloy. Usually the purpose of the cladding is to impart some specific property to the plate such as wear or corrosion resistance. Explosive spot and seam welding have been used to a much more limited extent.

$$L \propto \rho \sigma t^2 / E d$$

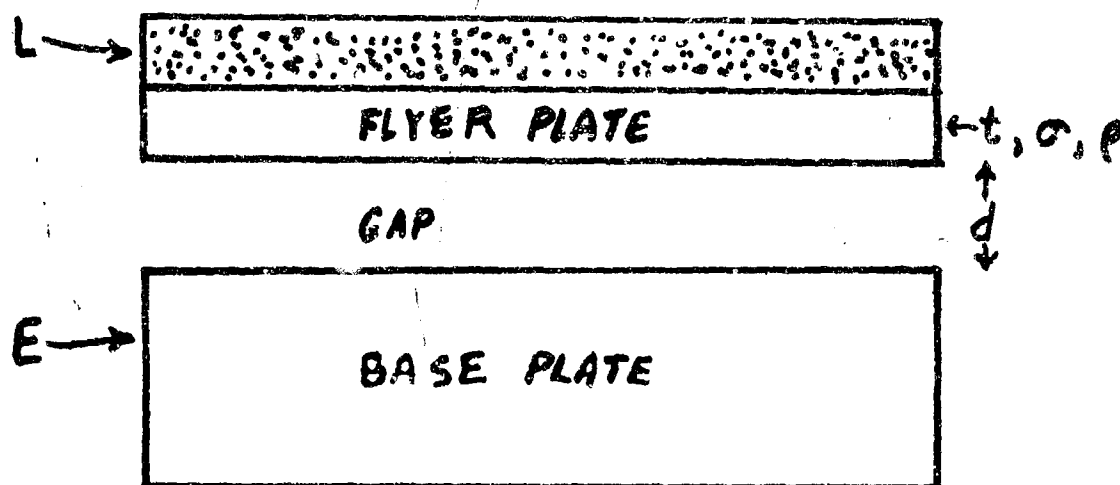


FIGURE 4. RELATIONSHIP BETWEEN GROSS PARAMETERS FOR EXPLOSIVE BONDING

Frankford Arsenal has demonstrated that all of the basic weld joints with the exception of the butt can be made with the explosive bonding process. A variety of structural materials have been bonded using lap, tee corner and edge joints. No known butt joints have been accomplished although a considerable amount of effort has been expended in this area.

Base Materials. Many base metals have been joined by explosive bonding including iron, low carbon steel, medium carbon steel and alloy steels in similar and dissimilar combinations. The process has also proved suitable for joining various combinations of aluminum, copper, beryllium, tin and magnesium alloys as well as refractory alloys and precious metals.

Explosion bonding appears to be adaptable to most metal systems except those in which the base materials have low impact resistance or low melting temperatures. It has been reported <sup>15</sup> that metals which have very low impact resistance are not usually bonded with explosives because they tend to fragment during the explosion. Also, metals with very low melting ranges have been difficult to bond with the usual explosives since there is a tendency for the metals to fuse under the high pressures generated during bonding. However, these difficulties may be overcome with further improvements in techniques and the development of new explosives with lower detonation velocities. For example, Carpenter and Otto <sup>16</sup> have recently obtained high quality explosive welds of lead, a low melting point material, to steel at ambient temperature by using a low velocity (1000 m per second) free-running dynamite, namely DuPont "Red Cross" Blasting FR dynamite.

Most explosive bonding work has been conducted on materials in the worked condition although some bonding has been performed with castings. Cladding materials ranging from a few mils to more than one inch in thickness have been bonded to backer materials ranging in thickness from less than 1/4 inch to 18 inches. The size of the welded assemblies have varied from small coupons to at least 7 feet by 20 feet. Steel forgings clad with stainless steel are used to prevent salt water corrosion. Aluminum clads are used in turbine engine applications. Nuclear power plants employ explosively bonded reactor tubes.

Advantages. The basic advantages of explosives bonding are derived from the fact that bonding depends only on the establishment of dynamic conditions for jetting and thus the restrictions to fusion and solid-state methods for welding do not apply. Some of these advantages may be listed as follows:

1. Metals with widely different melting points, thermal expansions or hardnesses can be bonded.
2. Large areas can be bonded.
3. Field fabrications can be made in inaccessible locations.
4. Thin sheets or foil can be bonded to heavy plates.
5. Heat affected zones are not produced since only a very small rise in temperature occurs during bonding.
6. Unusual geometrical configuration, welds and joints can be bonded.

#### ACKNOWLEDGEMENTS

The authors express their appreciation to Messrs. T. Q. Ciccone and I. G. Betz, of the Pitman-Dunn Research Laboratories, Frankford Arsenal, for their helpful suggestions.

# REFERENCES

1. Rolsten, R., Hunt, H. & Dean, W., AFML-TR-67-15, U. of Dayton, Contract AF 33(615)-2040 (February 1967). AD # 813605.
2. Linse, V., Wittman, R., & Carlson, R., DMIC Memorandum 225, September 15, 1967. AD # 820736
3. Addison, H. et. al., Welding Journal, American Welding Soc., 42, No. 8, (1963).
4. Addison, H., ASME paper no. 64-MD-47.
5. Cavell, W., Addison, H., & Kowalick, J., Frankford Arsenal Memorandum report (to be published).
6. Hay, D. R., and Kowalick, J. F., Select Conference on Explosive Welding, (London), (September, 1968).
7. Cavell, W. & Eves, R., Springfield Armory Report, SA-TR-1-7020, (26 february, 1963), AD # 350787.
8. Ohart, J., Major, Elements of Ammunition, J. Wiley & Sons, N. Y., (1946).
9. Abrahamson, G., J. Applied Mechanics, 519-528 (1961).
10. Crossland, B., Black, T., & Bahrahni, A., Proceedings of the Royal Society, A, 296, pp. 123-136 (1967).
11. Cowan, G., et. al., TAIME, 236, (May 1966).
12. Von Rosensteil, Zeitschrift Fur Metallkunde 55, 732-734, (1964).
13. Carpenter, S., Wittman, R., & Carbon, R., First Intl.Conf. of Center for High Energy Forming (U. of Denver), Estes Park, Colorado, (June 1967).
14. Hay, D. R., & Kowalick, J. F., Artillery Ammunition & Technology Division, AOA Meeting, Nellis A.F.B., (Sept. 1968).
15. Holtzman, A., & Cowan, G., Ordnance Magazine, (March-April, 1966).
16. Carpenter, S., & Otto, H., TAIME, 239, (November 1967).

EARLY EXPLOSION PHENOMENA

John Wisotski

Ralph E. Williams

Denver Research Institute

University of Denver  
Denver, Colorado

Presented at the Pyrotechnics Seminar

August 12 - 16, 1968

Estes Park, Colorado

#### ABSTRACT

Photographic and photometric measurements made on the detonation processes from 20 ton and 100 ton spherical TNT explosions delineate the existence of two shock waves. Total radiation measurements reveal the primary shockwave breakout from the fireball at a time correlating with the second radiation maximum. The secondary shockwave occurs when the detonation front is reflected at the charge surface. This reflected shockwave causes secondary brightening in the fireball and radiation measurements indicate a third maximum. The expansion of the fireball surface area, with time, overrides the unit radiation decay so that the total radiation from the fireball increases to the maximum (shockwave breakout). This process is repeated by the secondary shockwave. Ultra high-speed photography and rapid response pyrometry were utilized in correlating shockwave breakout with radiation intensity.

### INTRODUCTION

For a number of years there has been an interest in the early-explosion phenomena from high explosive (HE) charges. This interest was nurtured when vacuum chamber tests indicated gross variations in the piezoelectric and photoelectric data from gram-size charges. In order to better understand the results, different models were considered in the detonation process. The one chosen for consideration took into effect the detonation wave at the air-explosive boundary where whole or part continued as a shock in air, obeying the usual hydrodynamic equations. If this did occur, the motion of the expanding hot gas sphere behind this transmitted air shock would be quite different from the expansion into air that had not been shocked. In addition, there would be an effect of the rarefaction wave, if only part of the shock were transmitted into the air. If all or part of these conditions exist, the shock generation from an explosion of a sphere of explosive then would necessarily be different from that produced in a spherical shock tube.

The study of the early-time phenomena from pound-size HE explosions has been conducted by the Denver Research Institute. These early-time studies consisted of recording ultra high speed photographic, spectrographic and photoelectric data from the events during the first few milliseconds of the detonation process.

This research afforded the opportunity to acquire data from the early-time detonation phenomena of large charges. Some of the similarities as well as discrepancies between the performance of ton-size and pound-size charges were investigated in an attempt to reach a better understanding of the detonation processes. The 20-ton TNT events provided an expanded time scale of approximately 17 times the scale from an 8-pound charge. This magnification of the time scale allowed more precise measurements of early-time detonation phenomena.

#### EXPERIMENTAL PROCEDURE

The early-, intermediate- and late-time photographic and photoelectric data were recorded using high and ultra high speed cameras and oscilloscopes. These units were generally located at one position for each event at distances ranging from 945 to 1691 feet.

The early-time microsecond photographic results were obtained on colored film with a Bechman and Whitley 192 or 189A camera at framing rates of one-fourth to one-half million frames per second. Millisecond sequences, showing later-time photographs, were obtained with Dynafax cameras at framing rates of approximately 25,000 frames per second. Intermediate-time results were procured with Fastax and Eastman High Speed cameras employing a variety of filter and film combinations. Later-time fireball and cloud growth were photographed with D. B. Milliken cameras at 128 and 400 frames per second.

The photoelectric information was recorded with two four-beam oscilloscopes. The sensing devices, used to record total radiation, were silicon solar cell, photodiode and photomultipliers. A time-resolved optical pyrometer (PyI), utilizing a solar cell as a sensing element, was employed to register unit-density light output in three different radiation bands. The numerical ratios between the bands were utilized to determine temperature-time values. Another time-resolved optical pyrometer device (Mod PyI) was modified to obtain unit-area, broad-band, radiation-time information which was used to generate the total area, broad-band, radiation-time pulse as recorded by the solar cell.

## RESULTS

The results presented in this paper cover data obtained with photographic and photoelectric devices used on Events 1, 1a, 3, 5 and 6. The 20-ton TNT data from Events 1, 1a, 3 and 5 and the 100-ton TNT data from Event 6 are compared, wherever possible, to 1- and 8-pound spherical pentolite data obtained with the same recording equipment.

A general description of the experimental setups and the type of data obtained are given before the presentation of the results.

Event 1 - The charge was a 20-ton TNT sphere, 9.2 feet in diameter. It was constructed on a tower from 32.5-pound blocks of TNT. The center of the charge was located 85 feet above the ground surface. The recording devices were 1336 feet from ground zero, bearing approximately  $114^\circ$ . Most photographic results were obtained. Photoelectric data were sparse due to too high a gain.

Event 1a - The charge configuration was the same as for Event 1 with the exceptions that the center of the charge was only 29.5 feet above the ground and cradled with styrofoam instead of wood. Most recording devices were stationed at the main camera position located 1458 feet from ground zero at a bearing of  $154^\circ$ . Most photographic and photoelectric data were recorded.

Event 3 - The charge was a 20-ton TNT sphere, 9.2 feet in diameter, half buried in the ground. The recording devices were 945 feet from ground zero, bearing approximately  $136^\circ$ . Data were obtained covering all fields of interest.

Event 5 - This event was a repeat of Event 3 with the exceptions that the detonation took place under winter conditions and the devices were located 1332 feet from ground zero, bearing approximately  $180^\circ$ . All data, with the exception of one scope record containing photoelectric information were lost due to a premature detonation.

Event 6 - The charge for this event was a 100-ton TNT sphere, 15.7 feet in diameter, tangent to the ground surface and cradled with styrofoam. The recording devices were 1690 feet from ground zero at a bearing of approximately  $171^\circ$ . All photoelectric data were lost due to pretriggering. Most of the photographic data were recorded on time.

### A. Photoelectric Results

Past and present thermal measurements obtained from large HE explosions indicate that there are three distinct radiation maximums in the pulse shape. These maximums are easily recorded whenever the sensing device is a broad-band, red-sensitive unit which observes the total presented

radiation. Narrow-band, blue-sensitive sensors indicate the presence of only one maximum occurring very early in the detonation process. The lack of sensitivity in the red region of the spectrum prevents these devices from readily recording radiation at later times when the second and third maximums appear.

In order to obtain photoelectric data in different spectral regions of the radiation spectrum, an assortment of photoelectric devices were used which consisted of both wide- and narrow-band recording units, such as a silicon solar cell (SPR-08) and a photodiode (SD-100), an ultraviolet sensitive photomultiplier (1P23), a blue sensitive photomultiplier (931A), a time-resolved optical pyrometer (PyI) and a modified optical pyrometer (Mod PyI).\*

The SPR-08 solar cell and SD-100 photodiode are sensitive to a relatively broad band of radiation, 5250 to 9050  $\text{\AA}$  and 4400 to 10,600  $\text{\AA}$ , respectively. The solar cell has a response of about seven microseconds, whereas, the photodiode has a response of better than 10 nanoseconds. The SD-100 photodiode unit was calibrated with a model 580-20 EG&G radiometer so that its pulse record could be converted to the light-time output from Event 1a. Both of these devices looked at the total radiation from the detonations.

The fast response pyrometers (PyI and Mod PyI) have as sensing units the SPR-08 solar cell. The PyI's are units which focus on a unit area of the surface of the source of radiation. The unit area of coverage was variable dependent upon the distance of the device to the charge. The area of coverage for the PyI had the dimensions given by the formulas:

$$h = .00532d, \quad b = .00089d, \quad \text{where "h" is the height, "b" is the breadth and "d" is the distance from the PyI to the charge.}$$

The PyI obtained three relatively narrow band records whose peaks were at 7250, 6250 and 5550  $\text{\AA}$ . The PyI unit was calibrated to give temperature-time history from the band ratio-time values.

The Mod PyI was developed after Events 1 and 3 in order to prove that

- \* a) Silicon solar cell, manufactured by International Rectifier Company, 50% points of 5250 and 9050  $\text{\AA}$  peak at 8250  $\text{\AA}$ . Silicon solar cells were also used as sensing units in the PyI and Mod PyI.
- b) RCA Electron Tube Handbook H-B3, Photomultiplier, 1P23, S-5 response curve, 70% points, 2300 and 4500  $\text{\AA}$ , peak at 3600  $\text{\AA}$ . Photomultiplier 931A, S-4 response curve, 70% points, 4450 and 5700  $\text{\AA}$ , peak at 5100  $\text{\AA}$ .
- c) Edgerton, Germeshausen and Grier, Inc., data sheet #412, SD-100 photodiode, 50% points, 4400 and 10,600  $\text{\AA}$ , peak at 9400  $\text{\AA}$ .

the radiation-time history per unit area could be used to generate the total radiation-time record recorded by a similar sensing unit which looks at the total radiation. In order to accomplish this feat, the Mod PyI was developed as a focused device which recorded wide-band, unit-area radiation from the surface of the charge. The photomultiplier units (1P28 and 931A) were used to sense the total radiation in the ultraviolet and blue regions of the spectrum. These devices are relatively narrow-band with fast nanosecond response. The ModPyI focused on an area 50 percent greater than the PyI unit located at the same distance to the charge.

#### 1. Photoelectric Results from 1-Pound Pentolite Spheres.

Prior to participating in Events 1 and 3, tests were conducted, using 1-pound spherical pentolite charges to determine the light output response of the photoelectric devices which were to be used on the 20-ton detonations.

The silicon solar cell records of the fireball luminosity time history obtained from detonated 1-pound pentolite spheres contained three peaks, similar to those observed from present and past HE explosions. The first maximum occurred at approximately 12 usec, the second at about 150 usec, and the third (secondary brightening) at about 2.5 ms, all measured from first light.

A very simplified description of the possible steps associated with the detonation process which may cause these maximums and minimums to exist is as follows:

- a. The first peak of light is produced by the detonation front in the explosive as it passes across the air-explosive surface boundary. This peak, which radiates substantially in the ultraviolet region, because of the high temperature, decays rapidly as the initial radiating species cool. The rate of decay in temperature during this period of time is much faster than the presented area expansion of the fireball so that the total radiation decreases to the first minimum.
- b. The change in the rate of decay in temperature at about the time of the first minimum and the continued fireball expansion caused an overall increase in total radiation from this point in time until the second peak.
- c. The second peak, which follows, is near the limit of expansion of the fireball. The decay from this point follows the breakout of the main shock from the fireball.
- d. The time of third maximum is the time when the secondary brightness occurs. This brightening is thought to be caused by the reflected wave which is generated when the initial detonation

wave in the explosive comes in contact with the air-surface interface. This wave re-radiates from the center of the charge causing an acceleration in the chemical process as it passes through the fireball.

## 2. Photoelectric Results from 8-pound Pentolite Spheres

Comparisons of the photoelectric results from Events 1 and 3 to those from the detonation of 1-pound pentolite spheres indicated decided differences in the amplitude and time of the early peaks. These differences seem to infer that the point of initiation affected the density-time of the short-lived radiation species which are present in the very early stages of the detonation process. As a result, pentolite charges, which had a near-center initiation point, were cast and detonated at the East Range facility of the Denver Research Institute (DRI) for the purpose of obtaining comparable photoelectric data. Eight-pound size charges were selected for these tests in preference to the 1-pound since the exact location of the initiation was not as critical for the smaller size.

Comparisons of narrow-band and wide-band photoelectric results from Events 1 and 3 indicated the possibility of generating by other means, the pulse shape recorded by a wide-band sensor, like the solar cell, which looked at the total radiation. This assumption led to the construction of the Mod PyI unit which looked at the radiation from a fixed area of the charge. The output signal from this device was independent of the total expansion of the presented surface of the fireball. By multiplying the total presented area of the fireball by the total unit-area amplitude value recorded at the same instant of time, a wave shape was generated which was similar to the total radiation signal recorded by the solar cell. This development is shown in Figure 1. The Mod PyI signal is A, the variation in area with time is indicated by plot  $R_0^2$ , the total radiation-time signal, generated by multiplying A by  $R_0^2$  is given by the plot,  $A \times R_0^2$ . The  $R_0^2$  values were those obtained from ultra high speed pictures of the detonation of an 8-pound sphere.  $R_0^2$  values were extrapolated from 46 to 80  $\mu$  sec.

The results from the 20 and 100-ton TNT explosions scaled reasonably well to the 8-pound results.

### SUMMARY

The following provides a summary of results from the 20 and 100-ton TNT explosions.

- A. There are three maximums in the total radiation produced by an HE detonation which are easily detected by wide-band photoelectric devices.
- B. The unit radiation from an HE detonation decays exponentially.
- C. The expansion of the presented fireball surface area with time over rides the unit radiation decay so that the total radiation from the fireball increases from the first minimum toward the second maximum, at which time the main shockwave breaks out of the fireball.
- D. The total radiation decays from the second maximum to a second minimum at which time the secondary shock generates the secondary brightening; i.e., third maximum.
- E. Time-of-occurrence of the first peak as recorded by photoelectric instruments from the detonation of tone-size TNT spherical charges scale fairly well to centrally initiated 8-pound spherical pentolite charges.
- F. The peak radiation output as recorded by the solar cell compares from event to event when corrected for distance to and size of charge.
- G. The temperature-time calculations made from the measurements recorded with a time-resolved optical pyrometer on Event 1a indicate a decay in temperature from about  $6500^{\circ}\text{K}$  at 90 micro-seconds to about  $4000^{\circ}\text{K}$  at 720 microseconds, if the fireball is assumed to be a black or gray body with constant emissivity.
- H. The spectral records from the events show continuum with selective emission and absorption of atomic and molecular species.
- I. Photographic records on XR and H. S. Infrared films indicate good correlation in the times of breakout of the main and secondary shockwaves to the results obtained with wide-band photoelectric devices.
- J. Good radius-time correlation was exhibited between values calculated from ultra high speed camera measurements at 264,000 frames per second and the high speed camera measurements at 7,812 frames per second.



THE EXPLOSIVE FORMING OF METALS

by Arthur A. Ezra, Ph.D.  
Center for High Energy Forming  
University of Denver

## THE EXPLOSIVE FORMING OF METALS

by Arthur A. Ezra, Ph.D.  
Center for High Energy Forming  
University of Denver

### 1. INTRODUCTION

Explosive forming uses the short sharp energy release from the detonation of a high explosive to form a metal blank to a desired shape. A diagram of the process is shown in Figure 1, along with an identification of a number of important variables. The shock wave from the explosive in the energy transfer medium impinges on the metal blank, forcing it into a female die or over a male die. The energy transfer medium is commonly, though not exclusively, water.

The major advantage of explosive forming is the almost unlimited amount of force and energy that can be provided cheaply from chemical explosives, which are readily available, with a correspondingly low capital investment in facilities. For example, one pound of dynamite, costing a few cents, contains as much energy as a 100 ton drop hammer. Alternatively, one pound of dynamite contains about 2 million joules of energy. A capacitor bank this size would cost almost half a million dollars.

Explosive forming, therefore, shows the greatest potential economic benefits for forming limited numbers of large parts which exceed the capability of existing equipment. On the other hand, for this sort of application, there is not much room for trial and error process development, which is the basis for practically all metal forming processes. This emphasizes the necessity of being able to predict process parameters as accurately as possible, since the cost of errors can be amortized over only a few parts.

There are other advantages of explosive forming too. The charge can be shaped at will to provide the pressure distribution that is best suited for forming a given shape of part. This flexibility does not exist for most of the other sheet or plate forming processes. Limited evidence exists (1) that the attendant high strain rates can be used to provide increased ductility during forming. Care has to be taken however, to avoid excessive strain rates which can cause a decrease of ductility (Fig. 2). A good surface finish can be obtained on the formed part if stand-off operations are used under water; i.e., if the charge is placed at a distance from the metal blank, and if water is used as the energy transfer medium.

The present major drawbacks to explosive forming are the slowness of the operation, the variability of the energy release from the explosive, and the low efficiency of the process. The first problem of slowness will eventually be solved by the use of properly designed quick-release fixtures. The variability of energy release, which must be minimized if close tolerances are to be held, can be solved by the careful preparation and quality control of the explosive charge. The low efficiency which has been measured (2) of the order of 5-10%, is a more serious problem. Since the cost of explosives is low, not too much attention has been paid to this factor. However, the large percentage of unused energy (90-95%) can damage the explosive forming pool, die and fixtures, and the facilities must be designed to withstand it, thus adding indirectly to the investment costs. Contact explosives have been used for the purpose of maximizing the efficiency of energy transfer to the blank. The attendant problems of blank damage have been partially solved by using low velocity explosives, but unfortunately they show large variability in energy release. The use of low detonation velocity contact explosives was investigated by Savitt (3) using nitroguanidine under the sponsorship of the Air Force Materials Laboratory, and is also under investigation by the West German Defense Ministry.

Other techniques for increasing the efficiency of energy transfer are emerging. It has been shown by Johnson (4) that the use of an air cell between the explosive and the blank in underwater stand-off operations, will substantially increase the efficiency of energy transfer. Other devices exist which try to focus the energy from the charge on to the blank, but they have not yet been exploited (5). The growing requirements of forming large diameter thick shells of high strength steel for underwater exploration may provide the required impetus to the research needed to improve the efficiency of energy transfer for explosive forming.

The main hindrance to the exploitation of explosive forming, however, is the lack of sufficient knowledge to predict all the required process parameters without resorting to trial and error. Without this knowledge, it will not be possible to fully exploit the potential economic benefits which lie in the limited production of very large parts.

### 2. SCALING LAWS AND SUBSCALE PROCESS DEVELOPMENT

The number of variables governing the process is relatively large, and adequate mathematical models to express their interrelationships are still being developed.

If full scale trial and error were the only way to explosively form large parts, most of the potential savings from this process would be wiped out. However, the use of sub-scale models to provide full scale data is a well-known engineering technique that has been used for many years in ship and airplane design. Scaling laws and similitude requirements for valid scale model work in explosive forming were derived by the author at the Martin Company (6,7,8). This makes it possible for quick and inexpensive cut-and-try process development on a small scale to yield results that can be applied to all sizes.

The scaling law and corresponding similitude requirements that must be observed to ensure validity of the scaling law are shown below. The length scale factor is  $N$ .

Scaling Law: Weight of full scale charge =  $N^3$  x small scale charge.

Similitude Requirements:

1. Complete geometrical similitude between small and full scale.
2. Same blank material for small and full scale.
3. Same explosive type, density and shape for small and full scale.
4. Same clamping pressure for small and full scale.
5. Same coefficient of friction between blank and clamping restraints for small and full scale.
6. Full scale spring constants for die clamps and supports =  $N$  x small scale spring constants.
7. Blank material must not be appreciably strain rate sensitive.
8. Mass of full scale die =  $N^3$  x mass of small scale die.
9. Same vacuum pressure in die cavity for small and full scale.

It is usually difficult to provide exact geometrical similitude between model and full scale explosive forming pools. However, satisfaction of this similitude requirement will not be necessary if the full scale pool is large enough so that forming is complete before the shock wave returns to the die after being reflected off the walls of the pool.

Although the same material should be used for both model and prototype, there may be differences in the stress-strain relationship between model and full scale material, because the model will require sheet stock and the full scale prototype may require plate stock. Since the amount of explosive required is proportional to the strain energy of deformation, the modification to the charge size will depend on the relative areas under the stress-strain curves of the small and full scale blank materials. Experience to date with 2014-O aluminum has shown this to be a negligible factor.

Ductility differences between the model and full scale material may be accounted for in the following manner. If the model material is the less ductile of the two, there will be no scaling difficulty since a forming process that is successful with a less ductile model material will certainly be successful with a more ductile full scale material. However, if the model material is the more ductile of the two, care must be taken in developing the process to ensure that the maximum strain in the model blank is kept below the corresponding allowable value of strain for the full scale blank material.

The friction coefficient between the blank and its clamping restraints should be the same for model and full scale. However, if the clamping pressure is low, this requirement need not be precisely met.

The vacuum pressure in the die must be the same for both small and full scale. However, this is difficult to achieve and the full scale vacuum pressure should be at most less than small scale value.

The requirement for scaling the mass of the die is important only if it is a light-weight shock mounted die. A massive rigidly supported die need not obey this similitude requirement precisely, although it is easy to do so.

If the material is strain rate sensitive, then application of the scaling law without modification will overestimate the amount of explosive required for the full scale. Even if a strong enough die can be readily provided, this does not avoid the potential problem of forming at a strain rate that is higher than necessary (Fig. 2). This emphasizes the importance of related research on the effect of high strain rates on metals, so that the necessary corrections can be provided to the scaling law for strain rate sensitive materials.

An illustration of the use of scale models in explosive forming is shown in Figure 3: The 1/5 scale model dome of 2014-O aluminum 0.150 inches thick was formed with a single shot of 0.214 pounds of Composition A-3. The full scale dome of 2014-O aluminum, 0.75 inches thick was formed with 26.8 pounds of Composition A-3 in a single shot using a thin shell fiberglass die. The details of the entire process were worked out on the 1/5 scale model.

### 3. THE MECHANICS OF EXPLOSIVE FORMING

#### A. Prediction of Blank Deformation

Many attempts have been made to set up and solve mathematical models for predicting the deformation of metal blanks under blast or impulsive type loading. The incentive for some of the earlier work by Cole (9) was to use the measured deflection of a metal diaphragm as a gage to determine the explosive pressures and impulses incident on it. Attempts to simplify the mathematical description of the large dynamic plastic deformation of a blank under impulsive loading were made using the concept of a moving-plastic hinge and a rigid-plastic material (10,11,12).

The analytical work of Enhamre (13) represents a theoretical attempt at predicting the response of a circular metal plate to a blast pressure, but it is limited to the elastic range, and is thus of no value for explosive metal forming predictions.

The limited usefulness of these theoretical methods and their unsatisfactory agreement with experimental results led to a much more thorough analytical and experimental investigation by Witmer, et. al. (14,15).

Finite difference equations were derived which can be interpreted as the representation of a lumped-parameter model consisting of ring masses connected by massless frustra. The thickness of the blank is idealized by 2 discrete layers of material that can carry normal stresses in planes parallel to the surface, whereas the material between these layers cannot carry normal stress but has infinite shear rigidity. Each layer is taken to be elastic, perfectly-plastic with a strain rate dependent uniaxial yield stress, and the von Mises-Hencky yield condition and flow rule are used to solve this plane stress problem.

The finite difference equations were programmed for solution on a IBM 7094 digital computer. Experimental checks so far have shown that a proper selection of the magnitude of the strain rate dependence of the material will yield good agreement with theoretical predictions. However, this computer program is very expensive to run, and the programmed boundary conditions do not represent the flow of the flange material into the die cavity, which has a profound effect on the formability limits.

The desire to provide a simpler mathematical model and computer program better adapted to the needs of explosive metal forming led to the work by Boyd (16) and Thurston (17), which includes the effect of edge pull-in of the blank into the die cavity. Boyd (16) makes the following assumptions to come up with simplified equations of motion in an effort to obtain meaningful answers with a minimum of computations:

1. Small finite deflection theory is used in the derivation. This assumption is the most restrictive one and limits the validity of the results to shallow draw depths.
2. Bending strains are neglected to give a membrane theory.
3. Radial inertia terms are neglected in the equations of motion.
4. Elastic strains are neglected compared to plastic strain components. Deformation theory of plasticity is used with a power law effective stress - effective strain relation for the material as follows:

$$\bar{\sigma} = K \bar{\epsilon}^n$$

where  $\bar{\sigma}$ , the effective stress =  $\left[ \sigma_r^2 - \sigma_r \sigma_\theta + \sigma_\theta^2 \right]^{1/2}$

$\bar{\epsilon}$ , the effective strain =  $\frac{2}{\sqrt{3}} \left[ \epsilon_r^2 + \epsilon_r \epsilon_\theta + \epsilon_\theta^2 \right]^{1/2}$

$\epsilon_r$ , the radial strain =  $\frac{2u}{r} + \frac{1}{2} \left( \frac{dw}{dr} \right)^2$

$\epsilon_\theta$ , the circumferential strain or hoop strain =  $\frac{u}{r}$

$u$  = the radial displacement of a point on the blank

$w$  = the vertical displacement of a point on the blank.

The equations of motion are as follows:

$$\frac{\epsilon_0 - \epsilon_r}{h} - \left[ 2 + \frac{2}{3}(n-1)A_n^2 \right] \frac{\partial \epsilon_r}{\partial h} - \left[ 1 + \frac{2}{3}(n-1)A_n A_0 \right] \frac{\partial \epsilon_0}{\partial h} = 0$$

where 
$$\frac{\partial^2 w}{\partial t^2} = \frac{p}{\rho h} \left( 1 + \frac{u}{h} \right) \left( 1 + \frac{\partial u}{\partial h} \right) + \frac{2K}{3\rho} \frac{\partial}{\partial h} \left[ h A_n \bar{\epsilon} \frac{\partial u}{\partial h} \right]$$

$$A_r = \frac{3}{2} \bar{\epsilon} \left( \frac{\partial \bar{\epsilon}}{\partial \epsilon_r} \right) = 2\epsilon_r + \epsilon_0$$

$$A_0 = \frac{3}{2} \bar{\epsilon} \left( \frac{\partial \bar{\epsilon}}{\partial \epsilon_0} \right) = 2\epsilon_0 + \epsilon_r$$

$p$  = pressure normal to the blank surface.

$\rho$  = density of blank material.

$r$  = radial distance from center of blank.

$t$  = time.

Replacing the strain terms in the equations of motion by their relationship in terms of  $u$  and  $w$  we get two non-linear partial differential equations with  $u$  and  $w$  as the unknowns. Thurston (17) uses Newton's method in getting a numerical solution to the equations of motion, using specified amounts of edge pull-in. A typical example of the results he obtains is shown in Fig. 4, taken from (17).

It is difficult to compare theoretical predictions of blank deformation with experimental results because of the uncertainty in specifying the pressure-time history of the explosive pressure on the blanks. Published results on pressure-time histories and impulses from underwater explosions (9) are based on free field measurements. The motion of the blanks causes a rarefaction wave to move off its surface which in turn interacts with the pressure pulse. This rarefaction wave can be strong enough to cause cavitation, and this has been observed in some high speed photographs of blank motion (18). It is also possible that the gas bubble from the underwater explosion can contribute to the forming operation. Another complication is the effect of water head. Johnson has shown (19) that the head of water above a charge, strongly influences the efficiency of the energy transfer.

Another uncertainty underlying the analytical prediction of blank deformation is the unknown constitutive equation of the blank material at high strain rates. It has been established by many investigators that the stress-strain relationships of metals at high strain rates differ from those obtained at slow strain rates. Quantitative results for stress-strain relationships at the high strain rates characteristic of explosive forming, are lacking, and it is not known whether the plastic strain energy of deformation for large strains differs markedly at high strain rates from the corresponding values at low strain rates. Wittmer (14,15) shows that good agreement between theory and experiment can be obtained with properly chosen numerical values for the strain-rate effects. The strain rates characteristic of the explosive forming process can range from 100 to 1000  $\text{sec}^{-1}$ . It is quite difficult to determine experimentally stress-strain relationships at these strain rates, though active research is being conducted in this area. It can be seen, therefore, that considerable progress needs to be made towards predicting pressure-time histories on explosively formed blanks and towards specifying bi-axial stress-strain relationships at high strain rates before conclusions can be drawn regarding the validity of any one method of predicting blank deformations. A first step should be made by conducting a carefully controlled set of experiments where metal blanks of materials which are not appreciably strain-rate sensitive are deformed under impulsive loads which have a duration that is short compared to the duration of blank motion.

#### B. Formability Limits.

Formability limits provide advance information on whether a blank of a particular material, size, and thickness can be explosively formed to a desired shape without failure. To understand and control the factors governing formability, the failure modes must be defined and understood. There are three failure modes: tearing, buckling and uneven pull.

The tearing mode of failure is shown in Fig. 5. This occurs when the maximum strain exceeds the ultimate elongation of the material. Actually, the uniform elongation or the strain at onset of necking, is a much more useful criterion for metal forming. At present time, it is not possible to predict this value for a given material under explosive forming conditions from the results of a conventional uniaxial tensile test at a low rate of strain. The strain at onset of necking depends on the state of stress, the rate of strain, and possibly even the magnitude and duration of the forming pressure. The effect of strain rate on uniform elongation is shown in Fig. 2, and it can be seen that both decreased and increased ductility can be obtained, depending on the strain rate. The ability to predict the strain rate is therefore a valuable asset, and this provides yet another justification for research in the analytical prediction of blank deformation. The ability to predict ductility under a biaxial stress state from the results of a uniaxial tensile test is a universal metal forming problem, not restricted to explosive forming alone. Equating the octahedral shear stress in a uniaxial test specimen at the onset of necking to the octahedral shear stress in a one-to-one biaxial stress state will give a predicted value of surface strain at onset of necking that is one half the uniaxial value. There is much experimental evidence (19) to show that more ductility is obtained in the biaxial deformation of sheet metal rather than less. The theoretical predictions of biaxial ductility from uniaxial values in reference (19) show better agreement with experimental results, but the theoretical basis of these predictions is not rigorous. What is needed is the ability to predict accurately the biaxial ductility from measurements of uniaxial values, as a function of state of stress and strain rate. If the duration of the explosive pressure is comparable to the duration of forming, it is conceivable that the Bridgman effect of increased ductility under high hydrostatic pressure could occur. This, however, is a speculation and conclusive experiments have yet to be conducted. There is some basis, however, for this speculation in the recent unpublished results of explosive forming work at the Technical Metal Working Institute in Holland by van Wely, and similar experiments at the MAK Co. in Kiel by Nemitz. They found in metal forming experiments with contact explosives, that high detonation velocity explosives ruptured the metal blanks while low detonation velocity explosives formed them successfully.

The buckling mode of failure is shown in Fig. 6, and occurs when the blank is too thin for the diameter of part to be formed. With an increase of blank thickness, buckles in the part may disappear, while wrinkles remain in the flange. This is shown in Fig. 7. For deeper draws the flange wrinkles will in turn lead to uneven draw of the blank as shown in Fig. 8.

Flange wrinkling can be eliminated by increasing the stiffness and/or hold down pressure of the clamps. However, even though flange wrinkling can be cured by this method, instability or uneven draw can still occur as shown in Fig. 9.

Until satisfactory mathematical models become available for prediction, these problems can be avoided by the experimental construction of formability limits using sub-scale models. Examples of formability limits developed, using sub-scale models are shown in Figures 10 to 16, for the following six materials: 2014-O aluminum alloy, 7039-O aluminum alloy, 18 percent Ni Maraging steel, 12Ni-5Cr-3Mo Annealed Maraging steel, 9Ni-4Co Annealed Maraging steel, annealed D6AC steel. (These are taken from unpublished results of the Martin Company under AF Contract AF 33(615)3167, Advanced Explosive Forming Processes, sponsored by AF Materials Laboratory, Wright Field).

These formability limit curves are used as follows. All points below the curves represent combinations of draw depth ratios and die diameter to blank thickness ratios that can be successfully formed without buckling, tearing, or instability, provided the charge is centered carefully, and a stand-off distance of 1/6 the diameter of the die opening is used. While TWT was used to develop these curves, they are not restricted to this explosive, since formability is much more heavily dependent on material properties and geometry. The formability limits for 2014-O aluminum were developed using a clamping arrangement that was not very stiff and reliance was therefore placed on holddown pressure. When this curve is used for a different size of die, care must be taken to keep the value of the parameter  $f/D^2$  the same for all die sizes, where  $f$  is the total clamping force on the flange,  $\sigma$  is the yield stress of the blank material, and  $D$  is the diameter of the die opening.

The remaining formability limit curves (Figures 11-16) were developed using a die with a six inch diameter opening and a very stiff clamping arrangement. When applying these results to different size of die, care must be taken to scale up the clamp stiffness shown in the figures by the factor  $1/6 \times \text{diameter of the die opening in inches}$ . The clamping force should be scaled up by the square of this factor. For example, a 12 inch diameter die will require a clamp stiffness which is twice as stiff and a holddown force four times as great as the value shown in these figures.

The combinations of clamp stiffness and holddown force shown in Figures 11 to 16 are not unique. Different combinations of clamp stiffness and holddown pressure may be found that will maintain formability. In general, a lower clamp stiffness will require increased holddown force to prevent flange wrinkling and vice-versa. The advantage of using high clamp stiffness and low holddown force is that the blank material will flow more easily into the die opening.

At the present time, the fastest and surest way to determine required clamp stiffness and holddown force is by means of carefully scaled model tests. The same is true for finding the minimum blank width to diameter ratio (B/D) to ensure against uneven blank pull.

In general, it can be said that if flange wrinkling occurs, it can be prevented by either increasing the blank thickness, or increasing the stiffness (or number) of holddown clamps. If uneven pull occurs, use a larger blank, or decrease the stand-off distance, i.e., the distance between the charge and the blank. The latter method stretches the blank more during forming, and hence pulls it in by a lesser amount.

#### 4. EFFECT ON EXPLOSIVE FORMING ON MATERIAL BEHAVIOR

The high pressure and strain rates that occur in the explosive forming process can cause the material to behave differently during forming, and can change the material properties permanently afterwards.

The effect of velocity of deformation on material ductility is illustrated in Fig. 2. It can be seen that both increased ductility and decreased ductility may be caused by the velocity of forming, and that it is possible to exploit the former while avoiding the latter.

Permanent changes in material properties can also be brought about by explosive deformation. Like ductility, they can be either adverse or beneficial. The susceptibility of explosively formed parts to stress corrosion has been questioned. Work done by C. A. Verbraak (21) shows that explosively formed stainless steel exhibits an increased susceptibility to stress corrosion. Investigations conducted by the National Aeronautics and Space Administration's Marshall Space Flight Center at Huntsville, Alabama, show increased stress corrosion in explosively formed 311 stainless steel, but no increase in stress corrosion in explosively formed 2014 and 2219 aluminum alloys. Results of Martin Company investigations have shown no adverse stress corrosion effects in explosively formed 2014-O aluminum alloy.

Some recent work by Verbraak at the Technical Metalworking Institute in Holland suggests that most of the microstructural damage leading to increased stress corrosion is caused by impact of the blank with the die surface. His experiments show a decrease in susceptibility to stress corrosion when a plastic die rather than a steel die is used.

Without testing, there is not enough information to predict whether a particular material will suffer increased stress corrosion after being explosively formed. In view of the present state of knowledge, any load-bearing part formed by either conventional methods or by explosive forming should be checked to determine its resistance to stress corrosion. Good explosive-forming practice requires a minimum amount of explosive to form a part, and subscale process development makes it possible to determine the minimum amount needed. Larger amounts of explosives than necessary may still form the part to the required dimensions and tolerances, but will most certainly cause microstructural damage.

The explosive forming process can increase the strength of the material being formed. Results of experiments on 2014-O aluminum at the Martin Company, show that the material after forming, solution heat treating and aging to the T-6 condition, exhibits strengths about 5% higher than normal. Normal standoff forming operations under water provide incident pressures of the order of 100,000 psi, whereas the use of contact explosives will raise this pressure level by an order of magnitude. At these higher levels, there is a much more pronounced strengthening and hardening effect and the existing results of shock hardening research which have been done at these higher levels, may prove applicable.

#### 5. CHOICE OF EXPLOSIVE

The desired qualities in an explosive used for metal forming are the following:

- a. The explosive must be safe during handling and placing.
- b. The energy released should be consistent, i.e., all charges of the same weight should release the same energy upon detonation.
- c. It should be able to hold its shape without the necessity of enclosing it in a container, since the fragmentation of a container disturbs the uniformity of the shock wave and may cause the metal blank to draw in a non-uniform manner.
- d. The charges should not absorb moisture and should not deteriorate under exposure to direct sunlight over a period of at least four hours.
- e. It must be possible to press it or cast it to a consistent density.

- f. The charge should not absorb moisture and should detonate readily under water.
- g. The charge should be inexpensive.
- h. The charge should be readily available, i.e., should preferably be a standard brand of explosive.
- i. It should be possible to detonate it readily under water with a blasting cap alone, without the necessity of adding a booster to initiate detonation.

The first and last requirements tend to be contradictory since the harder a charge is to detonate, the safer it is. Two explosives that meet all the above requirements are pentolite and Composition A-3. The advantage of Composition A-3 is that it can be pressed to a consistent density at 10,000 psi under vacuum. Small scale charges can be readily made up on demand to any size required. However, it requires a large press and elaborate facilities for preparing large charges. Pentolite on the other hand can be readily cast to a consistent density in large charges without elaborate facilities. However, it must be cast hot, and it is quite sensitive and therefore dangerous to handle while molten. Small scale charges, therefore, cannot be readily cast to any required size without some delay.

It may be that the newer cold cast explosives that are becoming available may combine the advantages of both pentolite and Composition A-3. This has yet to be investigated.

Composition C-4 has been used to explosively form large domes, such as the end-closures for Sea Lab II. However, it is practically impossible to control the density of this charge, and hence expect a consistent energy release. It must also be enclosed in a container, which then disturbs the uniformity of the shock wave when it shatters, tending to cause a non-uniform draw.

Primacord has been extensively used in explosive forming. However, it is not well suited to the assembly of large charges (20 pounds or more) and is difficult to position accurately. When explosively forming domes, a ring of primacord causes much more metal stretch at the center than an equal amount of the identical explosive placed centrally over the metal blank.

When small scale models are used to develop the process, the importance of not having to use a booster along with a cap for detonation becomes readily apparent, since the contribution of the booster and cap to the total energy release from the small scale charge is not negligible. This causes inaccuracies when scaling up to the full size charge.

It is therefore not possible at the present time to say what the "best" choice of explosive is for metalworking. Future experience will narrow down the choice, and it may well be that the choice of a particular explosive will be related to the type of metal it is required to form.

## 6. THE EFFECT OF STAND-OFF DISTANCE

The distribution of incident pressure on the blank strongly influences the ease of forming and the efficiency of the process. It can be varied by changing the shape of the explosive charge or by changing the stand-off distance.

The stand-off distance is the easiest thing to alter. The effect of stand-off distance on the free formed shape of a metal blank is shown in Fig. 17. The effect of stand-off distance on the magnitude and distribution of radial strains is shown in Figs. 18 and 19. It will be seen that an L/D ratio of 0.25 will produce the lowest and most uniform distribution of radial strains, and the lowest circumferential strain for most of the formed part. However, there is a correspondingly large edge pull-in which can cause the blank to draw unevenly. An L/D ratio of 1/6 produces strains that are almost as low, but pulls in the blank much less, thus avoiding problems of uneven pull. A stand-off distance ratio of 1/6 is a good compromise value to use for explosive forming operations.

## 7. DIES FOR EXPLOSIVE FORMING

In the explosive forming process, matched male and female dies are not necessary. A female die alone will do the job, with the incident shock wave from the explosive acting as the male die. Many kinds of dies have been used in explosive forming, male, female and open bottom dies (Fig. 20). The open bottom dies are good research tools permitting an observation of the blank deformation process under the action of the incident shock wave. Male dies are less frequently used because explosive forming is usually done under water, and the blank must be free to deform the die contour without resistance to motion which would be caused by water between the blank and the die.

Female dies are generally used since the die cavity can easily be evacuated (usually to an air pressure of less than 3 mm Hg) to permit the metal blank to move freely into it.

Dies for explosive forming have been made of many different kinds of material. Some examples are cast steel, meehanite, kirkite, concrete, epoxy lined concrete, concrete encased in a steel shell, Fiberglas, etc. An example of a low cost thin shell Fiberglas and steel die is shown in Fig. 21.

The holddown mechanism is extremely important since it has to ensure uniform draw, avoid buckling in the flange and at the same time permit the blank material to flow into the die. Its effect on formability has been explained previously. Hydraulic holddowns are popular because of the very large clamping pressures they can exert. They are expensive, and the hydraulic fluid lines have to be protected from blast wave pressures. Bolts and C-clamps are cheaper and do not need much protection from the explosive pressures. On the other hand, the clamping forces they can provide are restricted and they require considerably longer times for clamping and release. In either case general analytical relationships between the required stiffness of holddown, clamping pressure, material thickness and material properties have yet to be established. Limited empirical data have been derived from previous experience and knowledge is steadily increasing.

The die is the largest single item of expenditure in the explosive forming process, and an overdesign can cancel the potential economic benefits. On the other hand, the die must obviously be strong enough to serve its purpose.

At the present time a complete satisfactory set of design criteria for explosive forming dies does not exist. Partial criteria have been developed based on the modes of failure that have been experienced and they are presented here.

1. Sharp corners must be avoided. Oblique shock waves in the body of the die reflect off the die boundaries as rarefaction waves. If two rarefaction waves intersect in a corner, failure will result. This is shown schematically in Fig. 22.
2. Most die failures have occurred with the final sizing shot, when the blank has almost conformed to the die surface, and therefore cannot provide much cushioning action against the shock. A limit therefore has to be set on the maximum sizing shot permitted in a die. This has to be determined on the basis of how much explosive charge can be detonated inside the die cavity without die failure and without relying on the cushioning action of the blank. Scale model tests to destruction are perhaps the most reliable way of doing this, or approximate analyses using pressures and impulses given by standard empirical formulae for underwater explosions.
3. If the die is a lightweight, thin shell, spring and damper mounted die (as in Fig. 21), the shell enclosing the die cavity can buckle under the water pressure caused by movement of the die through the water. Also, in this case the bolts connecting the thin shell die body to the draw ring may be sheared due to shell deformation caused by this water pressure. A thin shell buckling analysis is therefore necessary. The design philosophy behind this kind of a die is that it merely keeps the water out of the way to permit the metal blank to deform freely under explosive forces. With this kind of a die, it is therefore mandatory to shape to incident shock wave so as to bring the blank to its final shape with the very minimum impact of the blank on the surface of the die.

Nevertheless, the impact of the blank on the thin shell die is another source of die failure, and the die must be designed to withstand this force. Because of the complexities in the analyses, the most practical method at the present time is to design the die experimentally on a small scale, relying on a cut-and-try procedure to arrive at a configuration that works. The resulting dimensions and details can then be scaled up to any size with confidence.

## 8. EXPLOSIVE FORMING POOLS

Water is a much more efficient energy transfer medium than air. Since it is cheap and readily available, it is the most popular medium in the practice of explosive forming.

Any body of water will be a satisfactory pool for explosive forming, provided it is large enough or has strong enough walls so that the shock wave from the exploding charge will not damage them.

Cylindrical tanks have been used quite often as explosive forming pools by a number of aerospace agencies or companies, e.g., North American Aviation, Aerojet General, The Marshall Space Flight Center, Lockheed. In these cases, the walls have to be strong enough to withstand the reflected shock, or ingenious techniques such as a bubble curtain have been used.

The bubble curtain concept was originated by Lockheed, and has also been used by the Martin Company and the Marshall Space Flight Center. It consists of an annulus made of a perforated pipe, surrounding the die, or placed at the walls of the cylindrical pool. A stream of compressed air is pumped through the perforation. The resulting bubble curtain attenuates the shock wave as it passes through the bubble curtain on its way to the walls of the pool.

Another technique for reducing the strength of the reflected shock is to use sloping walls as shown in the Martin Company Explosive Forming Pool in Fig. 23. This pool is 105 feet in diameter and is 30 feet deep in the middle. A dolly on an inclined track lowers the explosive forming die to the top of the concrete pad at the bottom of the pool. A bubble curtain in the form of a perforated pipe surrounds the draw ring of the die. A 26.8 pound explosion of Composition A-3 in this pool is shown in Fig. 24. This explosion was used to form a 10 foot diameter dome of 2014-O aluminum with an ellipsoidal shape to draw a depth ratio of 0.39.

The inclined walls of this pool are made of six inch thick reinforced concrete with a rubber membrane over its surface. However, a pool of comparable size (80 feet) has been used by Lockheed, with sloping dirt walls lined with a waterproof membrane of polyethylene. A charge of 14 pounds of RDX primacord has been fired in the Lockheed pool with no adverse effects.

The San Francisco Naval Shipyard has used San Francisco Bay as an explosive forming pool. A hundred pound charge of Composition C-4 was used to form the 12 foot diameter steel end closure of Sea Lab II in a massive concrete die, which was suspended by a crane over the end of a pier.

It can be seen, therefore, that explosive forming pools can take many forms, the only requirement being that they withstand the force of the explosive charge without damage. It is important to be able to predict this, and design criteria need to be developed relating the explosive charge in the pool to the structural characteristics of its walls.

#### 9. APPLICATIONS OF EXPLOSIVE FORMING

Used in the proper places, explosive forming is a powerful and economical extension of conventional metal forming processes. Many useful applications have been found for it, and a number of typical examples are shown in Figs. 25-29.

#### 10. RECOMMENDATIONS FOR FUTURE RESEARCH

Research is more important to the future of explosive forming than perhaps for any other high energy rate forming process, but not because it is more complicated. It is because the greatest potential economic benefits occur in the forming of the largest size of parts - where the fewest mistakes can be tolerated for economic reasons. Large parts can be undertaken today most economically on the basis of small scale cut-and-try process development with extrapolation to full scale by means of scaling laws. However, in order to optimize the process it is necessary to be able to predict theoretically the full scale process parameters and the costs fairly accurately.

A summary is provided below in tabular form indicating the research problems that need to be undertaken, and their relationship to the different parameters of the explosive forming process. Some of the research programs are already under way, e.g., items 5, 6, 7, 13, at the Center for High Energy Forming at Denver, Colorado, a joint effort between the University of Denver and the Martin Company, sponsored by A.R.P.A. (Advanced Research Projects Agency) and monitored by U.S. A.M.R.A. (United States Army Materials Research Agency). Most of these research problems apply equally well to all types of high energy rate forming, the major exceptions being items 1, 2, 3 and 4.

A coordinated research program as summarized in the table, advancing simultaneously on all fronts, would reduce explosive forming, before too long, to a routine predictable manufacturing process.

SUMMARY OF NECESSARY RESEARCH AND DEVELOPMENT PROBLEMS  
RELATED TO PROCESS PARAMETERS FOR HIGH ENERGY RATE FORMING

Research and Development	Energy Requirements Type - Size - Shape	Number of Shots and Intermediate Anneals	Determination of Formability Limits	Design of Dies and Accessory Equipment	Pool Requirements	Economics of Process
1. Consistency of Energy Yield	X	X				
2. Prediction of Pressure Time History on Moving Blank	X	X				
3. Increased Efficiency of Energy Transfer	X			X	X	X
4. Effect of Water Head on Energy Transfer	X				X	X
5. Effect of bi-axial stress, high strain rates and pressures on ductility of metal blank		X	X	X		X
6. Prediction of large dy- namic plastic deformation of blanks with moving boundaries	X	X		X		X
7. Stress-strain relation- ships at high strain rates	X	X		X		X
8. Prediction of Spring back		X		X		X
9. Analysis of flange wrinkling		X	X	X		X
10. Analysis of blank buckling		X	X	X		X
11. Analysis of blank instability (uneven pull)	X	X	X	X		
12. Forming techniques for thin blanks		X		X		X
13. Effect of forming on Material Properties, e.g., changed heat treat, stress corrosion, fatigue life, etc.		X		X		X
14. Determination of die loads				X	X	X
15. Quick blank placement and release techniques				X		X
16. Low cost dies				X		X

#### BIBLIOGRAPHY

1. Wood, W. W., "Increased Formability", Product Engineering, Sept. 30, 1963.
2. Johnson, W. and Sowerby, R., "Experiments on Clamped Circular Blanks Subject to Underwater Explosive Charge", Proceedings of the Institution of Mechanical Engineers, 1964-65, Vol. 179, Part 1, No. 7.
3. Savitt, J. and Conover, R. E., "Final Report on Direct Contact Detonation Explosives Metalforming", Technical Report NR-AFML-TR-65-422; Dec. 1965.
4. Ezra, A. A., "The Development of Scaling Laws for Explosive Forming", Experimental Mechanics, August 1962.
5. Filler, W. S., "Measurements on the Blast Wave in a Conical Tube", The Physics of Fluids, Vol. 3, No. 3, May-June 1960.
6. Ezra, A. A., "Scaling Laws and Similitude Requirements for Valid Scale Model Work", A.S.M.E. Colloquium on Scale Modelling, Dec. 1963.
7. Ezra, A. A., "The Use of Scale Models in Explosive Forming", International Symposium on High Energy Rate Forming, Prague, Czechoslovakia, Sept. 1966.
8. Johnson, W., "A Review of Some Experiments in, and Efficiency Considerations of High Rate Forming", International Symposium on High Energy Rate Forming, Prague, Czechoslovakia, Sept. 1966.
9. Cole, R. H., "Underwater Explosions", Princeton University Press, Princeton, New Jersey, 1948.
10. Wang, A. J., "Permanent Deflection of a Plastic Plate Under Blast Loading", Journal of Applied Mechanics, Vol. 22, pp. 375-376, 1955.
11. Hudson, G. E., "Theory of the Dynamic Plastic Deformation of a Thin Diaphragm", Journal of Applied Physics, Vol. 22, No. 1, page 1, 1951.
12. Wang, A. J., and Hopkins, H. G., "On the Plastic Deformation of Built-In Circular Plates Under Impulsive Load", Journal of the Mechanics and Physics of Solids, Vol. 3, pp. 22-37, 1954.
13. Enhamre, E., "Effects of Underwater Explosions on Elastic Structures in Water", Bulletin No. 42 of the Institution of Hydraulics of the Royal Institute of Technology, Stockholm, Sweden.
14. Witmer, E. A., Balmer, H. A., Leech, J. W., and Pian, T. H. H., "Large Dynamic Deformations of Beams, Rings, Plates and Shells", A.I.A.A. Journal, Vol. 1, No. 8, pp. 1848-1957; 1963.
15. Witmer, E. A., Balmer, H. A., and Clark, E. N., "Experimental and Theoretical Studies of Explosive-Induced Large Dynamic and Permanent Deformations of Simple Structures", Presented at the S.E.S.A. Spring Meeting, Denver, Colorado, May 5-7, 1965.
16. Boyd, D., "Dynamic Deformation of Circular Membranes", Journal of the Engineering Mechanics Division, Proceedings of the A.S.C.E., Vol. 92, No. EM 3, June 1966.
17. Thurston, G. A., "On the Effects of Edge Pull-In on the Explosive Forming of Domes", Proceedings of the Seventh International Machine Tool Design and Research Conference, Sept. 12-16, 1966, Pergamon Press.

18. van Wely, F. E., "Explosive Forming", Presented at the International Symposium on High Energy Rate Forming, Prague, Czechoslovakia, Sept. 1966.
19. Johnson, W., et. al., "Some Contributions to High Rate Sheet Metal Forming", Proceedings of the Fourth International Machine Tool Design and Research Conference, Sept. 1963.
20. Foral, R., "The Stability of An Annular Plate of Strain Hardening Material", Report SR-0530-3-18, The Martin Company, Denver, Colorado.
21. Verbraak, C. A., "Explosive Forming Can Cause Problems", Metals Progress, Jan. 1963.

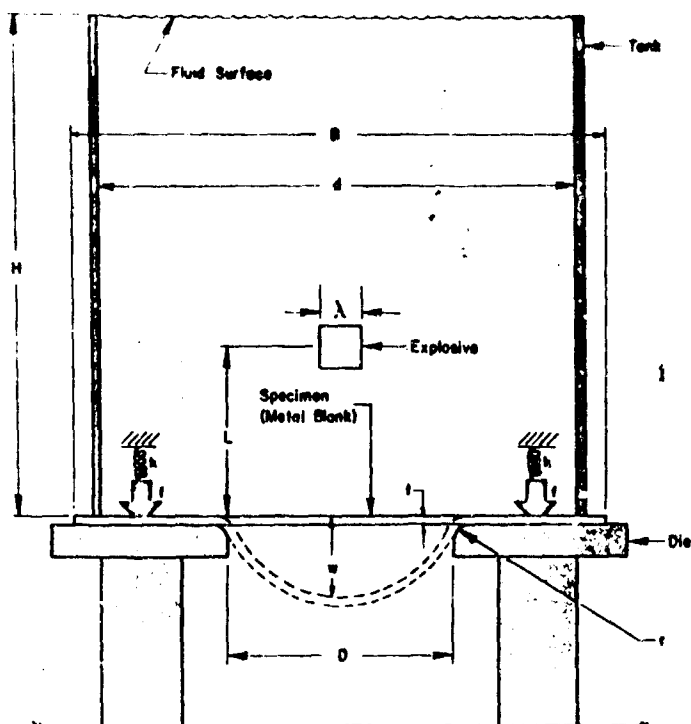


Fig. 1 Assembly for Explosive Forming

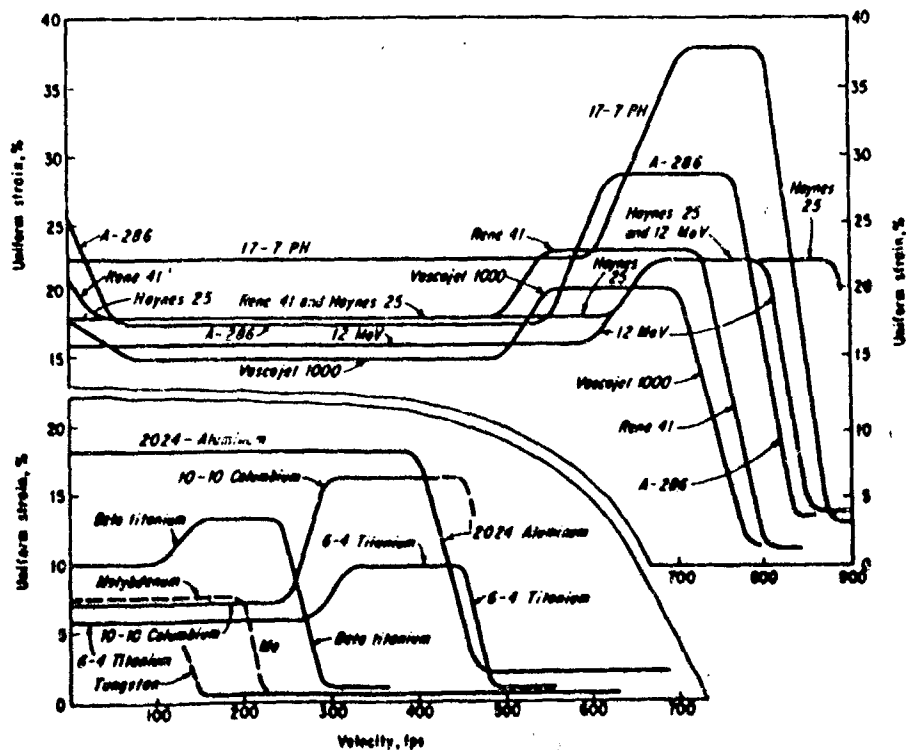


Fig. 2 Effect of Velocity on Dome Bulging.

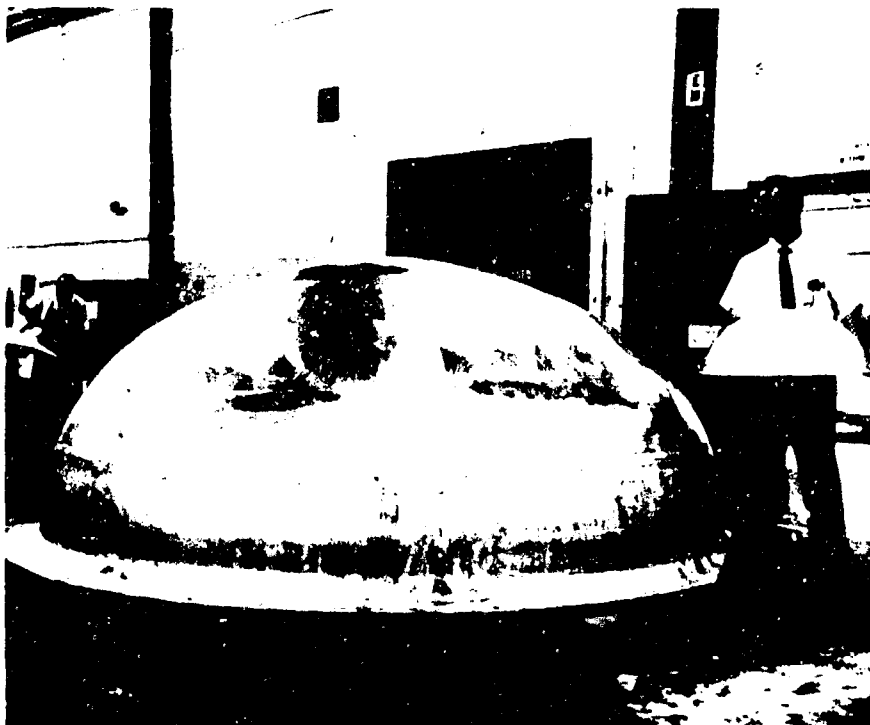


Fig. 3 Verification of Scaling Law for Explosive Forming.

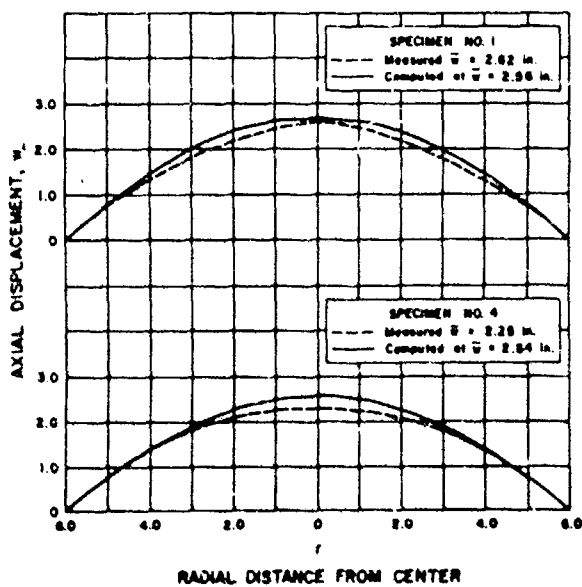


Fig. 4 Comparison of Predicted Deflection with Measured Values Including the Effect of Edge Pull-in.



Fig. 5 Tearing Mode of Failure



Fig. 6 Buckling Mode of Failure



Fig. 7 Flange Wrinkling



Fig. 8 Uneven Draw Due to Flange Wrinkling.



Fig. 9 Uneven Blank Draw.

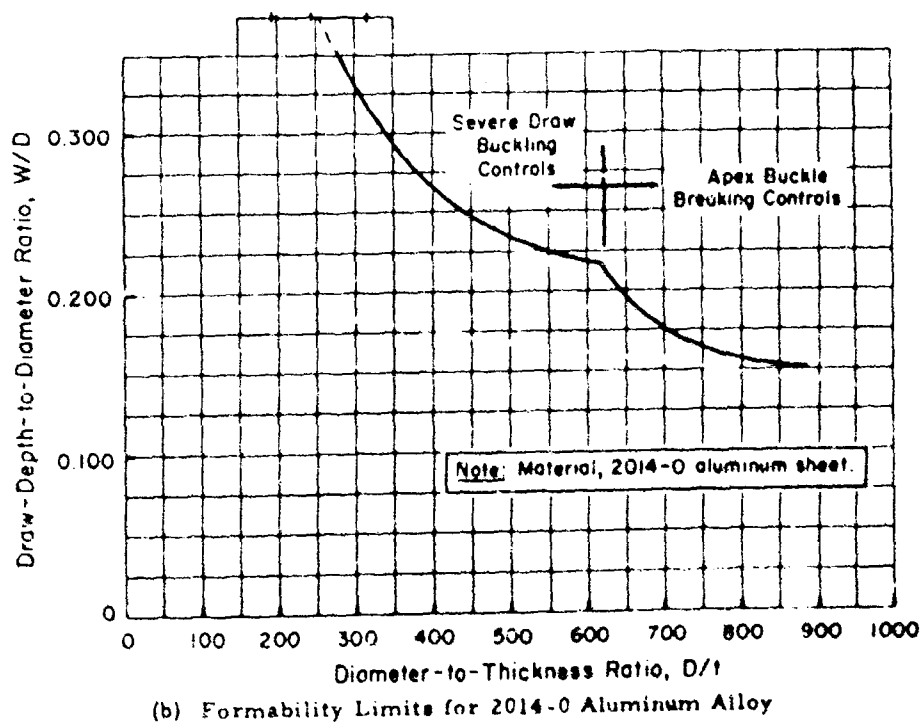
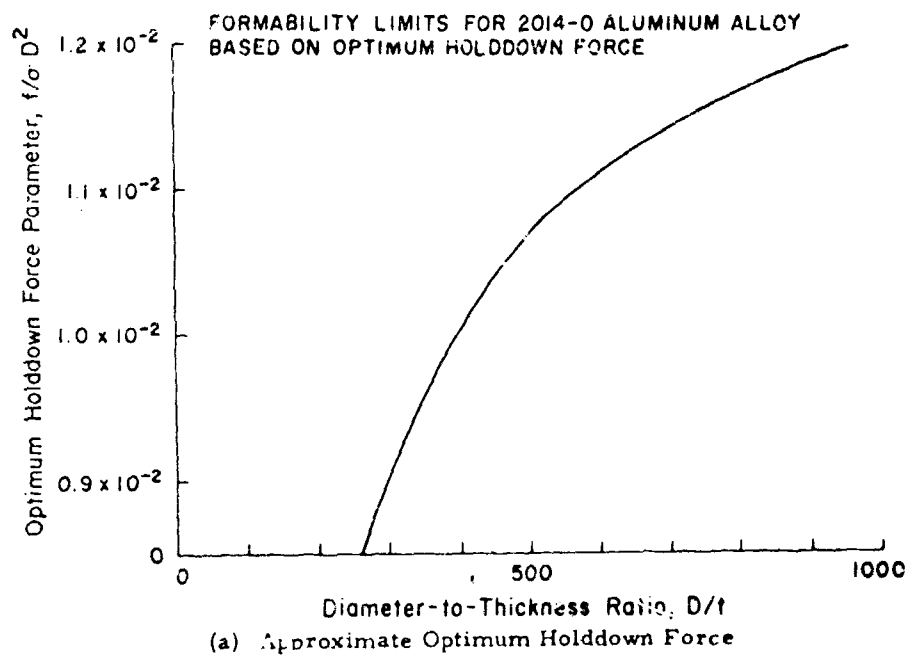


Figure 10. Formability Limits for 2014-0 Aluminum Alloy ( $B/D = 1.4$ )

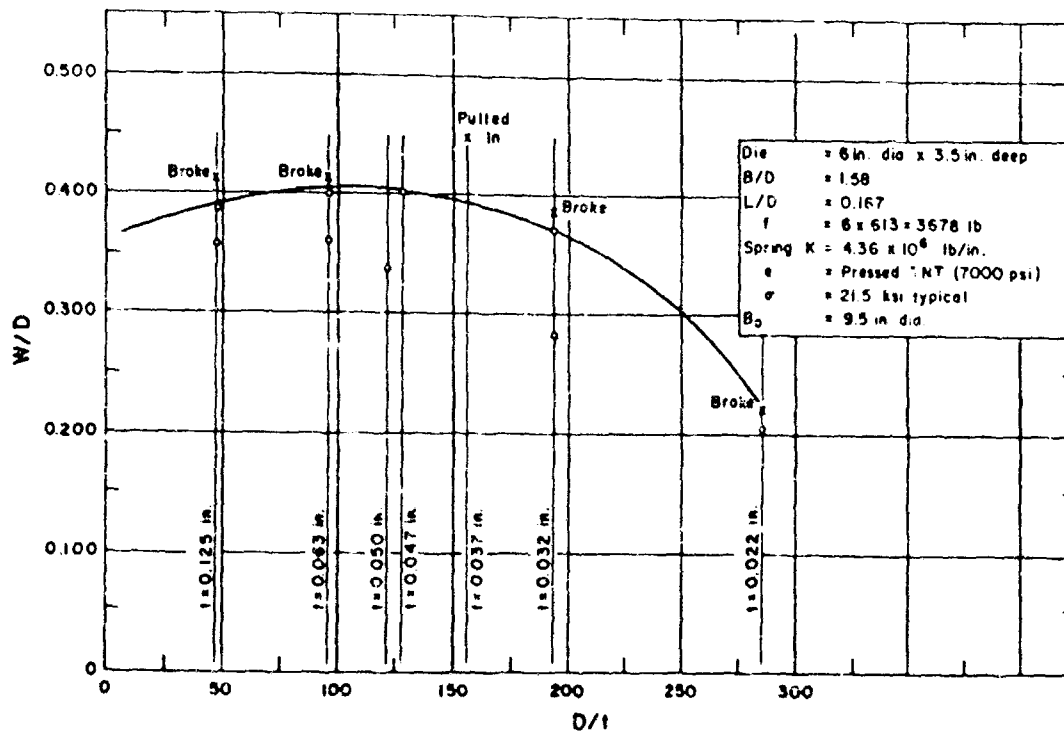


Fig. 11 Formability Limits for 7039-O Aluminum Alloy (R/D = 1.58).

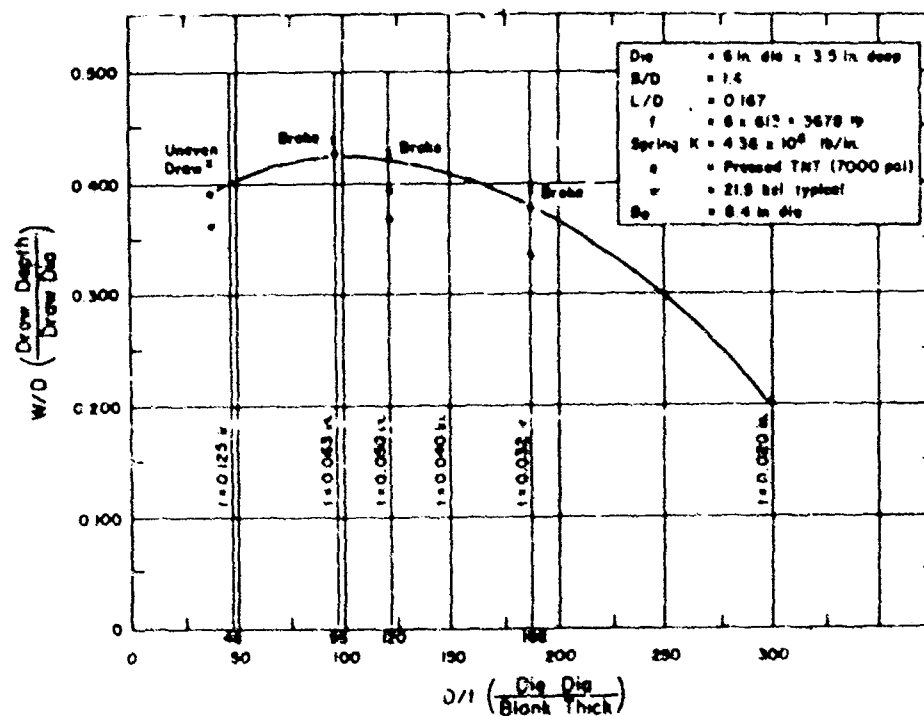


Fig. 12 Formability Limits for 7039-O Aluminum Alloy (R/D = 1.40).

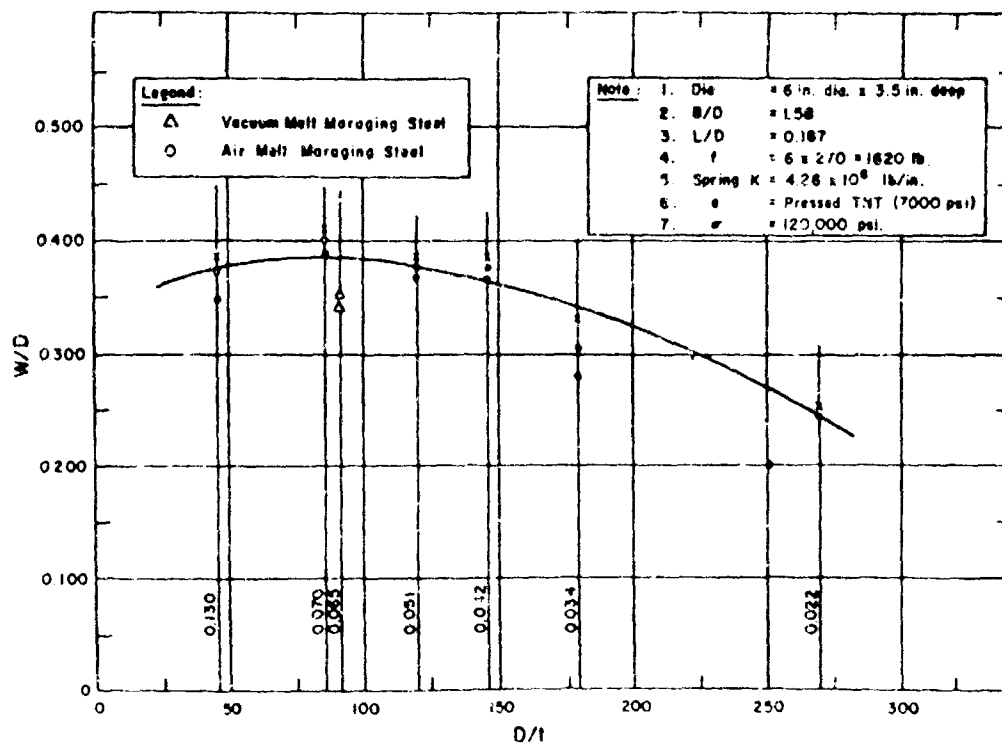


Fig. 13 Formability Limits for 1 1/2% Ni Maraging Steel (Annealed) ( $\sigma = 1.69$ ).

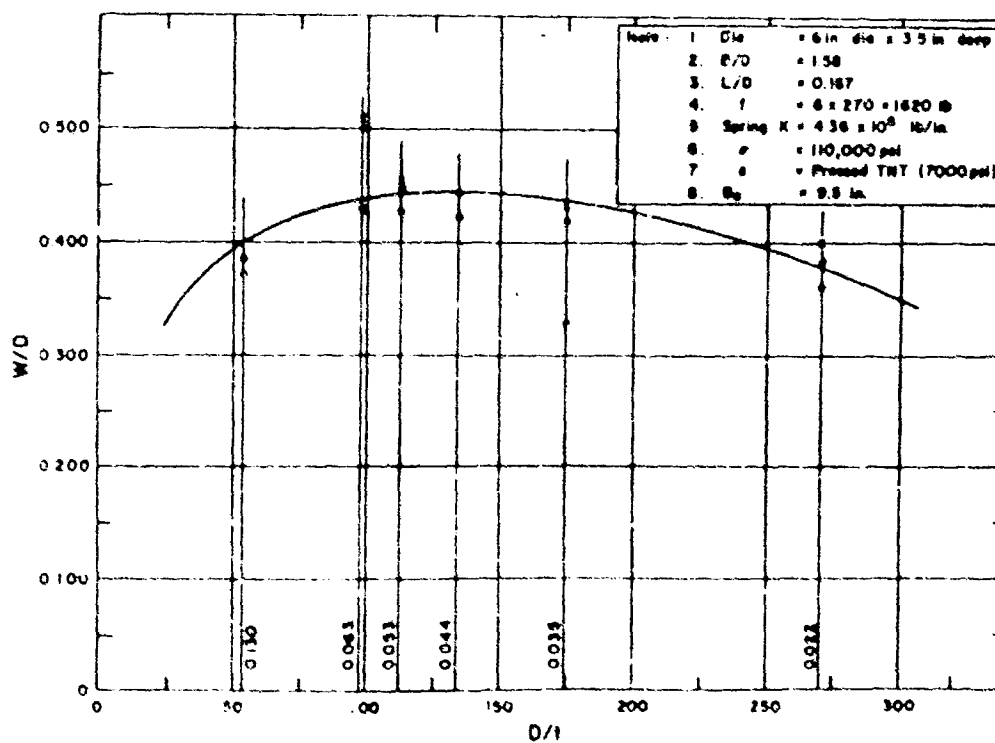


Fig. 14 Formability Limits for D-11 Steel (Annealed) ( $\sigma = 1.15$ ).

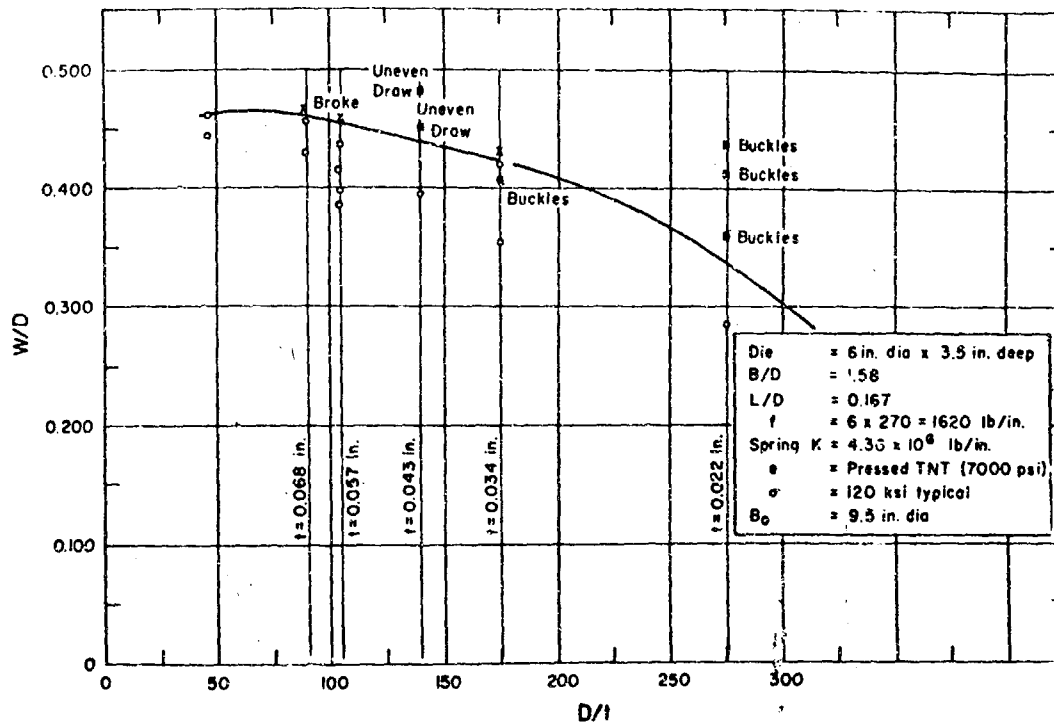


Fig. 15 Formability Limits for 9 Ni-4Co Maraging Steel Annealed (B/D = 1.58).

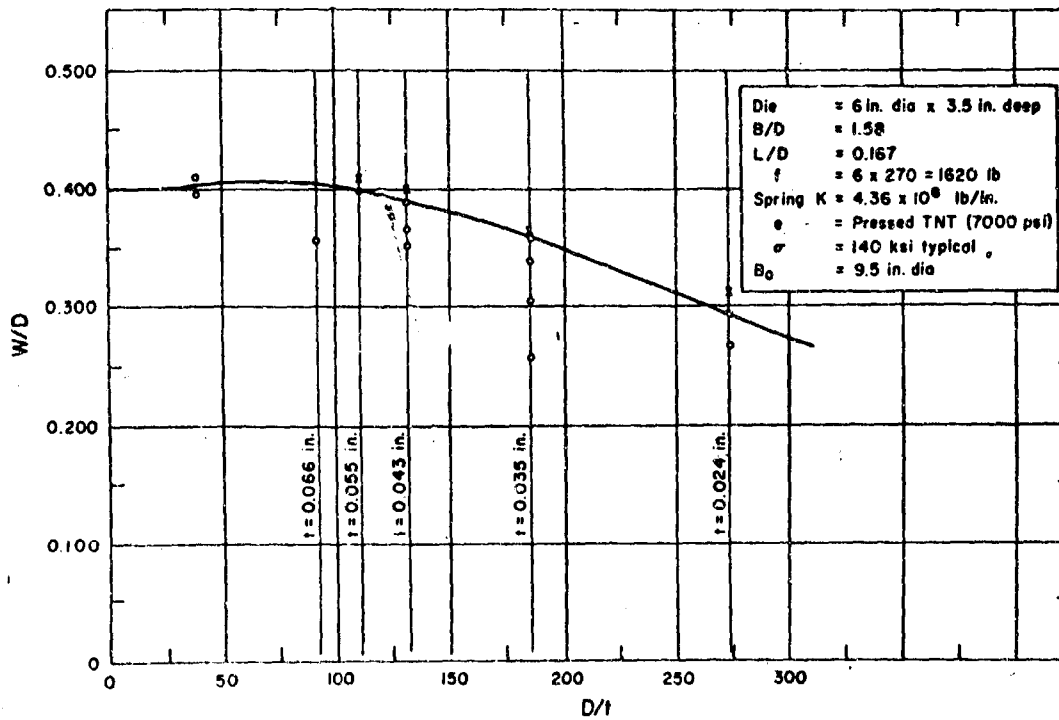


Fig. 16 Formability Limits for 12 Ni-5Cr-3Mo Maraging Steel Annealed (B/D = 1.58).

# EFFECT OF STANDOFF DISTANCE

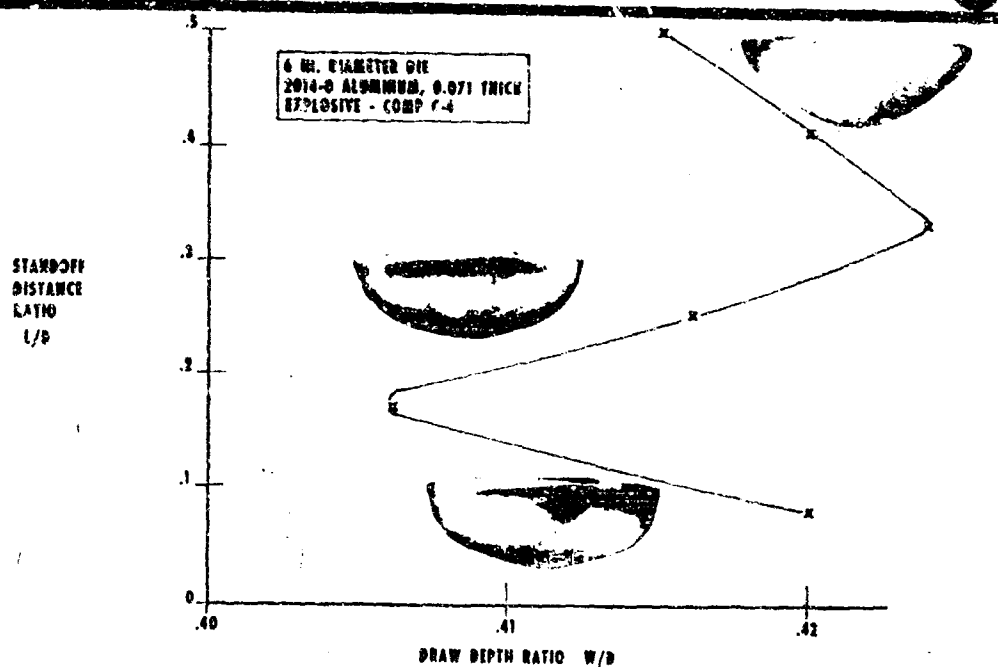


Fig. 17 The Effect of Stand-off Distance on Shape of Free Formed Part.

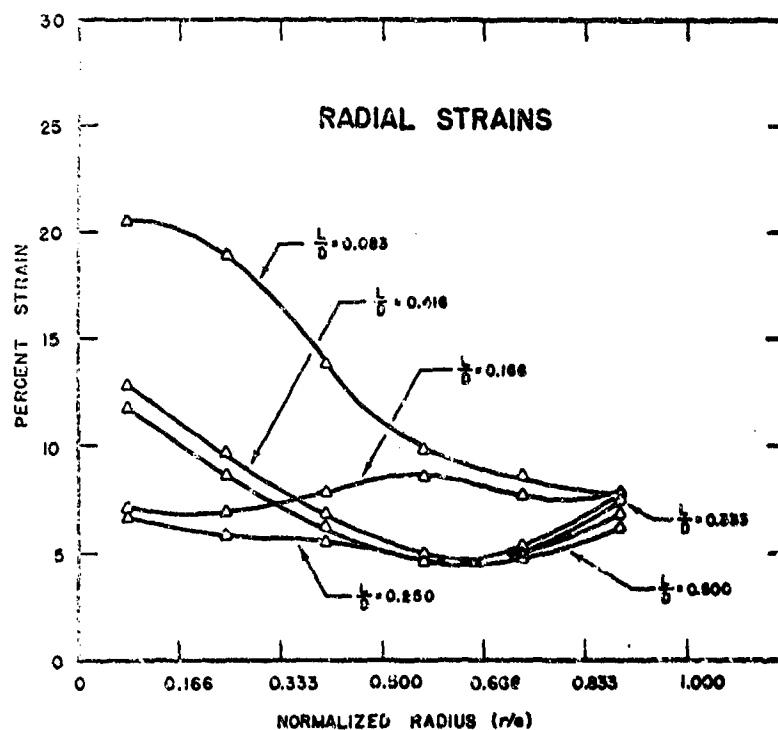


Fig. 18 The Effect of Stand-off Distance on the Magnitude and Distribution of Radial Strains.

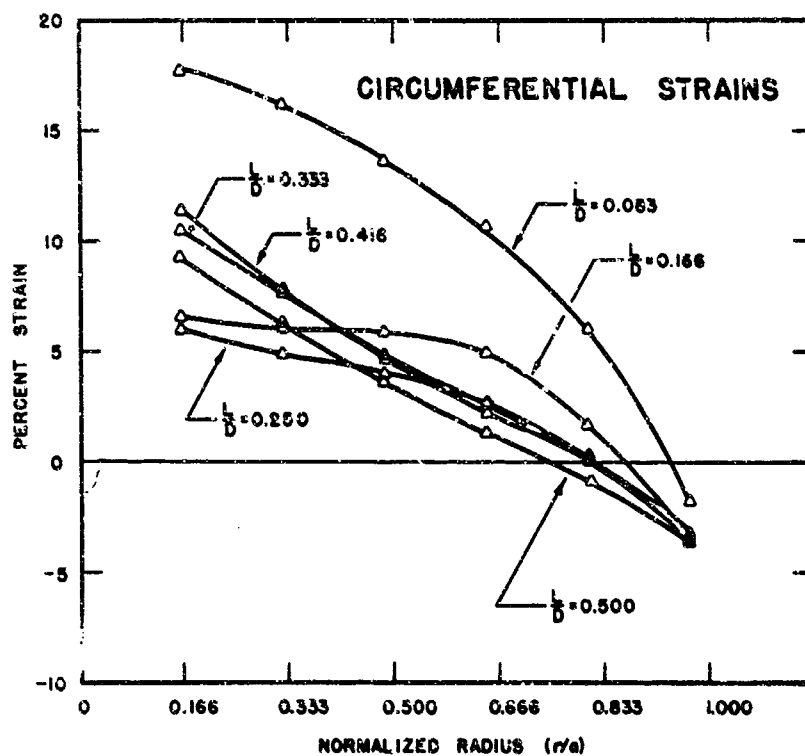


Fig. 19 The Effect of Stand-off Distance on the Magnitude and Distribution of Circumferential Strains.

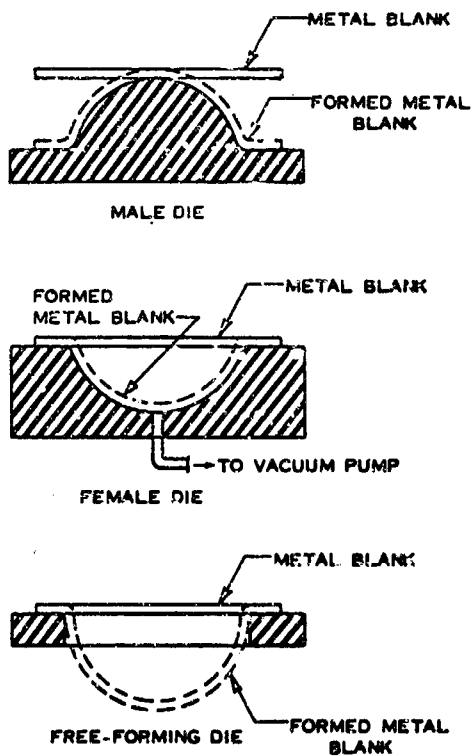


Fig. 20 Basic Die Configurations.

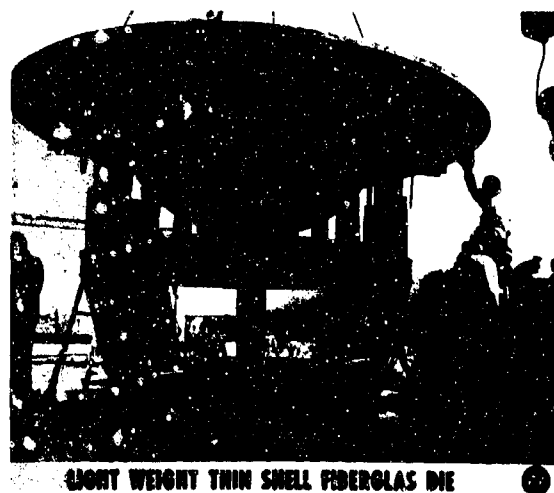
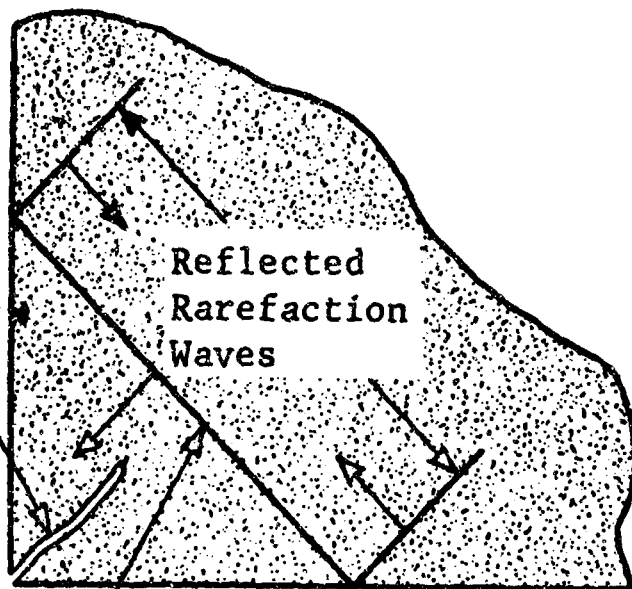


Fig. 21 Lightweight Thin Shell Fiberglass Die.

Resultant Crack Due  
to Intersection of  
Reflected Rarefaction  
Waves



Moving Compressive Shock  
Wave in Die Material

Fig. 22 Corner Cracks in Explosive Forming Dies.

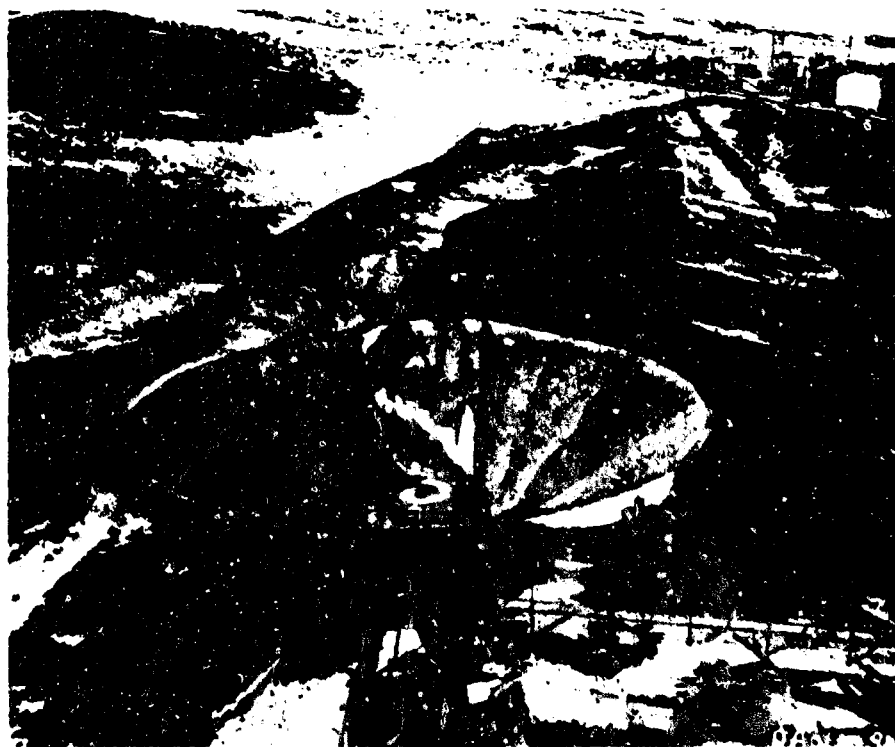


Fig. 23 Conical Explosive Forming Pool (Martin Co.).

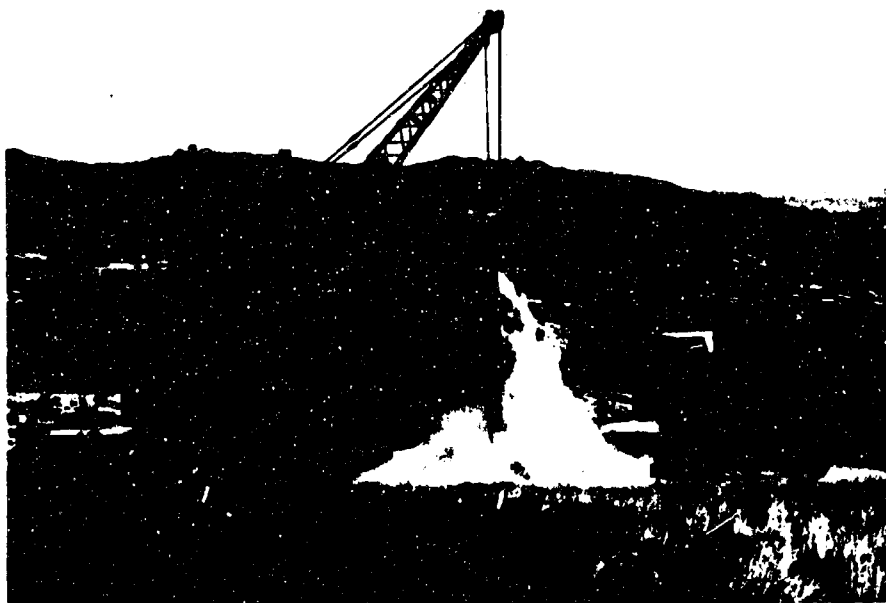


Fig. 24 Detonation of 26.8 Pound Charge of Comp. A-3 in Conical Explosive Forming Pool (Martin Co.) with Bubble Curtain Operating.



Fig. 25 One Hundred and Twenty Inch Diameter Explosively Formed 2014-0 Aluminum Domes (Martin Co.).



Fig. 26 Full Scale Core Segment Explosively Formed Out of 0.661 Inch Thick 2219-T37 Aluminum Alloy (Ryan Aeronautical Co.).

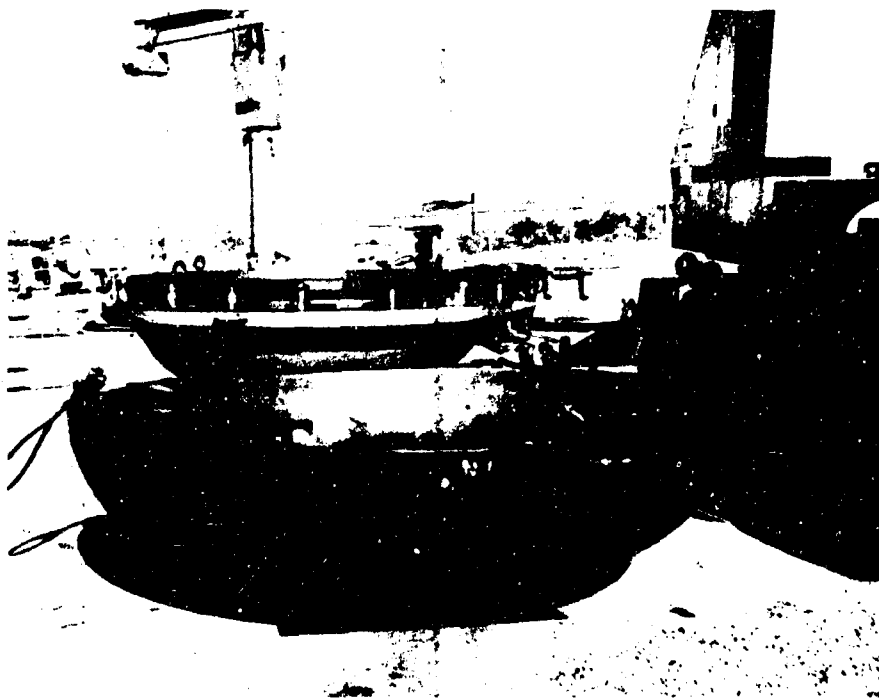


Fig. 27 Explosively Formed H-11 Tool Steel 156 Inch Diameter Dome (Ryan Aeronautical Co. ).



Fig. 28 Twenty-four Inch Aluminum Reflector Explosively Formed (Ryan Aeronautical Co.).



PROTOTYPE WHEEL COVER EXPLOSIIVELY FORMED FROM  
0.027 INCH THICK 304 STAINLESS STEEL

Fig. 29

COLORIMETRY AND RADIOMETRY

James A. Swinson  
U. S. Naval Ammunition Depot  
Crane, Indiana

## INTRODUCTION

There are few people today who do not have a general idea of the capabilities of computers. Most people realize that the digital computer can handle large volumes of data and reduce or analyze it very rapidly. However, one of the difficulties has been in getting data from the laboratory equipment and instrumentation into the computer by an efficient and sometimes feasible method. The discussion here will be how this obstacle can be overcome and some of its applications to pyrotechnics.

### Background

The major difficulty facing the data generator in utilizing digital computers is getting the real-world "analog" signals, generated as laboratory data, into the digital form required by computers. Usually the individual who is generating a large volume of data, is the one most interested in using a computer for data analysis, however, he also has the greatest problem acquiring his data in a form suitable for computer input.

Visualize the difficulty and sources of error in those situations where it is humanly possible to tabulate raw data in handwritten form or printed by some automatic printing device--the data must then be key punched into a card, paper tape or some other form for automatic processing.

Many times the data may be generated at such a high rate that recording by hand or mechanical printers is impossible. In such cases the automated high speed data acquisition systems solves most problems. The data can be converted to digital form and stored for computer input, thereby, by-passing the need for time consuming key punching.

High speed data acquisition systems are presently being produced by several manufacturers with the capability of continually sampling analog data 50,000 times per second with better than 0.1% definition and storing the data on digital magnetic tape ready for digital computer input. Such systems bridge the gap between the real analog world and that of the digital computer.

The U. S. Naval Ammunition Depot, Crane, Indiana recently installed such a data acquisition systems and the following describes its capabilities and the applications, both present and future, in the field of pyrotechnic research.

#### System Description

The NAD Crane system is typical of most high speed digital data acquisition systems with a small (of the order of 4,000 memory storage location) general purpose digital computer acting to control the various input/output devices.

These devices include: an Analog to Digital Converter, capable of 40,000 conversions or samplings of the input signal per second, a high speed digital magnetic tape allowing transfer and storage of 30,000 data values each second, an ASR 33 Teletype unit for operator control and unit for operator control and paper tape read and punch capability and

a digital X-Y plotter in the form of an oscilloscope with both axis and the beam intensity controlled by the computer.

The system also has a priority interrupt system allowing external input signals to command any programable function or subroutine including changing the meaning of any or all interrupts.

### Applications

This system was installed in a Spectroscopy Laboratory where a scanning spectrometer generated analog data which required sampling rates as high as 12,000 per second and desirable up to 30,000 per second, over period of one, two, or three minutes.

The only feasible and economic means of processing such large volumes of data was with digital computers and the data acquisition system was necessary to acquire and store the data.

A second application has been in converting analog data from the NAD Crane MAPI facility to digital magnetic tape. On this data the conversions were made at a rate of 100 per second and the Analog to Digital Converter was externally commanded to digitize by means of the computer priority interrupts.

It is planned to program the computer to digitize data from our densitometer and then a second program to calculate the radiant energy distribution illuminating the spectrograph.

In applications of spectrographic analysis the computer can be programmed to print out the per cent concentration or parts per million of elements being analyzed for.

In general, the data acquisition system can be used to digitize

and store data from any source for reduction at a later time.

#### Use of Computers in Data Reduction

The computer system designed to acquire data at a high rate usually, although not necessarily, does not have sufficient memory to store large programs and/or large amounts of data and therefore these systems are not capable of reducing large volumes of data that has to be stored at one time.

Usually the digital magnetic tape from these tape systems is sent to large memory machines where the data is input from the magnetic tape and processed.

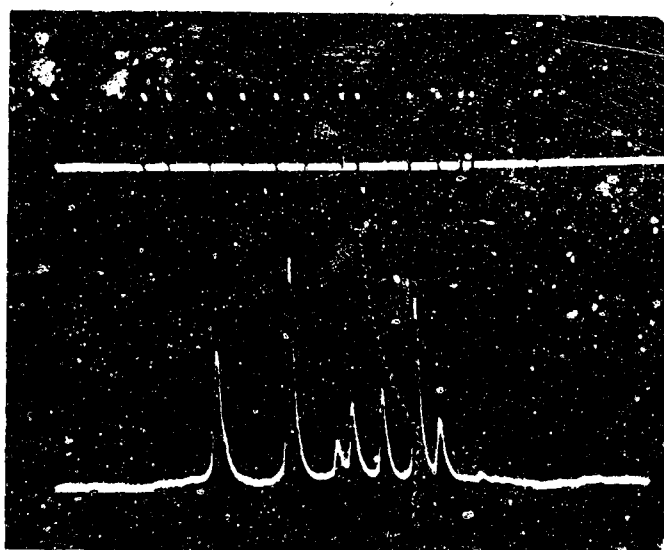
To show the capabilities of the large machine in volume data reduction usage consider the analysis of spectral data from the scanning spectrometer.

Our program uses the computer to make both the wavelength and intensity calibration for the spectrometer system and then to apply these calibration curves to raw data generating spectral radiant intensity distributions as a function of wavelength for a pyrotechnic item or any other light or infra-red source.

Wavelength calibration is accomplished by scanning the emitted spectra of vapor lamps and having the computer locate these spectral emission peaks and assign the appropriate wavelength. After several points are obtained in this manner the computer calculates by interpolation and extrapolation the wavelength associated with each digital sample throughout the spectral region scanned.

Figure 1 is a digital display of the data obtained from a Hg-Cd va-

FIGURE 1



por lamp. Figure 2 is a display of the wavelength calibration against the sample points in the data record.

The data generated by the spectrometer for a NBS calibrated "Illuminate A" lamp is shown in Figure 3 while Figure 4 depicts the actual radiate energy distribution vs wavelength emitted by the lamp. As can be seen by comparing these two curves the response of the spectrometer system to radiation in the longer wavelength region or on the right hand side in the graphs is very low, decreasing to zero at the extreme right.

The actual system response is determined by dividing the spectrometer data output for the lamp into the actual distribution emitted by that lamp at each sample point across the data record. A display of the system response is shown in Figure 5.

By multiplying the data record from the spectrometer, point by point by the system response at each respective point, the spectral distribution emitted by a pyrotechnic item or any other source is obtained.

The graph showing a spectrometer response to a Mk 24 Aircraft Parachute Flare is shown in Figure 6 while Figure 7 shows the radiant energy distribution emitted by the flare determined by the method just described.

Our spectrometer will generate 50 spectral distributions per second, and for each distribution 4,400 mathematical calculations are required to determine calibration and the actual radiant energy distribution emitted by the source. To make these calculations by hand requires approximately 30 man hours per distribution. Obviously, a person can not determine many spectral distributions by this method not to mention

FIGURE 2

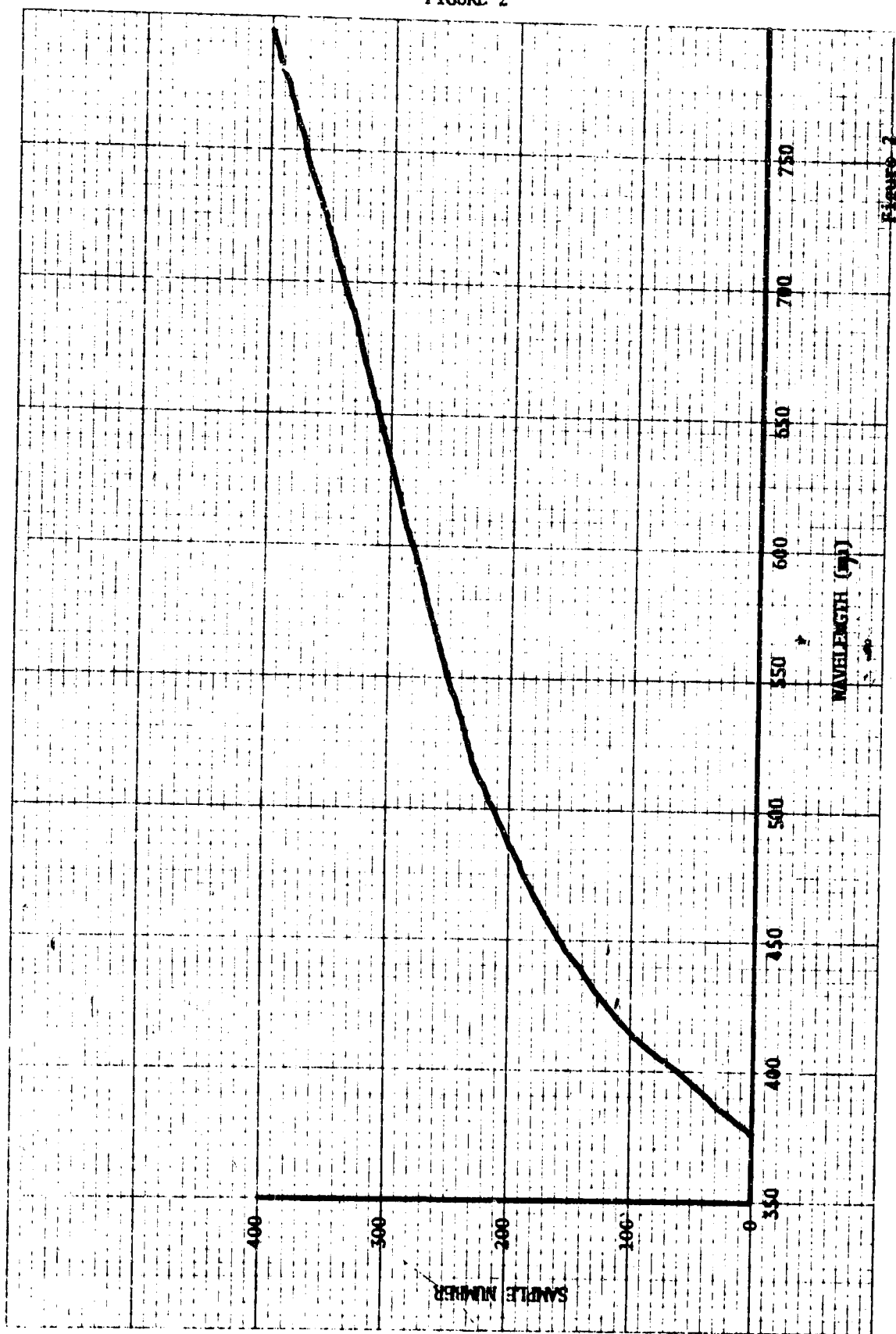
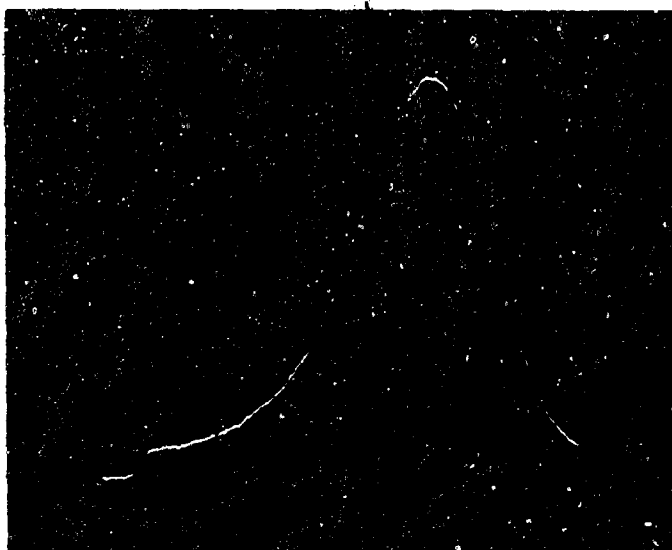


Figure 2

FIGURE 3



DAI

ILL. "A"

FIGURE 4

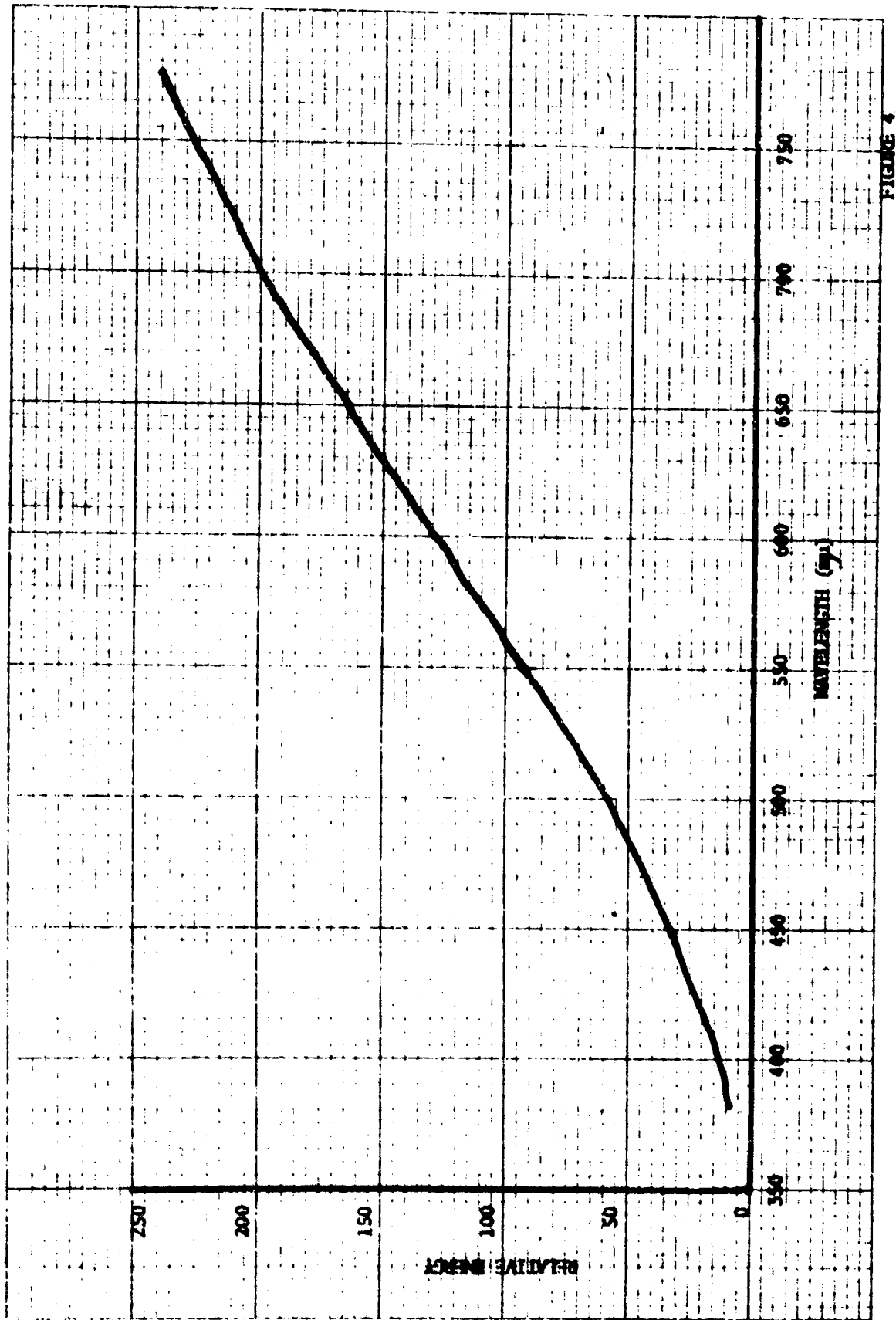


FIGURE 4

FIGURE 5

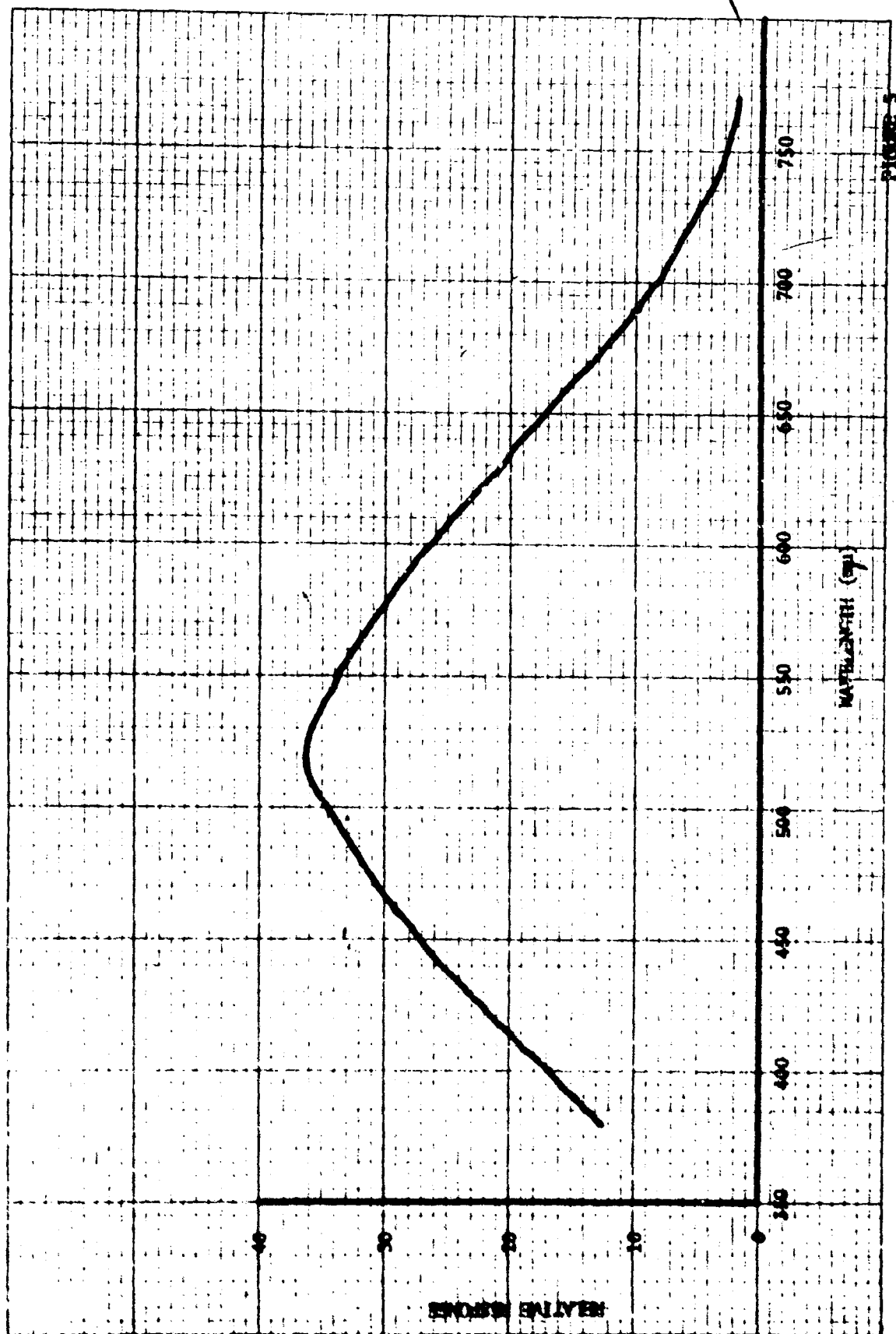


FIGURE 5

FIGURE 6

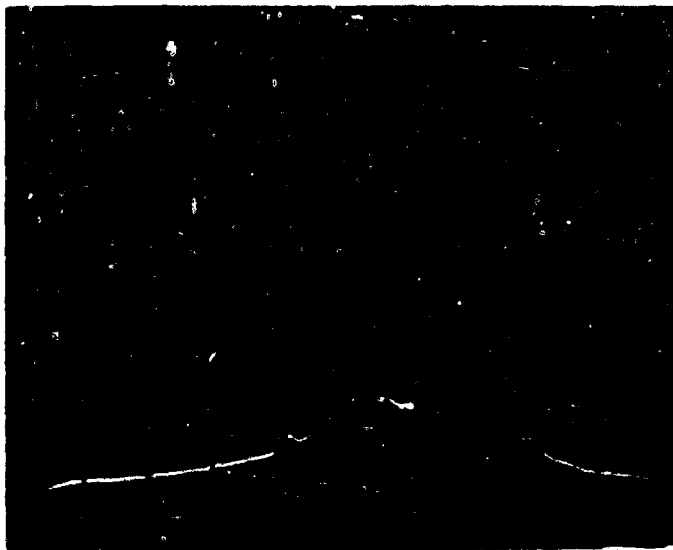
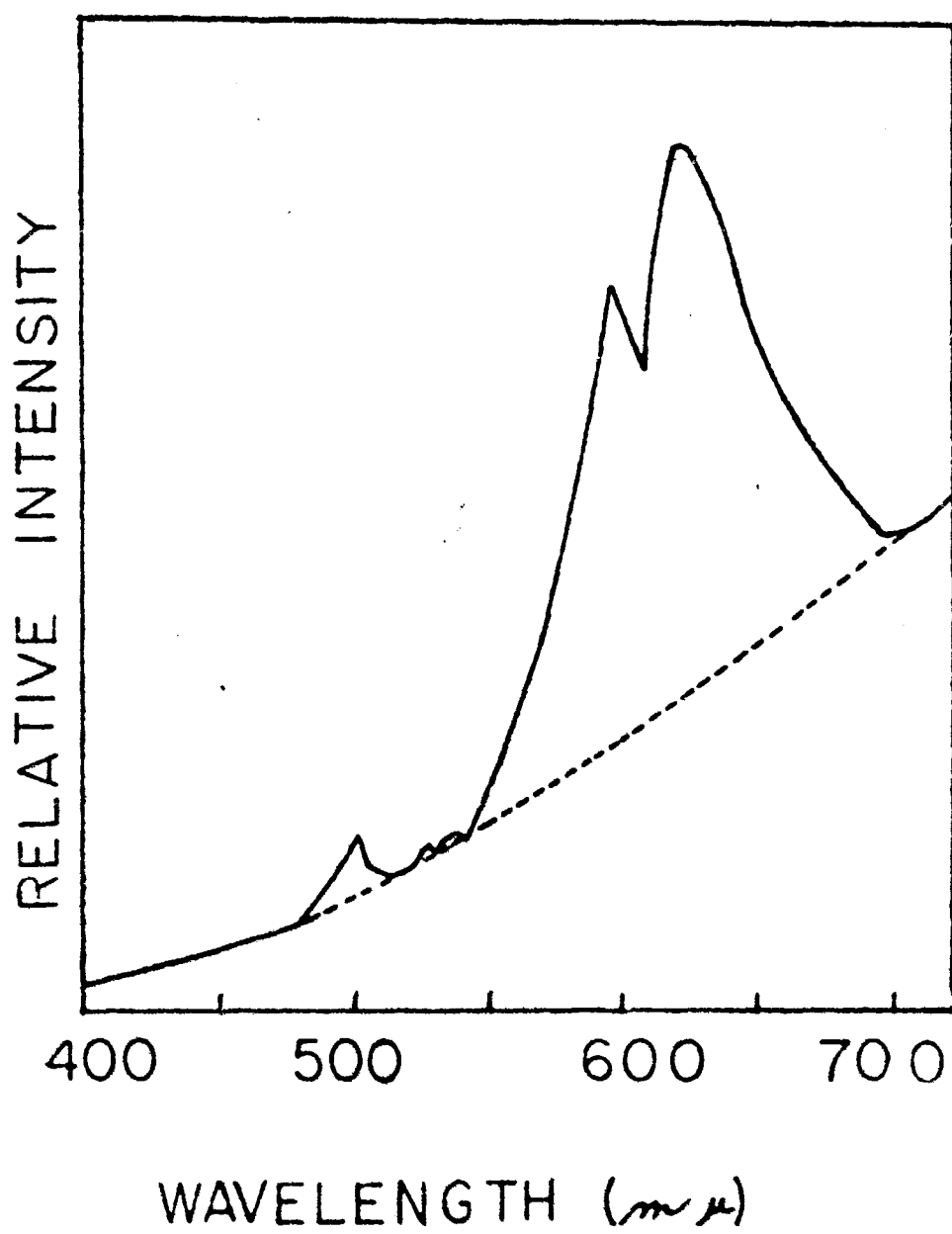


FIGURE 7



possible errors.

To perform these same calculations requires a computer approximately two seconds.

Additionally, the computer is programmed to modify the radiant energy distribution by the human eye response at each wavelength and then plot the luminous radiant energy distribution emitted by the device.

Candlepower is also determined by integrating the area under the luminous intensity curve and is output by the computer.

Dominant Wavelength and Purity are determined by multiplying, wavelength by wavelength, the radiant intensity distribution by the three primary color distributions adopted by the International Commission on Illumination. The chromaticity co-ordinants are calculated from the integrals under the three product curves, and then plotted on a chromaticity diagram to determine dominant wavelength and purity. These co-ordinates may be input to a separate computer program which determines dominant wavelength and purity eliminating the process of plotting the data on a chromaticity diagram.

UNCLASSIFIED

Security Classification

DOCUMENT CONTROL DATA - R & D

Security classification of title, body of abstract and indexing information must be entered when the overall report is classified.

1. ORIGINATING ACTIVITY (Corporate author) <b>Mechanics Division Denver Research Institute University of Denver, Denver, Colorado 80210</b>		2a. REPORT SECURITY CLASSIFICATION <b>UNCLASSIFIED</b>	
		2b. GROUP	
3. REPORT TITLE <b>PROCEEDINGS OF FIRST PYROTECHNIC SEMINAR</b>			
4. DESCRIPTIVE NOTES (Type of report and inclusive dates) <b>Proceedings August 13-16 1968</b>			
5. AUTHOR(S) (First name, middle initial, last name) <b>R. M. Blunt, General Chairman, Denver Research Institute</b>			
6. REPORT DATE <b>1 October 1968</b>		7a. TOTAL NO. OF PAGES <b>432</b>	7b. NO. OF REFS
8a. CONTRACT OR GRANT NO.		8b. ORIGINATOR'S REPORT NUMBER(S)	
9. PROJECT NO.			
c.		9a. OTHER REPORT NO(S) (Any other numbers that may be assigned this report) <b>RDTR No. 131</b>	
d.			
10. DISTRIBUTION STATEMENT <b>Distribution of this document is unlimited.</b>			
11. SUPPLEMENTARY NOTES		12. SPONSORING/MILITARY ACTIVITY <b>U. S. Naval Ammunition Depot Crane, Indiana</b>	
13. ABSTRACT <b>Contains proceedings of First Pyrotechnic Seminar held August 13-16, 1968 at Estes Park, Colorado.</b>			

DD FORM 1473

(PAGE 1)

S/N 0101-807-6801

UNCLASSIFIED

Security Classification

Security Classification

14 KEY WORDS	LINK A		LINK B		LINK C	
	ROLE	WT	ROLE	WT	ROLE	WT
Pyrotechnics Flares Signalling Illumination Mathematics Delays Smokes Explosives Radiometry Kinetics Colorimetry						